Theoretical and Experimental Studies on Combustion of Alternative Fuels in Cement Kilns

Ernst Petter Axelsen

Telemark University College
Faculty of Technology
Departement of Environmental Technology
Porsgrunn, Norway

Thesis submitted for the degree of Dr. Ing.
NTNU/HIT 2002

Contents

List of Figures

List of Tables

Preface

The former Scancem Group, now part of Heidelberg Cement, started a Doctors of Engineering programme in the spring of 1997 with approximately 15 doctoral students. The students goal was to conduct research and graduate with a doctor's degree in engineering within fields beneficial to Scancem's operations.

I have had the pleasure to take part in the Doctors of Engineering programme from September 1998 to September 2002. During this programme I have had the pleasure to be employed by Scancem International ANS in Brevik, where I have conducted most of my work in close collaboration with Telemark University College, Department of Technology, Institute of Environmental Technology.

During these years I have learned a lot about cement manufacturing and related subjects.

I would like to express my special thanks to many individuals and organizations as this work could not have been accomplished without their support and cooperation:

- Professor Dag Bjerketvedt, my supervisor, for his guidance and encouragement, and for introducing me to the "world of combustion". His positive thinking during my many practical challenges during design, construction and operation of the CFBC reactor will not be forgotten.
- Technical Director of Indocement, Øivind Høidalen, my former superior, project manager and initiator of this project, for making it possible for me to take part in the Doctors of Engineering programme. His encouragement is highly appreciated.
- R&D Director Birger Søpler at Norcem, for his encouragement and good advice. The many talks and discussions with Birger Søpler are highly appreciated.
- Dr. Ing. Lars-André Tokheim, my supervisor at Norcem Brevik, for his guidance and encouragement and for being there for questions and comments. His wide experience and knowledge during the full-scale experiments are highly appreciated.
- Associate Professor Dr. Ing. Vidar Mathiesen, at Telemark University College, for his help and guidance during my CFD simulations. His positive attitude and encouragement are highly appreciated.
- Associate Professor Dr. Tech. Ron Zevenhoven, at Helsinki University, for his support and guidance and for making my three months stay at Åbo Akademi University in Finland the best experience a scientist could get. My thanks also go to his family and all of the colleagues I met during my stay in Åbo.
- R&D Director Bo-Erik Eriksson, at Cementa AB, for his support and interest in the project. The extra funding from Cementa AB for technical equipment

is highly appreciated. I also thank the staff at Cementa AB who let me visit the Slite production plant and made my stay a very positive experience.

- Technical Director of Scancem International ANS, Klaus Hvassing, my present superior, for his good advise and encouragement. Many thanks also to all the employees at Scancem International ANS, especially to my former and present colleagues in Brevik who has been very supportive during my work.

- Dr. Ing. student M. Sc. Ursula Kääntee, at Finnsementti, my colleague in the Doctors of Engineering Programme, for her support and ideas.

- Norcem AS and its staff, for letting me execute full-scale experiments and letting me participate in the cement production team.

- Professor Miko Hupa, at Åbo Akademi University in Finland, for making it possible for me to work at Åbo Akademi for three months.

- Associate Professor Pia Kilpinen, at Åbo Akademi University in Finland, for her comments and support.

- Divisional Engineer Talleiv Skredtveit, at Telemark University College, for his contribution during the design, construction and operation of the CFBC reactor. His positive attitude and technical knowledge will not be forgotten.

- Dr. Ing student M. Sc. Nina Bjerkebo, at Telemark University College, for her support and execution of experiments in a modified muffle furnace.

- M. Sc. Steinar Voll, at Telemark University College, for executing experiments in a single particle reactor and a modified muffle furnace.

- M. Sc. Stig Myrland, at Hydro Porsgrunn, for his contribution on the instrumentation of the CFBC reactor.

- To all my friends, especially to M. Sc. Cato Michelsen, for his support during MATLAB programming and for encouraging talks.

Special appreciation is extended to my daughter Anna Louise - the apple of my eye; her understanding and patience during this work was more than any father could expect.

Porsgrunn, 2002
Ernst Petter Axelsen

Abstract

In this thesis, the utilization of alternative fuels for NO_x reduction by means of reburning and advanced reburning is considered. Laboratory experiments, full-scale experiments and computational fluid dynamic (CFD) simulations are the basis of the thesis.

The goal of the work was to characterize alternative fuels used in cement kilns, with focus on the processes taking place in the precalciner of the cement kiln.

To facilitate testing under controlled process conditions, a lab-scale circulating fluidized bed combustion (CFBC) reactor was designed and constructed. A comprehensive study on the fluidization regime in CFBC reactors and precalciners was required to ensure and verify that the operational regime in the CFBC reactor was similar to the regime in a precalciner.

Different alternative fuels, such as refuse derived fuel, animal meal and solid hazardous waste, were tested in the CFBC reactor, which proved well suited for characterization of alternative fuels and investigations of NO_x reduction, even though the operation of a CFBC reactor is quite complex and gives a certain variation in stability. Experiments with and without circulating mass in the CFBC reactor demonstrated the importance of executing the laboratory combustion experiments in an environment similar to that in the full-scale process, i.e. in the precalciner. Animal meal is believed to follow the reduction route of selective non-catalytic reduction or advanced reburning and to have a special capability of reducing NO_x during increased NO_x concentrations at the reactor inlet. The increased CO emissions during advanced reburning and reburning with animal meal are most likely to be due to the competition for the OH radical during oxidation of CO and of NH_3. Furthermore, it was shown, for all fuels, that an increased concentration of NO_x at the reactor inlet increases the ratio of NO_x at the exit and NO_x supplied.

Full-scale experiments were executed at Norcem's kiln 6 in Brevik, using solid hazardous waste in combination with urea pellets, as well as with animal meal, to obtain advanced reburning. The full-scale experiments showed that advanced reburning and reburning with animal meal are well suited for NO_x reduction. NO_x reductions of up to 73 and 63 % during advanced reburning and reburning (with animal meal), respectively, were obtained.

For the CFD simulations a grid of 240,000 cells was generated using GAMBIT. Euler-Euler granular multiphase simulations with FLUENT 4 were executed to verify the assumption of dilute flow and the importance of particle-particle collisions. Euler-Langrangian simulations were executed in FLUENT 6 to investigate the combusting particles, e.g. particles-trajectory, retention time and species concentrations. The CFD simulations revealed important information about the flow regime, e.g. low degree of mixing between the kiln side and tertiary air side of the calciner, which is important as far as burnout is concerned.

Nomenclature

0.1 Latin letters

Symbol	Unit	Description
A	$m^3/mol \cdot s$	Pre-exponential factor
A_p	m^2	Particle surface area
a_L		The content of the component of interest in lot L
a_m		The critical content of the component of interest in lot L
c_g	$J/kg \cdot K$	Specific heat of gas
c_p	$J/kg \cdot K$	Specific heat of particles
C_c	$-$	Cunningham correction
C_D	$-$	Drag coefficient
C_{deg}	%	Calcination degree
$C_{i \cdot S}$	$mol/g\ cat.$	Surface concentration of sites occupied by species i
C_{sw}	$-$	Swelling factor
d_p *or* d	μm	Particle diameter
D	m	Reactor diameter
D_e	cm	Equivalent size of particle sheet
E	kJ/mol	Activation energy
$E(t)$	$-$	Residence time distribution
f_h	$-$	Fraction of heat released by particle reaction
f_{v0}	$-$	Volatile fraction of a particle
f_{w0}	$-$	Volume fraction of the evaporating/boiling material at wet combustion
F	N/kg	Particle force
$F_{i,g}$	N/kg	Additional forces besides drag and gravity forces
$F_{i,s}$	N/kg	Lift force, virtual force or other additional forces
Fr_D	$-$	Froude number $= \frac{U_0^2}{gD}$
g	m/s^2	Acceleration of gravity
G_s	$kg/m^2 s$	Mass flux of solids
h	$W/m^2 K$	Convective heat transfer coefficient
H	m	Height of reactor
h_m		Total heterogeneity
H_{reac}	J/kg	Heat released by the surface reaction

I_q		Mass of increment
k	m^2/s^2	Turbulent kinetic energy
k_m	–	Solids reflux ratio
k_S	s^{-1}	Surface rate constant
k_f *or* k	$m^3/kmol \cdot s$	Rate constant
K_{gs}	–	Gas-solid particle exchange coefficient
K_{eq}	–	Equilibrium constant
K_{ss}	–	Solid-solid exchange coefficient
K_S	–	Surface reaction equilibrium constant
L	m	Riser height
L		One-dimensional lot
L_e	cm	Equivalent length of particle sheet
m_a	kg	Ash content in the particle
M_L		Mass of the lot L
M_m		Weight of component U_m
$m_v(t)$	kg	Volatile yield up to time t
N		Number of splits
N_u		Number of discrete units (e.g. increments)
P_{BFB}	$mbar$	Pressure in bubbling fluidized bed
P_O	Pa	Partial pressure of oxidant
P_s	Pa	Solid phase pressure
r_S	$mol/g\ cat.$	Surface reaction rate
R	$J/kmole \cdot K$	Universal gas constant
R_1	s^{-1} (1. order)	Rate expression on the Arrhenius form
R_2	s^{-1} (1. order)	Rate expression on the Arrhenius form
Re	–	Reynolds number
S		General source term
S_b	–	Mass of oxidant per mass of char
t	s	Time
$t_{injection}$	s	Injection time
T	K	Temperature
T_L	s	Lagrangian time scale
T_∞	K	Local temperature of the continuos phase
u_j	m/s	Velocity in the j-th direction
$u\prime$	m/s	Random velocity fluctuation
U_{CA}	m/s	Accumulative chocking velocity
U_e	m/s	Average velocity of particle sheet
U_m		Component U; m=1, 2, ..., N_u
U_{slip}	m/s	Slip velocity in the riser
$U_{slip,mean}$	m/s	Overall relative velocity
U_0	cm/s	Superficial gas velocity
v_t	m/s	Terminal velocity
$v\prime$	m/s	Random velocity fluctuation
$w\prime$	m/s	Random velocity fluctuation
x_j	–	Position in the j-th direction
Z_s	m	Height where the phenomenon of slugging appear

0.2 Greek letters

Symbol	Unit	Description
α	$-$	Yield factor
$\alpha_{g/s}$	$-$	Volume fraction of gas or solid
$\gamma_{\theta s}$	$kg/m \cdot s^3$	Collisional dissipation of energy
Γ		General diffusion coefficient
δ_e	$-$	Equivalent thickness of particle sheet
ΔP_R	$mbar$	Pressure drop across the riser
ϵ_p	$-$	Particle emissivity
ε	$-$	Bed-voidage / Void fraction of particles
ε	m^2/s^2	Dissipation of turbulent kinetic energy
ε_s	$-$	Volume fraction of solids
ε_{mean}	$-$	Average cross section bed-voidage
ζ	m	Integral length scale
ζ	$-$	Distributed random number
θ_R	K	Radiation temperature
Θ	$minutes$	Time steps
$\kappa_{\theta s}$	$kg/m \cdot s$	Diffusion coefficient for granular energy
λ	$-$	Excess air ratio
λ	m	Molecular mean free path
$\kappa_{N-ratio}$	$-$	$\frac{mass\ nitrogen\ emitted}{mass\ fuel\ nitrogen\ supplied}$
μ	cm/s^2	Dynamic viscosity
$\mu_{eff,g}$	m/s^2	Dynamic effective gas viscosity
μ_s	m/s^2	Viscosity for solids
ϖ	s^{-1}	Angular frequency
ρ_f	kg/m^3	Fluid density
ρ_g	g/cm^3	Gas density
ρ_s	g/cm^3	Solid density
σ	W/m^2K^4	Stefan-Boltzmann constant
σ_t	-	Prandtl number for turbulent dispersion
$\tau_{ij,g}$	g/ms^2	Shear stress of the gas phase
τ_e	s	Characteristic lifetime of an eddy
τ_p	s	Particle response time
τ_s	s	Solids residence time
τ_t	s	Turbulence time scale of particles
ϕ_{gs}	$kg/m \cdot s^3$	Energy exchange between fluid and solid phase
ϕ_{ls}	$kg/m \cdot s^3$	Energy exchange between solid phases l and s
χ	$-$	Mole fraction

0.3 Subscripts

Symbol	Description
bp	Boiling point
c	Calciner
e	Equivalent
f	Fluid
g	Gas
s	Slugging or solid
vap	Vaporization
p	Particle
0	Initial (e.g. time; mass)

0.4 Abbreviations

Symbol	Description
AE	Analytical error
AM	Animal meal
AR	Advanced reburning
BFB	Bubbling fluidized bed
CC	Char coal
CE	Continuous selection error
CFB	Circulating fluidized bed
CFBC	Circulating fluidized bed combustion
CRDF	Carbonized refuse derived fuel
DE	Delimitation error
DSC	Differential scanning calorimetry
ECT	Electrical capacitance tomography
EE	Extraction error
FBC	Fluidized bed combustion
H&B	Hartman&Braun
ILC	In-line calciner
k.g.	Kiln gas
LDA	Laser-doppler anemometry
LHW	Liquid hazardous waste
NDIR	Non dispersive infrared analyzer
NSR	Nitrogen stoichiometric ratio (ratio NH_3/NO_{in})
OE	Overall estimation error
PB	Packed bed
PC	Pet coke
PE	Preparation error
RDF	Refuse derived fuel
RMS	Root mean square
RTD	Retention time distribution
SE	Sampling error
SHW	Solid hazardous waste
SNCR	Selective non-catalytic reduction
SPR	Single particle reactor
SFT	The Norwegian State Pollution Agency
t.g.	Tertiary gas
TE	Total sampling error
TGA	Thermogravimetric analysis
TOC	Total organic compound
WO	Waste oil

Chapter 1

Introduction

1.1 Background

Today the society generates enormous amounts of solid wastes like e.g. municipal waste, medical and pathological wastes, solid hazardous wastes, and specialized industrial wastes. The Landfill Directive in the EU states that landfill disposal must be reduced to 35 % of 1995 levels by 2016. Waste-to-energy and material recovery are commonly practiced and currently the only viable alternatives to landfill. However, the energy recovery as a result of waste incineration is of secondary concern to the hazard destruction and volume reduction. Combustion of solid waste, from any source, typically generates significant public opposition based upon perceived risks associated with airborne emissions and solid (ash) products management. Solid waste, or so-called alternative fuels, is from this point of view best utilized in the cement industry for full energy recovery. Where high temperature, long residence time, intense turbulence, minimum waste disposal and an alkaline environment ensures destruction of organic compounds.

In the past few years we see a rapid increase in the use of alternative fuels in the cement industry. The driving forces are the prospect of reduction in fuel costs and the need of utilization of the enormous amount of waste that is produced in our society. Furthermore, conserving non-renewable fossil fuels contributes to CO_2 reduction, and alternative fuels may be utilized in NO_x[1] reduction.

Norcem is the sole cement manufacturer in Norway and part of Heidelberg Cement. Norcem has for several years used alternative fuels in the cement manufacturing process, see the recent development in Figure 1.1. At the cement plant in Brevik it has been decided to increase the use of refuse derived fuel (RDF), and an annual supply of 40,000 ton of RDF has been contracted for 2002. In addition the cement plant utilizes liquid hazardous waste (LHW), solid hazardous waste (SHW), animal meal (AM) and waste oil (WO) together with a mixture of coal and pet coke. Figure 1.2 presents the precalciner kiln in Brevik

Norcem, among several others, has experienced that alternative fuels have large differences in properties like specific weight, geometrical shape, moisture content, chemical composition, heat of combustion etc. These properties influence the fuel particle transportation, burning rate and formation of chemical elements in the precalciner cement kiln. The characteristics of the different alternative fuels may have significant effect on the clinker quality, kiln operation, energy consumption and emissions to the air (e.g. NO_x, CO, etc.). Hence, it is necessary to increase the knowledge about combustion and alternative fuels to achieve increased flexibility in the cement production.

[1] NO_x is the sum of NO_2 and NO calculated as NO_2.

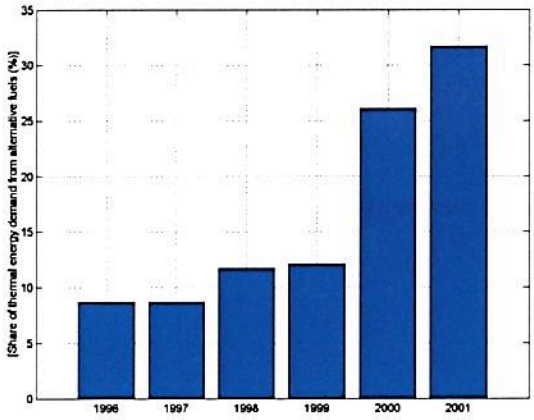

Figure 1.1: The development of alternative fuels share of the thermal energy used in precalciner kiln 6 at Norcem Brevik.

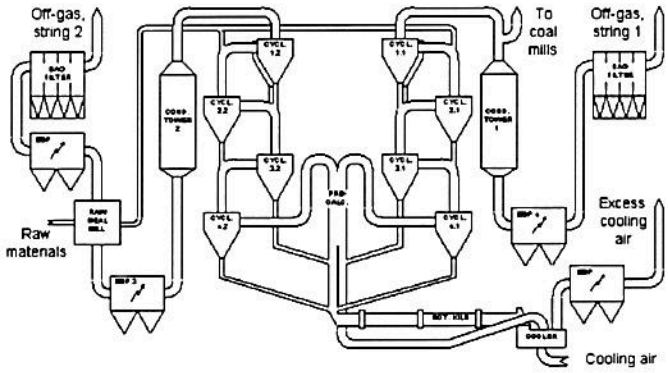

Figure 1.2: Precalciner kiln 6, Brevik, (Tokheim 2000*a*).

Optimizing the combustion of alternative fuels, and improving the knowledge of burning alternative fuels in precalciner cement kilns is a major challenge for the future.

1.2 Problem description

The motivation for research and development has been the requirement to reduce emissions levels (e.g. NO_x) and provide more sophisticated indications of fuel reactivity.

The objective for this thesis is to investigate combustion of alternative fuels in a precalciner.

Full-scale experiments in a precalciner do not give full control over process variables, such control is more obtainable in laboratory experiments. Furthermore, the number of full-scale experiments in a cement plant is restricted to the most essential ones.

It was decided to build a CFBC reactor to improve the knowledge about the process in the precalciner and how it is affected by the utilization of alternative fuels,

with special emphasis on NO_x reduction by reburning and advanced reburning. Experiments in a CFBC do not necessarily correlate with full-scale processes, but give an approximate picture of temperatures and emissions. Besides, it is well-suited for comparing the behavior of different types of fuel.

Similarities and differences between the CFBC and full-scale experiments is important to clarify. Therefore, full-scale experiments have been performed on kiln 6 at Norcem Brevik in order to investigate NO_x reduction - advanced reburning rich and reburning.

Not much has been published on characterization of cement kiln precalciner regimes. Hence, it is necessary to characterize the precalciner regime with reference to previous work on CFBC reactors and with the aid of Computational Fluid Dynamic (CFD) simulations. CFD simulations also give useful information on the precalciner particle paths, retention time and species concentrations.

1.3 Structure of the thesis

- Chapter 2 presents theory and previous work on formation and reduction of CO and NO_x, as well as fluidization regime and utilization of alternative fuels in cement kilns.
- Chapter 3 presents the full-scale experiments, as well as characteristics of the precalciner kiln 6 at Brevik. Experiments on NO_x reduction with alternative fuels by reburning and advanced reburning is emphasized.
- Chapter 4 presents the CFBC reactor and the laboratory experiments. Again, NO_x reduction with alternative fuels by reburning and advanced reburning is emphasized.
- Chapter 5 presents CFD simulations of the precalciner of kiln 6 at Brevik.
- At last, Chapter 6 gives a summary and a conclusion.

The formate of references is standard Scientific Work Place (SWP).

Chapter 2

Theory and related work

This chapter reviews related and previous work for the investigations on alternative fuels ability to reduce NO_x emissions and CO formation in full-scale and laboratory experiments. Characterization of the flow regime are discussed in order to form the basis of comparing execution of experiments in the laboratory to the full-scale experiments.

This chapter presents theory and previous work on:

- formation and reduction of NO_x and CO,
- fluidization regime and
- utilization of alternative fuels in cement kilns.

2.1 NO_x formation and reduction

NO_x formation and destruction processes in combustion systems are very complex. During combustion, nitrogen from the combustion air or fuel may be converted to nitrogen-containing pollutants such as NO, NO_2, N_2O, NH_3 and HCN. What pollutants are formed depends on the temperature and fuel/oxygen ratio in the combustion device (Hill & Smoot 2000). The conversion of NO to NO_2 in typical flame temperatures can be shown to be negligibly small in chemical equilibrium calculations, although significant concentrations of NO_2 in the exhaust gas of gas turbines and in the products of range-top burners have been reported. Kinetic models modified to include NO_2 formation and reduction showed that the conversion can be neglected in practical devices (Glassman 1996).

There are three major sources of NO formed in combustion (Glassman 1996), (Turns 1996), (Hill & Smoot 2000), (Bowman 1992):

- thermal NO mechanisms,
- prompt NO mechanisms and
- fuel NO mechanisms.

In addition, the N_2O-intermediate mechanism is a fourth source of NO, according to Turns (1996).

Different mechanisms reduce NO_x. Reburning and advanced reburning are discussed here. CO formation and oxidation are also discussed.

2.1.1 Thermal NO

The oxidation of atmospheric nitrogen (N_2) by the thermal mechanism is a major source of NO_x emissions at high temperatures in a fuel-lean environment and with fuels containing small or no nitrogen at all. This process is described by the Zeldovich two-step mechanism:

$$N_2 + O \rightleftarrows NO + N \tag{2.1}$$

$$N + O_2 \rightleftarrows NO + O \tag{2.2}$$

An extended Zeldovich mechanism is applied when the NO formation from the Zeldovich mechanism is under-estimated, that is in fuel-rich flames:

$$N + OH \rightleftarrows NO + H \tag{2.3}$$

The extended Zeldovich mechanism involves the O and OH radicals, which also play an important role in the fuel oxidation mechanism. Hence, in general, it is necessary to couple the thermal NO reactions to the reaction sequence describing oxidation of the fuel.

Since the overall ratio of NO formation by the thermal mechanism generally is slow compared to the fuel oxidation reactions it is often assumed, following the suggestion of Zeldovich, that the thermal NO formation reactions can be decoupled from the fuel oxidation process. In this situation, NO formation rates are calculated assuming equilibrium values of temperature and concentrations of O_2, N_2, O and OH, where the N-atom concentration is calculated from a steady-state approximation applied to reactions 2.1, 2.2 and 2.3 (Miller & Bowman 1989). The overall simplified rate expression is:

$$\frac{\mathrm{d}[NO]}{\mathrm{d}t} = 2k_{f1}[O][N_2] \tag{2.4}$$

$$k_{f1} = 1.8 \cdot 10^{11} \exp(-38,370/T) \tag{2.5}$$

The rate expression ($\frac{\mathrm{d}[NO]}{\mathrm{d}t}$) in Equation 2.4 and the rate constant (k_{f1}) in Equation 2.5 have units of $\mathrm{kmole \cdot m^{-3} \cdot s^{-1}}$ and $\mathrm{m^3 \cdot kmole^{-1} \cdot s^{-1}}$, respectively.

The first reaction is usually accepted to be the rate-determining step due to its high activation energy, and results in the Zeldovich mechanism being temperature-sensitive, which can be seen from Figure 2.1. The temperature dependence also results from the temperature sensitivity of the O atom equilibrium concentration (Hill & Smoot 2000).

Equation 2.3 is usually negligible except in fuel rich flames (Hill & Smoot 2000).

The rate equation, Equation 2.4, is coupled to the fuel oxidation process through competition for the oxygen atom, whose concentration must be estimated if a comprehensive scheme is not used to compute the fuel oxidation chemistry. Equation 2.6 applies to fuel-lean, secondary combustion zones, where oxygen atoms are assumed to be in equilibrium with O_2. Warnatz et al. (1999) state that assuming equilibrium, particularly at low pressures, underpredicts oxygen atoms concentration by a factor of up to 10. Following, Warnatz et al. (1999) presents a better approximation, in partial-equilibrium, for the oxygen atom concentration, see Equation 2.7 (Warnatz et al. 1999). Equation 2.8 applies to fuel-rich zones, where oxygen is in partial-equilibrium (Hill & Smoot 2000). Hill et al. (2000) reviewed previous work on methods to estimate the atomic oxygen concentration and stated that a general reliable estimation is far from resolved.

$$[O] = \{K_{eq}[O_2]\}^{1/2} \tag{2.6}$$

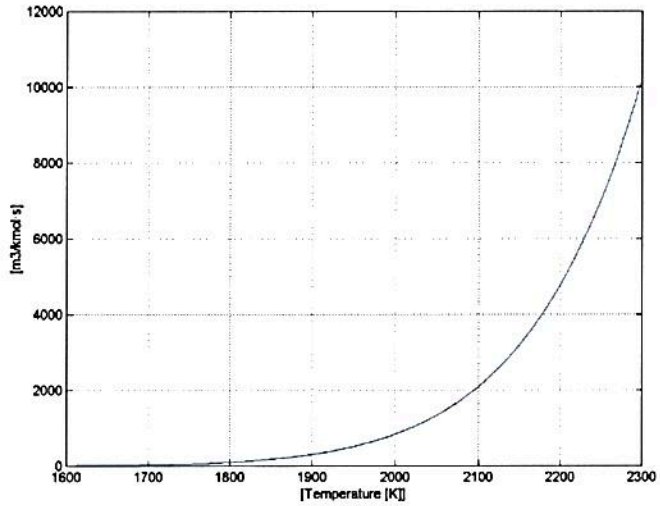

Figure 2.1: The forward rate coefficient of Equation 2.1.

$$[O] = \frac{k_{H+O_2} \cdot k_{OH+H_2} \cdot [O_2][H_2]}{k_{OH+O} \cdot k_{H+H_2O} \cdot [H_2O]} \tag{2.7}$$

$$[O] = K_{eq} \frac{[O_2][CO]}{[CO_2]} \tag{2.8}$$

It can be seen from Figure 2.1 that thermal NO formation by the Zeldovich mechanism is significantly reduced at temperatures below 1600 - 1800 K (Hill & Smoot 2000), (Turns 1996).

2.1.2 Prompt NO

Prompt NO formation occurs in fuel rich regions of the flames. It is formed by the reaction of atmospheric nitrogen with hydrocarbon radicals in the flame, which are then oxidized to form NO. This is the so-called Fenimore mechanism.

The main reactions are (Turns 1996):

$$N_2 + CH_i \rightleftarrows HCN + N + ... \tag{2.9}$$

$$N_2 + C \rightleftarrows CN + N \tag{2.10}$$

Reaction 2.9 is the primary path and is the rate limiting step in the sequence. It is estimated that HCN is involved in approximately 90 % of the prompt NO formed (Hill & Smoot 2000). For excess air ratios[1] higher than 0.9, the conversion of HCN to form NO follows the following chain reaction:

$$HCN + O \rightleftarrows NCO + H \tag{2.11}$$

$$NCO + H \rightleftarrows NH + CO \tag{2.12}$$

[1] Excess air ratio is defined here as $\lambda = (\frac{\frac{air}{fuel}}{(\frac{air}{fuel})_{stoic}})$.

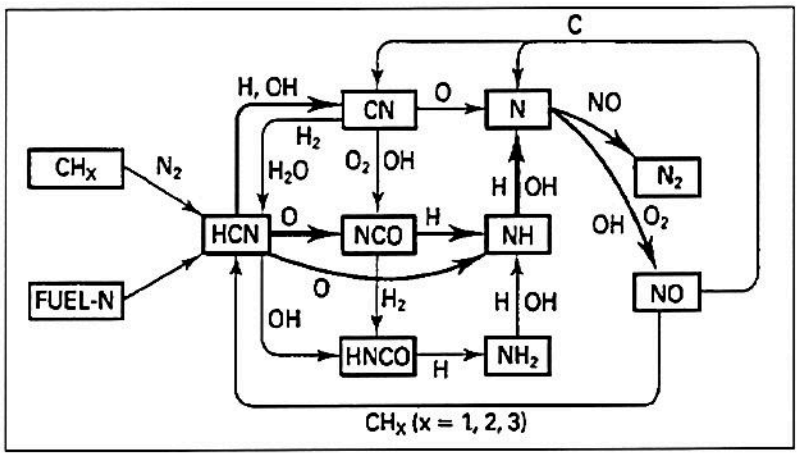

Figure 2.2: Illustration of prompt NO formation, fuel nitrogen conversion and reburning (Turns 1996).

$$NH + H \rightleftarrows N + H_2 \tag{2.13}$$

$$N + OH \rightleftarrows NO + H \tag{2.14}$$

For excess air ratio lower than 0.9, other routes open up and the chemistry becomes much more complex. Miller and Bowman (1989) state that the above scheme is no longer rapid and that NO is recycled to HCN, inhibiting NO production. Further details can be found in Miller and Bowman (1989).

The prompt NO mechanism is much more prevalent in fuel-rich than in fuel-lean hydrocarbon flames. Since prompt NO is only significant in very fuel-rich systems and most practical combustion systems, such as a cement kiln, is operated fuel-lean or close to stoichiometric, the contribution from prompt NO to the total NO formed is likely to be small. Staged combustion systems are, however, usually operated with a fuel-rich stage that will increase the importance of prompt NO formation. Also, in coal diffusion flames, the reaction zone is often slightly fuel-rich which can promote prompt NO formation (Hill & Smoot 2000). However, tests in which N_2 in the combustion air was replaced by argon showed no change in NO concentrations. Thus, prompt NO is most prevalent in cooler hydrocarbon flames containing no fuel-nitrogen and is less prevalent in hot, fuel-lean systems with substantial amounts of fuel-nitrogen (Hill & Smoot 2000).

From this statement, it is difficult to be conclusive about formation of prompt NO in precalciner cement kilns which base their NO_x reduction on staged combustion with alternative fuels containing fuel-nitrogen, such as Cement kiln 6 in Brevik. It can be stated that, even with an alternative fuel containing fuel-nitrogen, there will be some formation of prompt NO in a precalciner that employ staged combustion. In contrast it can be stated that there are negligible amounts of prompt NO in the main burner. The NO_x formation in the main burner is most likely to be solely thermal NO formation due to the high temperature (maximum temperature at about 2000 $°C$) and possibly fuel NO formation due to the nitrogen in the primary burner fuels.

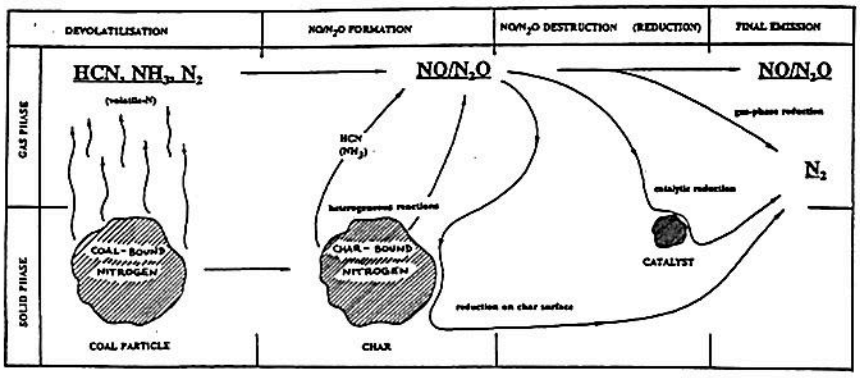

Figure 2.3: Conversion of fuel nitrogen in coal combustion (Wojtowicz et al. 1993).

2.1.3 Fuel NO

It is chosen here to treat both homogeneous and heterogeneous fuel NO reactions, though several authors choose to designate only homogeneous reactions as fuel NO reactions (Hill & Smoot 2000), (Glassman 1996), (Turns 1996). Figure 2.3 shows the conversion of fuel nitrogen in coal combustion.

Heterogeneous reactions

In combustion systems burning solid fuels, NO_x can be both formed and reduced by reactions involving the solid fuel:

$$char + O_2 \longrightarrow NO \tag{2.15}$$

$$char + NO \longrightarrow N_2 + ... \tag{2.16}$$

These heterogeneous reactions occur with the solid carbonaceous substance remaining after devolatilization. Shimizu et al. (1992) state that the net amount of NO_x formed from heterogeneous reaction is strongly dependent on the intrinsic reactivity and internal surface area of the char. These characteristics of the char will vary depending on several factors, including fuel-type, air-staging, burner injection and the conditions that led to the formation of the parent solid fuel (e.g. coal). This makes heterogeneous NO_x control more difficult.

The amount of nitrogen retained in the char after devolatilization appears to be a function of the stoichiometry, and as much as half of the nitrogen remains in the char (e.g. coal) after devolatilization (Hill & Smoot 2000). Hill et al. (2000) reports that up to 70 - 90 % of the coal nitrogen is devolatilized at temperatures above 1400 - 1500 K. Previous experiments have shown that 0 - 20 % of the nitrogen in the coal is evolved in the early volatiles, primarily as HCN and NH_3 (Hill & Smoot 2000).

Tillman (1991) states that nitrogen contained in the char is oxidized directly to NO, as shown in Figure 2.4. The fuel nitrogen conversion according to Figure 2.4 is prevailing for temperatures lower than 1480 $°C$. The oxidation may occur either with oxygen atoms (O), hydroxy radicals (OH), or other reactive species. The char may then react with CO and NO to form N_2, or it may react with NO at a reactive carbon site in the char to form N_2 and CO. Alternatively the NO may be generated directly as a gaseous product of combustion (Tillmann 1991).

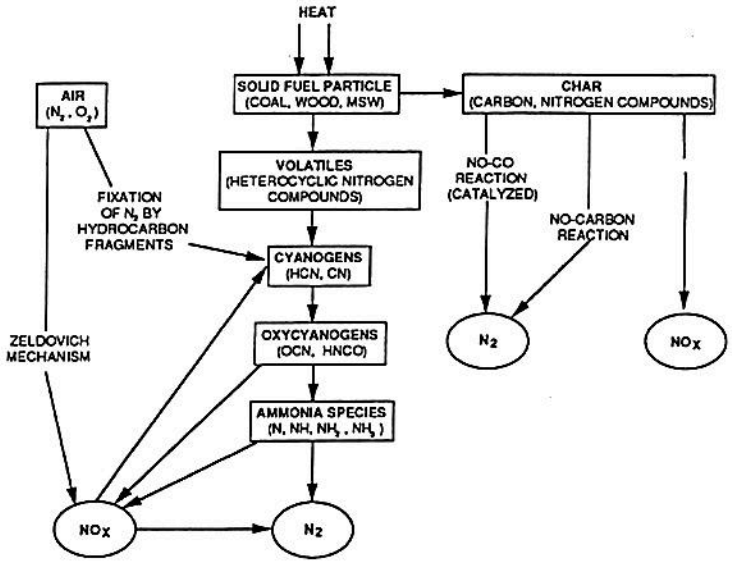

Figure 2.4: Alternative pathways for the formation of NO_x from burning solid fuel particles (Tillmann 1991).

De Soete (1990) made investigations on heterogeneous N_2O and NO formation from bound nitrogen atoms during coal char combustion and found that (De Soete 1990):

- the fractions of char-nitrogen transformed into NO and N_2O during combustion are roughly proportional to the degree of carbon burnout (unlike the fractions of char-nitrogen converted into HCN and NH_3),
- the amounts of N_2O and NO, measured at the end of the combustion, only account for about 30 to 70 % of total char-nitrogen content, respectively, due to heterogeneous reduction of these nitrogen oxides on bound carbon atoms, whereby N_2O is more readily reduced than NO,
- a suitable heterogeneous adsorption/desorption mechanism of NO and N_2O formation from char-nitrogen can only be proposed in connection with heterogeneous carbon combustion, since, at least at temperatures up to 1300 K, oxygen adsorption on (-C) and (-CN) sites controls the overall reactions of both phenomena,
- for particle sizes of 35 to 50 microns, oxygen concentrations between 1 and 30 % and temperatures between 800 and 1300 K, the adsorption reactions of oxygen have been found to be controlled by pore diffusivity.

De Soete et al. (1999) made investigations on heterogeneous formation of nitrous oxide from char-bound nitrogen and found that (De Soete et al. 1999):

- the conversion of char-nitrogen into N_2O increases with combustion temperature, see Figure 2.5,
- there is a triple trade-off between NO, N_2O and N_2, seen from Equation 2.17, 2.18 and 2.19.

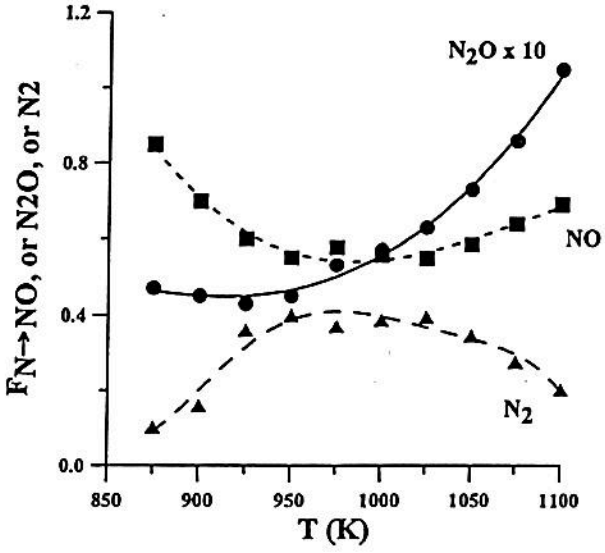

Figure 2.5: Fraction of char nitrogen atoms released in the steady state either as N_2O, NO or N_2, as a function of combustion temperature. Coal char particle size = 30-50μm; P_{tot} = 100 kPa; P_{O_2} = 34 kPa; O_2 in Argon (De Soete et al. 1999).

$$NO + (-C) \longrightarrow N_2 \tag{2.17}$$

$$NO + (-CNO) \longrightarrow N_2O \tag{2.18}$$

$$N_2O + (-C) \longrightarrow N_2 \tag{2.19}$$

At typical conditions (800 to 1200 K) the rate of reaction 2.18 seems to be about twice the rate of Equation 2.17. In the temperature range between 900 to 1050 K, only a small part of the NO (about 20 %) is converted into N_2 by Equation 2.17, whereas a major part of the N_2O (40 - 80 %) is reduced to N_2 by Equation 2.19. Moreover, a major part of the molecular nitrogen released originates from N_2O reduction (typically 60 %), rather than from NO reduction (typically 40 %). Thus, reduction of NO occurs preferentially via the intermediate formation of nitrous oxide (De Soete et al. 1999).

Goel et al. (1996) studied NO formation during char combustion on Newland coal particles, and they concluded that HCN is not released during char oxidation. Furthermore, they showed that cyano species are not released in significant amounts during char combustion, even in the presence of oxygen. Consequently, the nitric and nitrous oxides produced from the combustion of char nitrogen is not formed from the homogeneous oxidation reaction of HCN. The results reported are consistent with the hypothesis that oxygen is required to break the nitrogen containing aromatic rings and react with char nitrogen to form an intermediate, see Figure 2.6. The intermediate forms NO or reacts with NO to form N_2O (Goel et al. 1996).

Skaarup Jensen et al. (2000) made experiments showing that the intrinsic NO formation selectivity from char-N during pulverized coal char combustion at temperatures between 1050 and 1150 $°C$ is close to 100 % and about 65 % at 850 $°C$. Temperature is reported to only have a weak effect on the intrinsic NO formation selectivity, and no noticeable effect of O_2 concentration on NO formation selectivity

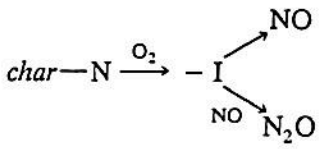

Figure 2.6: Oxygen reacts with the nitrogen atoms to form an intermediate. The intermediate splits to form NO and reacts with NO to form N_2O (Goel et al. 1996).

was found. Skaarup Jensen et al. (2000) state that since the fuel-N is mainly contained in the char, NO formation from char-N combustion is predominant for coal combustion up to 1200 $°C$. It was shown that reduction of NO by reaction with char is the main reaction accounting for net NO formation from char combustion being significantly lower than 100%. The results showed that NO/char reactions during combustion are of a dynamic nature. Hence, kinetic parameters determined at quasi-steady state conditions are not directly applicable to most combustion processes (Skaarup Jensen, Jannerup, Glarborg, Jensen & Dam-Johansen 2000).

Zevenhoven and Hupa (1998) investigated the reactivity of chars from coal, peat and wood towards NO, with and without CO. It was found that chars from lignite and peat are more reactive towards NO than chars from bituminous coals and wood, which is a trend inconsistent with char gasification. It was shown that chemical composition (12 elements) and char/NO or char/NO+CO reaction rate constants show a catalytic effect for calcium, magnesium and potassium. The effects are, however, very temperature dependent (Zevenhoven & Hupa 1998).

Homogeneous reactions

If the fuel-nitrogen is volatilized, the volatile species are fuel specific, and can be described by fuel reactivity. In the combustion environment these various nitrogenous volatiles may be either oxidized to NO or converted into N_2 by the following general reaction sequences:

$$NH_2 \longrightarrow NH \longrightarrow N \longrightarrow N_2 \tag{2.20}$$

or

$$NH_2 \longrightarrow NH \longrightarrow N \longrightarrow NO \tag{2.21}$$

Whether reaction 2.20 or 2.21 is being favored, depends on oxygen concentration (Tillmann 1991).

Tillman (1991) and Hill et al. (2000) state that formation of fuel NO is largely a function of the percentage of nitrogen in the fuel, the reactivity of the fuel, and the concentration of oxygen in the primary pyrolysis and initial combustion sections of the furnace or reactor (staged combustion).

It is reported by Miller and Bowman (1989) that measurements on laboratory-scale burners with a variety of model fuel-nitrogen compounds, such as methacrylonitrile, methylamine, pyridine and quinoline, indicate that the extent of conversion of fuel nitrogen to NO is nearly independent of the identity of the model compound, but is strongly dependent on the local combustion environment (temperature and stoichiometry) and on the initial level of nitrogen compounds in the fuel-air mixture (Miller & Bowman 1989). This supports the statement from Tillman (1991) and Hill et al. (2000) except for the temperature dependence. Miller and Bowman (1989) are supported by Hill et al. (2000) in that the gas-phase fuel-nitrogen reaction sequence is initiated by a rapid and nearly quantitative conversion of the

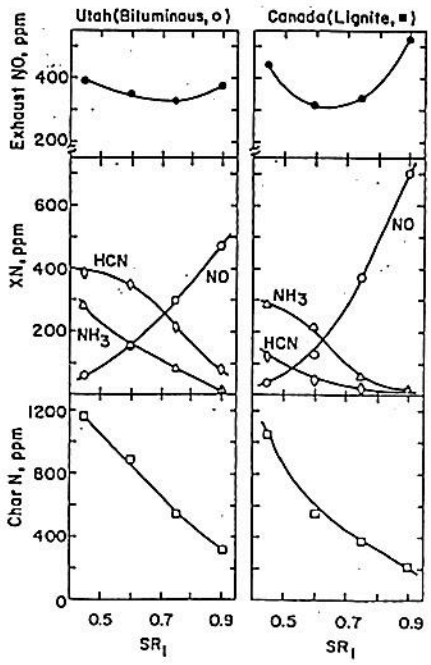

Figure 2.7: Exhaust NO, NH_3, HCN and char N as a function of stoichiometric ratio (SR) (Chen et al. 1982).

parent fuel nitrogen compounds to hydrogen cyanide (HCN) and ammonia (NH_3). Thus, hydrogen cyanide (HCN) appears to be the principal pyrolisis product when the fuel nitrogen is bound in an aromatic ring (pyridinic or pyrrolic structure), and ammonia (NH_3) when the fuel-nitrogen is in the form of amines[2]. Hence, the reaction mechanism for NO production from fuel nitrogen involves reactions important in the oxidation of HCN and NH_3. As in the the case of prompt NO, the mechanism is shown Figure in 2.2.

Chen et al. (1982) have made investigations on formation of NO, HCN, NH_3 and char nitrogen residue for a high and low rank coal, namely Utah (bituminous) and Canada (lignite), see Figure 2.7. The investigations show an essential difference in formation of NH_3 and HCN for two different rank coals.

Hämäläinen (1995) contradicts that the conversion of fuel-N to HCN and NH_3 only can be explained in terms of nitrogen functionality. If amino groups were responsible for the formation of NH_3, it would be released before HCN during pyrolysis of the fuel, since the thermal stability of amino groups is certainly lower than that of aromatic nitrogen compounds. And according to Hämäläinen (1995) experiments show that HCN is formed before NH_3. Even the different aromatic nitrogen functionalities of fuel do not appear to affect the conversion of fuel-N to NH_3(Hämäläinen 1995).

The studies made by Hämäläinen (1995), on several different fuels, showed that the oxygen containing functional groups, and particularly the OH-groups, are important in the conversion of fuel-N to HCN and NH_3. It was shown in experiments with model compounds containing phenolic OH-groups that the conversion of HCN increased, in contrast to NH_3. The concentration of OH-groups decreases with de-

[2]Amines: Organic compounds derived from ammonia by replacement of one or more of its hydrogen atoms by hydrocarbon groups (Sharp 1990).

creasing total oxygen concentration in the fuel, and it is probable that the OH/N ratio decreases proportional with the fuel O/N ratio. It was also found that the conversion of fuel-N to NO_x was dependent on the fuel O/N ratio, even at low temperatures (1073 K). It was shown that HCN/NH_3 ratio in pyrolysis gases decreases with the fuel O/N ratio. Correspondingly the N_2O emissions increase with increasing fuel O/N (Hämäläinen 1995).

Zevenhoven et al. (2000) investigated the behavior of nitrogen from polymers and plastics in waste-derived fuels during combustion. An almost reverse trend between fuel-N content and fuel-N to NO conversion. The following fuels with an increasing nitrogen content were considered: wood, RDF, coal, sewage sludge, PA6/PE, PU foam, PA6 and urea formaldehyde glue (Zevenhoven, Axelsen, Kilpinen, Hupa, Elomaa & Liukkonen 2000). Combining the theory of Hämäläinen (1995) and the work of Zevenhoven et al. (2000) shows an O/N ratio ranging from 225.4 to 0.6. The fuels with a low O/N ratio is followed by low fuel-N to NO conversion. The experiments by Zevenhoven et al. (2000) supports Hämäläinen (1995) in that the conversion of fuel-N to NO_x is dependent on the fuel O/N ratio.

Desroches-Ducarne et al. (1998) investigated co-combustion of coal and municipal solid waste in a circulating fluidized bed. It was observed, when coal was added to MSW, that the combustion rate decreased and char concentration in the whole combustion chamber increased. When the fraction of coal exceeded 30 wt-% the CO concentration increased. Furthermore, it was observed that an increasing part of the NO_x was reduced when coal was added. It was stated that the NO reduction was favoured by the reduction reactions by char or CO. Desroches-Ducarne et al. (1998) supports Hämäläinen (1995) in experiments of HCN/NH_3 ratios, showing a ratio of 1 - 2 and 0.7 for coal and MSW, respectively. Furthermore, it showed a volatile nitrogen release of 10 - 30 % and 67 % for coal and MSW, respectively.

2.1.4 The N_2O mechanism

The N_2O-intermediate mechanism plays an important role during natural gas combustion in the production of NO in very lean ($\lambda > 1.25$), low-temperature combustion processes, see Equation 2.22 (Turns 1996), (Bowman 1992).

$$O + N_2 + M \rightarrow N_2O + M \tag{2.22}$$

The principal homogeneous reactions forming N_2O in fossil fuel combustion can be seen from Equation 2.23 and 2.37 (Bowman 1992).

$$NCO + NO \rightarrow N_2O + CO \tag{2.23}$$

The primary removal steps can be seen from Equation 2.24 and 2.38 (Bowman 1992).

$$O + N_2O \rightarrow N_2 + O_2 \rightarrow NO + NO \tag{2.24}$$

Bowman (1992) reports that the calculated lifetime of N_2O in combustion products, at temperatures above 1500 K, is typically less than 10 *ms*. This indicates that N_2O emissions should not be significant, except in low-temperature combustion systems like fluidized bed combustors, and possibly in some post-combustion NO removal systems, the latter applying to cement kiln precalciners.

2.1.5 The importance of NH_3 and HCN

It appears adequate to take a closer look at the role of NH_3 and HCN, which have been referred to as important species in prompt NO formation and fuel nitrogen

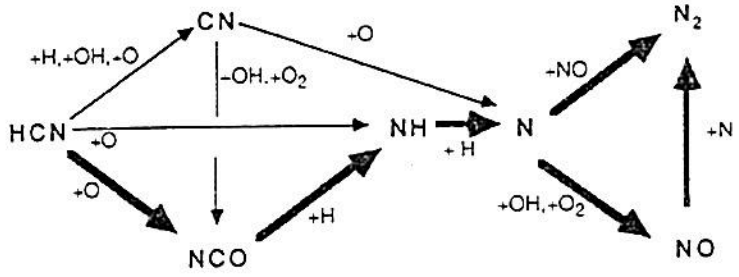

Figure 2.8: Reaction path diagram illustrating the reaction mechanism by which HCN is converted to NO and N_2 in low-pressure flames. The bold lines indicate the most important reaction paths (Miller & Bowman 1989).

conversion (see Subsections 2.1.2 and 2.1.3). Figure 2.7 shows formation of NO, HCN, NH_3 and char nitrogen residue for a high and low rank coal, namely Utah (bituminous) and Canada (lignite).

HCN

Miller and Bowman (1989) state in their analysis of the computed results that the reaction sequence indicated by the bold arrows in Figure 2.8 is the dominant mechanism for converting HCN to NO and N_2 in $H_2/O_2/Ar$ flames. The HCN removal is controlled by the reaction of HCN with oxygen atoms, even in rich flames, see Equation 2.25 and 2.26.

$$HCN + O \rightleftarrows NCO + H \tag{2.25}$$

$$HCN + O \rightleftarrows NH + CO \tag{2.26}$$

Miller and Bowman (1989) also investigated the removal of HCN by reaction with OH. Two routes were suggested. The first channel is first order, shown in Equation 2.27. The second channel is second order, shown in Equation 2.28 and 2.29.

$$OH + HCN \rightleftarrows HOCN + H \tag{2.27}$$

$$OH + HCN \rightleftarrows CN + H_2O \tag{2.28}$$

$$CN + OH \rightleftarrows NCO + H \tag{2.29}$$

Miller and Bowman (1989) found that the $OH + HCN$ reactions normally come into play only under conditions that are in a rich, nearly equilibrated state and that the $O + HCN$ sequence in Figure 2.8 almost always plays a major role.

Sensitivity analysis shows that the homogeneous NO removal occurs primarily by the $NO \longrightarrow HCN \longrightarrow N_2$ mechanism, with only a small contribution from the $NO \longrightarrow HNO \longrightarrow N_2$ (Miller & Bowman 1989). Figure 2.9 illustrates the reaction path diagram in the NO-added flames of Thorne et al. (1986). The bold lines indicate the most important reaction paths.

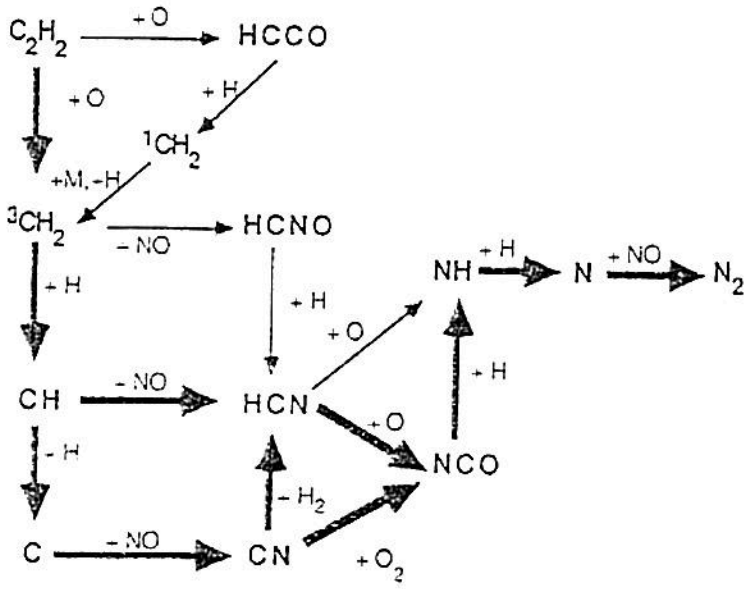

Figure 2.9: Reaction path diagram illustrating the $NO \rightarrow HCN \rightarrow N_2$ conversion mechanism in the NO-added flames of Thorne et al. The bold lines indicate the most important reaction paths (Thorne et al. 1986).

NH_3

This discussion of the mechanism of ammonia conversion to NO will be restricted to NH_3/O_2 flames, as reviewed by Miller and Bowman (1989). The important features of the ammonia oxidation mechanism can be summarized in Figure 2.10. The primary oxidation reaction can be seen from Equation 2.30. In lean conditions, reactions with oxygen atoms make significant contribution, see Equation 2.31, whereas in rich conditions, reactions with hydrogen make a significant contribution, see Equation 2.32.

$$NH_3 + OH \rightleftarrows NH_2 + H_2O \tag{2.30}$$

$$NH_3 + O \rightleftarrows NH_2 + OH \tag{2.31}$$

$$NH_3 + H \rightleftarrows NH_2 + H_2 \tag{2.32}$$

The chemical identity of the NH_i (i=1, 2) free radical is primarily responsible for determining the NO/N_2 product distribution and is dependent on the excess air ratio. For *lean flames*, the critical amine free radical is NH_2, but with a *lower excess* air ratio the grater abundance of hydrogen atoms results in a shift from NH_2 to NH and N.

The formation of N_2 from NO by reaction with NH_2 occurs either directly by Equation 2.33 or through the NNH intermediate Equation 2.34 through 2.36.

$$NH_2 + NO \rightleftarrows N_2 + H_2O \tag{2.33}$$

$$NH_2 + NO \rightleftarrows NNH + OH \tag{2.34}$$

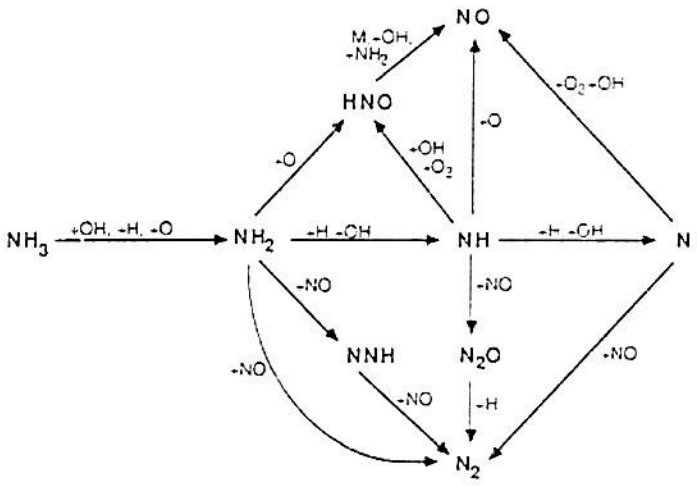

Figure 2.10: Reaction path diagram for the oxidation of ammonia in flames (Miller & Bowman 1989).

$$NNH \rightleftarrows N_2 + H \tag{2.35}$$

$$NNH + NO \rightleftarrows N_2 + HNO \tag{2.36}$$

The reaction of NH with NO produces N_2O, which is converted to N_2 principally by reactions with hydrogen atoms, see Equation 2.37 and 2.38.

$$NH + NO \rightleftarrows N_2O + H \tag{2.37}$$

$$N_2O + H \rightleftarrows N_2 + OH \tag{2.38}$$

The NO is removed primarily with nitrogen atoms by Equation 2.39, with only secondary contributions from Equation 2.33 through 2.36 and Equation 2.37 and 2.38 (Miller & Bowman 1989).

$$N + NO \rightleftarrows N_2 + O \tag{2.39}$$

Applying the works of Hämäläinen (1995) and the theory of Miller and Bowman (1989) in characterizing and verifying alternative fuels for NO_x reduction in a precalciner kiln in combination with characteristics made by Zevenhoven et al. (2000), will be of interest.

2.1.6 Reburning

Reburning or fuel staging involves the addition of a second fuel stream after the primary fuel burnout is completed, with the aim to reduce the NO_x already formed during combustion. Secondary fuel is added after the primary fuel burnout to create a moderately fuel-rich zone, see Figure 2.11 and Figure 2.12. Within this zone, radicals generated by the secondary fuel decomposition attack NO to produce N_2, HCN and NH_3. Under fuel-rich conditions, the formation of HCN depends strongly on the concentration of hydrocarbon species, see Equation 2.40. The HCN then decays through Equation 2.41, and ultimately reaches N_2 via the reverse Zeldovich

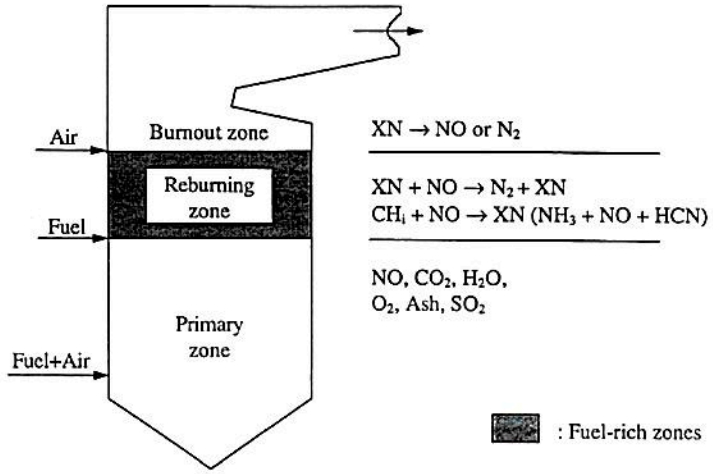

Figure 2.11: Schematic of reburning in a boiler (McCarthy et al. 1988).

reaction in Equation 2.44 (Smoot, Hill & Xu 1998), (Kramlich & Linak 1994), (Tokheim & Bjerketvedt 1998*b*), (Bjerketvedt & Høidalen 1994).

$$CH_i + NO \longrightarrow HCN + ... \tag{2.40}$$

$$HCN + O \longrightarrow NCO + H \tag{2.41}$$

$$NCO + H \longrightarrow NH + CO \tag{2.42}$$

$$NH + H \longrightarrow N + H_2 \tag{2.43}$$

$$N + NO \longrightarrow N_2 + O \tag{2.44}$$

Overfire air oxidizes combustibles formed in the reburning zone to CO_2 and H_2O, as well as the N-H and C-N species to NO, see Figure 2.11 and Figure 2.12. The reburning mechanism is also included in Figure 2.2.

In fuel-lean conditions, hydrocarbons react with oxygen and/or hydroxyl radicals through Equation 2.45 to form CO. Therefore, reactants in Equation 2.40 and 2.45 consume CH_i competitively. A goal in reburning optimization is to maximize the exposure of NO to CH_i and minimize CH_i interaction with oxygen (Smoot et al. 1998). This is to be kept in mind when discussing the CO level during utilization of alternative fuels for reburning purposes in the precalciner of cement kiln 6 at Brevik.

$$CH_i + O \longrightarrow CO + H + ... \tag{2.45}$$

The impact of particle size distribution on NO_x reduction with reburning has been studied by Smoot et al. (1998). The investigations showed that particles with a broad distribution in particle size gave the lowest level of NO. Mixing and segregation become important when particles of different sizes are located at different positions. Predicted NO levels were far more sensitive to the presence of small particles than to changes in mean particle diameter, even though only very small mass

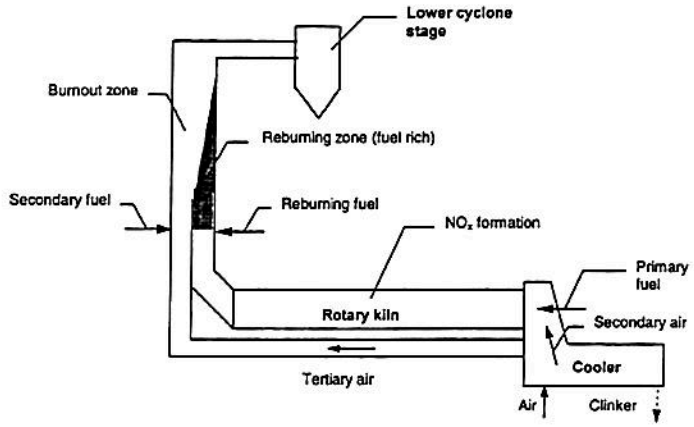

Figure 2.12: Illustration showing the principle of staged combustion in a precalciner cement kiln (Tokheim 1999).

percentages of very small particles were present (Smoot et al. 1998). Gajewski and Hoenig (1999) and Smoot et al. (1998) state that low NO levels can be reached with a finer grinding, but state that it depends on the burner type if the fuel (e.g. coal) is burnt in an internally staged flame with a well defined internal recirculation zone (Gajewski & Hoenig 1999).

Smoot et al. (1998) made studies on changes in the velocity used for injection of the reburning fuel (CH_4) on the predicted NO concentrations. The investigation showed that an increase of velocity also increased the NO reduction from reburning. This was probably because the CH_4 was able to penetrate further into the reactor before it was consumed, which resulted in a larger effective reburning region.

The optimum stoichiometric ratio in the reburning zone is given by the balance between the reduction in primary NO_x and formation of HCN from fuel-N and prompt NO. For hydrocarbon fuels the optimum stoichiometric ratio is about 0.9, see Figure 2.13. For more fuel rich conditions (i.e. stoichiometric ratio lower than 0.9) the additional fuel-N and possible prompt NO will decrease the overall NO_x reduction.

Chen et al. (1996) found a global rate expression for the reburning reaction, $\sum_{ij} C_i H_j + NO \longrightarrow HCN + ...$, for use in turbulent diffusion flames. The rate constant (k) recommended for a global NO_x kinetic model is shown in Equation 2.46 (Chen, Smoot, Hill & Fletcher 1996), (Chen, Smoot, Fletcher & Boardman 1996).

$$k = [(2.7 \pm 0.15) \cdot 10^6] \exp[(-18800 \pm 500)/RT)] \tag{2.46}$$

The rate coefficient in Equation 2.46 has units of mole·cm^{-3}·s^{-1}.

Kristensen et al. (1996) investigated the chemistry of nitrogen species in the burnout zone during reburning. It was found that the minimum in NO is related to the amount of CO, the oxidation of NH_3 or HCN, and the reduction of NO by NH_3 or HCN. The optimum temperature is strongly dependent on the amount of combustibles (CO) present. The NO reduction is accompanied by a high level of N_2O production, and the concentration of N_2O goes through a maximum as the temperature is increased. At temperatures above 1300 K, N_2O decomposes rapidly (Kristensen, Glarborg & Dam-Johansen 1996).

Lyngfelt et al. (1998) state that reversed air staging (delayed air staging), in a CFBC reactor, reduces N_2O, CO and SO_2 emissions during optimal control of the

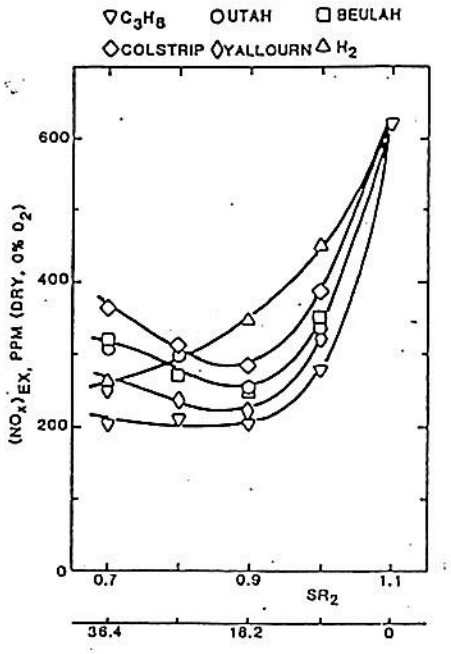

Figure 2.13: NO_x emissions as a function of stoichiometric ratio (SR) in the reburning zone (McCarthy et al. 1988).

combustor excess air ratio, increased bed temperature (from 850 to 870 $°C$) and increased limestone addition (Lyngfelt, Åmand & Leckner 1998).

2.1.7 Advanced reburning

A promising concept for NO_x reduction is advanced reburning (AR), by which up to 85 - 95 % reduction has been reported (Xu, Smoot & Hill 1999). Advanced reburning combines reburning with (concepts from) selective non-catalytic reduction (SNCR)[3], through the joint use of hydrocarbons and ammonia or urea. The nitrogen-containing NO reduction agent can be injected with or without promoters at one or two locations into the reburning zone, along with overfire air or downstream in the burnout zone.

In advanced reburning, the reburning zone is adjusted from the normal fuel-rich conditions to near-stoichiometric conditions. This results in high CO concentrations that improve the nitrogen-containing NO reduction agents effectiveness for removing NO by widening the temperature window. The combination of reburning and advanced reburning makes the NO reduction mechanisms more complex. The main reactions of advanced reburning can be described by Equation 2.47 and 2.48 (Xu et al. 1999).

$$NH_3 + OH, O, H \longrightarrow NH_2 + ... \tag{2.47}$$

$$NH_2 + NO \longrightarrow N_2 + H_2O \tag{2.48}$$

[3]In 1975 Lyon's patent defined the conditions for selective non-catalytic NO reduction to N_2 by ammonia at excess air conditions and temperatures between 850 to 1100 $°C$. Patent No. 3,900,554.

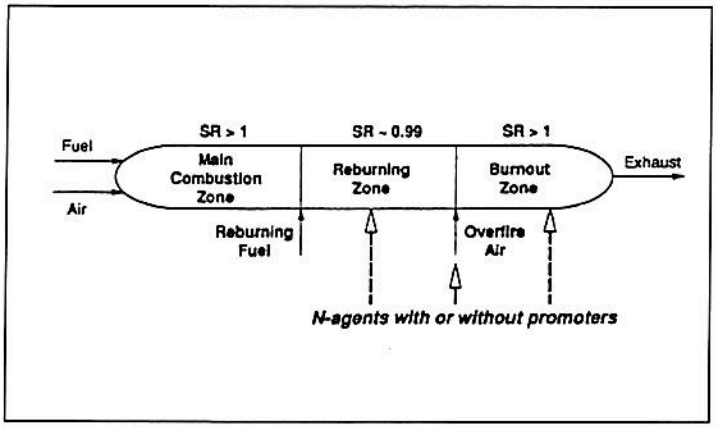

Figure 2.14: Schematic of different advanced reburning variants (Zamansky et al. 1997).

A comprehensive scheme of reactions does not yet quantitatively describe the experimental results due to insufficient understanding of the reactions according to Zamansky et al. (1996) cited in Xu et al. (1999).

There are six advanced reburning variants, and Figure 2.14 shows the general schematic (Zamansky et al. 1997):

- Advanced reburning lean: Injection of the nitrogen-containing NO reduction agent along with overfire air.
- Advanced reburning rich: Injection of the nitrogen-containing NO reduction agent and promoter (e.g. sodium carbonate) into the reburning zone.
- Multiple injection advanced reburning: Injection of nitrogen-containing NO reduction agent and promoters both into the reburning zone and with overfire air.
- Advanced reburning lean + SNCR: Injection of nitrogen-containing NO reduction agent and promoters with overfire air at about 1590 K and into the SNCR zone between 1230 to 1400 K.
- Advanced reburning rich + SNCR: Injection of nitrogen-containing NO reduction agent and promoters into the reburning zone and into the SNCR zone.
- Reburning + SNCR: Basic reburning followed by the promoted SNCR process.

Further in this report, only advanced reburning rich without a promoter will be considered since the most optimal feeding point of a nitrogen-containing NO reduction agent in the precalciner kiln 6 at Norcem Brevik is along with the reburning fuel. This is because this feeding point:

- gives no process intrusion and disturbance,
- requires practically no investments during experiments and
- quickly answers whether the technology can be applied in a precalciner.

Urea is used as the nitrogen-containing NO reduction agent in the advanced reburning (rich) experiments in the precalciner kiln 6 at Norcem Brevik, since:

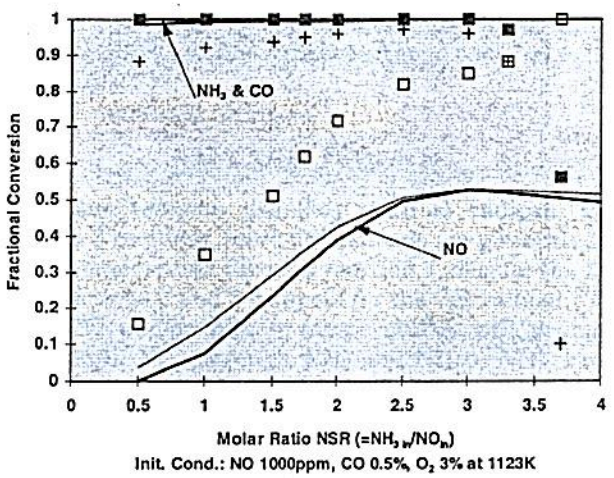

Figure 2.15: Effects of NSR (NH_3/NO_{in}) on NH_3, NO and CO at 1123 K. The main component is N_2. The solid lines are models, (-) seven-step model, (-) GRI-B96; +, CO measured; □, NO measured; ■, NH_3 measured (Xu et al. 1998).

- urea is a commercial goods and easy to handle in 40 kg bags,
- urea is easy to feed in a screw conveyor,
- urea is not hazardous during transport and feeding into the precalciner as long as it is handled according to the material safety data sheet supplied by the manufacturer.

The chemical reaction for urea decomposition is given in Equation 2.49.

$$H_2NCONH_2 \rightarrow HNCO + NH_3 \tag{2.49}$$

Chen et al. (1988) investigated NO_x reduction using -NH and -CN compounds in conjunction with staged air addition. The investigations indicated optimum conditions for NO reduction with:

- reaction temperatures at 800 $°C$,
- stoichiometric ratio at the injection location: SR = 0.99,
- minimal air addition to give slightly fuel lean conditions: SR = 1.02.

Using kinetic modeling it was suggested that the critical factor is an external source of OH radicals to initiate the decomposition of the agent. An excess of radicals can reduce the NO reduction efficiency by promoting the oxidation of the key intermediate, NH_2. For low CO concentrations the excess radicals are consumed by Equation 2.30 and 2.50, and NH_2 reacts according to Equation 2.48.

$$HNCO + H \rightleftarrows NH_2 + CO \tag{2.50}$$

The strong rich zone stoichiometry dependence is exerted mainly through the amount of CO entering the lean zone. Insufficient CO will limit the extent of the initial NH_3 or HNCO reaction (Chen, Cole, Heap & Kramlich 1988).

Xu et al. (1998) contributed with a reduced kinetic model for NO_x reduction by advanced reburning. A maximum was found in NO reduction that depended on the

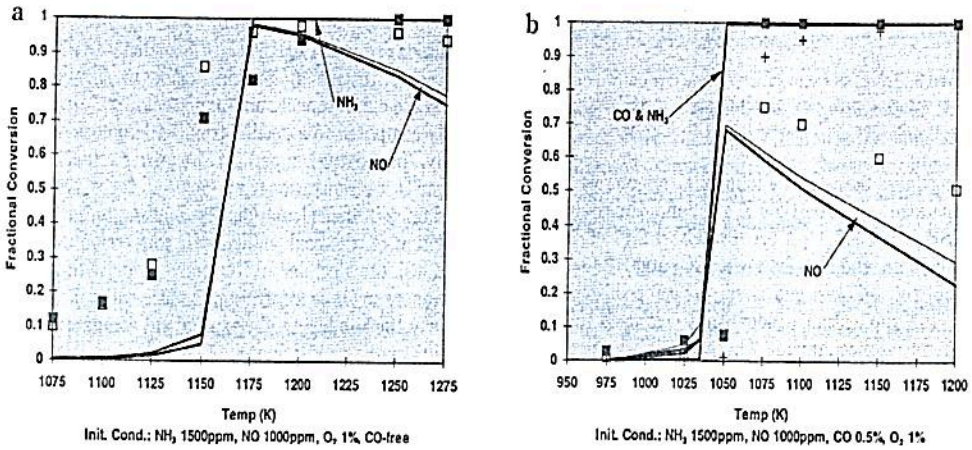

Figure 2.16: Effects of temperature on NH_3 and NO in a (a) CO-free system and (b) CO-containing system. The main component is N_2. The solid lines are models; +, CO measured; □, NO measured; ■, NH_3 measured (Xu et al. 1998).

concentrations of NO_{in}, CO, O_2, the ratio NH_3/NO_{in} (i.e. NSR) and temperature, see Figure 2.15 and Figure 2.16. In a mechanistic consideration, it is stated that the production of OH radicals is sufficient, even when Equation 2.47 and 2.55 compete for the OH radical. This is because Equation 2.55 produces more H radicals than Equation 2.56 requires, and more OH radicals are generated at lower temperatures through Equation 2.54 (Xu et al. 1998).

Chen et al. (1989) support Xu et al. (1998) in that particularly oxidation of CO could generate a significant amount of radicals via chain branching, which play an important role in the conversion of NO, HCN and NH_3 species to N_2 or NO during burnout (Chen, Kramlich, Seeker & Pershing 1989).

Brouwer et al. (1996) and Chen et al. (1989) support Xu et al. (1998) in that an increased level of CO lowers the temperature for optimal conversion of NO (Brouwer, Heap, Pershing & Smith 1996).

Alternative fuel reburning

Zamansky et al. (1997) made experiments with advanced reburning rich and found that the performance depends on the overfire air injection temperature. A lower overfire air injection temperature provides better NO reduction. 78 - 88 % NO control with overfire air at 1166 K and 70 - 77 % NO control with overfire air at 1300 K were reported, see Figure 2.17 and Figure 2.18. By-products during the experiments were reported to be about 30 % increase in CO emissions and HCN emissions up to 1.1 ppm @ O% O_2.

Maly et al. (1999) studied different alternative reburning fuels like: biomass, carbonized refuse derived fuel (CRDF), coal pound fines, Orimulsion, bituminous coal and low rank coal. An increasing NO_x reduction with initial NO_x concentration was reported, see Figure 2.19. Maly et al. (1999) support Zamansky et al. (1997) in that an increasing urea injection temperature gives a decreasing NO_x reduction, see Figure 2.20 (Maly et al. 1999). It was found that biomass gave a higher NO_x reduction than the other fuels tested.

Kicherer et al. (1994) investigated the reburning effect of the following fuels: coal, natural gas, straw and light fuel oil. It was concluded that homogeneous reduction mechanisms are more effective than the heterogeneous mechanisms. The

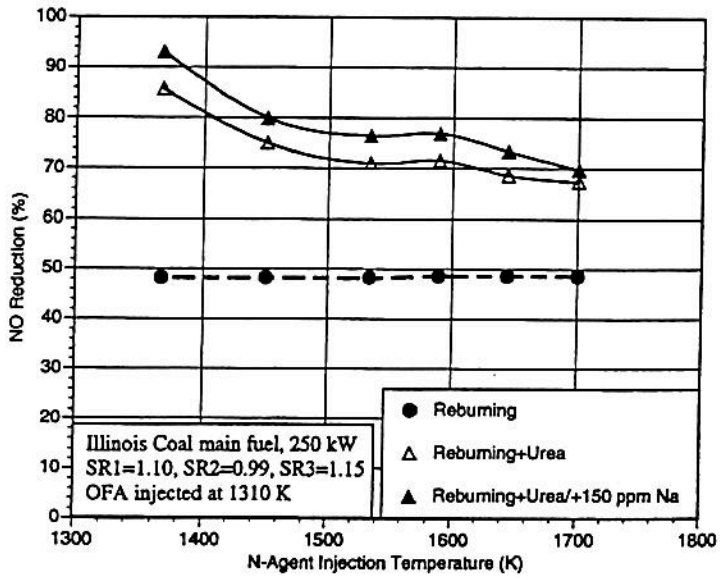

Figure 2.17: NO reduction by AR-rich with overfire air at 1166 K (Zamansky et al. 1997).

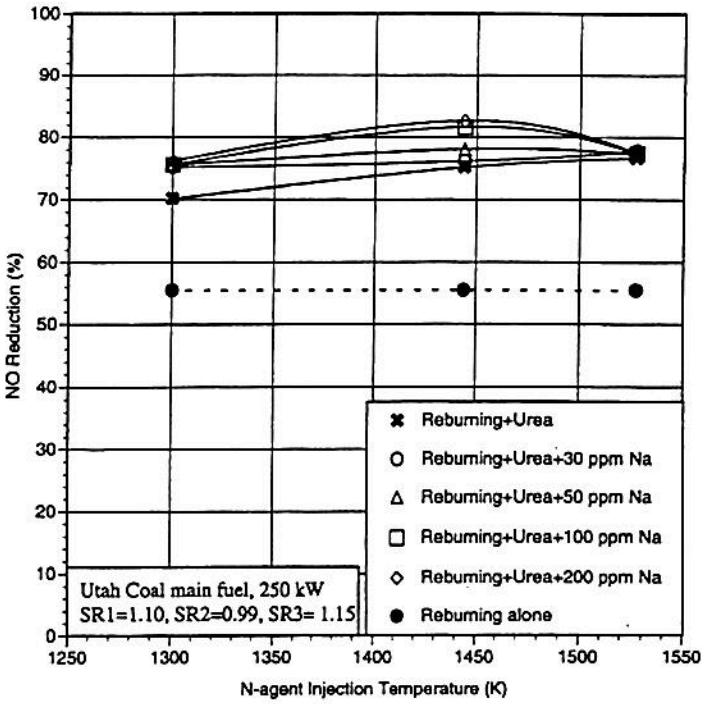

Figure 2.18: NO reduction by AR-rich with overfire air at 1300 K (Zamansky et al. 1997).

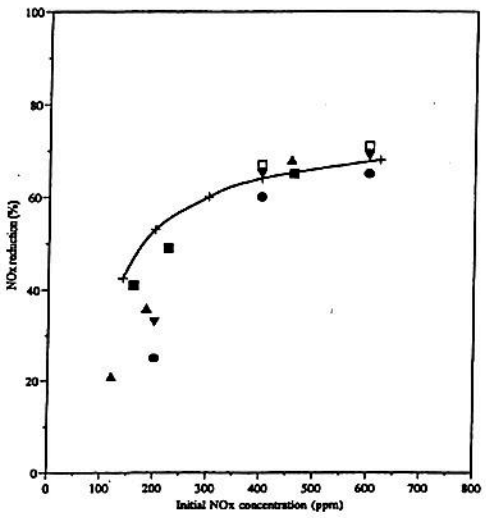

Figure 2.19: Effects of initial NO_x concentration on NO_x reduction for different reburning fuels. The main fuel is natural gas. Reburn heat input is 19%. Reburn zone residence time is 0.5 s. Reburning fuels: □, biomass; ■,Orimulsion; ▲, CRDF (carbonized refuse derived fuel); ▼, low rank coal; •, bituminous coal; +, natural gas (Maly et al. 1999).

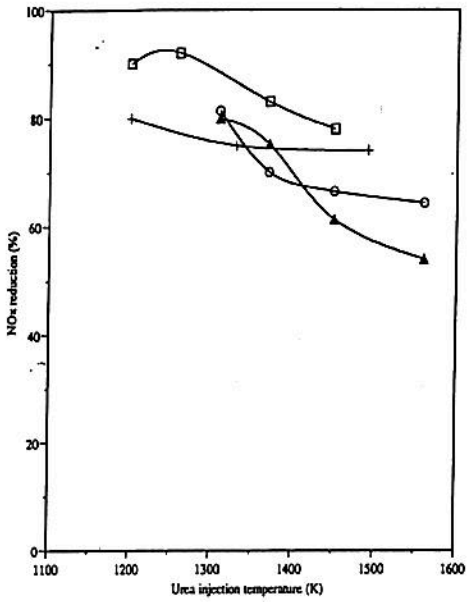

Figure 2.20: Effect of urea injection temperature on NO_x reduction for biomass and natural gas advanced reburning. The main fuel is natural gas. Initial NO_x concentration is 600 ppm. Reburn zone residence time is 0.6 s. Reburn heat input is 10%. Reburning fuels: □, biomass; ▲, CRDF (carbonized refuse derived fuel); ○, coal pond fines; +, natural gas (Maly et al. 1999).

best results, in regard of sufficient burnout as well as high NO_x reduction level, can be achieved under the following conditions (Kicherer, Spliethof, Maier & Hein 1994):

- high volatile matter of reburning fuel,
- maximum possible residence time to compensate for insufficient mixing,
- very fine grinding if solid reburning fuels and
- optimized mixing conditions.

Nitrous oxides emissions

The nitrous oxide (N_2O) emissions during NO_x control procedures have been reported to increase from 1 ppm in a gas-fired primary stage to 13 ppm with the use of coal reburning. In contrast, a 50 % reduction of the nitrous oxide emissions over a coal-fired primary stage with the use of gas as a reburning fuel has been reported (Kramlich & Linak 1994), (Rutar, Kramlich, Malte & Glarborg 1996).

Both modeling and experimental studies indicate that formation of N_2O in the SNCR technique is a minor product. The key difference between urea and ammonia is that urea can generate HNCO, NCO and N_2O as major products of reaction, ammonia does not. In comparison, thermal $DeNO_x$ control with urea or cyanuric acid injection gives about 10 - 15 % of NO_x reduction converted to N_2O. Comparison of urea and cyanuric acid as agents shows that urea generates less N_2O under equivalent conditions. This is expected since only half of the nitrogen contained in the urea becomes associated with HNCO after injection. The other half forms NH_3 which does not yield significant N_2O. In the case of cyanuric acid injection, all of the nitrogen initially becomes HNCO, and thus final N_2O yields are increased (Kramlich & Linak 1994). Experiments with CO showed an increase in the N_2O formation with increasing CO. A shift in NO_x to lower temperature with increasing CO was seen, but not any dramatically change.

Several studies have suggested that N_2O may be catalytically destroyed over calcium compounds. Also, certain alkaline materials appear to be capable of catalytically forming N_2O from NH_3. The alkaline surface that is actually exposed for reaction in the bed may be either CaO or $CaSO_4$. The high catalytic activity of CaO surfaces towards N_2O decomposition is well-documented (Kramlich & Linak 1994). Hansen et al.(1992) found that limestone with a high activation towards N_2O destruction is also the most reactive towards SO_2 (Hansen, Dam-Johansen, Johnsson & Hulgaard 1992).

Rutar et al. (1996) studied nitrous oxide emission control by reburning and found that free-radical destruction is predominant over thermal decomposition. Modeling strongly suggested that Equation 2.51 is responsible for the destruction of N_2O; the rate constant in Equation 2.52 having units of mole·cm^{-3}·s^{-1} (Rutar et al. 1996). The modeling by Rutar et al. (1996) showed that reburning effectiveness is governed by:

- the propensity of the fuel to generate H-atoms during oxidation and
- the reaction temperature, which acts primarily through the activation energy of the $N_2O + H$ reaction.

$$N_2O + OH \longrightarrow N_2 + HO_2 \tag{2.51}$$

$$k = 7.6 \cdot 10^{13} \exp(-15,200/RT) \tag{2.52}$$

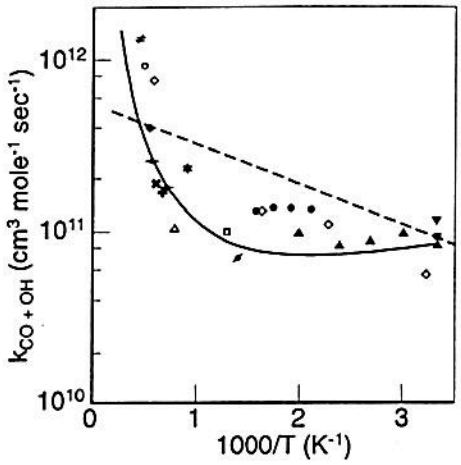

Figure 2.21: Reaction rate constant of the CO + OH reaction as a function of reciprocal temperature based on transition state (—) and Arrhenius (- -) theories compared with experimental data (Glassman 1996).

Hulgaard and Dam-Johansen (1992) state that nitrous oxide emissions usually are low (0-5 ppm) and that emission measurements are disturbed by interferences from CH_4, H_2O, SO_2 and to a minor extent from NH_3 (Hulgaard & Dam-Johansen 1992). Therefore, it is of importance to evaluate the N_2O emissions with caution.

2.2 CO formation and oxidation

The carbon monoxide oxidation mechanism with hydrogen-containing compounds present is referred to as "wet" CO oxidation, and it will apply to most practical combustion systems. The H_2O-catalyzed reaction essentially proceeds according to Equation 2.53, 2.54, 2.55 and 2.56 (Glassman 1996), (Bartok & Sarofim 1991).

$$CO_2 + O_2 \longrightarrow CO_2 + 2O \tag{2.53}$$

$$O + H_2O \longrightarrow OH + OH \tag{2.54}$$

$$CO + OH \longrightarrow CO_2 + H \tag{2.55}$$

$$H + O_2 \longrightarrow OH + O \tag{2.56}$$

Equation 2.55 is the principal CO oxidation reaction found in most combustion systems. At temperatures above 1500 K, the rate coefficient for Equation 2.55 is very temperature dependent, see Figure 2.21. It can be seen from Figure 2.21 that at temperatures below 800 - 1000 K, the rate coefficient is nearly independent of temperature. Hence quenching of CO at lower temperatures principally occurs by depletion of radical species, such as OH, by recombination reactions.

At high pressures (> 10 atm) and/or low temperatures (1000 - 1500 K) or in early stages of hydrocarbon oxidation, high concentrations of HO_2 can make reaction 2.57 competitive with reaction 2.55. Nevertheless, any complete mechanism for wet CO oxidation must contain all H_2-O_2 reaction steps including Equation 2.57 (Glassman 1996), (Bartok & Sarofim 1991).

$$CO + HO_2 \longrightarrow CO_2 + OH \tag{2.57}$$

Since combustion of alternative fuels in the precalciner typically occurs at temperatures of 1100 - 1200 K, it is useful to review the main oxidation mechanism for the $CO/H_2O/O_2$ reaction. In the present reaction system, where water is the source of hydrogen, reaction 2.55 is also the main producer of H-atoms. The hydrogen atoms are important because they initiate the main chain branching reaction 2.56. In previous experiments carried out at 1000 K, it has been found that the rate of the recombination reaction 2.58 is comparable in magnitude to that of reaction 2.56. Thus the competition of reaction 2.58 with reaction 2.56 serves to strongly moderate the chain branching (Roesler, Yetter & Dryer 1992). Furthermore, it is stated that the O-atom formed by reaction 2.56 reacts with H_2 and H_2O through the two chain branching steps 2.60 and 2.54, or with HO_2 through reaction 2.61. The HO_2 produced in reaction 2.58 primarily reacts with an H-atom through the chain propagating reaction 2.59 to produce more OH. It can be seen that reactions 2.56, 2.60 and 2.54 are more effective at producing OH radicals than reactions 2.58, 2.59 and 2.61. The rate of CO oxidation is strongly dependent on the production of OH radicals and consequently, on a number of reactions which determine the fate of the H, O and HO_2 radicals (Roesler et al. 1992).

$$H + O_2 + M \longrightarrow HO_2 + M \tag{2.58}$$

$$HO_2 + H \longrightarrow OH + OH \tag{2.59}$$

$$O + H_2 \longrightarrow OH + H \tag{2.60}$$

$$O + HO_2 \longrightarrow OH + O_2 \tag{2.61}$$

Roesler et al. (1992) further state that HO_2 chemistry is responsible for the increased inhibition of CO by addition of O_2. The addition of O_2 accelerates the competing reactions 2.56 and 2.58. The concentration of H-atoms in the system is therefore reduced. With less H-atoms in the system, the HO_2 is no longer consumed by the chain propagating reaction 2.59, but by the chain terminating reactions 2.62 and 2.63. The increase in chain termination at 1000 K is large enough to cause inhibition by the addition of oxygen. Additionally, presence of HCl will with increased HO_2 concentrations further enhance inhibition by promoting the chain terminating reaction 2.78 (Roesler et al. 1992).

$$O + HO_2 \longrightarrow OH + O_2 \tag{2.62}$$

$$OH + HO_2 \longrightarrow H_2O + O_2 \tag{2.63}$$

The CO formation reaction tends to be rapid in devices operating with excess air, and the CO oxidation rates in the product gases determine the CO levels in the exhaust gas. In this case CO quenching occurs by lowering the oxidation rate due to cooling and by reduction in radical concentration by gas-phase or wall recombination reactions (depletion of radicals), see Equation 2.64, 2.65 and 2.66 (Bartok & Sarofim 1991).

$$H + H \longrightarrow H_2 \tag{2.64}$$

$$H + OH \longrightarrow H_2O \tag{2.65}$$

$$H + O_2 \longrightarrow HO_2 \tag{2.66}$$

It has also been observed that HCl influences NO, CO, H_2O and O_2 reactions.

2.2.1 The impact of HCl on CO burnout

Desroches-Ducarne et al. (1998) observed that HCl perturbs the $CO/H_2O/O_2$ reaction system and provokes inhibition of the CO oxidation. Desroches-Ducarne et al. (1998) derived an expression for the CO oxidation rate (r_{CO}, with units of $mol/m^3 \cdot s$) in the presence of HCl, see Equation 2.67. The reactions controlling the inhibition from HCl are identified in Equation 2.68 through 2.71. Equation 2.69, 2.70 and 2.71 consume H, OH and HO_2 radicals which are necessary reactants in the CO oxidation reaction (Desroches-Ducarne, Dolignier, Marty, Martin & Delfosse 1998), (Gokulakrishnan & Lawrence 1999), (Roesler et al. 1992), (Roesler et al. 1995). The relative importance of the different pathways were found to vary with temperature (up to 1100 K) and Cl/H ratio (up to 0.017). In particular the reactions involving HO_2 became rapidly less important at higher temperatures. The addition of O_2 to the reaction system was found to strongly reduce the CO oxidation rate in the presence of HCl. And it has been shown that this effect occurs even in the absence of HCl at 1000 K, due to the importance of the HO_2 chemistry (Roesler et al. 1992).

$$r_{CO} = \frac{3.25 \cdot 10^7 \exp(-16098/T)[CO][O_2]^{0.5}[H_2O]^{0.5}}{2.9 \cdot 10^{11} \exp(-22709/T)[HCl] + 11.2} \tag{2.67}$$

$$HCl + O \longrightarrow OH + Cl \tag{2.68}$$

$$HO_2 + Cl \longrightarrow HCl + O_2 \tag{2.69}$$

$$HCl + OH \longrightarrow H_2O + Cl \tag{2.70}$$

$$H + Cl + M \longrightarrow HCl + M \tag{2.71}$$

Roesler et al. (1995) found that the coupling effect between NO and HCl generates considerable synergistic inhibition of the CO oxidation rate. Each component individually inhibits the oxidation of CO, however, considerably more inhibition occurs when both species are present. The main source of inhibition from the NO/HCl coupling originates from the chain terminating cycle in reaction 2.72 and 2.73,

$$NO + Cl + M \longrightarrow NOCl + M \tag{2.72}$$

$$NOCl + \{H, Cl\} \longrightarrow NO + \{HCl, Cl_2\} \tag{2.73}$$

where the overall effect is reaction 2.74.

$$Cl + H, Cl \longrightarrow \{HCl, Cl_2\} \tag{2.74}$$

Under incinerator postflame conditions, this cycle generates a 50 % decrease in the CO oxidation rate, with 250 ppm of NO present in the system, see Figure 2.22.

The cycle in reaction 2.75 and 2.76,

$$NO + HO_2 \longrightarrow NO_2 + OH \tag{2.75}$$

$$NO_2 + \{H, O\} \longrightarrow \{OH, O_2\} + NO \tag{2.76}$$

where the overall effect is reaction 2.77, is the key element in interpreting the different behavior of the fuel-lean and the stoichiometric mixtures to NO addition. At stoichiometric conditions, the cycle competes with reaction 2.59 for HO_2, where

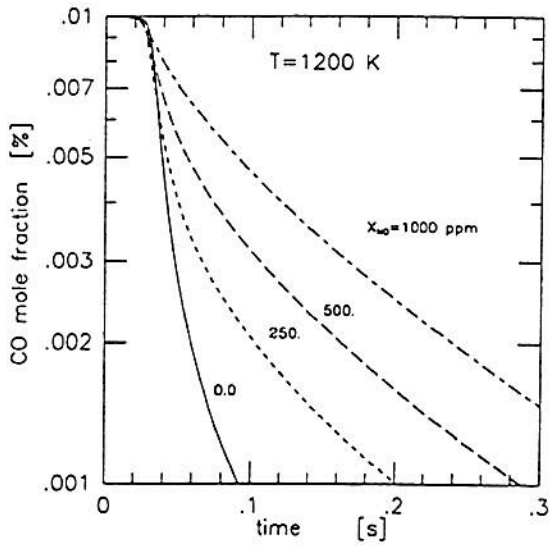

Figure 2.22: Numerical modeling of the effect of NO on CO burnout in the postflame region of incinerators when HCl is present. The calculations correspond to an isothermal reaction system with initially 1 % mole fraction CO, 5 %O_2, 15 % H_2O, 5 % HCl, 9 % CO_2, and a balance of N_2 at 1 atm and 1200 K, corresponding to reaction products from a mixture with equal molar contents of CH_4 an CH_3Cl and with excess air (Roesler et al. 1995).

both channels result in chain propagation. However, for fuel-lean conditions the cycle competes with the chain terminating reactions 2.61 and 2.63.

$$HO_2 + \{H, O\} \longrightarrow OH + \{OH, O_2\} \tag{2.77}$$

Experiments with NO and HCl for a fuel-lean mixture at 1000 K shows a slower oxidation of CO than in the stoichiometric case. This is due to the HO_2 chemistry under these conditions. In contrast, when adding NO alone an acceleration of the oxidation of CO is observed. The reaction of NO with HO_2 counteracts the kinetic effect that causes inhibition from O_2 by converting HO_2 to an active radical species (Roesler et al. 1995).

Ho et al. (1992) state that reaction 2.70 is the major cause of OH loss. This decrease of OH effectively stops CO burnout. Furthermore, it is stated that reaction 2.54, which usually forms OH during hydrocarbon incineration, reacts in the reverse direction when HCl is present at concentrations comparable to CO due to the large extent of OH depletion. It is suggested that addition of moderate levels of high-temperature steam will facilitate CO conversion by shifting the equilibrium to more OH for reaction 2.70 and 2.54 (Ho, Barat & Bozzelli 1992).

Gokulakrishnan and Lawrence (1999) made an experimental study of the inhibiting effect of chlorine in a fluidized bed combustor. It was found that combustion radicals (H/OH/O) play a major role in converting HCN and NCO to NO_x. Thus, the decrease in NO_x caused by HCl is due to the suppression of O, H and OH radicals. Furthermore, it was found that an increase in the concentration of N_2O at 825 and 900 $°C$ is due to the suppression of H and OH radical by HCl. It was found that the inhibiting effect of HCl is caused by a sharp reduction in the concentration of OH radicals, which prevents the oxidation of CO through reaction 2.55. In short, reaction 2.78 diverts HO_2 radicals from the chain propagating reaction

2.59, which is the main producer of OH radicals for the oxidation of CO to CO_2 (Gokulakrishnan & Lawrence 1999).

The presence of $CaCO_3$ and CaO will probably reduce the effect of HCl on CO in a precalciner kiln, see Equation 2.79 and 2.80. However, a temperature below 650 to 700 $°C$ is needed for reaction between CaO and HCl for HCl capture in a fluidized bed combustor (Zevenhoven 2001).

$$Cl + HO_2 \rightleftarrows HCl + O_2 \tag{2.78}$$

$$2HCl + CaO \longrightarrow CaCl_2 + H_2O \tag{2.79}$$

$$2HCl + CaCO_3 \longrightarrow CaCl_2 + CO_2 + H_2O \tag{2.80}$$

2.2.2 CO in heterogeneous combustion

Hayhurst and Parmar (1998) investigated if a solid carbon particle burned in oxygen gives the gaseous intermediate CO or produces CO_2 directly. A review on previous work supported that the ratio of CO/CO_2 increases with temperature. It was reported by Arthur (1951), cited in Hayhurst and Parmar (1998), that the primary products at temperatures between 730 - 1170 K is given by Equation 2.81.

$$\frac{[CO]}{[CO_2]} = 2500 \exp(\frac{-6240}{T}) \tag{2.81}$$

Hayhurst and Parmar (1998) state that carbon mainly produces gaseous CO at temperatures between 1000 - 1400 K. At the lower temperatures the rate of oxidation of CO is relatively slow, so there is hardly time for it to burn before being swept away in the gas passing over the particles. At higher temperatures, approaching 1400 K, CO evidently oxidizes rapidly close to the carbon surface, to which it donates its heat of combustion. Furthermore, CO burns close to the carbon when the size of the particles (and U_{mf}) is small. The burning of CO in a fluidized bed of sand is different from the situation without any sand, because radicals (OH, HO_2) are lost by recombination (Hayhurst & Parmar 1998).

Bews et al. (2001) studied the order, Arrhenius parameters and mechanism of the reaction between gaseous oxygen and solid carbon. Studies on the oxidation of graphite particles with an initial diameter of 115 μm, at fluidized bed temperatures ranging from 973 to 1173 K, showed that (Bews, Hayhurst, Richardson & Taylor 2001):

- the oxidation occurs by reaction 2.82, thereby producing CO, which burns either in bubbles ascending through the fluidized sand or on top of the bed,

$$C_s + \frac{1}{2}O_2 \longrightarrow CO \tag{2.82}$$

- a feature of a fluidized bed is that the sand is a surface where free radicals like HO_2 and OH recombine,
- the reaction rate was found as: $r = k_1 \cdot [O_2]^{1/2}$; the rate coefficient, which has units of $\text{mole}^{1/2}\text{s}^{-1}\text{m}^2$, is seen from Equation 2.83.

$$k_1 = 1.1 \cdot 10^4 \exp(-179/RT) \tag{2.83}$$

The heterogeneous reaction of CO can also be explained by a single- or dual site (S) mechanism, which is referred to as the Langmuir-Hinshelwood kinetics, see Equation 2.84 and 2.85 (Fogler 1992). The single site rate of surface reaction is shown in Equation 2.86, where k_S, $C_{i\cdot S}$, and K_S denote the reaction rate, surface concentration of sites occupied by species i (A or B) and surface reaction equilibrium constant.

$$A \cdot S \rightleftarrows B \cdot S \tag{2.84}$$

$$A \cdot S + S \rightleftarrows B \cdot S + S \tag{2.85}$$

or

$$A \cdot S + B \cdot S \rightleftarrows C \cdot S + D \cdot S$$

$$r_S = k_S(C_{A\cdot S} - \frac{C_{B\cdot S}}{K_S}) \tag{2.86}$$

In each of the cases above, the products of the surface reaction adsorbed on the surface are subsequently desorbed into the gas phase like e.g. in Equation 2.87.

$$B \cdot S \rightleftarrows B + S \tag{2.87}$$

Kilpinen et al. (2000) developed a new simplified formula for the kinetics of CO oxidation in the presence of water vapor to cover the whole temperature range of 973 - 1673 K. The accuracy of previous simplified CO oxidation schemes is poor outside their range of validity (Kilpinen & Norstrom 2000). However, the new formula is good in the whole temperature range at low CO concentrations. Relatively good accuracy is obtained in a wider range $X_{CO}/X_{O_2} < 0.65$, where X is mole fraction. The new rate equation is given in Equation 2.88; the temperature functions ($f_0(T)$, $f_2(T)$, $f_3(T)$ *and* $f_4(T)$) can be found in the original paper for different conditions (Kilpinen & Norstrom 2000). In Equation 2.88, χ is mole fraction, t is time and T is temperature.

$$-\frac{d\chi}{dt} = \exp(f_0(T) + f_2(T)\frac{\chi_{CO}}{\chi_{O_2}})\chi_{CO}\chi_{O_2}^{7.89\cdot10^{-4}T-0.90}\chi_{H_2O}^{f4(T)+f3(T)\frac{\chi_{CO}}{\chi_{O_2}}} \tag{2.88}$$

2.3 Fluidization regime

When designing the laboratory CFBC reactor it is crucial to have knowledge about the fluidization regime in order to achieve similar conditions as in the precalciner of cement kiln 6 at Brevik. Therefore, previous work on fluidization regime will be presented before discussing the regimes of the precalciner and the CFBC reactor.

2.3.1 Introduction

It is important to describe the contact regime and fluidization characteristics of the bed material to be able to compare different reactor regimes. The contact regime is most easily described by mean particle size (d_p), density (ρ_s) and superficial gas velocity (U_0), see Figure 2.23 (Kunii & Levenspiel 1991). In general there are three contact regimes: packed bed (PB), bubbling fluidized bed (BFB) and circulating fluidized bed (CFB) with belonging subregimes: turbulent fluidized bed, fast fluidized bed and pneumatic transport. Fluidization characteristics for different particle sizes and classes can be described by Geldart classification (Kunii & Levenspiel 1991).

Geldart classification describes how different particles behave at fluidization, see Figure 2.24.

In order to evaluate the contact regime with the use of Figure 2.23 the dimensionless particle size and gas velocity have to be calculated, as given by the following equations:

$$d_p^* = d_p \left[\frac{\rho_g \left(\rho_s - \rho_g\right) g}{\mu^2} \right]^{\frac{1}{3}} \tag{2.89}$$

$$U^* = U_0 \left[\frac{\rho_g^2}{\mu \left(\rho_s - \rho_g\right) g} \right]^{\frac{1}{3}} \tag{2.90}$$

Here ρ_g (g/cm^3) and ρ_s (g/cm^3) denote gas- and solid density, μ $(g/cm \cdot s)$ denotes dynamic viscosity, g (cm/s^2) denotes acceleration of gravity, U_0 (cm/s) denotes superficial gas velocity and $d_p(\mu m)$ denotes particle diameter.

In the design of a laboratory reactor, slugging of gas has to be considered. It is known from the literature that particle size and distribution show no correlation with slugging of gas, but on the other hand the relations of diameter (D) and height of the reactor have (Kunii & Levenspiel 1991). Slugging in a reactor can be found by employing empirical equations expressing the height (Zs) at which the phenomenon is prevailing, see Equation 2.91 (Kunii & Levenspiel 1991). To avoid poor gas and solids contact, the reactor height has to be lower than the height at which slugging is prevailing.

The phenomenon of choking has generally been used to describe an abrupt change in the behavior of a gas-solids conveying system. Zenz and Othmer (1960) defined choking as the point at which slugging occurred in such an extent that extremely unsteady flow conditions ensued (Bi, Grace & Zhu 1993). The minimum transport velocity, which corresponds to the accumulative choking velocity, U_{CA}, is an important parameter for pneumatic transport and for particle entrainment in the freeboard. From the pneumatic transport point of view, it sets the minimum superficial gas velocity required to make a given flux of solid particles fully suspended in the whole transport line without accumulation. The accumulative choking velocity is shown in Equation 2.92 (Bi et al. 1993). Here v_t, $G_s(\mathrm{kg/m^2 \cdot s})$ and ρ_s denote terminal velocity, solids recirculation rate and solids density, respectively. Terminal velocity can be estimated from fluid mechanics, see Equation 2.93. Where, C_D denote the experimentally determined drag coefficient.

$$Zs = 60 \cdot D^{0.175} \tag{2.91}$$

$$U_{CA} = 10.74 \cdot v_t \left(\frac{G_s}{\rho_s} \right)^{0.227} \tag{2.92}$$

$$v_t = \left[\frac{4 d_p \left(\rho_s - \rho_g\right) g}{3 \rho_g C_D} \right]^{1/2} \tag{2.93}$$

In addition, a fluidization regime can be characterized by physical and chemical particle composition, void fraction, gas (τ_g)- and particle (τ_s) retention time and reactor turbulence. Previous work in this area will be utilized in the evaluation of both the precalciner and the CFBC reactor.

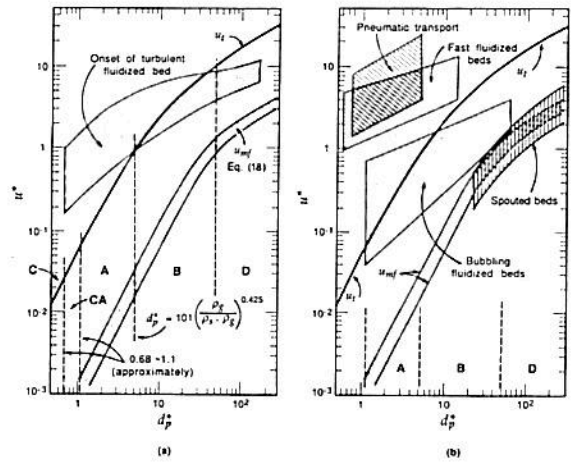

Figure 2.23: General contact regimes, (Kunii & Levenspiel 1991).

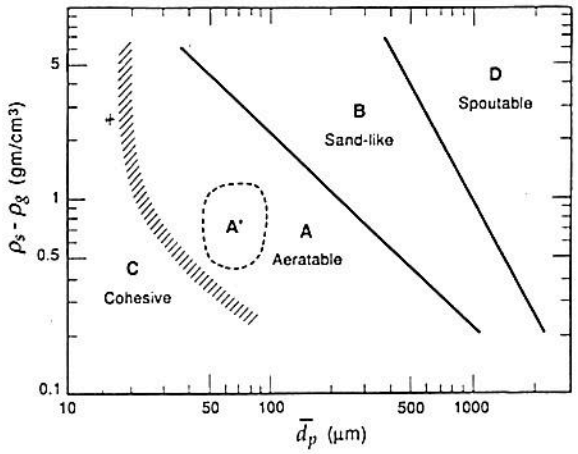

Figure 2.24: Geldart particle classification, (Kunii & Levenspiel 1991).

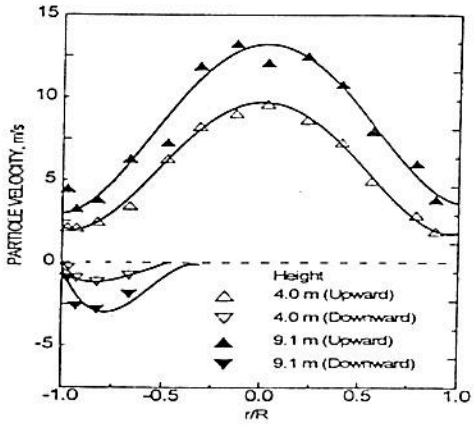

Figure 2.25: Radial distribution of upwards and downwards particle velocity in a dilute region of a CFB riser, (Lim et al. 1995).

2.3.2 Previous work

Core-annulus flow

Mechanistic approaches based on core-annulus flow structure are also used to predict the residence time on a more fundamental basis (Smolders & Baeyens 2000), (Hundebøl & Kumar 1987), (Van der Meer, Thorpe & Davidson 2000). A core-annulus flow structure was proposed by Bierl and Gajdos (1982) and later adopted by others (Bierl & Gajdos 1982). The riser is assumed to consist of a dilute core region, occupying most of the cross-section, and a dense annular region adjacent to the wall where solids mainly travel downwards. All observed radial distributions profiles of particle velocity support the core-annulus flow structure, in which solids are mainly entrained upwards in the core region and descend in the annular region. A typical radial distribution of particle velocity is shown in Figure 2.25 (Lim et al. 1995). Although the upflow and downflow particle velocities are similar in magnitude near the wall in Figure 2.25, the downflow solids flux is much higher since there are many more particles travelling downwards there.

It has been suggested that there may be a universal radial profile of bed voidage (ε) for any time-averaged solids concentration, for different particles at different superficial gas velocities and solids circulation rates in different risers (Lim et al. 1995). Hence, Tung et al. (1989) and Zhang et al. (1991) suggested a universal radial profile of bed voidage:

$$\varepsilon = \varepsilon_{mean}^{0.191+(r/R)^{2.5}+3(r/R)^{11}} \tag{2.94}$$

Here, ε_{mean} denotes average cross-section bed voidage. At a given velocity, radial profiles of mass flux change very little with changes in the mean solids flux in the riser. Accordingly, it is suggested that the thickness of the annular region is independent of the solids mass flux and is only a function of superficial gas velocity (Berruti, Chaouki, Godfroy, Pugsley & Patience 1995). However, investigations on the radial solids concentration distributions in a laboratory-scale CFB and in an industrial riser, show that the solids distribution in the tangential direction is not always uniform, even in the fully developed region (Lim et al. 1995).

Malcus et al. (2000) investigated the dense bottom zone of a CFB riser using the noninvasive electrical capacitance tomography (ECT) measurement technique. The radial profiles showing very low solids concentration close to the center-line

of the riser and a continuous increase of the local solids concentration towards the wall region indicate the existence of a core-annulus type of behavior in the bottom zone of the CFB riser. The probability density distribution functions and the radial standard deviation profiles also indicate that a core-annulus flow structure exists in the dense bottom zone, with a rather homogeneous gas-solids suspension around the center-line of the CFB riser and a heterogeneous behavior of the suspension in the wall region. Measurements at two different heights in the bottom zone showed that there is barely a change in the hydrodynamic behavior of the gas-solids suspension with a change in height. Malcus et al. (2000) state that solids concentration near the wall will always be much higher than at the center-line of the riser, independently of operating conditions, and that it will have a magnitude of about 40 % by volume (Malcus, Chaplin & Pugsley 2000).

Micro flow structure

A phenomenon affecting the hydrodynamics is particles that tend to exist in aggregated forms, also called clusters. Several methods have been used to characterize the time variation of solids concentrations. The micro-flow structure has been observed by employing a two-dimensional column, and also by using a video camera and a special optical fibre image probe showing that there are two distinct phases: a dispersed phase, in which solid particles are essentially present individually, and a cluster phase (Bai, Jin, Yu & Zhu 1992), (Lim et al. 1995). This is consistent with photos of Kuroki and Horio (1994), cited in Lim et al. (1995), who observed that clusters exist even under very dilute conditions. Clusters were observed to transform from strands at the centre of the column into near-spheres adjacent to the wall. Furthermore, significant axial and radial variations have been found by optical observation. Cluster size and frequency of appearance increased from the riser centre to the wall. The cluster size and the frequency of appearance decreased with increasing superficial velocity and/or decreasing solid circulation rate. Cluster size decreased with height.

The definitions of solids agglomeration, proposed by Bi et al. (1993a) are summarized in Table 2.1 (Lim et al. 1995); D_e, L_e, U_e, ε and δ_e denote equivalent size, equivalent length, average velocity, equivalent voidage and equivalent thickness of particle sheets, respectively.

The overall relative velocity ($U_{slip,mean}$) in circulating fluidized beds has been found to be higher than the terminal velocity of single particles, and has been attributable to the existence of particle clusters or streamers[4] (Lim et al. 1995). The overall relative velocity in a CFB is given by:

$$U_{slip,mean} = \frac{U_0}{\varepsilon} - \frac{G_s}{\rho_p (1-\varepsilon)} \tag{2.95}$$

Here U_0, ε, ρ_p and G_s denote superficial gas velocity, average voidage, particle density and solid circulation rate, respectively.

Gas and solids mixing in a CFB

The downward motion of particles in the wall region by the various forms of clusters causes backmixing of solids and may also lead to downflow (backmixing) of gas in the annulus. This gives a radial dispersion of gas and solids, which is usually favorable to overall conversion. Hence axial gas flow deviates significantly from plug flow. One-dimensional dispersed plug flow models have been employed to correlate experimental data; the dispersion mostly range from 0.1 to 0.6 m^2/s.

[4] Streamers are vertically elongated groups of particles travelling together close to the wall.

Table 2.1: Summary of solids agglomeration forms in CFB, Lim et al. (1995)

Forms of congregation	**Region**	**Shape**	**Character**	**Scale**	**Origin**
Particle clusters	Core and annulus	Various	D_e<1cm, $\varepsilon \approx \varepsilon_{mf}$	Micro	[1)]interparticle forces, [2)]particle wake interaction
Particle streamers/strands	Core and annulus	Bands	L_e>1cm, $\varepsilon \approx$ 0.7-0.95, U_e>0	Meso	[1)]resemble clusters, [2)]breakup of particle sheets, [3)]non-uniform introduction of particles
Particle swarms	Annulus	Approx. spherical	L $\approx$ 1-1.5 cm, U_e $\approx$-0.3 $\approx$-0.4 m/s	Meso	[1)]wall particle interaction
Particle sheets	Annulus	Layer	δ_e $\approx$ 0-3 cm, U_e $\approx$-1cm	Macro	[1)]resemble particle swarms, [2)]particles diffusing to the wall region and swarms

Gas backmixing is reported to be closely related to the operating conditions; it increases with solids circulation rate and decreases with superficial gas velocity (Lim et al. 1995), (Bai, Yi, Jin & Yu 1992).

Bai et al. (1992) measured residence time distributions, showing larger peak values with shorter tails as the superficial velocity is increased, but smaller peak values with longer tails as the solids circulation rate is increased. Experiments were performed by applying a fixed gas velocity and increasing the solids circulation rate, which increases the average solids holdup and the radial non-uniformity of solids distribution, this led to a less uniform radial gas distribution. The increased local gas velocity in the centre and the reduced (or increased downwards) gas velocity at the wall cause more gas to pass through the core region, increasing gas dispersion. The opposite occurs when gas velocity is increased at a fixed solids circulation rate (Lim et al. 1995). Bai et al. (1992) also investigated the backmixing and axial dispersion of gas and solids in a circulating fluidized bed with the use of residence time distribution (RTD) experiments. The experiments were carried out in a circulating fluidized bed, with an inside riser diameter of 140 mm and a height of 10 m. Experiments were conducted for gas velocities and solid circulation rates in the range of 2 to 10 m/s and 10 to 100 $kg/(m^2 \cdot s)$, respectively. The investigations led to the following conclusion (Bai, Yi, Jin & Yu 1992):

- The flow patterns of gas and solids in circulating fluidized beds are quite different from plug flow. Compared to the extent of solids backmixing, the gas backmixing is considerable and should not be ignored.
- In the mixed solids the flow patterns of particles of different size are quite different. Generally, the flow pattern of fine particles is closer to plug flow

than that of coarse particles in circulating fluidized beds.

The influence of operating conditions on radial gas dispersion appears to be complex. Werther et al. (1992) reported that radial gas dispersion is independent of superficial gas velocity and solids circulation rate between 0 and 70 kg/m^2·s for the core region in the upper part of the riser (Werther, Hartge & Krause 1992). In contrast, Zheng et al. (1992) suggested that there is a threshold of solids circulation rate below which radial gas dispersion increases with superficial gas velocity and above which radial gas dispersion decreases with superficial gas velocity (Zheng, Wei & Lou 1992).

Kruse et al. (1995) investigated the upper dilute zone of a CFB riser with the use of a tracer gas technique. Based on experimental findings, a two-dimensional two-phase model for gas/solids-flow and gas mixing in the upper dilute zone of a CFB riser was developed. The model accounts for radial gas dispersion and gas backmixing. An increase in the solids rate yields and increase in the interfacial mass transfer coefficient and the solids volume concentration were found (Kruse, Schoenfelder & Werther 1995).

Grace et al. (1997) state that the exit geometry configuration affects the back-mixing in the riser exit. A very strong restrictive (T-shape) exit gives higher solids concentration at the riser top, with violent turbulence and significant solids back-mixing in the riser exit region. A smooth (C-shape) exit, on the other hand, will give no significantly high solids holdup in the region of exit and no additional solids back-mixing activity (Grace, Avidan & Knowlton 1997).

Effects of particles on turbulence

The effects of particles on turbulence are discussed by Chomiak (2000) and Peirano et al. (1998). Investigations into turbulence with the aid of CFD modelling, e.g. proposed by Peirano et al. (1998), is followed up in Section 5.2. In addition, the impact of particles on turbulence is investigated in the two-way coupling region with the aid of the map of Elgobashi (1991), see Figure 2.26 (Chomiak 2000), (Peirano & Leckner 1998), (Elgobashi 1991). In order to make use of the proposed map, it is necessary to calculate particle response time[5] (τ_p), the turbulence time scale[6] (τ_e) and the volume fraction of particles (ε_s)[7]. The particle response time and the turbulence time scale are defined as:

$$\tau_p = \frac{1}{a} \text{ and } a = \frac{36\mu}{(2\rho_p + \rho_f)\, d^2} \tag{2.96}$$

$$\tau_e = C_\mu \frac{k}{\varepsilon} \tag{2.97}$$

Here ρ_p, ρ_f, d, μ , ε and k denote particle density, fluid density, particle diameter, dynamic viscosity, dissipation and turbulence kinetic energy, respectively. The constant $C_\mu = 0.09$.

Chomiak (2000) states that small particles by the way they physically interact with the fluid can only induce dissipation and not turbulent energy. Only particles having diameters at least close to 0.1 ζ can have an effect on energy (Chomiak 2000). ζ[8] denotes the integral length scale[9]. This is illustrated by the results reported in

[5] Particle response time defines the necessary time a particle need to react on a change in the flow pattern.

[6] Turbulence time scale is the characteristic time for a turbulent whirl.

[7] Denoted as α_p in Figure 2.26.

[8] Denoted as l_e in Figure 2.27.

[9] Integral length scale physically represents the mean size of the large eddies in a turbulent flow: those eddies with low frequency and large wavelength.

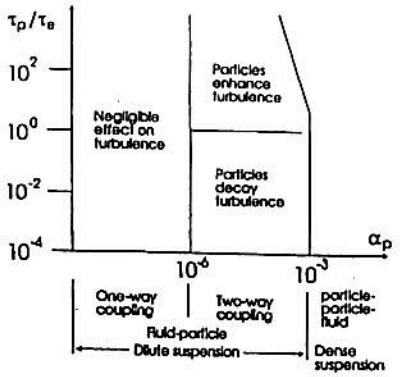

Figure 2.26: Proposed map for particle-turbulens modulation Elghobashi (1991).

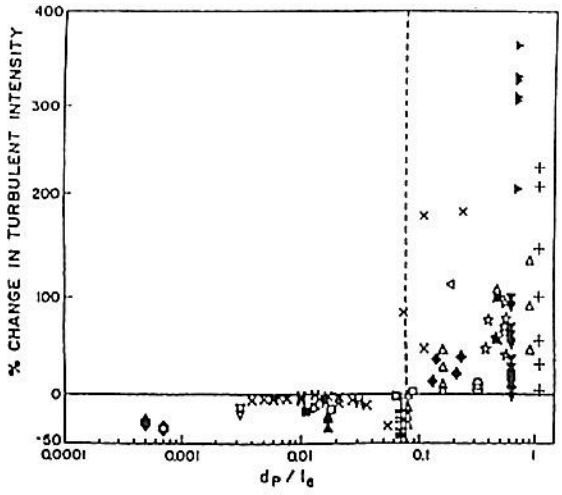

Figure 2.27: Experimental data on the effect of the particle diameter/turbulence length scale on the turbulence intensity of the carrier fluid (Gore & Crowe 1989).

Chomiak (2000), presented in Figure 2.27. Chomiak (2000) also states that little is known about the generation of turbulence in dense suspensions.

Void fraction

The void fraction is defined by: $\varepsilon = 1 - \varepsilon_s$, where $\varepsilon_s = \frac{\text{volume of solids}}{\text{volume of gas and solids}}$, is the volume fraction of solids. Calculating the void fraction from the process influx gives a theoretical void fraction in which one disregards accumulation and recirculation. The void fraction can be calculated by measuring the static pressure drop in the reactor, which reflects the hydrostatic head of solids:

$$(1 - \varepsilon) = \frac{\Delta P_R}{g \rho_s L} \tag{2.98}$$

Here ρ_s denotes solid density, ΔP_R denotes pressure drop across the riser, g denotes acceleration of gravity and L denotes riser height. Comparing directly measured solids holdup along the riser by using a series of quick-closing valves with the values inferred from differential pressure, it was found by Arena et al. (1986),

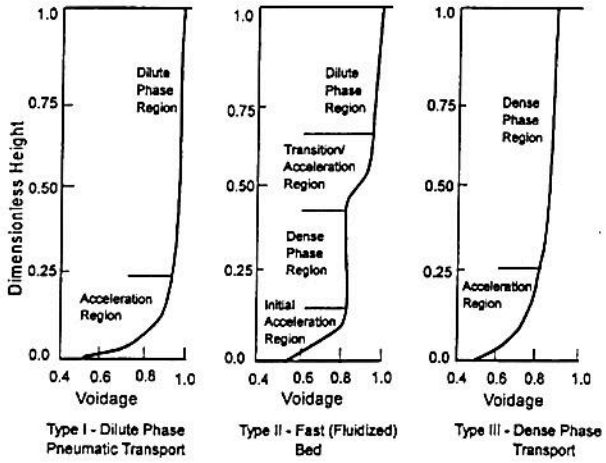

Figure 2.28: Axial bed voidage profiles observed in the riser of circualting fluidized beds, (Lim et al. 1995).

cited in (Lim et al. 1995), that the values calculated from differential pressure measurements are significantly higher in the transition region, where particles accelerate very quickly. Hence, when the acceleration pressure drop is neglected, correct calculations can only be made over the hydrodynamically fully developed region. See Figure 2.28 for the transition regions and classification of types of axial bed voidage profiles in the riser of circulating fluidized beds (Lim et al. 1995).

Particles physical composition

Interparticular bonds are mainly van der Waals forces, electrostatic forces and capillary forces[10]. Their relative magnitude are shown in Figure 2.29 for equally sized particles. It can be seen in Figure 2.30 that van der Waals forces are stronger when the particles are close, whereas electrostatic forces are stronger when the distance increases. In addition to increasing distance, moisture and roughness reduce the van der Waals forces. Neither electrostatic nor capillary forces are influenced by roughness, but moisture has a considerable effect on electrostatic forces. If binding between particles is with fluid or material bridges, it will dominate other binding forces. Interparticular forces with material bridges can consist of same solid as the particles, created through sintering, crystallization or partial fusion and congelation at the contact tips. It can also consist of a different substance, e.g. adhesive or crystals from dried up solutions. Interparticular forces with fluid binding are characterized by the pendular state, the funicular state and the capillary state.

Prevailing interparticular forces in a precalciner or a CFBC are mainly van der Waals forces, electrostatic forces and capillary forces. The particle size distribution of a circulating mass, in a precalciner or a CFB, contributes to characterization of the operating conditions of a reactor, in regard of how cohesive the material will behave. A cohesive material can be defined as when interparticular bonds are large compared to the gravity of the particles, hence particles in the range of 10 μm have a decisive influence on cohesivety, see Figure 2.29. About 30 % of the particles in the raw meal supplied to the precalciner kiln 6 in Brevik is below 10 μm. Hence, interparticular bonds will probably have an influence on the prevailing flow regime

[10]It must be noted that forces between different materials are different from those between particles of the same material.

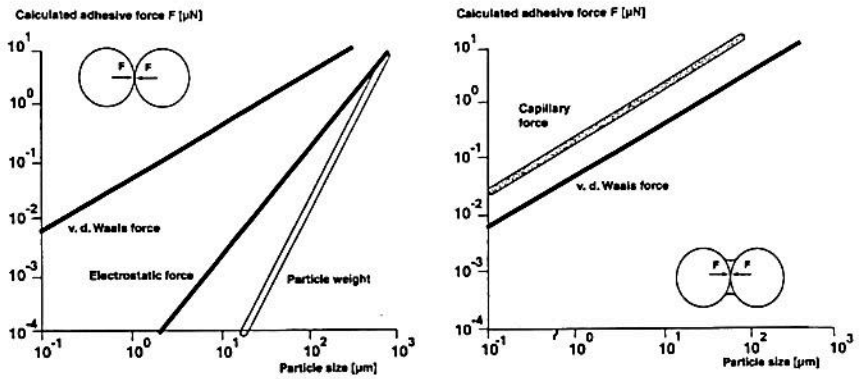

Figure 2.29: Magnitude of forces between particles (de Silva 2001).

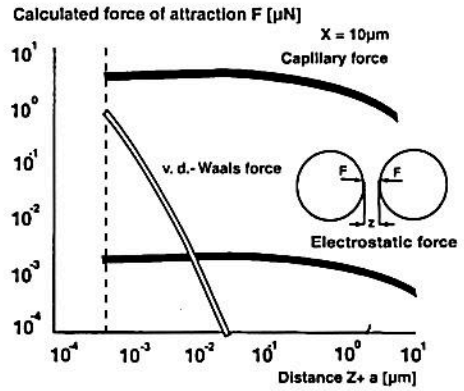

Figure 2.30: The effect of interparticular forces on the distance between particles (de Silva 2001).

in a precalciner (de Silva 2001). Therefore, it is desirable to use an approximately similar circulating material (i.e. particle distribution, mean particle size, etc.) in the CFB reactor as in the precalciner.

Dimensionless groups

van der Meer et al. (1999) have compared different sets of dimensionless groups from the literature used for scaling of circulating fluidized bed. The dimensionless groups are classified according to the number of groups in the set. van der Meer et al. (1999) state that at least five dimensionless groups are required for full hydrodynamic scaling. A survey concludes that most experimental results reported in the literature on scale up better match to catalyst cracking CFB's than to CFB combustors.

In the literature on dimensionless analysis of fluidized beds, it has been common to neglect particle shape and size distribution, particle/particle and particle/wall coefficients of restitution and friction, electrostatic forces and cohesion. Apart from the requirements for geometrical similarity, this leaves eight parameters of importance to flow in the riser of a CFB. The input parameters are:

- superficial gas velocity U_0,

- external solids circulation flux G_s,
- Sauter mean particle diameter d,
- particle density ρ_p,
- riser hydraulic diameter D,
- gas density ρ_g,
- gas viscosity μ,
- acceleration due to gravity g.

The input parameters described above determine the following output parameters, thus describing the flow pattern:

- riser pressure drop ΔP_R,
- riser solids holdup,
- local solids volume fraction ,
- local solids mass flux and velocity,
- slip velocity in the riser U_{slip}.

The input parameters can describe the flow pattern in the riser only if G_s is controlled. Experimental evidence by Chang and Louge (1992) indicates that if G_s is controlled, the flow in the riser is virtually independent of conditions in the feeder and solids return column. Hence, if G_s is controlled, the nature of the riser flow is isolated from other parts of the CFB and is a unique function of the input parameters and geometry of the riser and its exit. If G_s is not controlled, then the properties in the return column do influence the nature of the flow in the riser (Van der Meer, Thorpe & Davidson 1999). The eight input parameters have three independent dimensions, mass, length and time: it follows that five appropriate dimensionless groups, representing all eight parameters will yield complete similarity. However, van der Meer et al. (1999) state that for practical reasons it is usually not possible to match the parameters so that all five dimensionless groups remain constant.

In the following a short presentation of the different dimensionless groups will be given.

Two dimensionless groups If the axial solids volume fraction profile in the riser is investigated, a fair similarity with a large unit may be achieved with: $\frac{U_0}{v_t}$ and $\frac{G_s}{\rho_p U_0}$ where v_t denotes the terminal velocity of a single particle. Including slip velocity ($U_{slip,mean}$) instead of the terminal velocity in the first group will probably give a better interpretation of fluidization regime.

Three dimensionless groups The three dimensionless groups $Fr_D = \frac{U_0^2}{gD}, \frac{U_0}{v_t}, \frac{G_s}{\rho_p U_0}$ are expected to maintain the fluidization regime, riser solids holdup by volume and macroscopic movements of solids. The groups are recommended for $Re_d < 15$, where $Re_d = \frac{\rho_g U_0 d}{\mu}$.

Four dimensionless groups Through the use of four dimensionless groups the riser solids holdup by weight is properly non-dimensionalised, hence the pressure drop and -gradients will be appropriate output parameters to study. It is suggested that the set $Fr_D, \frac{U_0}{v_t}, \frac{G_s}{\rho_p U_0}, \frac{\rho_p}{\rho_g}$ holds for much of the CFB flow regime.

Five dimensionless groups If particle shape and size distribution, particle/particle and particle/wall coefficients of restitution and friction, electrostatic forces, cohesion and adhesion can be neglected, then assuming geometric similarity, full hydrodynamic similarity of CFB may be obtained by: Fr_D, $\frac{d}{D}$, $\frac{G_s}{\rho_p U_0}$, $\frac{\rho_p}{\rho_g}$, Re_d. It is suggested that for dilute flows, the Reynolds number may need to be based on the bed diameter (D), rather than on particle diameter (d).

For simple design of fluidized beds the important aspect of geometrical similarity is the design of the exit, which can significantly affect flow conditions in the top section of a riser and sometimes even in the middle section (Jin, Yu, Qi & Bai 1988).

Flow pattern and retention time in a CFB

Smolder et al. (2000) has studied the residence time distribution (RTD) in a CFB . Experiments were performed with salt as a tracer in a riser with a diameter of 0.1 m and a height of 6.5 m. The exit of the riser was made with a 90° sharp connection (short extension blind T). The results from the experiments was used to: 1) make a correlation with a fitting procedure, 2) make a model based on one-dimensional quasi plug flow with dispersion, 3) make a model based on the core/annulus flow. The correlation with a fitting procedure gave, for the specific riser, two equations, one for the average solids residence time of the total system ($\tau_{s,mean,riser}$) and one for solids residence time ($\tau_{0.5}$)[11]:

$$\tau_{s,mean} = 56 \cdot \frac{Gs^{0.333}}{U_0^{2.4}} \tag{2.99}$$

$$\tau_{0.5} = 60 \cdot \frac{Gs^{0.325}}{U_0^{2.6}} \tag{2.100}$$

Here G_s ($kg/m^2 \cdot s$) and U_0 (m/s) denote solids circulation rate and superficial gas velocity, respectively. Measurements demonstrated that the average solids residence time (τ_s), which reflects the hydrostatic head of solids in the reactor, was lower than the actual-average solids residence time ($\tau_{s,mean,riser}$), except for high gas velocities. τ_s is found by measuring hydrostatic head (shown in Equation 2.98). Actual-average solids residence time is found with the following equations and RTD experiments:

$$\tau_{s,mean} = \int_0^\infty tE(t)dt \tag{2.101}$$

$$\tau_{s,mean,riser} = \tau_{s,mean} - \frac{t_{injection}}{2} \tag{2.102}$$

Here $\tau_{s,mean}$, t, $E(t)$ and $t_{injection}$ denote average residence time of the total system (s), time (s), residence time distribution of injection and riser system and injection time (s), respectively (Smolders & Baeyens 2000).

Modelling of a one-dimensional quasi plug flow with dispersion resulted in a rather small Peclet number[12], varying from 1 to 20. The Peclet number decreases with increasing loadings and confirms the higher backmixing at higher solid fluxes. Theory of plug flow with axial dispersion is valid only for Peclet numbers larger than 100, which proves that with this approach of modelling the particle flow in the riser is questionable, although it predicts a residence time distribution curve that fits the experiments very well. Smolders and Baeyens (2000) report that Peclet numbers in earlier RTD experiments, presented by (Diguet 1996), are higher and

[11] $\tau_{0.5}$ with $F(\tau_{0.5})$=0.5, $F(\tau)$ is the cumulative residence time distribution.
[12] Peclet number is defined as: $\mathrm{Pe} = \mathrm{Re} \cdot \mathrm{Pr}$.

state that the difference is the exit of the two risers. Backmixing in a CFB with a T-shaped exit will be larger than in a CFB with a smooth exit. It has been reported by Rhodes et al. (1991) that the dispersion of the solids decreases with increasing riser diameter (Rhodes, Zhou, Hirama & Cheng 1991). The experimental results by Smolders and Baeyens (2000) showed that the downflow along the riser wall increases with increasing solids circulation rate and hence results in a higher back-mixing, contrary to the results by Rhodes et al. (1991), which showed that the Peclet number has a linear relation.

A mathematical model, based on the core/annulus flow structure, was proposed by Smolders and Baeyens (2000) to characterize the flow and to predict the residence time distribution of solids in the riser. The model was used to predict the experimental values. The interchange flux between core and annulus corresponded well with radial fluxes reported in the literature. The core/annulus model approach has proved to be a practical tool for predicting the backmixing of solids in a riser flow.

Solids flow patterns were observed and measured by van der Meer et al. (2000) in a laboratory CFB with a diameter of 0.14 m . van der Meer et al. (2000) state that there is core/annulus flow, with downward solids flow near the riser walls and upward solids flow in the central area of the riser. The detailed design on the exit bend at the top of the riser was investigated, and it was found to have an important impact on the solids reflux ratio (k_m)[13] throughout the riser. The observation that the reflux ratio is affected is in conflict with the statements made in a review article by Lim et al. (1995) (Van der Meer et al. 2000). No explanation for this difference is given. van der Meer et al. (2000) state that if the bend outlet design affects solids inventory throughout the riser, this in turn may affect overall performance, e.g., in respect of heat transfer to the walls of a CFBC, carbon burnout, combustion efficiency and emission control. Furthermore the laboratory CFB was compared with an industrial CFBC, and a scale-up effect was found: the thickness of the region adjacent to the wall, within which there is a net solids down flow, amounts to a smaller fraction of the reactor diameter for large (industrial) units than for smaller (laboratory) units.

He et al. (1995) made approaches in the modelling of gas-solids flow through a riser, for which the theory suggested that there are two different mechanisms for solids flowing through a riser, namely, dragging and entrainment (He & Rudolph 1995). Dragging is understood as the mechanism for solids circulation by which the riser voidage is reduced by the pressure drop over the riser. This condition is dragging exerted on the particulate solids by the percolating gas, see Type I Figure 2.28. Entrainment is understood as if the gas rate in the system were increased, the level of the dense phase in the riser will rise and the entrainment rate increases, see Type II Figure 2.28. The model only considers the dragging regime, where particulate solids in the riser are relatively evenly distributed along the whole height of the riser with a lower volume average voidage than would be determined by the gas flow alone. The drag force exerted on the particulate solids by the percolating gas is greater than the solids gravity force, resulting in the solids flow. He et al. (1995) state that solids in this regime are constantly dragged through the riser by the flowing gas. He et al. (1995) do not consider the internal circulation of solids in contrast to van der Meer et al. (2000), Smolders and Baeyens (2000) and Hundebøl et al. (1987). He et al. (1995) consider only two regimes, namely, dragging and entrainment. Lim et al. (1995) contradict that there are only two regimes, but also a Type III. Furthermore, Lim et al. (1995) state, based on previous investigations, that the bottom dense region may not always be present and a denser region may exist at the top for constricted exits, see Figure 2.28. Operating variables, such

[13] $k_m = \frac{G_d}{G_{ex}}$, G_d is solids interior mass flux, G_{ex} is solids external mass flux

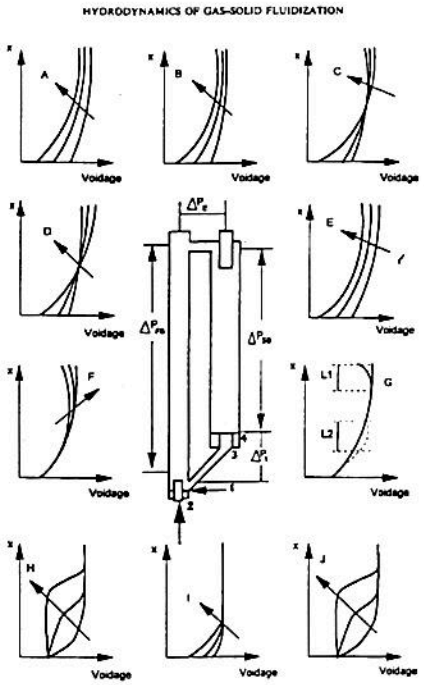

Figure 2.31: Illustration of the various factors influencing average voidage distribution: the arrows indicating effect of: (A) decreasing gas velocity; (B) increasing solids circulation rate, (C) decreasing particle diameter, (D) decreasing particle density, (E) decreasing column diameter, (F) decreasing exit restriction, (G) influence of bed height with different exit restrictions, (H) decreasing inlet restriction, (I) increasing solids inventory with strong inlet restriction and (J) increasing solids inventory with weak inlet restriction Bai et al. (1992).

as solids circulation rate, total solids inventory, particle size and density, solids inlet configuration, riser exit structure, secondary air inlet and the level of solids reintroduction into the riser, affect the axial voidage profile (Lim et al. 1995), (Bai, Jin, Yu & Zhu 1992). Bai et al. (1992) conducted experiments on how operating conditions all affect the axial voidage profile. As summarized in Figure 2.31, it was found that:

- decreasing superficial gas velocity and increasing solids circulation rate increase the solids holdup, especially in the bottom region,
- increasing particle size or particle density has a mixed effect, resulting in slightly less solids holdup in the upper region, but much higher solids holdup in the bottom region where it may form a rather dense bed,
- decreasing riser diameter leads to a reduction in bed voidage, especially in the bottom region.

CFD modelling of CFB reactors Simulations with computational fluid dynamics (CFD) have also been used to investigate the flow pattern of CFB reactors. CFD gives a more complete picture of the flow pattern by combining experimental data with more fundamental models of calculation.

Berutti et al. (1995) reports that Dasgupta et al. (1994) were able to determine the physical cause of the segregation of particles toward the wall, requiring fulfillment of force balance in the radial direction. The equations were closed using a $\kappa - \varepsilon$ turbulence model developed for a constant-density, homogeneous, incompressible fluid. The output of the model indicated qualitative agreement with experimental observations, and a sensitivity analysis proved that the model results were relatively insensitive to the parameters in the $\kappa - \varepsilon$ turbulence model. The model was compared with the experimental data of Bader et al. (1988), and very good agreement was found (Berruti et al. 1995).

Mathiesen et al. (1999) made experiments with a laboratory scale circulating fluidized bed using Laser Doppler Anemometry (LDA) and a modified Shape Discrimination Technique[14] on FCC catalysts. Experiments showed no significant agglomeration in the gas/solids flow system. Typical annulus-core flow behavior was observed, and the relative velocity between particles of different sizes was measured. Different fluctuating velocities of different particle sizes were observed. The largest particles showed the highest fluctuating velocity. This was caused by gas/solids interactions. Significant radial segregation of particles of different sizes was observed, and the mean particle diameter increased from the center of the riser towards the wall. A CFD multiphase gas/solids model for the riser was developed, using two different particle sizes in a two-dimensional Cartesian system. The observed core-annulus flow with a correct relative velocity between the solid phases was calculated. However, the computed fluctuating velocity showed lower values than the experimental data, but demonstrated the same form and behavior. The divergency between simulations and experimental results was explained by the differences between actual and simulated geometry as well as particle-size distribution. (Mathiesen, Solberg, Arastoopour & Hjertager 1999).

Mathiesen et al. (2000) made an experimental and computational study of a cold flow laboratory-scale fluidized bed in order to investigate mean and fluctuating velocity, diameter and solids concentration. The experiments, which were performed with LDA and Phase Doppler Anemometry techniques on group B particles, showed much of the same trends as in Mathiesen et al. (1999), apart from;

- turbulent velocity was almost constant in the center of the riser and increased in the shear layer,
- a relative particle RMS velocity was observed in the lower part of the riser. Smaller particles fluctuated more than larger ones. In the upper part the of the riser, the turbulent velocity seemed to be nearly independent of the particle size.

The CFD simulations also showed much of the same trends as in Mathiesen et al. (1999), apart from:

- the relative velocity between the solid phases was somewhat overpredicted. This was explained with a possibly underestimated turbulent kinetic energy in the lower part of the riser, since the particle-particle drag is proportional to the square root of the granular temperature[15].
- in the upper part of the riser, the computed turbulence had a correct form and magnitude, although the turbulence in the shear layer was too low. Underestimation of the turbulence in the lower part may be a reason for the divergency

[14] Shape Discrimination Technique is an extended LDA measurement technique. Based on the amplitude of a Doppler burst, the technique can estimate the particle size of unspherical particles.

[15] Kinetic theory for granular flow is applied to determine the granular temperature in the particle phases. The granular temperature is defined as one-third times the fluctuating velocity squared. The solid phase pressure, bulk viscosity and shear viscosity are deduced from this theory (Gidaspow 1990).

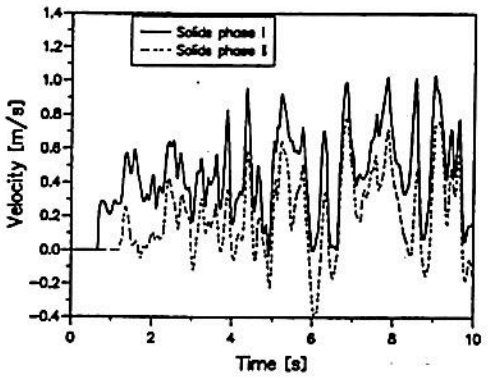

Figure 2.32: Large scale velocity fluctuations. Solid phase I: $d_p = 120\ \mu m$, $\rho = 2400\ kg/m^3$, form factor = 1.0, restitution coefficient, solid = 0.99; Solid phase II: $d_p = 185\ \mu m$, $\rho = 2400\ kg/m^3$, form factor = 1.0, restitution coefficient, solid = 0.99 (Mathiesen et al. 2000).

between measured and simulated mean diameter in the wall region (Mathiesen et al. 2000).

Mathiesen et al. (2000) state that a gas/solid flow system, such as a circulating fluidized bed, never will reach a steady state condition. The system will exhibit a fluctuating behavior. Simulations of large scale fluctuations for each solid phase showed that they had the same frequency, and that the relative velocity between the solid phases was nearly constant, see Figure 2.32 (Mathiesen et al. 2000). This observation is very interesting in the evaluation of the CFB reactor and precalciner of the present work.

Flow pattern and retention time in a precalciner

Retention time distribution Hundebøl et al. (1987) investigated the particle retention time for calciners with the intention of describing the fuel particle retention time. An experimental test calciner was set up (Hundebøl & Kumar 1987). A series of holdup measurements with raw meal and air led to the conclusion that the ratio of solids retention time to gas retention time (τ_s/τ_g) was a fairly high constant, varying only with the Reynolds number of the calciner. The retention time distribution (RTD) in a 3200 tpd calciner was mapped using radioactive tracers. The ratio τ_s/τ_g was established to be approximately 4. A simplified model states that the number of particles is so high that collisions frequently occur. Therefore particles gather in "showers" (clusters, strands) of considerable size and begin to fall quickly opposite to the gas flow. The "showers" fall some length and then split up into separate particles. In this way the particles caught in "showers" must travel the same distance twice or more, and the passage through the calciner is retarded. The following correlation, deduced from the simplified model, explained the experiments very well:

$$\frac{\tau_s}{\tau_g} = \frac{\exp(\alpha) - 1}{\alpha} \tag{2.103}$$

Here $\alpha = f(\mathrm{Re})$. The correlation shows:

- τ_s/τ_g is independent of particle size (as long as it is small), particle shape and density.

- τ_s/τ_g does not depend on the solids feed rate/gas feed rate ratio.
- τ_s/τ_g depends somewhat on gas velocity at smaller Reynolds numbers, but is independent of gas velocity at high Reynolds numbers.
- τ_s/τ_g varies with the gas temperature at smaller Reynolds numbers. A high gas temperature means a high dynamic viscosity, a lower Re-number, and therefore a high τ_s/τ_g.
- τ_s/τ_g depends on the scale; small calciners have higher τ_s/τ_g than large ones, if the gas velocity is maintained constant.
- τ_s/τ_g depends on the height to diameter ratio (H_c/D_c) of the calciner. For constant volume and gas flow, a higher H_c/D_c causes the τ_s to drop.

Hundebøl et al. (1987) concluded that in an industrial calciner of the FLS-SLC[16] type, small particles, such as raw meal and coal meal, remain in suspension for about 12 seconds, although the gas passes the calciner in only 3 seconds. This was explained by the "shower" mechanism. The rather intensive backmixing of the solids phase accounts for the uniform temperature profile of the precalciner. The coal combustion efficiency in a calciner can be estimated with the knowledge of the particle retention time and the residence time distribution. Hundebøl et al. (1987) used the retention time distribution to calculate the degree of burn-out with the use of a kinetic expression of the coal combustion, in which only the fixed carbon was considered.

CFD modelling of precalciners Giddings et al. (2000) investigated the performance of a precalciner with the use of a three-dimensional model in CFD. The aim of the work was to improve the understanding of the fluid dynamics and chemical reaction behavior inside a precalciner. See Figure 2.33 for simulations made by Giddings et al. (2000). After studying previous work Giddings et al. (2000) stated that the CFD tools available now offer a more accurate and fuller analysis of the precalciner than previously, especially because of the improvement in the geometry meshing technique. The precalciner geometry studied by Giddings et al. (2000) resemble a circular CFB with a short-blind T exit. The reported measurements are consistent with the results calculated by the model, indicating a fair validation. The temperatures correlated well, with not more than a 60 $°C$ difference. The CFD data showed that (Giddings, Eastwick, Pickering & Simmons 2000):

- the gases undergo distinct recirculation,
- there is significant recirculation of some particles in the main cylindrical section before exit,
- the coal particles entering at one inlet have significantly different trajectories and temperature histories from those entering at the second diametrically opposed inlet,
- there is 90 % completion of coal combustion at the exit,
- 73 % limestone in the raw meal is calcined to calcium oxide at the exit from the precalciner,
- the highest reaction rate of the raw meal is closer to one side of the vessel due to interaction with the gas flows,

[16] FLS is F.L.Smidth & Co.; SLC is "separate-line calciner", where the tertiary air is the only gas entering the calciner and the off-gas from the precalciner is not subsequently mixed with the kiln gases. If mixing occurs, the term semi-SLC (SLC-S) is used.

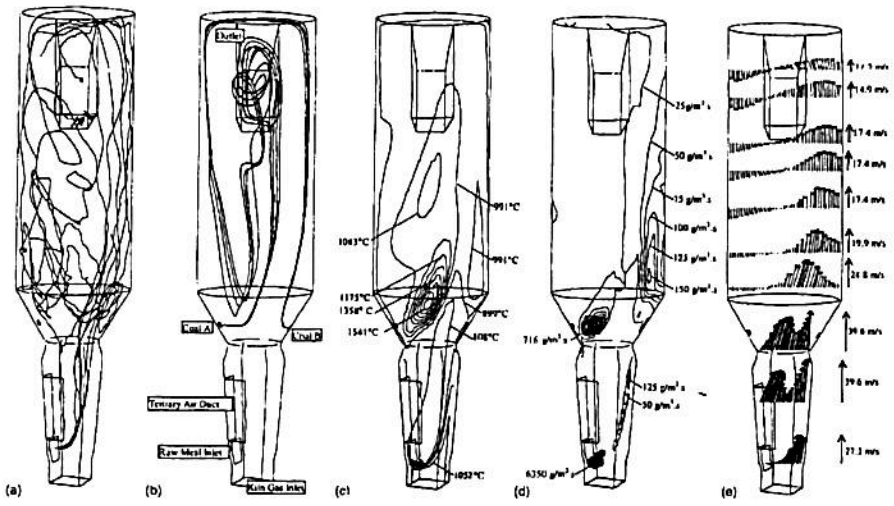

Figure 2.33: (a) Single raw meal particle, showing six stochastic attempts. (b) Coal injection from the two inlets A and B (mean path only). (c) Contours of temperature showing the high-temperature core. (d) Contours showing the release of volatiles. (e) Velocity vectors on selected lines through the precalciner Giddings et al. (2000).

- there is a core-annulus flow inside the precalciner with temperatures varying from about 800 to 1850 $°C$.
- the effect of turbulence in the real installation tends to disperse the particles in random patterns. CFD shows that the initial common trajectory is towards the right-hand side of the precalciner in the conical section despite turbulence effects. The effects of turbulence is significant in dispersing the particles beyond the throat of the conical section.

Giddings et al. (2000b) extended the above mentioned model for combustion of car tires in combination with coal (Giddings, Pickering, Simmons & Eastwick 2000). Differences compared to previous results showed that:

- the model suggest that about 85 % of the raw meal has undergone calcination,
- the coal particles from inlet A has a residence time from 0.6 to 1.0 seconds and coal particles from inlet B from 5 to 18 seconds, hence char oxidation of coal B has completed whereas 20 % of coal A is not oxidized before exit.
- the tire chips fall and then recirculate in the same way as the coal injected at inlet A.

Belot et al. (1993) used CFD to model a down-flow in-line precalciner with a three-dimensional model. The model gave indications of the raw meal calcination, coal combustion and fluid dynamics. Measurements showed that the CO profile was predicted too low whereas the temperature and O_2 profiles were predicted too high in the simulations. This may be due to mean reaction rates (unmixedness) in the CFD simulations. The results indicated temperatures from 800 to 1900 $°C$ and incomplete combustion, and modifications were made in accordance with suggested improvements (Belot, Goffe, Grouset, Bertrand, Homassel & Philippe 1993).

2.4 Alternative fuels in cement kilns

This section starts with a brief presentation of cement production. A more detailed description of the cement production process in the precalciner kiln 6 in Brevik is given in Section 3.1. Furthermore, this section presents alternative fuels used in cement kilns.

2.4.1 Cement production

The production of cement[17] requires the following components in the raw material feed:

- calcium carbonate ($CaCO_3$),
- silica (SiO_2),
- alumina (Al_2O_3) and
- iron oxide (Fe_2O_3).

Limestone typically provides the calcium carbonate while clay or shale provide the remaining components. If necessary, the silica, alumina or iron oxide content of the raw materials can be supplemented by sand, bauxite or iron ore, respectively.

After being blended and ground, the mixed raw materials are fed into the kiln i.e., a cylinder lined with heat-resistant bricks, inclined 3 to 4 % from the horizontal, and rotated one to four revolutions per minute, see Figure 2.34. The raw material undergoes drying, preheating, calcination and at last burning before the clinker enters the cooler. Calcination is the endothermic decomposition reaction of calcium carbonate according to Equation 2.104.

$$CaCO_3 \rightarrow CaO + CO_2 \tag{2.104}$$

In order to complete the production of cement, the cooled clinker is ground with a small amount of gypsum. The gypsum added gives a total sulfate composition of 2 to 3 % in the cement. Without the additional gypsum, the cement would set to quickly.

Production of cement may be done in one of three processes:

- wet process - using slurry with a water content between 25 and 45 %, to allow for pumping and blending,
- semi-dry process - using nodular feed produced by mixing dry raw feed in a pan or drum mixer with a water content between 8 and 15 %, or
- dry process - using raw feed with a moisture content of less than 1 %.

In Europe, the production of clinker normally takes place in dry process kilns, which account for more than 50 % of the total clinker production (Hoenig, Høidalen & Bergamaschi 1997). The so-called suspension preheater kiln is the most common, while the so-called precalciner kiln, as kiln 6 in Brevik, represents a further development enabling higher production capacities of the kiln system, see Figure 2.34.

The difference between a precalciner kiln and a preheater kiln is that the latter calcines most of the raw meal in the rotary kiln, while the former calcines up to 90 % in a vertical parallel-flow reactor, where additional fuel is supplied, before the raw meal enters the rotary kiln, see Figure 2.34.

[17] Cement is to be understood as a synonym to Portland cement, which is a certain composition of lime and clay named by Joseph Aspdin in 1824.

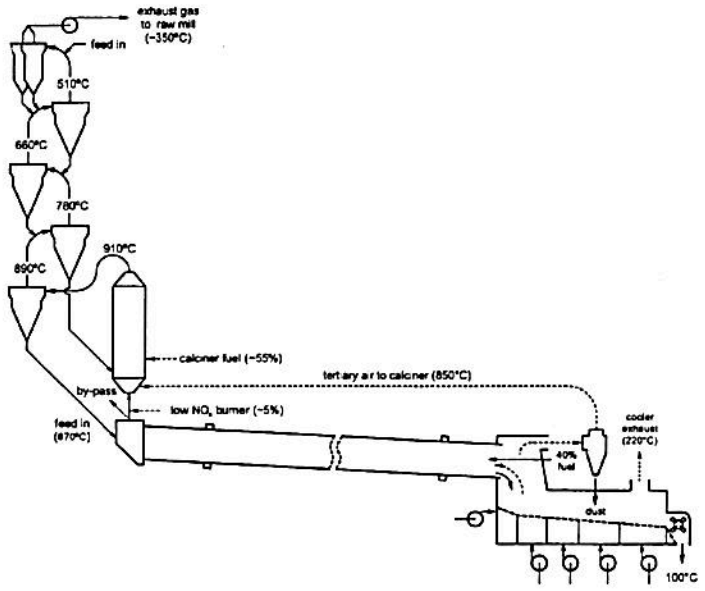

Figure 2.34: Sketch of a 5-stage air separate (AS) in- line calciner (ILC) system (Taylor & Isaksson 2001).

2.4.2 Alternative fuels

The production of cement is an energy intensive process. About 30 to 40 % of the production cost is derived from the primary fuel, usually pulverized coal, which is burnt in the rotary kiln.

After the energy crisis in the 1970s the pulverized coal was reintroduced in the cement production industry to substitute oil and gas. Due to the continued economic pressure on the cement manufacturers, a byproduct of the oil-refining cracking processes - petroleum coke - was also introduced (Lockwood & Ou 1993).

Today, combustion of solid and hazardous waste adds benefits to the cement manufacturers and the community by:

- conserving non renewable fossil fuels,
- using existing technology,
- recovering the energy in solid and hazardous waste,
- reducing manufacturing costs by charging a fee for the disposal and
- ensuring safe destruction of organic compounds.

It is generally recognized that all organic compounds are adequately destroyed if exposed to a temperature of 1200 $°C$ for 2 seconds under oxidizing conditions (Herat 1997), (Mantus 1992). The oxidizing conditions in a cement kiln exceed these requirements by a wide margin, which is due to the following (Mantus 1992):

- High temperature - in order to produce clinker for cement production it is necessary to reach a material and gas temperature of about 1450 and 2000 $°C$, respectively. Hence, the combustion gas temperature in cement kilns is much higher than in commercial incinerators.

- Intense turbulence - this facilitates mixing.
- Long gas residence time - 6 to 10 seconds is typical.
- High thermal capacity - temperature oscillations and sudden temperature reductions are avoided due to the amount of materials.
- Alkaline environment - emissions of HCl are significantly lower than from commercial incinerators due to the alkaline materials capturing acidic gases.
- A minimum of waste is generated. Combustion of hazardous wastes in commercial incinerators generates ash, which must be treated as hazardous waste. In the cement production process no ash is generated. And cement kiln dust collected by the flue gas clean-up system is usually returned to the kiln with the raw feed.

Application and types of alternative fuel

Alternative fuels can be used both in the main firing system at the primary burner and in the secondary firing system for calcining the raw meal.

Fine and liquid alternative fuels with sufficient heating value like e.g. liquid hazardous waste (LHW), waste oil, sewage sludge, refuse derived fuel (RDF), animal meal (AM) and plastic can be insufflated or atomized in the main burner. Long residence times and high material and gas temperatures are ideal combustion conditions, which ensure the destruction of the most stable compounds (Neumann 1992), (Liebl & Gerger 1993).

Coarse and low grade alternative fuels like e.g. solid hazardous waste (SHW), refuse derived fuel, animal meal, plastic, car tires, rubber, paper and biomass are preferably introduced into the precalciner or the kiln inlet. Substances requiring high destruction temperatures, such as hazardous waste, may not be used at the precalciner because the temperature is only between 800 and 1000 $°C$ (Neumann, Duerr & Kreft 1990).

Impact of fuel variations

Variations in the chemical properties of the fuel will always have an impact on the cement produced. A change in the fuel ash composition, for example, will have an effect on the clinker mineral phases[18] tricalcium silicate (C_3S), dicalcium silicate (C_2S), calcium aluminate (C_3A) and tetra calcium aluminoferrite (C_4AF), which determine the properties of the cement made from the clinker, such as strength development, workability and color (Turnell 2001).

Sulphur Fuel sulphur entering a dry kiln system usually exits the kiln as sulfates in the clinker and in the preheater bypass dust. Fuel sulphur is reported by Turnell (2001) to have little effect on the SO_2 emissions. Giugliano et al. (1999) and Inverardi (1993) report lower SO_2 emissions during utilization of car tires and RDF, respectively (Giugliano, Cernuschi, Ghezzi & Grosso 1999), (Inverardi 1993). However, Carrasco (1998) reports an increase in the SO_2 emissions during utilization of car tires (Carrasco, Bredin, Gningue & Heitz 1998). Brooks et al. (1992) reports 50 % reduction of SO_3 in the clinker during combustion of RDF. Decreases were also observed in the alkalies and in $CaSO_4$ as a direct result of the decrease in SO_3 (Brooks, Blankenship & Daugherty 1992). Also, an increase in the free lime

[18] In the cement industry, the following abbrevations are often used in order to simplify the complex formulas frequently occuring: $CaO \equiv C$, $SiO_2 \equiv S$, $Al_2O_3 \equiv A$, $Fe_2O_3 \equiv F$, $K_2O \equiv K$, $Na_2O \equiv N$ and $SO_3 \equiv \bar{S}$.

content of about 35 % was observed, because the raw mix content was not adjusted for the CaO content in RDF. Schwab et al. (1999) report that SO_2 emissions from cement plants range from less than 100 ppm to more than 600 ppm, depending on the raw materials, the scrubbing efficiency of the preheater tower and, to a much lesser degree, the combusted fuels (especially when calciners are involved) (Schwab, Wilber, Riley & Hawks 1999).

Chlorine Fuels with a higher content of chlorine, compared to coal, like e.g. RDF will possibly result in higher emissions of HCl and favour formation of PCDDs (polychlorinated dibenzodioxins) and PCDFs (polychlorinated dibenzofurans) (Lockwood & Ou 1993), (Inverardi 1993). However, in the experiments by Zorzi (1988), no increase in the amount of PCDDs and PCDFs was detected from the stack emissions (Zorzi 1988). Furthermore, it is stated that no consideration has to be taken to the clinker quality during utilization of RDF up to 50 %. It is suggested by Lockwood and Ou (1993) that the higher chlorine/hydrogen atom ratio in RDF compared to coal, will facilitate PAH (polynuclear aromatic hydrocarbons) and soot formation. Hence, combustion of RDF may produce a larger amount of PAH than coal combustion. Carrasco et al. (1998) reports that a blend of car tires and coal, compared to coal, lower the PCDD/PCDF and PAH emissions with 60 and 10 %, respectively.

Trace elements The heavy metal content of the waste may be higher than that of fossil fuels. During the combustion process, the metals may vaporize in the high-temperature combustion zone to form oxides and chlorides. Metal compounds can be categorized into three classes, based on the volatility of the metals and their salts (European Commision 1999):

1. Non-volatile (Ba, Be, Cr, As, Ni, V, Al, Ti, Ca, Fe, Mn, Cu and Ag). Non-volatile metal compounds remain within the process and exit the kiln as part of the cement clinker composition.

2. Semi-volatile (Sb, Cd, Pb, Se, Zn, K and Na). Semi-volatile metal compounds are partly taken into the gas at sintering temperatures to condense on the raw material in cooler parts of the kiln system. This leads to cyclic effects within the kiln system (internal cycles), which builds up to the point where an equilibrium is established and maintained between the input and the output via the clinker.

3. Volatile (Hg, Tl). Volatile metal compounds condense on raw material particles at lower temperatures and potentially form internal or external cycles, if not emitted with the flue gas of the kiln.

Volatile components (metal compounds) in alternative fuels (or materials) can evaporate, and are not readily bound in the clinker. Therefore, utilization of solid and hazardous wastes containing high concentrations of volatile metals (e.g. mercury, thallium) can result in an increase in the emissions of such metals (European Commision 1999).

Schäfer and Hoenig (2001) carried out long term Hg-balance trials for the first time on rotary kilns, and found for the plants investigated that (Schäfer & Hoenig 2001):

- the Hg inputs were determined essentially by the input via the raw meal,

- the majority of the Hg is collected in the dedusting system, so that a recirculating Hg system is formed between the preheater, raw mill and exhaust gas filter and

- it is expedient to remove some of the raw materials from the exhaust gas cleaning system in order to relieve the external recirculating Hg system and therefore to limit the Hg emissions. However, the removal of meal cannot be used to reduce the Hg emissions to any required level as the effectiveness of removing meal limits to the recirculating Hg system, which decreases with decreasing quantity of Hg in the external recirculating system.

Stephan et al. (2001) investigated the influence of Cr, Ni and Zn on the manufacture and use of cement and found that (Stephan, Knöfel & Härdtl 2001):

- concentrations of the heavy metals Cr, Ni and Zn, at levels many times higher than the natural levels in cement, showed no detectable changes in the pure clinker phases or the clinker,
- Ni and Zn increased the strength while Cr decreased the strength due to increased free lime formation and
- at extremely high additions (2.5 wt-%) changes occur in the clinker composition, or new phases are formed, which influence the cement hydration and the resulting mortar properties. Furthermore, Ni and Zn were almost completely fixed in the cement, while Cr leached out more readily and the concentration in the eluate rose in proportion to the total Cr content.

Phosphorus Utilization of animal meal in cement kilns has been tried out, with reported effects on cement quality due to the high phosphorus content. The CBR cement company in Belgium reports that increased presence of P_2O_5 in cement clinker, i.e. utilization of animal meal in the cement kiln, at levels above 1 % has negative influence on cement performance. Accordingly, to avoid negative consequences, it is suggested to limit the P_2O_5 content in clinker to 0.6 % (CBR 2001).

Similar experiments have been made on Kiln 6 in Brevik, where a lower tolerance level of 0.2 % P_2O_5 in the cement has been set (Thyholdt 2002).

Material build-ups Material build-ups are mainly due to chlorine (Cl), sodium (Na), potassium (K) and sulphur (S). These components evaporate in the burning zone and condense in the cooler area, such as the preheater tower and kiln feed end. Typically, the material build-ups are more evident when the molar ratio of sulphur and alkalies is not balanced. Low sulphur-to-alkali molar ratios tend to generate alkali build-ups in the kiln feed end area. Depending on the raw meal and alternative fuel composition this problem could be solved by adding a 'raw meal curtain' near the kiln feed. Feeding a portion of the raw meal from the second lowest cyclone near the kiln feed, gives a 'raw meal curtain', which quenches the kiln vent gases and the volatile elements. Another preventative measure to reduce build-ups is to install air cannons in the affected area of the kiln system (Turnell 2001).

In the Ph. D. thesis of Tokheim (1999), it is found that a supply of alternative fuels at the kiln inlet leads to reducing conditions. This promotes the decomposition of sulfates in the precalcined meal, and impedes capture of gaseous sulphur oxides by the meal. Hence, sulphur is transported to the precalciner by the kiln gas (from the kiln), where sulphur dioxide is converted to sulfate under oxidizing conditions and returned to the kiln. The increased level of sulfates in the precalciner leads to deposit formation (Tokheim 1999), (Hoenig et al. 1997).

Auxiliary equipment capacity The amount of combustion air needed per unit of fuel energy is larger for alternative fuels than for coal. Hence, the amount of alternative fuels fed may be restricted by fan capacity. A trade-off between lower

production and higher alternative fuel feeding is a possibility if the production plant benefits from alternative fuel fees.

Fuel feeding A first step in the effort to utilize alternative fuels successfully is to ensure a stable, continuous, balanced feed rate. Utilization of alternative fuels in cement kilns can very often give process disturbances due to an inadequate feeding system, e.g. due to fire protection, belt scale calibration errors and blockages in screw feeders, bends and flap valves. Such problems may, in a start-up period, take away focus from the role of combustion in the exploitation of alternative fuels in cement kilns.

Cement kilns vary in design, and alternative fuels come in various forms (e.g. fluffy, lumpy) and composition (e.g. moisture content), which means that a lot of the experience with alternative fuel feeding has to be regained at each new installation. However, experience with feeding systems for the main burner and for car tires at the kiln inlet are documented by several authors (Helmreich 2000), (Greco 2000), (Helmreich 2002), (Kaldeway 1985), (Hock 2001) and will not be discussed in detail here.

Preparation of different types of solid and hazardous waste fuels is usually performed outside the cement plant by the supplier or by waste-treatment specialist organizations. Since supplies of waste suitable for use as fuel tend to be variable whilst waste material markets are rapidly developing, it is advisable to control the composition by representative sampling. Harting (2000) reports that the Phoenix cement plant in Germany take grab samples from every load, and an automatic sampler collects samples from the metering belt. Harting (2000) found that by continuous analysis of all delivery samples, especially of chlorine, it was possible to reduce the chlorine content in the secondary fuels by 0.2-0.3 wt-% and increase the feed rate of alternative fuels by 2-2.5 ton/h (Harting 2000). Subsection 3.1.3 shows the importance of representative sampling on an RDF fuel feed stream at the cement plant in Brevik.

2.4.3 NO_x reduction in cement kiln

The two main categories for NO_x reduction in cement kilns are primary and secondary methods. The primary methods are applied to prevent formation of NO_x in the kiln burning zone, whilst the secondary methods convert NO_x in the post-combustion zone (precalciner).

The NO_x reduction techniques applied in precalciner cement kilns are:

- application of low NO_x burners, which is a primary method. Low NO_x burners are designed to reduce flame turbulence, delay fuel/air mixing, and establish fuel-rich zones for initial combustion. The longer, less intense flames resulting from the staged combustion, lower the flame temperature and reduces the thermal NO_x formation,

- reburning or so-called fuel-staged combustion, which is applied in the precalciner, as previously described in Subsection 2.1.6,

- selective non-catalytic reduction (SNCR). Reagents that contain NH_x (e.g. urea, ammonia etc.) are supplied into the precalciner (post-combustion gases) at temperatures between 830 and 1050 $°C$, and

- advanced reburning, which is a secondary method that combines reburning with selective non-catalytic reduction. Advanced reburning is previously described in Subsection 2.1.7.

The formation of NO_x in cement kilns are influenced by several factors besides temperature (Hoenig et al. 1997):

- oxidizing conditions,
- flame shape (main burner),
- combustion chamber geometry (design),
- raw materials - raw meal composition and degree of heterogeneity,
- fuels - physical (size) and chemical composition and
- plant operations

NO_x reduction in the cement industry has been investigated by several researchers and approached with different techniques and fuels (Neuffer 1994), (Scheuer 1987). NO_x reduction has been investigated at the precalciner cement kiln 6 at Brevik since the end of the 1980's. The investigations dealt with reburning fuels as: car tires, plastics, wood chippings and RDF in the precalciner (Høidalen 1990), (Syverud, Thomassen & Gautestad 1994), (Syverud, Thomassen & Høidalen 1994), (Tokheim 1999).

Modern plants in Europe today are built as precalciner kilns with separate tertiary air ducts, and equipped with staged combustion. It is stated that there is practically no further potential for NO_x reduction available in the primary methods due to the implementation of low NO_x burners during the past years (Hoenig, Hoppe & Bodendiek 2001*b*). However, research shows additional potential for NO_x reduction and understanding of the mechanisms of NO formation in the low NO_x burners (Smart & Jenkins 1999), (Gajewski & Hoenig 1999). In Cembureau, European cement manufacturers have been participating for several years in the work on lowering NO_x emissions, and Cembureau has developed a list of best available techniques (BAT) (Xeller 1999).

Several secondary methods are implemented and examined for further NO_x reduction in cement kilns. The most frequently implemented technique in conventional plants today is the SNCR process with ammonia water (Hoenig et al. 2001*b*), (Hoenig, Hoppe & Bodendiek 2001*a*). The so-called NO_xOUT (SNCR) technique applies urea pellets with successful results in precalciner kilns as well as preheater kilns (Steuch, Hille, Sun, Bisnett & Kirk 1996), (Harpe 1998). Lower specific costs (per ton clinker) for urea pellets than for ammonia water have been shown (Harpe 1998). Furthermore, investigations on the combination of staged combustion with the injection of ammonia water has proved successful in three full-scale experiments (Rose, Adler & Erpelding 2001). The previous work on SNCR in cement kilns has shown that there is a trade-off between reduced NO_x emissions and increased CO emissions, with a possibility of NH_3 slip.

Staged combustion, or so-called reburning has been employed for several years by the cement kiln manufacturers like e.g. KHD, Polysius and Technip-CLE. The major difference is the physical design of the cement kiln precalciners and preheaters. Investigations with staged combustion has proven to be well suited for NO_x reduction in precalciner cement kilns (Dusome 1995). Staged combustion with alternative fuels, like e.g. plastics, has proven to be successful (Tokheim, Bjerketvedt, Husum & Hoidalen 1998), (Jeschar, Jennes, Kremer & Kellerhof 1999). However, operational difficulties from interference with the internal sulphur cycles and the stepped raw meal feeding showed that utilization of alternative fuels in reburning needs closer attention than SNCR.

Remark

There is a scarcity on previous work regarding utilization of alternative fuels for NO_x reduction. Changes in NO_x emissions due to utilization of alternative fuels have been reported, but little investigations are made to understand the reasons and to investigate the possibilities for NO_x reduction with alternative fuels (Neumann 1992), (Schmidthals & Rose 2001). One statement is that fuels containing large amounts of fuel nitrogen will give large amounts of fuel-NO - without further consideration (Xeller 1999). Last statement seem to contradict the work of Zevenhoven et al. (2001) and will be addressed in this work.

Chapter 3

Full-scale experiments

Full-scale experiments in the precalciner of kiln 6 at Norcem Brevik were carried out in two campaigns; the first one in February 2001, the second one in April 2001. The experiments comprised:

- combustion of an alternative fuel with a high nitrogen content, namely animal meal (AM),
- combustion of solid hazardous waste (SHW) with and without injection of urea, the latter to obtain advanced reburning,
- temperature measurements along the flow direction of the precalciner during combustion of AM,
- traverse measurements of CO to obtain concentration profiles in the precalciner, and
- representative sampling of RDF.

The objective of this chapter is to document NO_x reduction experiments with solid alternative fuels used in the precalciner cement kiln 6 in Brevik. The first section gives a presentation of the precalciner characteristics and its flow regime to give an insight into the prevailing conditions, whereas the rest of the chapter is dedicated to the discussion of the experiments.

3.1 Precalciner kiln 6 in Brevik

3.1.1 Characteristics of kiln 6

Precalciner kiln 6 in Brevik is a so called "in-line calciner" (ILC), which means that the off-gas from the kiln is led through the precalciner (Tokheim 1999). A sketch of the precalciner kiln is shown in Figure 3.1. Raw meal is fed to the first cyclone stage of the system. In the cyclone tower the raw meal is dried and heated through the first three cyclone stages from about 50 °C to about 700 °C, before entering the precalciner. At the same time the gas, flowing in the opposite direction, is cooled from about 900 °C to about 350 °C. In the precalciner the meal is calcined in parallel flow with the gas at about 900 °C to a calcination degree of about 90 %. The meal then enters the rotary kiln, where the rest of the carbon dioxide is driven off. At the end of the rotary kiln the formation of clinker occurs from 1260 °C and upwards to about 1450 °C, as a result of the counterflowing gas with a maximum temperature of about 2000 °C. In the grate cooler the clinker is cooled down to approximately 150 °C. The cooling air is divided in three parts: secondary

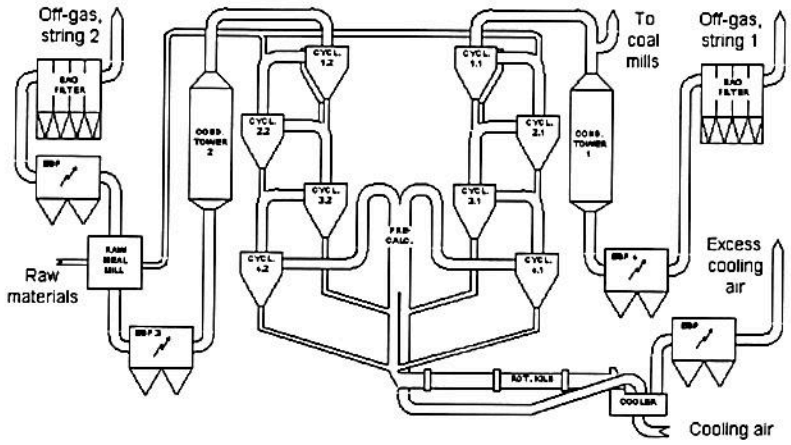

Figure 3.1: Precalciner kiln 6, Brevik, (Tokheim 2000*a*).

air, tertiary air and off-gas. Secondary air is heated to about 1000 °C and used for oxidation of the primary fuel in the main burner located at the end of the rotary kiln. Tertiary air is heated to about 800 °C and fed through the tertiary air duct into the precalciner for oxidation of secondary fuels. Off-gas is drawn through the cooler, exits at about 300 °C and is dropped to the surroundings (Tokheim & Bjerketvedt 1998*a*). Primary air is ambient air for feeding (and oxidation) of the fuels (e.g. coal and animal meal) in the main burner.

Characteristics of the precalciner kiln are presented in Table 3.1 and 3.2. Increasing flow rate through the rotary kiln and precalciner is due to the calcination of the raw meal in addition to the supply of tertiary air. False air, transport air and water vapor, which is supplied in the cooling tower and through the drying of raw materials, are the cause of the higher flow rate in the two chimneys.

Table 3.1: Characteristics of kiln 6, Brevik

Kiln length	68 m
Outer kiln diameter	4.4 m
Nominal production capacity	3300 tons clinker/day
Typical specific fuel consumption	3300 kJ/kg clinker
Approximate static pressure loss in the preheater	7000 Pa
Specific cooler load at nominal production capacity	48 tons clinker/m^2·day

Table 3.2: Gas flow characteristics of kiln 6, Brevik

Rotary kiln inlet	70.000 Nm^3/h
Rotary kiln outlet	100.000 Nm^3/h
Tertiary air duct	70.000 Nm^3/h
Precalciner inlet	170.000 Nm^3/h
Precalciner outlet	250.000 Nm^3/h
Chimney string 1	150.000 Nm^3/h
Chimney string 2	200.000 Nm^3/h

Solid feed characteristics are shown in Table 3.3, and the chemical composition

of the different fuels fed to the precalciner kiln is shown in Table 3.4.

Table 3.3: Solid feed characteristics of kiln 6, Brevik

Solid feed	Feeding point	Typical feed rate
Raw meal	Upper cyclone stage	220 tons/h
Coal mixture	Rotary kiln burner. Calciner, tertiary air side.	8-14 tons/h[1]
Liquid hazardous waste (LHW)	Rotary kiln burner	1-2 tons/h[2]
Solid hazardous waste (SHW)	Calciner, kiln riser duct	2-3 tons/h[3]
Refuse derived fuel (RDF)	Calciner, tertiary air side	2-6 tons/h
Waste oil	Rotary kiln burner	0-3 tons/h
Animal meal (AM)	Rotary kiln burner	2-4 tons/h
Diesel oil	Rotary kiln burner	Minor[4]

Table 3.4: Chemical composition of fuels fed to the precalciner kiln. Oxygen by difference. LHW = liquid hazardous waste; SHW = solid hazardous waste; RDF = refuse derived fuel; AM = animal meal; WO = waste oil.

Parameters	Unit	Coal	LHW	SHW	RDF	AM	WO
Moisture	% (as rec.)	2.80	45.70	10.70	25.00	4.50	0.00
Volatiles	%	31.60	100.00	46.30	53.0	59.70	100.00
C.fix	%	45.5	0.00	7.70	10.50	7.50	0.00
Ash	%	20.1	0.00	35.30	11.50	28.30	0.00
LHV	MJ/kg (as rec.)	24.74	17.88	15.75	18.0	15.80	41.60
C	wt-% (daf)	82.60	48.20	65.20	52.30	56.30	86.00
H	wt-% (daf)	5.80	10.40	9.80	6.60	8.30	12.00
N	wt-% (daf)	2.90	2.70	2.0	1.0	11.60	0.00
O	wt-% (daf)	7.60	35.70	21.80	39.0	14.40	0.00
S	wt-% (daf)	1.10	2.10	0.70	0.30	0.60	2.00
P	wt-% (daf)	-	-	-	-	8.30	-
Cl	wt-% (daf)	<0.1	1	0.5	0.8	0.5	<0.1
H/C	molar ratio	0.84	2.59	1.80	1.50	1.55	1.67
O/C	molar ratio	0.07	0.57	0.26	0.57	0.20	0.00
O/N	molar ratio	2.29	11.89	7.76	34.80	1.12	-
C.fix/Volat.	-	1.44	0.00	0.17	0.20	0.13	0.00

The coal mixture is a blend of pulverized coal (70-100%), petcoke (PC; 0-30%) and charcoal (0-10%), and is the main fuel in the primary burner and calciner. A typical coal mixture is 80 % coal, 15 % PC and 5 % charcoal. A typical composition (weight percent) of raw meal is about 75 % $CaCO_3$, 15.2 % SiO_2, 4 % Al_2O_3, 2.3 % Fe_2O_3, 2 % MgO, 0.6 % K_2O, 0.3 % Na_2O, 0.6 % SO_3 and 0.009 % Cl. The endothermic decomposition reaction of calcium carbonate into carbon dioxide and

[1] If there is no feed of alternative fuel. The feed rate of coal mixture is about 18 tons/h.
[2] Following permission from The Norwegian State Pollution Control Agency(SFT)
[3] Following permission from The Norwegian State Pollution Control Agency (SFT)
[4] Used during startup

calcium oxide at about 900 °C requires approximately 1.7 MJ/kg $CaCO_3$. The raw meal median and mean particle diameter are 25 and 50 μm, respectively, with a particle density of 2745 kg/m^3.

Typical emissions from the precalciner kiln are shown in Table 3.5 along with emission limits from The Norwegian State Pollution Control Agency (SFT) (Norcem 1999).

Table 3.5: Emission characteristics of kiln 6, Brevik

Component (mg/Nm^3@11%O_2)	Limit	2001 emissions[5]
Dust	40	8
Total organic carbon (TOC)	10	6.8
Chlorine compound calculated as HCl	10	5.9
Fluorine compound calculated as HF	1	0.15
SO_x calculated as SO_2	400	209
NO_x calculated as NO_2		707
Sum Cd + Tl	0.1	0.002
Mercury	0.1	0.016
Sum of other metals[6]	1.0	0.030
Dioxines	0.1[7]	0.078[8]

Traverse CO measurements

The traverse measurements were carried out in order to determine the CO concentration profiles in the precalciner. The measurements were made during combustion of AM, since experience has shown that combustion of this fuel in the calciner gives relatively high CO concentrations, thus giving more distinct concentration profiles compared to e.g. combustion of SHW.

Similar concentration profile measurements have been reported in a previous project (Tokheim 2000*b*), and the same sampling ports, as described in Table 3.6 and shown in Figure 3.2, have been used in the current CO measurements.

Table 3.6: Average fuel and solid feed into the precalciner kiln 6 during experiments.

Ports	Location	Gas residence time
1, 2	Square duct	0.50 sec.
3, 4, 5, 6	Square-to-circular transition	0.75 sec.
8, 9, 10, 11	Loop duct 1^{nd} part	1.74 sec.
12, 13, 14	Loop duct 2^{nd} part	2.07 sec.

The measurements were discontinuous in time and space. Measurements were taken 0.2, 0.8 and 1.8 m from the wall at ports 1 and 2, and 0.1 and 0.8 m from the wall at ports 3, 4, 5, 6, 8, 9, 10 and 11. It can be seen from Figure 3.3 that the CO concentration above the tertiary air channel (2) is decreasing 0.8 meter from the wall, in contrast to the measurement above the kiln riser duct (1).

The preheated meal from string 1 enters below port 1, which is opposite to port 3. The increase of CO concentration close to the wall at port 3 may be explained with the flow of preheated meal interfering with the flow of alternative fuels. A similar effect should have been observed at port 5, where the preheated meal enters opposite to and below port 2.

[5] Mean weight of string 1 and string 2
[6] Sb, As, Pb, Cr, Co, Cu, Mn, Ni, V, Sn
[7] I-TE ng/Nm^3
[8] I-TE ng/Nm^3

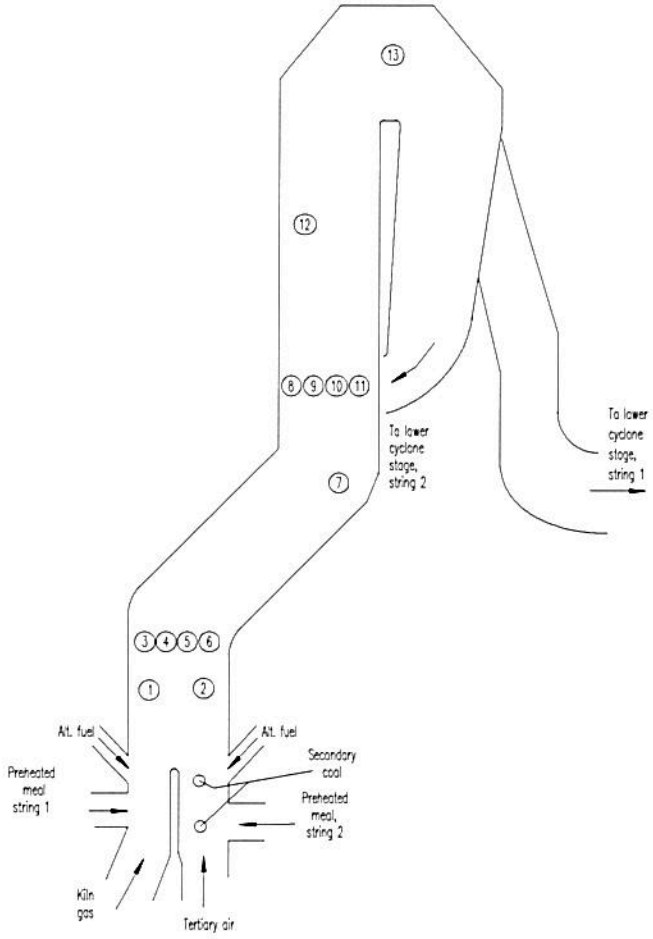

Figure 3.2: Sketch of the precalciner in Brevik showing sampling points 1 to 13 (Tokheim 2000*a*).

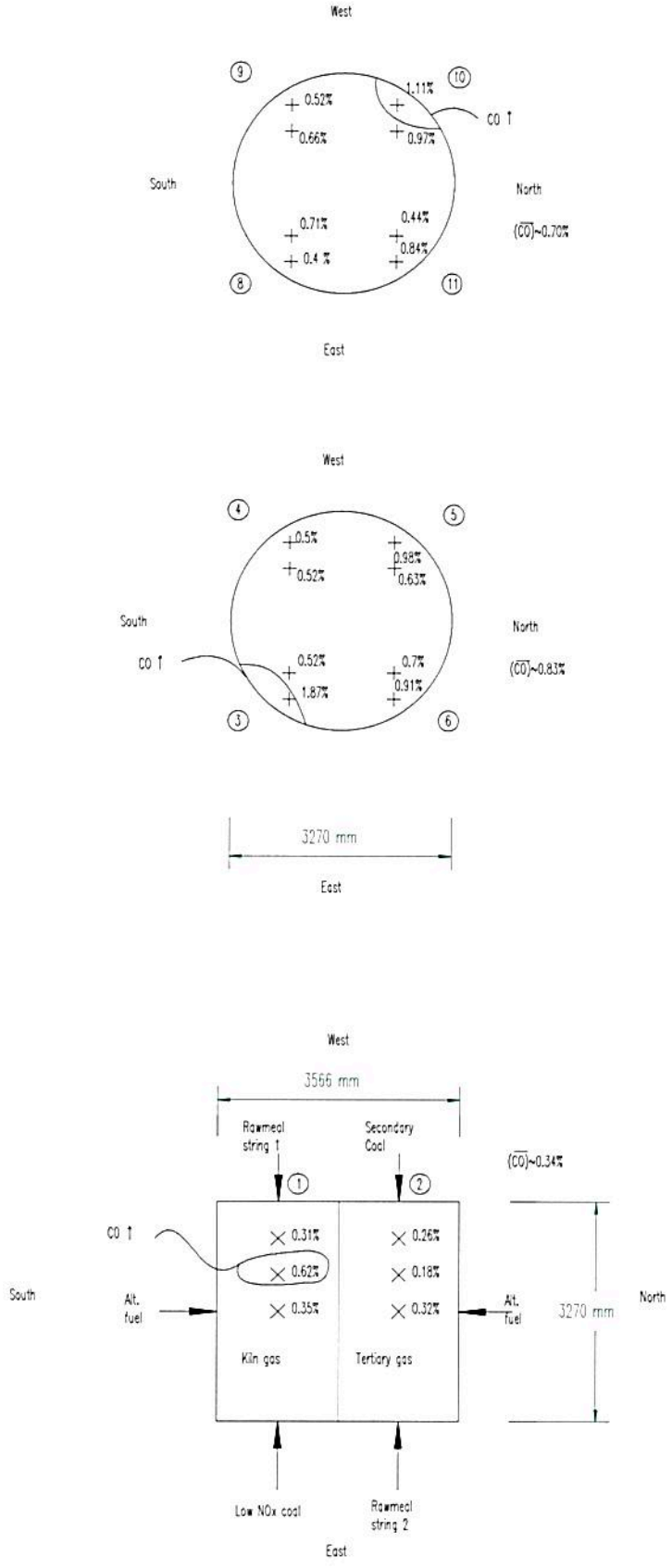

Figure 3.3: Traverse CO concentration measurements in the precalciner during combustion of animal meal.

The results from the concentration profile measurements in combination with CFD simulation results may reveal important details about the flow regime in the precalciner.

Axial temperature measurements

The temperature measurements along the flow direction of the precalciner during combustion of solid hazardous waste and animal meal were accomplished with the use of a thermoelement type K. The sampling ports are described in Table 3.7, with reference to Figure 3.2. Similar measurements in the same precalciner have also been carried out previously (Tokheim 2000*b*). The temperature results of experiment 13 and 16 are shown in Table 3.7.

Table 3.7: Average fuel and solid feed into the precalciner kiln 6 during experiments.

Port	Location	Gas residence time	# 13	# 16
	Above the alternative fuel inlet	0.33 sec	960 °C	938 °C
1	Square duct	0.50 sec	962 °C	911 °C
3	Square-to-circular transition	0.75 sec	NA	919 °C
9	Loop duct 1^{st} part	1.74 sec	821 °C	834 °C
12	Loop duct 2^{nd} part	2.07 sec	882 °C	881 °C
13	Loop duct 3^{rd} part	2.41 sec	875 °C	872 °C

3.1.2 Precalciner flow regime

Precalciner characteristics are presented in Table 3.8 and 3.9. Calculations of precalciner characteristics are based on the prevailing regime after joining the tertiary air channel and the kiln riser duct, see Figure 3.2. Figure 2.23 and 2.24 describe the contact regime and fluidization characteristics of the bed material as pneumatic transport and Geldard A particles, respectively. These are applied on the outer edge, hence the results have to be applied with precaution. The indication of pneumatic transport is supported by the void fraction being larger than in a typical CFBC reactor (Van der Meer et al. 1999).

Turbulence or dissipation generated by particles has to be considered because the particles are very small, and the solids fraction is in the region of two-way coupling, see Subsection 2.3.2 and Figure 2.26. This is a subject to be followed up by Euler-Euler CFD simulations in Chapter 5.

In consideration of the Re_D-number, there is obviously turbulence in the precalciner. Viscosity and velocity are the causes of the large Re_D-number. In calculations of the viscosity it is necessary to predict the various mole ratios of the main components in the precalciner. For subsequent comparison of dimensionless groups between the precalciner and the CFB reactor, a similar temperature, excess air ratio (λ) and fuel mix is assumed, see (Axelsen 2001*a*). It is taken into account that calcium carbonate decomposes into carbon dioxide and calcium oxide in the precalciner, whereas it is assumed an inert circulating mass in the CFB reactor.

[10] Based on average hydraulic diameter.

[11] Hydraulic mean diameter calculated for the upper part of the calciner.

[12] Terminal velocity (v_t). Its value is a unique function of the input parameters. Derivative of a force balance on a single particle with the use of Stokes law.

[13] Assumption according to Hundebøl et al. (1987).

Table 3.8: Characteristic parameters of the precalciner.

Parameter	Unit	Typical values	Reference
U_0	m/s	22[10]	(Tokheim 2000*a*)
G_s	$kg/m^2 \cdot s$	6.81	See table 3.3
d	μm	52	(Axelsen 2001*a*)
ρ_p	kg/m^3	2745	Appendix A
D	m	3.38[11]	(Tokheim 2000*a*)
ρ_g	kg/m^3	0.387	(Tokheim 2000*a*)
μ	$Pa \cdot s$	$4.08 \cdot 10^{-5}$	(Axelsen 2001*a*)
[12] $v_t = \frac{(\rho_p - \rho_g)d^2 g}{18\mu}$	m/s	0.057	(Geankoplis 1993)(?)
τ_s	s	9.2	Section 2.3.2[13]
τ_g	s	2.3	(Tokheim 2000*a*)
$U_{slip,mean} = \frac{U_0}{\varepsilon} - \frac{G_s}{\rho_p(1-\varepsilon)}$	m/s	15.81	(Lim et al. 1995)
P	Pa	-700	
T	$°C$	890	

Previous work on precalciner flow regimes is rather scarce compared to the work on CFB's. However, there are obvious similarities between the flow regime in a precalciner and the one in a CFB. It can be seen from the CFD simulations made by Giddings et al. (2000a and 2000b) that recirculation, backmixing of gas and solids and core-annulus flow in a precalciner are comparable to those in a CFB. The major differences are probably the solids loading and the particle distribution, hence the interparticle forces defining raw meal as cohesive. Therefore, it is important to be cautious in the use of empirical correlations and dimensionless groups that have been derived for CFB. Nevertheless, experiments on the influence of flow regime, like for example exit design, will probably apply for both precalciners and CFB reactors.

3.1.3 Representative sampling of fuels

It is generally accepted that alternative fuels, such as RDF, are less homogeneous, i.e. have a higher heterogeneity, than e.g. coal. Therefore, is it important for the cement industry to get correct information about trends in dispersion and fluctuation of some important values e.g., calorific value and contents of Hg, Cl, S, trace elements and alkali metals. The foundation of a precise analytical result is a representative sample. A lot of money is being spent on high tech analytical equipment that can analyze concentrations as low as ppb (10^{-9}) or ppt (10^{-12}). In contrast, samples for analysis are often picked up more or less randomly from containers and piles. It is obvious that an analytical result cannot be more precise than the samples taken for the analysis. Therefore, it is of interest to get information about the heterogeneity of the material and answering the question: how can a representative analysis sample be extracted from a continuous alternative fuel feed stream?

Figure 3.4 illustrates the general sampling problem of a flowing feed stream. The second and the third sampling steps are not problematic since there exists a lot of experience in splitting of lots. The critical point is the primary sampling step, since it is difficult to apply standard procedures.

Table 3.9: Characteristic dimensionless groups of the precalciner.

Dimensionless groups	Unit	Typical values	Reference
$Fr_D = \frac{U_0^2}{gD}$	[−]	14.60	
$\frac{U_0}{v_t}$	[−]	733	
$\frac{G_s}{\rho_p U_0}$	[−]	$1.128 \cdot 10^{-4}$	
$\frac{\rho_p}{\rho_g}$	[−]	7093	
$\frac{d}{D}$	[−]	$2.814 \cdot 10^{-6}$	
$Re_d = \frac{\rho_g U_0 d}{\mu}$	[−]	1.98	
$Re_D = \frac{\rho_g U_0 D}{\mu}$	[−]	$7.05 \cdot 10^5$	
ε	[−]	0.9996	(Axelsen 2001*a*)
τ_s/τ_g	[−]	4	(Hundebøl & Kumar 1987)
$U^* = U_0 \left[\frac{\rho_g^2}{\mu(\rho_s - \rho_g)g}\right]^{\frac{1}{3}}$	[−]	11.32	(Kunii & Levenspiel 1991)
$d_p^* = d_p \left[\frac{\rho_g(\rho_s - \rho_g)g}{\mu^2}\right]^{\frac{1}{3}}$	[−]	0.96	(Kunii & Levenspiel 1991)

Results of representative sampling

RDF is the main alternative fuel utilized on kiln 6. Hence, this fuel was selected as the adequate material to investigate. RDF is a shredded fuel derived from municipal solid waste (MSW). The MSW has been processed to remove metals, glass and compostables and shredding has been applied, resulting in a particle size of less than 30 mm. The material composition corresponds to the ASTM standard STP 832 for RDF-3. The RDF is delivered by trucks and discharged into reception bins, with subsequent transportation on conveyor belts to the precalciner, without further treatment.

During the period from the 5th to the 17th of January 2000, variographic experiments were carried out at kiln 6 in order to investigate the fluctuations of the RDF feed. The objective was to provide a representative sample with an average weight of 0.001 kg from a flowing stream of heterogeneous solid material with an average flow rate of 2,000 kg/h. A simple sampling system was implemented, sampling theory was employed in the design of a correct sampling plan, samples were taken, and variography was used in the estimation of the heterogeneity of the materials, see Appendix I.

Four systematic sampling campaigns were carried out. And, in order to compare the systematic sampling to the traditionally grab sampling from containers, grab samples were also taken during all sampling campaigns.

The results show that:

- the mean value of the gross calorific value and the chlorine content is constant in the long range,
- the cyclic fluctuation is about 5 minutes in the short range, which can be caused by an upstream process during preparation or delivery, hence
- a systematic sampling system with a sampling interval between 5 to 20 minutes would give representative samples,

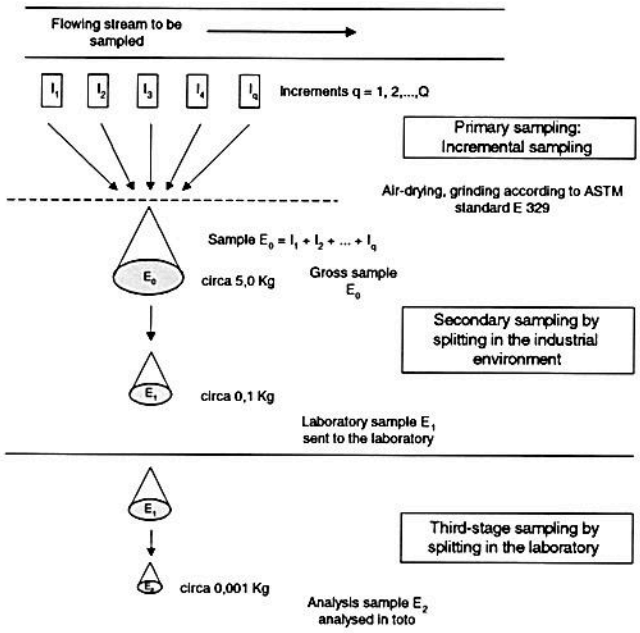

Figure 3.4: The general sampling problem (Gy 1998).

- a larger heterogeneity of the chlorine content leads to the question of the representativeness of the chlorine content determinations,
- the representativeness improved, with a factor of 10, in comparison to grab sampling from containers, thus grab sampling will not give representative sampling.

Control of feed streams is important for the stability of continuous process operations. This simple and relatively low-cost sampling system shows that there is a degree of uncertainty connected to the results from full-scale- as well as laboratory experiments.

(To accomplish laboratory CFBC experiments it is necessary to extract two tons of raw meal from the full-scale process. The extracted mass is not necessarily a representative sample of the continuous flow of raw meal being fed to the cement kiln. However, a representative extraction of that size would be very expensive and practically impossible within this program. But representative sampling should be carried out for experiments in small scale laboratory experiments, e.g. when a 100 mg sample or less is representing an annual deliverance of 40,000 tons. Accordingly, representative sampling of the fuels used in the laboratory CFBC reactor was executed.)

Raw meal is the major input flow in a cement kiln, with a large influence on the kiln operations. Kiln 6 at Norcem Brevik features an automatic sampling system for the raw meal feed. The next step for improved control of the kiln operations should be to install an automatic sampling system for the fuels as well.

Further details on representative sampling can be found in Part I (Appendix A).

3.2 Execution of combustion experiments

The experiments in the precalciner were accomplished with variation of the fuel feed and injection of urea to the kiln gas side according to Table 3.10, 3.11 and

3.12. The feed of the other fuels as well as the raw meal were kept approximately constant during the trials.

The reference condition is no feed of alternative fuel into the kiln gas side of the precalciner, as in experiment 1 and 8.

Experiment 2 and 9 are pure reburning trials, i.e. tests with no urea addition.

Experiment 3, 4 , 5 and 6 as well as experiment 10, 11, and 12 show increasing feed of urea to obtain advanced reburning (AR) rich. Each campaign was run for 30 minutes. Two longer-lasting AR trials were also executed, in experiment 16 (1 hour) and 17 (1 hour). By comparing these trials with trials 2 and 9, advanced reburning is compared with reburning.

Utilization of animal meal in the precalciner is shown in experiment 7 and 13.

Experiment 14 and 15 reveal the impact of using AM in the main burner on reburning and AR, respectively.

Details about the gas sampling method are found in Table B.1.

Table 3.10: Average fuel- and solid feed into the precalciner kiln 6 during experiments in February 2001.

Parameters		**No feed**	**SHW**	**SHW + 38 kg/h urea**	**SHW + 153 kg/h urea**	**SHW + 269 kg/h urea**	**SHW + 386 kg/h urea**	**AM**
		# 1	**# 2**	**# 3**	**# 4**	**# 5**	**# 6**	**# 7**
Coal$_{PrimaryBurner}$	t/h	4.1	3.6	3.8	3.8	3.6	3.5	4.2
Coal$_{Precalciner}$	t/h	9.9	9.0	9.7	8.8	9.2	9.0	8.9
LHW	t/h	1.5	1.7	1.8	1.8	1.8	1.8	1.5
SHW	t/h	0.0	3.0	3.0	3.0	3.0	3.0	0.0
RDF	t/h	2.9	2.5	2.0	2.3	2.0	2.0	3.1
AM$_{Precalciner}$	t/h	0.0	0.0	0.0	0.0	0.0	0.0	2.6
AM$_{PrimaryBurner}$	t/h	0.0	0.0	0.0	0.0	0.0	0.0	0.0
WO	t/h	2.5	2.6	2.2	2.2	2.5	2.7	2.5
Raw Meal	t/h	238	238	237	224	237	237	239

Table 3.11: Average fuel- and solid feed into the precalciner kiln 6 during experiments in April 2001.

Parameters		**No feed**	**SHW**	**SHW + 153 kg/h urea**	**SHW + 386 kg/h urea**	**SHW + 770 kg/h urea**	**AM**
		# 8	**# 9**	**# 10**	**# 11**	**# 12**	**# 13**
Coal$_{PrimaryBurner}$	t/h	6.0	8.0	8.0	8.0	8.0	8.0
Coal$_{Precalciner}$	t/h	8.0	5.0	6.0	5.0	6.0	6.0
LHW	t/h	2.0	0.0	0.0	0.0	0.0	0.0
SHW	t/h	0.0	4.0	4.0	4.0	4.0	0.0
RDF	t/h	4.0	6.0	5.0	6.0	6.0	6.0
AM$_{Precalciner}$	t/h	2.0	0.0	0.0	0.0	0.0	3.0
AM$_{PrimaryBurner}$	t/h	0.0	0.0	0.0	0.0	0.0	0.0
WO	t/h	0.0	0.0	0.0	0.0	0.0	2.0
Raw Meal	t/h	220	218	220	220	220	226

The urea pellets were fed into the precalciner at the kiln gas side along with

the alternative fuel (SHW) to obtain so-called advanced reburning rich. The proportioning of urea pellets was accomplished using a small screw feeder mounted on the SHW screw conveyor. The proportioning screw feeder is previously described by Axelsen (2001).

Table 3.12: Average fuel- and solid feed into the precalciner kiln 6 during experiments in April 2001.

Parameters		SHW # 14	SHW + 386 kg/h urea # 15	SHW + 153 kg/h urea # 16	SHW + 386 kg/h urea # 17
$Coal_{PrimaryBurner}$	t/h	7.0	6.0	7.0	7.0
$Coal_{Precalciner}$	t/h	5.0	4.0	5.0	4.0
LHW	t/h	1.0	1.0	1.0	2.0
SHW	t/h	4.0	4.0	4.0	4.0
RDF	t/h	6.0	6.0	5.0	6.0
$AM_{Precalciner}$	t/h	0.0	0.0	0.0	0.0
$AM_{PrimaryBurner}$	t/h	2.0	2.0	0.0	0.0
WO	t/h	1.0	0.0	0.0	0.0
Raw Meal	t/h	213	220	220	220

3.3 Experimental results and discussion

In this section, the main results from the full-scale experiments will be discussed. Further details can be found in Appendix B.

Figure 3.5, 3.6, 3.7 and 3.8 show decreasing NO_x[14], HCl and HF emissions throughout the experiments carried out in February (experiment 1 to 7) and April (experiment 8 to 13). A systematic trend of decreasing NO_2 with decreasing NO_x is however not observed. The average NO_2 emissions are about 1.6 % of the total NO_x emissions for all experiments.

An illustration on the development of NO_x and CO emissions during the advanced reburning experiments is shown in Figure 3.9 and 3.10, respectively.

The experiments with animal meal in the precalciner as reburning fuel showed up to 63 % (# 12) reduction in NO_x emissions while the CO emissions increased, see Table 3.13. It is believed that the NO_x reduction with animal meal is most likely to originate from NH_3 released during devolatilization. Thus, the NH_3 released during combustion of animal meal may follow a similar reduction route as in advanced reburning or selective non-catalytic reduction. As will be shown in Chapter 4, the laboratory experiment results support this.

Different average NO_x levels at the kiln inlet in the February and April campaigns are probably due to variation in primary burner flame temperature, which brings about a change in the formation of thermal NO_x. The change in flame temperature may be due to several factors, such as different secondary air temperature, fuel composition, heating value, main burner configuration, materials composition, ambient (outside) temperature and weather.

There is a substantial overall NO_x reduction when animal meal is supplied to the main burner in combination with reburning and advanced reburning in the

[14] $NO_x = NO + NO_2$

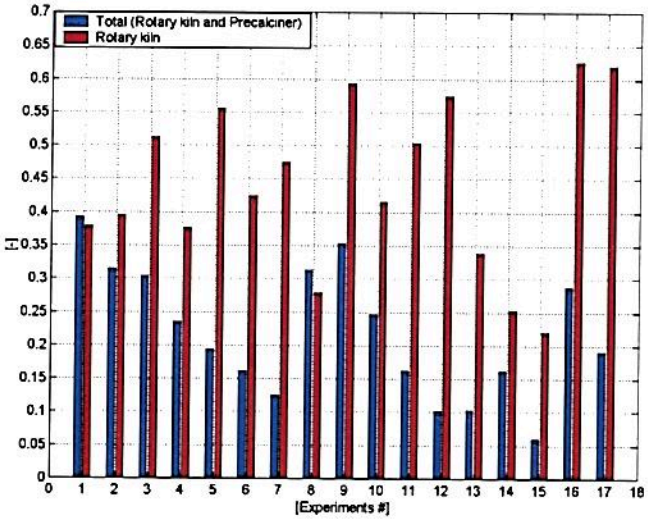

Figure 3.5: Ratio of N emitted and fuel-N supplied ($\kappa_{N-ratio}$) during experiment 1 to 17.

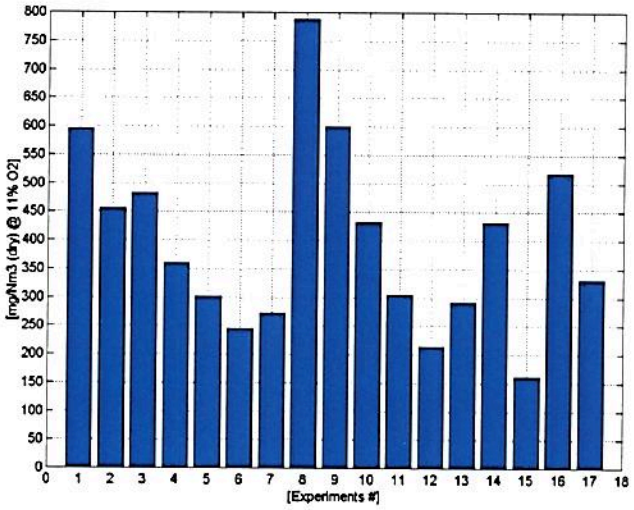

Figure 3.6: NO_x emitted from kiln 6 during experiment 1 to 17.

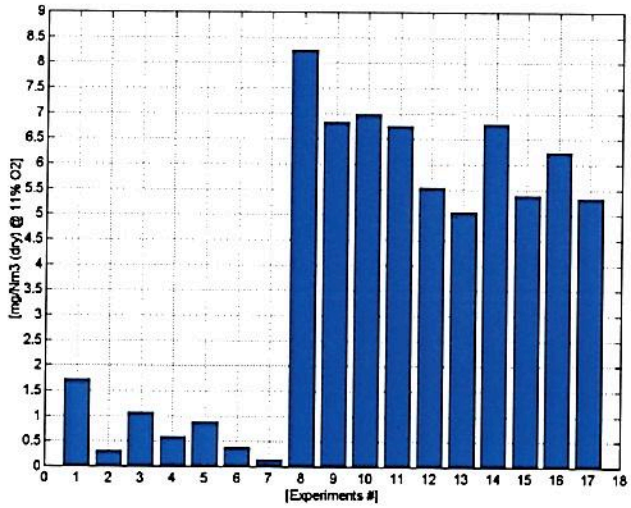

Figure 3.7: HCl emitted from kiln 6 during experiment 1 to 17.

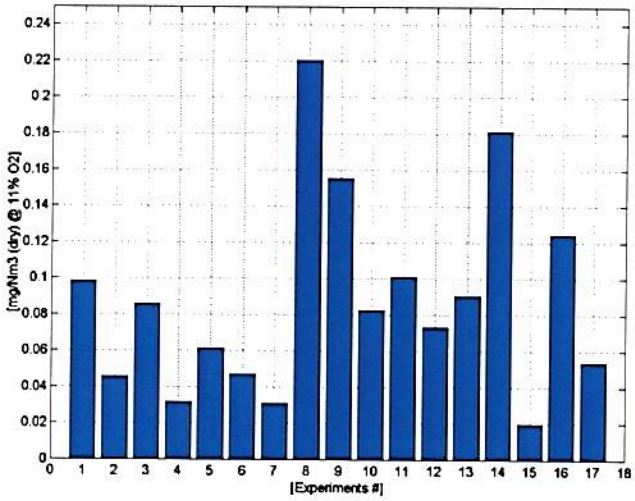

Figure 3.8: HF emitted from kiln 6 during experiment 1 to 17.

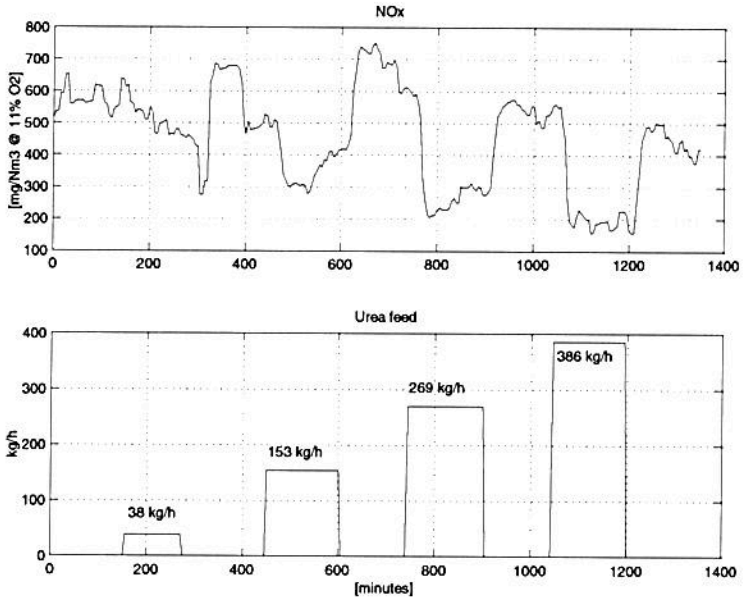

Figure 3.9: NO_x emissions during alteration in urea feed into kiln 6 for experiments 10, 11, 12, 16 and 17 (April campaign).

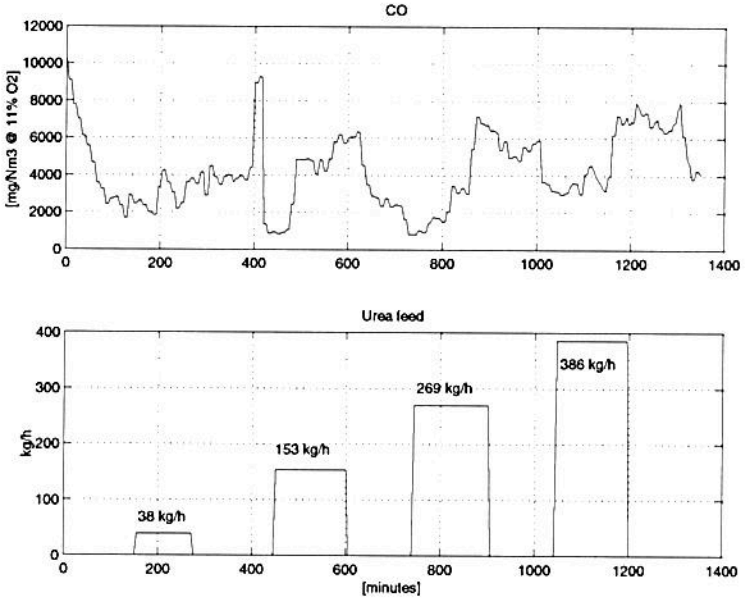

Figure 3.10: CO emissions during alteration in urea feed into kiln 6 for experiments 10, 11, 12, 16 and 17 (April campaign).

Table 3.13: Alteration in the emissions of NOx, CO, NH3 and the molar ratio of urea/NO into the precalciner during experiments in February and April 2001. Showing alteration between the reference exeperiment 1 and and 8 for the February and April campaign, respectively.

Experiment		NO_x	CO	NH_3 emission	$(Urea/NO)_{in}$
		Alter. %	Alter. %	mg/Nm^3	mol/mol
# 1	No feed (ref.)	0	0		
# 2	SHW	-22	85		
# 3	SHW + 38 kg/h urea	-17	21		0.36
# 4	SHW + 153 kg/h urea	-38	64		1.75
# 5	SHW + 269 kg/h urea	-48	27		2.46
# 6	SHW + 386 kg/h urea	-58	66		3.62
# 7	Animal Meal	-53	130		
# 8	No feed (ref.)	0	0		
# 9	SHW	-24	644	2.6	
# 10	SHW + 153 kg/h urea	-45	458	25.7	1.30
# 11	SHW + 386 kg/h urea	-61	753		1.51
# 12	SHW + 770 kg/h urea	-73	998	37.9	2.72
# 13	Animal Meal	-63	865	62.9	
# 14	SHW	-45	432	1.1	
# 15	SHW + 386 kg/h urea	-80	1402		1.54
# 16	SHW + 153 kg/h urea	-34	451		0.52
# 17	SHW + 386 kg/h urea	-58	826		1.32

precalciner. The overall NO_x reduction with animal meal in the main burner can not be explained with lower NO_x concentrations in the kiln inlet, since the relative reduction in the kiln inlet is only 4 % and 2 % compared to the overall reduction of 21 % (# 9 vs. # 14) and 19 % (# 11 vs. # 15). A combination of animal meal in the main burner and advanced reburning in the precalciner gives up to 80 % (# 14) in NO_x reduction in comparison to 73 % (# 11) with no AM in the main burner (and twice the amount of urea), see Table 3.13. The increased amount of NH_3 released by the animal meal in the main burner probably follows the reduction route of SNCR in the rotary kiln, as in the precalciner.

The HCl and HF emissions show a decreasing trend with increasing supply of urea into the precalciner. It is believed that the ammonia reaction will dissipate hydrogen radicals, thus the chlorine and fluorine finds other elemental forms. Furthermore, a surplus of ammonia will probably (in addition) convert HCl to NH_4Cl (Zevenhoven 2001). Neither of these components are measured.

CO and TOC show increased emissions during experiments of advanced reburn-

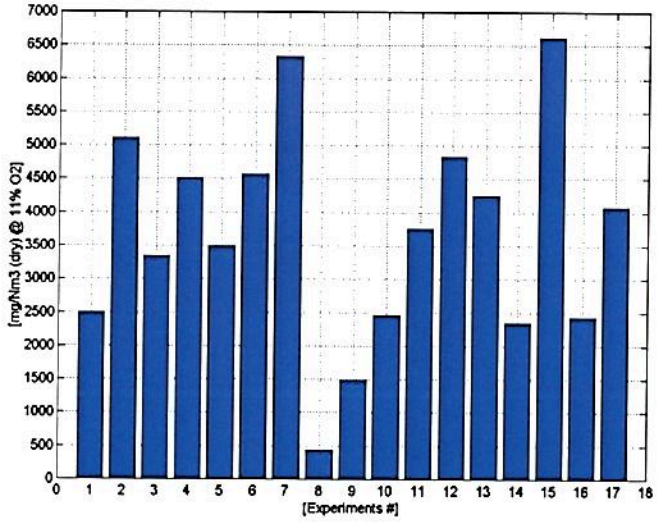

Figure 3.11: CO emitted from kiln 6 during experiment 1 to 17.

ing and combustion of animal meal in the precalciner and main burner, see Figure 3.11. The increasing amount of ammonia in the process, which leads to a competition for the OH radicals, is most probably the reason for the increased CO emissions. It can be shown from the reaction rate constants that the primary reduction reaction for ammonia is about ten times faster than the CO oxidation, see Figure 3.12. An evaluation of the primary abstraction reaction rate for NH_3 and the CO oxidation can be found in Appendix F. Furthermore, increased CO levels in the kiln inlet, when animal meal is supplied in the main burner, are also observed.

The excess air ratio in the reburning zone at the kiln gas side is mainly varying between 0.65 and 0.87 during the experiments. Chen et al. (1998) indicated optimum conditions for NO reduction (AR) with reaction temperatures at 800 $°C$, a stoichiometric ratio of about 0.99 and minimal air addition to give slightly fuel lean conditions (SR =1.02). It is reasonable to believe that a higher excess air ratio in the reburning zone at the kiln gas side during experiments would decrease the CO emissions and probably result in a higher NO_x reduction, nevertheless a substantial NO_x reduction has been achieved.

The injection temperature (938 to 960 $°C$) of alternative fuel and urea in the precalciner is optimal compared to what is recommended from previous experiments, see Figure 2.20 (Maly et al. 1999). Furthermore, it is reported that low overfire air temperature (893 $°C$), equivalent to the tertiary air gas side of the precalciner (about 800 $°C$), improves NO_x reduction.

The ammonia emissions were measured during five experiments and showed an increasing trend with increasing supply of urea and combustion of animal meal in the precalciner, see Table 3.13 and B. The highest ammonia emissions originate from combustion of animal meal in the precalciner, corresponding to 34.3 % of the NO_x reduction. In comparison the ammonia slip is small when animal meal is supplied into the main burner, only 0.8 % of the NO_x reduction. The slip of ammonia during combustion of animal meal, in comparison with SHW, could support that a low O/N ratio signify a smaller HCN/NH_3 ratio release during pyrolysis.

It can also be shown that an increasing molar ratio of $(\text{urea}/NO_{kiln\ inlet})$ lowers the NO_x emissions, see Figure 3.13 and Table 3.13.

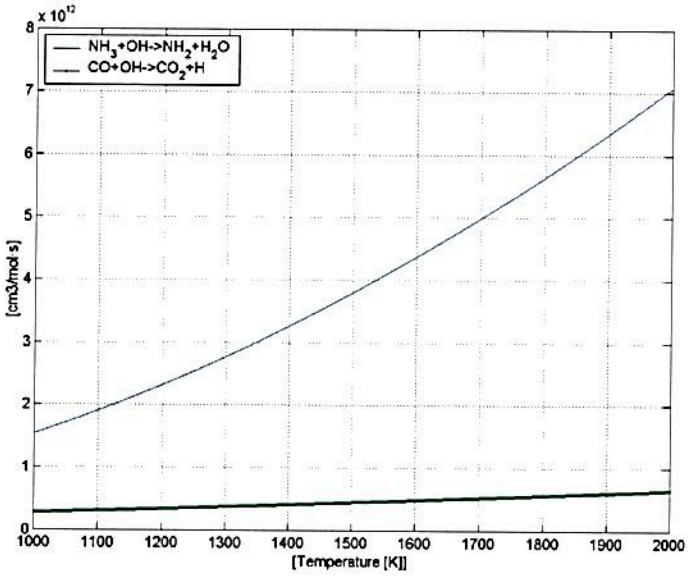

Figure 3.12: Comparision between the reaction rate constant for reaction: $CO + OH \rightarrow CO_2 + H$ and $NH_3 + OH \rightarrow NH_2 + H_2O$ (Warnatz et al. 1999).

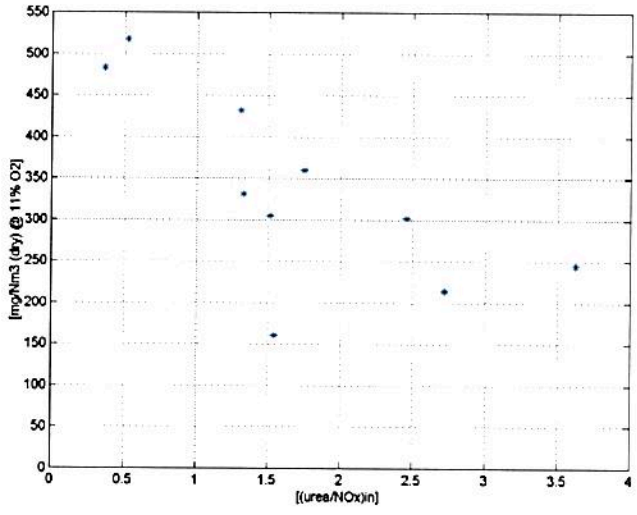

Figure 3.13: NO_x emission concentration as a function of the molar ratio (urea/NO_{in}).

The nitrous oxide emissions are fairly stable during advanced reburning and combustion of animal meal in the main burner, in contrast to combustion of animal meal in the precalciner - except for the last period. Alteration of the urea feed does not influence the nitrous oxide emissions. The nitrous oxide emissions during advanced reburning, reburning combined with combustion of animal meal in the main burner (two experiments) and combustion of animal meal in the precalciner give 46, 49, 24 and 74 mg/Nm^3, respectively. The parallel emission measurements with reburning combined with combustion of animal meal in the main burner show that measurements for a long period, 12 hours apart, under approximately similar conditions give a high element of uncertainty for the nitrous oxide emissions. It is difficult to state whether the uncertainty is caused by the measurement technology or process operations. However, the measurements contribute with relative values during experiments. No correlation between CO and N_2O emissions was observed.

3.4 Conclusion of full-scale experiments

The following can be concluded from the full-scale experiments:

- Advanced reburning and combustion of animal meal in the precalciner are well suited for NO_x reduction in the precalciner kiln 6 at Norcem Brevik, with up to 73 and 63 % NO_x reduction, respectively.
- Combustion of animal meal in the main burner gives additional overall NO_x reduction and lowers the NO_x concentration in the kiln inlet, even though AM gives a significant increase in fuel-nitrogen supply.
- Combustion of animal meal probably follows a similar reduction route as in advanced reburning or selective non-catalytic reduction because of a low HCN/NH_3 ratio.
- A change in the main burner flame temperature may be the reason for alteration of the NO_x level in the kiln inlet.
- Increasing amounts of ammonia in the process lead to a competition for the OH radicals, which probably is the reason for increased CO and TOC emissions.
- The reduction in HCl may be explained by the formation of e.g. NH_4Cl and/or increased amount of $CaCl_2$ in the precalciner.

The optimum NO_x reduction would be:

- optimal flame temperature at the main burner,
- control of the excess air ratio in the reburning zone at the kiln gas side of the precalciner and
- control of the $(NH_3/NO_{kiln\ inlet})$ ratio or $(\text{urea}/NO_{kiln\ inlet})$.

This will give lower NO_x, CO, TOC, HCl, HF and NH_3 emissions during advanced reburning or combustion of alternative fuels on the kiln gas side of the precalciner. It is recommended to utilize animal meal in the main burner and on the kiln gas side of the precalciner since it will reduce the expense of a secondary NO_x reduction agent as for instance urea.

Chapter 4

Laboratory experiments

The objective of this chapter is to document:

- the laboratory experiments, carried out in order to characterize solid alternative fuels used in the precalciner cement kiln 6 in Brevik,
- the CFBC reactor developed for this purpose, and
- a comparative study of the CFBC reactor and the precalciner at Norcem Brevik.

  The main purpose is to investigate different fuels characteristics during:

- reburning,
- advanced reburning and
- combustion without circulating mass[1].

Laboratory experiments were executed at Telemark University College, using the CFBC reactor described in Section 4.1. The experiments were carried out in two campaigns; the first in the autumn of 2000 and the second in the autumn of 2001. The experiments comprised:

- introductory experiments with and without inert circulating mass; the latter with wood chipping,
- reburning with refuse derived fuel (RDF), coal, animal meal (AM) and mixtures of RDF/AM, Coal/AM and char coal (CC)/AM,
- advanced reburning rich with RDF and coal,
- combustion of RDF, coal, AM and solid hazardous waste (SHW) without circulating mass in the riser

4.1 The CFBC reactor

The CFBC reactor is to be understood as the complete experimental installation.

[1] Circulating mass is, in this thesis, to be understood as the solid material (inert and/or raw meal) fed to the BFB and lifted up into the riser (CFB) for collection after the cyclone. There are continous feed of fresh circulating mass.

4.1.1 Design determining characteristics

Physical similarity and limitation

The goal is to achieve similarity between the precalciner and the CFBC reactor. Parameters of major importance in this context are:

- temperature (T),
- pressure (p),
- particle- and gas retention time (τ_s, τ_g),
- particle size distribution,
- turbulence,
- void fraction (ε),
- gas composition,
- reactive- versus inert circulating material.

In order to limit the complexity of the CFBC reactor it was chosen to run the process with a blend of inert circulating material and raw meal, hence the mole fraction of carbon dioxide is less than in the precalciner because of the decomposition of the calcium carbonate. This can be compensated with the supply of carbon dioxide to the CFBC reactor, hence the gas composition will be approximately the same as in the precalciner.

To achieve a particle size distribution of circulating mass similar to the preheated meal, the sand quality of Millisil®M6 was chosen, see (Axelsen 2001*a*). Mean- and median particle size of Millisil®M6 are 50.2 and 30 μm, respectively. In comparison preheated meal has a mean- and median particle size of about 52 and 25.7 μm, respectively.

The void fraction (ε) of particles in the CFBC reactor mainly depends on exit design, particle distribution, superficial gas velocity (U_0) and solids circulation rate (G_s). All of these parameters obviously reflect the ratio of the particle- and gas retention time (τ_s/τ_g). As a consequence of this, it was chosen to operate the CFBC reactor with the same gas retention time (τ_g) and to control the void fraction (ε) by measuring the static pressure drop.

The temperature and pressure in the CFBC reactor will be almost the same as in the precalciner, but there will be some differences in temperature profiles since the CFBC reactor is operated with inert circulating mass.

The turbulence in the CFBC reactor will be much less than in the precalciner due to lower velocity.

Consequence of dissimilarity

The above mentioned physical similarities and limitations can be summarized with the 3 T's; Temperature, Time and Turbulence.

The consequence of not achieving the same turbulence level will probably affect the particle retention time and the diffusion of oxidizer to the fuel particles.

Utilization of inert circulating material will affect the heat and mass transfer, which affects the drying and devolatilization of the fuel particles. It will be of interest to carry out experiments with a blend of raw meal and Millisil®M6 to determine the temperature profiles in the CFBC reactor, and compare these to the temperature profiles in the precalciner measured by Tokheim (2000b). It will also be of interest to investigate if the difference in gas composition (different volume fraction of CO_2) affects the burnout of particles.

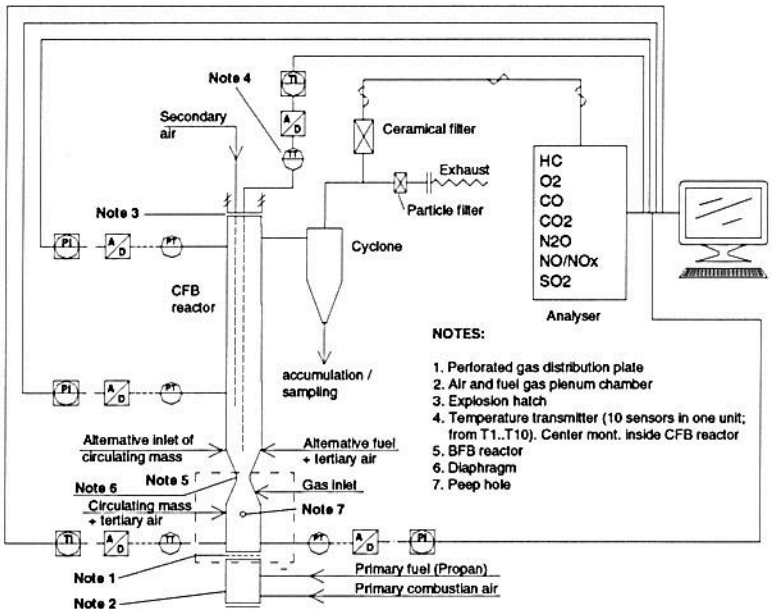

Figure 4.1: Sketch of the CFBC reactor.

Physical design

The physical design is limited by manpower, laboratory height and supply of combustion air, i.e. one person, 6 m and 45 kg/h, respectively.

For the following discussion, a sketch of the CFBC reactor is shown in Figure 4.1. A supplementing dimensional sketch and a PID can be found in (Axelsen 2001*a*).

Process description

In order to attain a similar flow regime, temperature and gas composition as from the rotary kiln into the precalciner, the CFBC reactor is split in two sections; a lower bubbling fluidized bed (BFB) and an upper circulating fluidized bed (CFB). A diaphragm is installed between the BFB and the CFB to retain combustion of solid fuel in the riser when the solid fuel is fed into the CFB, and a more even distribution of circulating mass when the circulating mass is fed into the BFB.

It was chosen to feed both the alternative fuel and circulating mass into the CFBC reactor with screw feeders (K-TRON-SODER-K2MVS60) having screw diameters of 15 and 25 mm, respectively. A screw feeder limits preheating and circulation of the circulating mass; on the other hand it gives good control of the influx of circulating mass (G_s). Hence, if G_s is controlled, the nature of the riser flow is isolated from other parts of the CFB and is a unique function of the input parameters and geometry of the riser and its exit.

Primary combustion air and primary fuel (propane) are fed to the plenum box and premixed before entering the BFB. This plenum box is connected to the BFB with a pair of flanges. A distribution plate is installed between the two flanges. Detailed design of the BFB is reported earlier (Axelsen 1998).

Below the diaphragm it is possible to feed alternative gas and extract gas samples. An alternative inlet for circulating mass in the opposite position of the alternative fuel inlet is also installed. Both the circulating mass inlet and the alternative

fuel inlet are equipped with tertiary air, which contributes to feeding the solids into the CFBC reactor. Secondary air is supplied through a 6 mm pipe mounted inside the CFB and flows out 0.5 m above the diaphragm. It is also possible to supply secondary air through the mid pressure sensor.

The CFBC reactor is equipped with three pressure sensors (Druck PTX 1400) with a range of 100 mbarg. The lowest pressure sensor is mounted just above the distribution plate, the mid pressure sensor 2 m above the distribution plate and the upper pressure sensor 4.46 m above the distribution plate.

Along the axis of the CFB is mounted a temperature transmitter with 10 sensors (Multi element TK-6.0-Multi-10-TK-1). There is one sensor for every 0.45 m, starting with measuring temperature 0.2 m below the feed point for alternative fuel. Furthermore, in the BFB, just above the distribution plate, a temperature transmitter is mounted to assure a temperature below 950 °C.

The exit of the CFBC reactor is executed with a 90° sharp connection (short extension blind T). At the exit is mounted a cyclone, which is described earlier (Lidal, Kleppe, Bjørnson & Andreassen 2000). At the cyclone exit, a filter cell is connected to remove the smallest particles before the exhaust gas is released to the surrounding.

At the exit of the cyclone, a part of the flue gas is drawn through a ceramic filter and a tube with heating jacket into a Hartman & Braun (H&B) emission analyzer. The H&B is equipped with:

- two Uras 14 NDIR analyzers for measurement of CO, CO_2, SO_2, N_2O and NO,
- a Multi-FID-14 for measurement of hydrocarbons (HC),
- an electrochemical cell for measurement of O_2,
- a NO_x/NO converter CGO-K.

Details of the H&B analyzer are reported previously (Feria, Loland, Pleym, Thoresen & Ulltang 1999), (Broll 2000).

Sampling of emissions, temperatures and pressures are made possible with an ADAM modular system for serial communications, with a sampling frequency of 500 $msec^{-1}$, see principle drawing in (Axelsen 2001*a*). The sampling data are made available through Delphi and processed in Matlab, see Matlab scripts in (Axelsen 2001*a*).

The combustion air is provided through a compressor installation. Before entering the CFBC reactor, the combustion air flows through an air drier and a filter which removes particles larger than 0.01 μm. The maximum oil content after the filtration is 0.01 ppm.

The flow rate of primary fuel (propane), primary-, secondary- and tertiary air are controlled with flow meters mounted on pressure reducing valves.

The construction material selected is acid resistant AISI 316 L steel tube with main dimension 114.3×2.0. Alkalies in the circulating mass and fuels may dissolve chromium oxide, which will result in minor holes. An inner ceramic lining might have been installed, but vanadium tends to have an equivalent effect on the ceramics as the alkalies have on stainless steel. However, the main problem with the choice of material is not degradation, but rather catalytic effects affecting the emission measurements. On the other hand, the effect on the emission measurements is believed to be small compared to other effects, for instance reproducibility of experiments (fuel combustion, circulating mass, exhaust draft etc.) and measurement equipment (calibration, stability etc.), so no lining is installed.

The CFBC reactor is insulated all the way from the BFB and up to the explosion hatch with two layers of insulation and an outer encasing. Details of the insulation are shown in Lidal et al. (2000).

4.1.2 CFBC regime

The CFBC reactor characteristics are presented in Table 4.1 and 4.2. The calculated CFBC reactor characteristics are based on the prevailing regime after the diaphragm, see Figure 4.1.

Table 4.1: Characteristic parameters of the CFBC reactor.

Parameter	Unit	Typical values	Reference
U_0	m/s	1 - 4	Experimental value
G_s	$kg/m^2 \cdot s$	0 - 1.6	Experimental value
d	μm	50.2	(Axelsen 2001*a*)
ρ_p	kg/m^3	2650	(Axelsen 2001*a*)
D	m	0.11	Design criteria
ρ_g	kg/m^3	0.31 - 0.35	Variabel with temperature in CFBC reactor
μ	$Pa \cdot s$	$3.9865 \cdot 10^{-5}$	(Axelsen 2001*a*)
g	m/s^2	9.81	
$v_t = \frac{(\rho_p - \rho_g)d^2 g}{18\mu}$	m/s	0.060	(Geankoplis 1993) and (?)
τ_s	s	4.4 - 8.8	Assumptions according to Hundebøl et al. (1987)
τ_g	s	1.1 - 4.3	Experimental value
$U_{slip,mean} = \frac{U_0}{\epsilon} - \frac{G_s}{\rho_p(1-\epsilon)}$	m/s	2.87	(Lim et al. 1995)
P	Pa	900	
T	$°C$	910	

Figure 2.23 and 2.24 describe the contact regime and fluidization characteristics of the bed material as pneumatic transport and Geldard A particles, respectively. These figures apply somewhat better for the CFBC reactor than for the precalciner because of the difference in velocities between the CFBC reactor and precalciner. The indication of pneumatic transport is supported by the high void fraction, which is determined experimentally by measuring the static pressure drop in the reactor.

The argument for using static pressure drop to calculate the void fraction is the investigation by Arena et al. (1986) and Yang (1988), shown in Figure 2.28, cited in (Lim et al. 1995). It can be seen from Figure 2.28 that for pneumatic transport the dilute phase is approximately constant through the riser, except in the acceleration region, which is prevailing in the first quarter from the inlet. Hence, from the dimensional sketch in Axelsen (2001) it can be seen that the mid pressure sensor is placed with a good margin above the acceleration region.

It has been shown in previous investigations (Axelsen 1998) that there is no slugging in the BFB. Slugging in the CFB is not a problem since it is a dilute-phase transport with small particles ($d < 60\mu m$) and the superficial gas velocity is larger

Table 4.2: Characteristic dimensionless groups for the CFBC reactor.

Dimensionless groups	Unit	Typical values	Reference
$Fr_D = \frac{U_0^2}{gD}$	[−]	0.93 - 14.83	
$\frac{U_0}{v_t}$	[−]	16.7 - 66.7	
$\frac{G_s}{\rho_p U_0}$	[−]	$3.77 \cdot 10^{-5}$ - $1.51 \cdot 10^{-4}$	
$\frac{\rho_p}{\rho_g}$	[−]	8548 - 7571	
$\frac{d}{D}$	[−]	$1.24 \cdot 10^{-4}$	
$Re_d = \frac{\rho_g U_0 d}{\mu}$	[−]	0.12 - 0.48	
$Re_D = \frac{\rho_g U_0 D}{\mu}$	[−]	854 - 5700	
$\varepsilon = 1 - \frac{\Delta P_R}{g \rho_s L}$	[−]	0.95	Target: Similar to Precalciner (Experimental value)
τ_s / τ_g	[−]	4	Assumptions according to Hundebøl et al. (1987)
$U^* = U_0 \left[\frac{\rho_g^2}{\mu(\rho_s - \rho_g)g} \right]^{\frac{1}{3}}$	[−]	0.49 - 1.96	(Kunii & Levenspiel 1991)
$d_p^* = d_p \left[\frac{\rho_g(\rho_s - \rho_g)g}{\mu^2} \right]^{\frac{1}{3}}$	[−]	0.86	(Kunii & Levenspiel 1991)

than the choking velocity (Grace et al. 1997). The choking velocity is found to be approximately 0.12 m/s using Equation 2.92 and parameters in Table 4.1.

Turbulence and dissipation affected by particles has to be be considered since the solids fraction is in the regime of two-way coupling, see Subsection 2.3.2 and Figure 2.26. Dissipation has to be considered because the particles are very small (20 % of the particles are less than 10 μm). Considering the Reynolds number the turbulence is only a fraction of the turbulence in the precalciner. According to Chomiak (2000) the magnitude of turbulence is either enhanced or damped by the small particles. However, results reported in Chapter 5 indicate that the particles in the precalciner enhance turbulence, although the CFBC reactor operates on the border line of laminar flow for the range of residence times (τ_g). Low superficial gas velocity is the reason for the low Reynolds number (Re_D). Although a small contribution to the turbulence is made with the choice of exit design; Grace, Avidan and Knowlton (1997) stated that a short extension blind T will give violent turbulence and significant solids back-mixing in the riser exit region.

Smolders and Baeyens (2000) used a fitting procedure to make a correlation of an average solids retention time of the total system ($\tau_{s,mean}$) as a function of superficial gas velocity (U_0) and solids circulation rate (G_s). The physical design of their reactor is similar to the CFBC, but they used a particle size about 7 times larger than in this work in their experiments. Nevertheless, it could be of interest to compare the solids retention time calculated with the correlation of Smolders and Baeyens (2000) with the solids retention time found in the CFBC experiments, using equation 4.1 (and solving for the unknown solids retention time (τ_s)):

$$\varepsilon = \frac{volume\ of\ solids}{volume\ of\ gas + volume\ of\ solids} = \frac{\dot{m}_s \cdot \rho_g}{(\dot{m}_g \cdot \rho_s + \dot{m}_s \cdot \rho_g)} \cdot \frac{\tau_s}{\tau_g} \tag{4.1}$$

Here $\dot{m}_s$, $\dot{m}_g$, ρ_s, ρ_g, τ_s and τ_g denote feed rate of solids and gas, density of solids and gas, and solids and gas retention times, respectively. However, when comparing with Smolders and Baeyens (2000) it is to note that the similar exit (short extension blind T) gives a higher backmixing compared to previous work, and that the Pe-number is quite low (1-20) (Smolders & Baeyens 2000), (Van der Meer et al. 2000). Peclet numbers decrease with higher loadings and confirm the increased backmixing with increased solid fluxes. The solids loading reported in Smolders and Baeyens (2000) are about 3 to 15 times higher than in the CFBC reactor. Therefore, comparing the Peclet number reported by Smolder et al. (2000) with the one for the CFBC reactor will probably not be very meaningful.

It could be of interest to do more work on the Peclet number of the CFBC reactor in order to investigate plug flow theory with axial dispersion, which is only valid for Peclet numbers larger than 100. It has been stated by Lim et al. (1995) and Bai et al. (1992b) that downward motion of particles cause backmixing of solids and may lead to downflow (backmixing) of gas in the annulus. This is also supported by Giddings et al. (2000) in CFD simulations of a precalciner. Thus, the choice of a turbulence-generating exit at the CFBC reactor (compared to the smooth exit of the precalciner) will to some extent compensate for having to compromise on the gas- and solids retention time during experiments. The magnitude of this compensation, if any, is however unknown. In fact, it only proves the complexity of scaling.

Similarity between the CFBC reactor and the precalciner

The CFBC reactor and the precalciner shows similarity for Fr_D, $\frac{U_0}{U_{slip,mean}}$, $\frac{Gs}{\rho_p U_0}$ and $\frac{\rho_p}{\rho_g}$, which are the four dimensionless groups discussed in Subsection 2.3.2, see Table 4.3. (Five similar dimensionless groups are somewhat difficult to obtain since the CFBC/precalciner ratios of $\frac{d}{D}$, Re_d and Re_D are about 44:1, 4:1 and 180:1, respectively.)

It is expected that the four dimensional groups roughly give:

- the same fluidization regime,
- the same riser solids holdup by volume and
- the same macroscopic movements of solids.

Inclusion of the density ratio provides a better similarity. In particular the riser solids holdup by weight is properly non-dimensionalized and so the pressure drop/gradients will be appropriate output parameters. It is suggested that the set (Fr_D, $\frac{U_0}{U_{slip,mean}}$, $\frac{Gs}{\rho_p U_0}$, $\frac{\rho_p}{\rho_g}$) holds for much of the CFB flow regime (Van der Meer et al. 1999).

Particles physical composition can best be described by Geldart classification as discussed in Subsection 2.3.1. The particle distribution in the precalciner and the chosen particle distribution in the CFBC reactor are classified as Geldart A, which means aeratable or particles having a small mean particle size. Normal fluidization is extremely difficult for these solids because interparticle forces are greater than those resulting from the action of gas (Kunii & Levenspiel 1991). This supports the previous discussion of interparticular forces also shown in Figure 2.29.

The difference in turbulence is the largest difference between the precalciner and the CFBC reactor. The consequence of not achieving similar turbulence will

Table 4.3: Comparision of characteristic dimensionless groups for the CFBC reactor and the Precalciner.

Dimensionless groups	Unit	Typical values in the CFBC reactor	Typical values in the Precalciner
$Fr_D = \frac{U_0^2}{gD}$	[−]	0.93 - 14.83	14.60
$\frac{U_0}{v_t}$	[−]	16.7 - 66.7	733
$\frac{U_0}{U_{slip,mean}}$	[−]	1.4	1.4
$\frac{Gs}{\rho_p U_0}$	[−]	$3.77{\cdot}10^{-5}$ - $1.51{\cdot}10^{-4}$	$1.128{\cdot}10^{-4}$
$\frac{\rho_p}{\rho_g}$	[−]	8548 - 7571	7093
$\frac{d}{D}$	[−]	$1.24{\cdot}10^{-4}$	$2.814{\cdot}10^{-6}$
$Re_d = \frac{\rho_g U_0 d}{\mu}$	[−]	0.12 - 0.48	1.98
$Re_D = \frac{\rho_g U_0 D}{\mu}$	[−]	854 - 3860	$7.05{\cdot}10^5$
ε	[−]	Found in experiments	0.9996
τ_s/τ_g	[−]	Found in experiments	4

probably affect the particle retention time and the diffusion of oxidizer to the fuel particle as discussed in Subsection 4.1.1. The effect of the large difference in the Re_D (180:1) is uncertain compared to the smaller difference in Re_d (4:1).

4.1.3 CFBC reactor, summary

The literature review showed that there is similarity between a CFB and a precalciner regarding the phenomena of:

- gas and solids mixing,
- core-annulus flow,
- micro flow structure of particles, and
- effects of particles on turbulence.

One large difference between a CFB and a precalciner is in the solids loading and the particle distribution, hence the interparticular forces defining raw meal as cohesive. Nevertheless, experiments on the influence of flow regime, like for example inlet and exit design, will probably apply for both precalciner and CFB.

There is similarity between the CFBC reactor and the precalciner at Norcem Brevik regarding the dimensionless groups applied, namely Fr_D, $\frac{U_0}{U_{slip,mean}}$, $\frac{Gs}{\rho_p U_0}$ and $\frac{\rho_p}{\rho_g}$. It is expected that equality in the four dimensional groups roughly obtains the same:

- fluidization regime,
- riser solids holdup by volume, and
- macroscopic movements of solid.

From this similarity the pressure drop gradient will be an appropriate output parameter, and it is anticipated that the set holds for much of the flow regime. The

particles selected for use in the CFBC reactor have the same Geldart A classification as raw meal and will most likely be suitable, except for the chemical decomposition of calcium carbonate.

Another large difference between the CFBC reactor and the precalciner is the difference in turbulence level. Turbulence affects the particles retention time and the diffusion of oxidizer to the fuel particle. However, the precalciner has a smooth exit, whereas the exit design of the CFBC reactor is a blind T short extension, which will enhance turbulence and increase backmixing.

Previous investigations showed increasing thickness of the core layer in a smaller CFB compared to a larger one. This difference must be assumed to be found also in the scaling between the CFBC reactor and the precalciner.

In any case the:

- gas retention time,
- particle size distribution,
- pressure,
- gas composition and
- void fraction

are more or less similar. This makes experiments in this laboratory CFBC reactor comparable to experiments in the precalciner.

4.2 Execution of experiments

In the CFBC experiments, a lot of parameters have to be set correctly. The parameters are indirectly connected to each other, and this can make the operation of such a process quite complex. The following parameters put limitations to the operation of the reactor, later referred to as the state-parameters:

- The temperature in the BFB and in the remaining reactor must not exceed 1000 $°C$ due to the risk of sintering and damage on the construction material.
- The gas concentrations must be within the measuring range of the analyzers. Hence, to avoid too high CO emissions, the influx of alternative fuel should not be too high.

The following parameter is constant during all experiments:

- influx of tertiary air. It is set to about 5 and 8 kg/h in order to ensure a stable inflow of circulating mass and secondary fuel, respectively.

The following parameters are set for each experiment:

- the influx of primary air,
- the influx of primary fuel,
- the influx of secondary air,
- the influx of secondary fuel,
- the solids circulation rate.

The parameters set for each experiment affect:

- the excess air ratio,
- the superficial gas velocity, which implies a change in the Reynolds number and the gas retention time,
- the void fraction, which implies a change in heat transfer and mass transfer,
- solids retention time, which implies a change in the burnout of particles and a change in combustion efficiency,
- the input power, which implies a change in the temperature in the BFB and CFB and in turn a change in density and viscosity of the gas mixture.

A set of parameters are chosen in order to achieve similar conditions as in the precalciner, from now on called state-parameters. These state-parameters are:

- the excess air ratio,
- the gas retention time,
- the void fraction,
- the temperature profile in the CFB.

The state-parameters are controlled by rotameters, emission measurements, distributed temperature nodes within the reactor and pressure drop measurement over the riser.

A start-up procedure is followed before execution of the experiments:

- completion of a test plan that controls the state-parameters,
- calibration of the H&B gas analyzer, and logging of deviation,
- a first step of heat up and stabilization of the reactor with primary fuel and excess air ($\lambda = 1.5$) until stable CO emission measurements and relatively stable temperature measurements in the temperature nodes are achieved,
- a second step of heat up and stabilization of the reactor feeding circulating mass and/or alternative fuel until CO emission measurements and the temperatures are relative stable.

A sketch of the CFBC reactor is shown in Figure 4.1, including the position of sampling points.

The chemical composition of the different solid alternative fuels fed to the CFBC reactor are shown in Table 4.4 and 4.5.

4.3 Experimental results and discussion

Through a series of introductory experiments it was found that it is possible to control the conditions in a laboratory reactor better than in a full-scale reactor, such as a calciner. For instance, using a well-defined particle size for different fuels makes it easier to determine whether an increase in CO emissions is due to different temperature profiles or fuel characteristics or subject to a change in flow pattern (backmixing). In this way, the CFBC reactor was found to be a useful tool for investigations of fuel specific emissions from combustion in a regime equivalent to that in a precalciner (Axelsen 2001*a*). A summary of the introductory experiments are presented in Appendix G, and a discussion of reactor stability is given in Appendix H.

The principal experiments include:

Table 4.4: Chemical composition of fuels fed to the CFBC reactor. Oxygen by difference. AM = animal meal; RDF = refuse derived fuel; SHW = solid hazardous waste.

Parameters	Unit	Coal	RDF	AM	SHW
Moisture	wt-% (as rec.)	5.2	7.7	3.9	10.7
Volatiles	wt-%	28.7	70.4	62.8	46.3
C. fix	wt-%	56.5	10.3	8.9	7.7
Ash	wt-%	9,6	11.6	23.0	35.3
LHV	MJ/kg (as rec.)	28.82	18.14	17.10	15.75
C	wt-% (daf)	86.4	54.0	56.6	65.2
H	wt-% (daf)	5.2	7.4	8.2	9.8
N	wt-% (daf)	1.5	0.4	12.0	2.0
O	wt-% (daf)	5.9	37.0	16.6	21.8
S	wt-% (daf)	1.1	0.4	0.7	0.7
P	wt-% (daf)	-	-	5.4	-
Cl	wt-% (daf)	<0.1	0.8	0.5	0.5
N in char @ 800 °C	wt-% (daf)	1.48	0.015	3.40	-
N in char @ 950 °C	wt-% (daf)	1.44	0.010	1.70	-
H/C	molar ratio	0.72	1.64	1.74	1.8
O/C	molar ratio	0.05	0.53	0.23	0.26
O/N	molar ratio	3.44	82.7	1.25	9.8
C.fix/Volat.	-	1.97	0.15	0.14	0.17

- reburning,
- advanced reburning, and
- combustion without circulating mass.

These three operational modes are discussed in separate subsections. But first, in an introductory subsection, the fuel particles, the circulating mass, the emissions of N_2O, SO_2, NO_2, TOC and CO as well as the temperature profiles are presented and discussed.

4.3.1 Introduction

In the experiments with reburning and advanced reburning it was of interest to investigate alternative fuels behavior in a precalciner environment, i.e. with circulating mass and supply of up to 2000 mg/Nm^3 of NO into the CFBC reactor. In the experiments without circulating mass, fuel specific differences were expected.

It was initially decided to vary the supply of NO in four steps for the experiments with advanced reburning and combustion without circulating mass in order to investigate the impact of increasing supply of NO.

The reburning experiment was executed with pure fuels as well as blends of fuels. However, due to limited time, it was decided to execute the reburning experiment with only one input concentration of NO (about 1930 mg/Nm^3).

In the following discussion, it is reasonable to expect that the influence of fuel-NO is suppressed (hard to detect) due to the amounts of NO supplied into the reactor.

Table 4.5: Chemical composition of fuels fed to the CFBC reactor. Oxygen by difference. AM = animal meal; CC = coal char; RDF = refuse derived fuel.

Parameters	Unit	Wood	Coal/AM	RDF/AM	CC/AM
Moisture	wt-% (as rec.)	12.2	3.8	9.2	9.6
Volatiles	wt-%	72.3	35.5	65.4	50.1
C. fix	wt-%	15.4	47.3	10.8	17.0
Ash	wt-%	0.10	13.4	14.6	23.4
LHV	MJ/kg (as rec.)	16.53	26.5	16.07	16.70
C	wt-% (daf)	55.0	82.0	50.7	63.6
H	wt-% (daf)	6.8	5.9	7.0	7.8
N	wt-% (daf)	0.3	3.6	1.2	10.4
O	wt-% (daf)	37.7	6.4	40.3	13.8
S	wt-% (daf)	0.20	0.9	0.4	0.6
P	wt-% (daf)	-	1.2	0.4	3.9
N in char @ 800 $°C$	wt-% (daf)	0.044	-	-	-
N in char @ 950 $°C$	wt-% (daf)	0.019	-	-	-
H/C	molar ratio	1.48	0.86	1.66	1.47
O/C	molar ratio	0.51	0.06	0.60	0.16
O/N	molar ratio	110	1.56	29.4	1.2
C.fix/Volat.	-	0.21	1.33	0.17	0.34

Table 4.6 shows the principal operating conditions during the experiments, including the levels of SO_3 and Cl and the calcination degree.

Fuel particles

The reburning and advanced reburning experiments were run with a particle size less than 1 mm. The experiment without circulating mass was tested with two sets of particle sizes, namely less than 1 and 2 mm, to investigate the impact on combustion behavior. The solvents in SHW evaporates at relatively low temperatures, and grinding below 2 mm expose the particle for higher heat generation. Accordingly, the SHW particles were ground down to 2 mm in order to change them as little as possible, but still be able to feed them properly. SHW is a difficult fuel to feed because of its stickiness, so only one experiment with SHW was carried out.

Circulating mass

The circulating mass fed into the CFBC reactor is a 50/50 blend of raw meal and Millisil®M6, from now on referred to as the circulating mass, see Subsection 4.1.1 for further details. A circulating mass influx of 29 kg/h was applied in all experiments, which corresponds to about 67 % of the theoretical input to the precalciner (Axelsen 2001*a*).

As described in Section 3.1 the preheated meal entering the precalciner has a temperature of about 700 $°C$. In comparison, the circulating mass enters the BFB at 20 $°C$. Thus, the circulating mass is preheated in the BFB before entering the riser through the diaphragm, see Figure 4.1. During the preheating free water (up to 200 $°C$), adsorbed water (100 to 400 $°C$) and chemically combined water (400 to 750 $°C$) is expelled (Tokheim 1999).

Table 4.6: Principal results from the reburning, advanced reburning and combustion without circulating mass experiment

Parameters	Unit	Reburning	Advanced reburning	Comb. without circ. mass
λ	[−]	1.11 - 1.21	1.12 - 1.26	1.52 - 1.82
Alt. fuel	*% energy*	49 - 64	36 - 56	28 - 57
q	kW	37.5 - 53.1	35.7 - 55.8	20 - 29
τ_g	*sec.*	0.64 - 0.69	0.63 - 0.67	0.86 - 1.06
v_{riser}	m/s	6.3 - 6.8	5.9 - 6.8	4.0 - 5.0
Re	[−]	5300 - 5700	5570 - 5670	4520 - 4810
ε_{riser}	[−]	0.99996	0.99996	-
G_s	kg/h	29	29	-
$NO_{supplied}$	mg/Nm^3	1931	72 - 1457	74 - 1450
Calcination	%	70 - 86	83 - 87	-
SO_3	*wt%*	0.36 - 0.6	0.075 - 0.45	-
Cl	*wt%*	0.01 - 0.14	0.01 - 0.01	-

N_2O emissions

The Hartman & Braun Uras 14 NDIR analyzer has a deficiency in the nitrous oxide (N_2O) measurement. This has been shown through parallel batch analysis with a gas chromatograph (GC), see Table I.1 in Appendix I. The parallel analysis showed 2.1 to 2.87 higher emissions with the H&B analyzer compared to the GC analysis.

The N_2O emissions are high compared to emission levels reported by Hulgaard and Dam-Johansen (1992), who state that the nitrous oxide emissions in ordinary combustion devices are usually low (0 - 5 ppm). However, nitrous oxide emissions up to 150 ppm (CFBC) and 200 ppm (FBC), respectively, have been reported (Hulgaard & Dam-Johansen 1992), (Werther & Ogada 1999).

Taking into consideration the uncertainties in the N_2O emission measurements, it is important to evaluate the nitrous oxide emissions with caution. Hence, in the rest of this thesis only relative N_2O values are used.

SO_2 emissions

The SO_2 emissions are low in all experiments and are therefore presented in one common graph, see Figure J.1. The sulphur from the circulating mass (raw meal) and fuels is released and then captured in the circulating mass.

A mass balance on sulphur has been carried out, showing an imbalance of about 35 %, see Appendix J. The imbalance is probably due to inaccuracies in the:

- SO_3 analysis of the raw meal,
- SO_3 analysis of the calcined meal,
- S analysis of the coal,
- mass flow of coal,
- mass flow of circulating mass,
- SO_2 analysis in the gas and
- accumulation of sulphur in the CFBC reactor (possibly the largest contribution).

Because of the sulphur imbalance, the SO_2 emissions are not emphasized in this thesis.

NO_2 emissions

The H&B analyzer is equipped with an NO/NO_2 converter. Thus, the analyzer is restricted to measure either NO or NO_x. Operations including the NO/NO_2 converter, i.e. measurements of NO_x, influence the remaining emission measurements. It is therefore necessary to carry out parallel experiments for NO and NO_x in order to balance the NO_2 emissions. Thus, the NO_2 emissions are presented for all experiments in Figure K.1. More details are given i Appendix K. The NO_2 emissions during advanced reburning and combustion of animal meal during reburning and combustion without circulating mass is between 9 and 19 %, whereas in the rest of the experiments they are below 6 %. The reason for the increased NO_2 emissions during supply of urea and animal meal will be discussed in the following subsections.

CO and TOC emissions

The measurements of CO and TOC (details are given i Appendix L) show the following:

- There is almost no correlation between the level of NO supplied and the CO or TOC concentrations.
- Increasing CO and TOC emissions are observed during reburning with AM. This is probably due to competition for the OH radical between Equation 2.30 and 2.55. In contrast, during combustion without circulating mass, the AM is well (4 times) below coal in CO emissions. The major difference between these two operational modes is that there is no rich zone during combustion without circulating mass. This could imply that competition between Equation 2.30 and 2.55 is of minor importance when fuels with a high nitrogen content, like e.g. AM, is burnt in a lean environment and not undergoing reburning or staged combustion. In lean flames the critical amine radical is NH_2, and the reduction of NH_2 produces enough OH radicals.
- A comparison of experiments without circulating mass using $coal_{d<2}$ and $coal_{d<1}$ shows higher CO emissions with increased particle size.
- It is important to emphasize that $coal_{d<1}$ emits more than twice the amount of CO compared to $RDF_{d<1}$ and $AM_{d<1}$ at similar conditions during combustion without circulating mass. In contrast, $AM_{d<2}$ emits a higher amount of CO compared to $SHW_{d<2}$ and $coal_{d<2}$.

Temperature profiles

The temperature profiles for the reburning, advanced reburning and combustion without circulating mass is discussed and presented in Appendix M. The results demonstrate reproducibility and the fact that increased amounts of volatiles release more energy in the lower parts of the CFBC reactor.

4.3.2 Reburning

The reburning experiments were executed with the following fuels and mixtures:

- refuse derived fuel (RDF),
- animal meal (AM),

- coal,
- RDF/AM (75/25 wt %),
- coal/AM (75/25 wt %) and
- CC/AM (25/75 wt %).

The reason for executing experiments with fuel mixtures is to investigate the impact on NO reduction and CO emissions.

Animal meal was mixed with RDF, coal and char coal. The weight fraction of AM was 25, 25 and 75 %, respectively. The argument for blending a larger amount of AM into char coal is to investigate if an increased number of free carbon sites could affect e.g. N_2O emissions, see Equation 2.19.

The experiments were carried out with additional supply of NO into the reactor at a concentration of about 1930 mg /Nm^3 (average of all experiments).

The investigation of Hämäläinen (1995), referred to in Subsection 2.1.3, show that the HCN/NH_3 ratio in pyrolysis gases decreases with the fuel O/N ratio. It can be seen from Table 4.4 and 4.5 that the O/N ratio is low for animal meal and coal in comparison with solid hazardous waste (SHW) and refuse derived fuel (RDF), which signify a smaller HCN/NH_3 ratio for AM. In experiments by Zevenhoven et al. (2000) it was found that a smaller O/N ratio favours NO_x reduction.

Comparing experiments made by Desroches-Ducarne et al. (1998) to the experiments with RDF/AM, coal/AM, CC/AM, shows that adding a fuel with a low O/N (HCN/NH_3) ratio in combination with RDF lowers the NO_x emissions. Desroches-Ducarne et al. (1998) state that the NO reduction is favoured by char or CO at CFB conditions. It is shown that homogeneous reduction of NO by CO is not significant at FBC conditions (750-950°C) (Johnsson 1994).

The NH_3 released during combustion of animal meal can be expected to follow a similar reduction route as advanced reburning or selective non-catalytic reduction (SNCR). Equation 2.30 and 2.55 is the primary oxidation reactions for NH_3 and CO, respectively. Hence, the competition for the OH radical between Equation 2.30 and 2.55 is probably the reason for the increased CO and TOC emissions of up to 5 and 15 times, respectively.

It must be noted that the NO emissions may have been affected by the differences in NO supplied in the different experiments. This will be shown later. A conservative assumption is that the percentual increase of NO supplied contributes to a reduction in NO emitted of the same size. Therefore, the numbers have been modified applying a superposition reduction in the percentual difference in NO supplied, to give the most modest profit on NO reduction, see Table 4.7. The actual NO reduction is supposed to lie somewhere between the conservative assumption and the NO reduction measured.

In a regime comparable to that in a precalciner, the following order of optimal NO reducing fuels and mixtures are:

- RDF/AM (20.6 to 41.4 % improvement relative to coal),
- RDF (18.7 to 39.5 % improvement relative to coal),
- CC/AM (22.9 to 34.5 % improvement relative to coal),
- AM (13.4 to 25 % improvement relative to coal),
- coal/AM (18.3 % improvement relative to coal) and
- coal.

Table 4.7: The table shows improvement in NO reduction relative to coal during the reburning experiments. The table presents reduction improvements actually measured as well numbers that were modified, using a superposition reduction in the percentual difference in NO supplied.

		CC / AM	RDF / AM	RDF	Coal / AM	AM	Coal
$NO_{supplied}$	$\frac{mg}{Nm^3}$	1945	2106	2106	1743	1945	1743
$\frac{NO_{out}}{NO_{supplied}}$	[-]	0.199	0.178	0.225	0.304	0.279	0.372
$1 - \frac{Reduct.\ ratio,i}{Reduct.\ ratio,coal}$	%	**34.5**	**41.4**	**39.5**	**18.3**	**25**	-
$1 - \frac{NO_{supplied,i}}{NO_{supplied,coal}}$	%	11.6	20.8	20.8	0	11.6	-
$NO_{modified\ reduction}$	%	**22.9**	**20.6**	**18.7**	**18.3**	**13.4**	-

NO_x emissions during the animal meal combustion were expected to be lower than during RDF and coal combustion, since AM is likely to release more NH_3 during devolatilization. An increase is seen in the NO_2 and N_2O emissions during combustion of AM, compared to the rest of the reburning fuels, and there is a possibility of ammonia slip via the exhaust gas. Increased NO_2 emissions can possibly be due to elemental phosporus released from animal meal in the flue gas stream. Previous investigations with direct injection of elemental phosphorus into the flue gas stream shows that NO is converted to NO_2, where NO_2 is subsequently removed using a conventional flue gas scrubber (Digest 2000).

The subplot in Figure 4.2 shows a trend of lower NO emissions with increasing volatiles ratio. This is supported by Kicherer et al. (1994), who state that one of the conditions required to achieve sufficient burnout as well as high NO_x reduction is a high level of volatile matter in the reburning fuel, see Subsection 2.1.7.

4.3.3 Advanced reburning rich

The advanced reburning rich experiment were carried out with:

- 25 wt % urea in RDF (RDF_{25}),
- 5 wt % urea in RDF (RDF_5) and
- 5 wt % urea in coal ($coal_5$).

The experiments were executed with a four step variation in the NO supplied (72 - 1457 mg /Nm^3).

RDF_5 versus RDF_{25}

The major difference is between the RDF_5 and RDF_{25} experiments, see Figure 4.3. The level of $NO_{supplied}$ at the break-even point ($NO_{out}/NO_{supplied} = 1$) is about twice as high for RDF_{25} as for RDF_5. Thus, a higher ammonia slip for RDF_{25} than for RDF_5 should be expected, but from parallel batch samples it was found 2 mg/Nm^3 @ 11 % O_2 and 8 mg/Nm^3 @ 11 % O_2, respectively.

The surplus of urea, which did not contribute to a proportional reduction in NO, and was not emitted as ammonia, can be seen as a increase in the N_2O or NO_2 emissions.

The chemical identity of the NH_i (i=1, 2) free radical is primarily responsible for determining the NO/N_2 product distribution that is dependent on the excess air ratio. For rich flames, as in parts of advanced reburning rich, a grater abundance of hydrogen atoms results in a shift from NH_2 to NH to N. Furthermore, the reactions

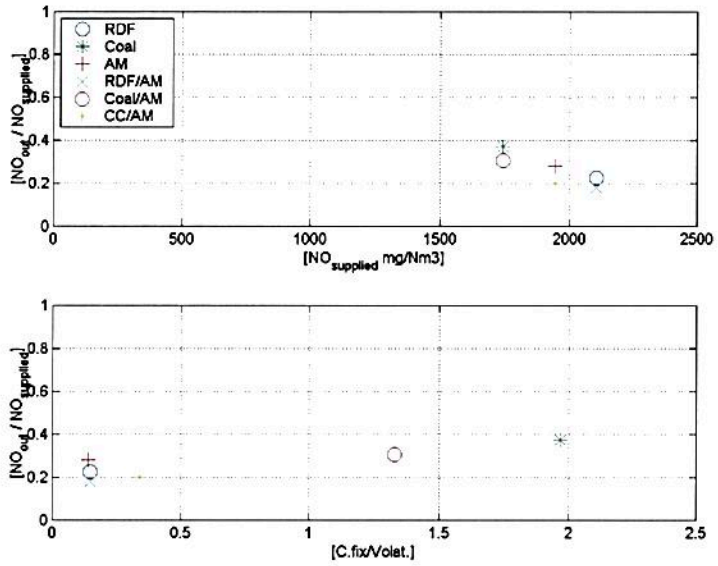

Figure 4.2: Main plot: NO $_{supplied}$ with respect to $NO_{out}/NO_{supplied}$ ratio during reburning experiments with RDF, coal, AM, RDF/AM, coal/AM and CC/AM. Subplot: C.fix/Volat. ratio with respect to $NO_{out}/NO_{supplied}$ ratio. .

of NH with NO produce N_2O, which is converted to N_2 principally by reactions with hydrogen atoms, see Equation 2.37 and 2.38 (Miller & Bowman 1989).

From this statement and with a probable scarcity of hydrogen atoms, it is possible that the increased nitrous oxide emissions from RDF_{25} originates from Equation 2.37. This will also be a probable route for the formation of N_2O during reburning with animal meal and its blends.

RDF_5 versus $coal_5$

The subplot in Figure 4.3 shows, at the break-even point for $coal_5$, a 55 % higher reduction for RDF_5 than for $coal_5$. Furthermore, it can be seen that the two experiments follow a similar gradient. This could imply that different fuels with the same amount of urea have a similar gradient, but different break-even points.

Precalciner conditions

The advanced reburning rich experiments show substantial NO reduction at higher levels of NO supply, as in a precalciner, when a favorable fuel and/or amount of urea is chosen. At conditions similar to those in a precalciner (1000 mg/Nm^3 $NO_{supplied}$) a NO reduction of up to 8, 50 and 60 % for $coal_5$, RDF_{25} and RDF_5, respectively, can be expected. Previous investigations by Maly et al. (1999) support these experiments; they found that an increasing initial NO_x concentration was followed by an increasing NO_x reduction, see Figure 2.19. They also found that biomass gave a higher NO_x reduction than other fuels, see Subsection 2.1.7 (Maly et al. 1999).

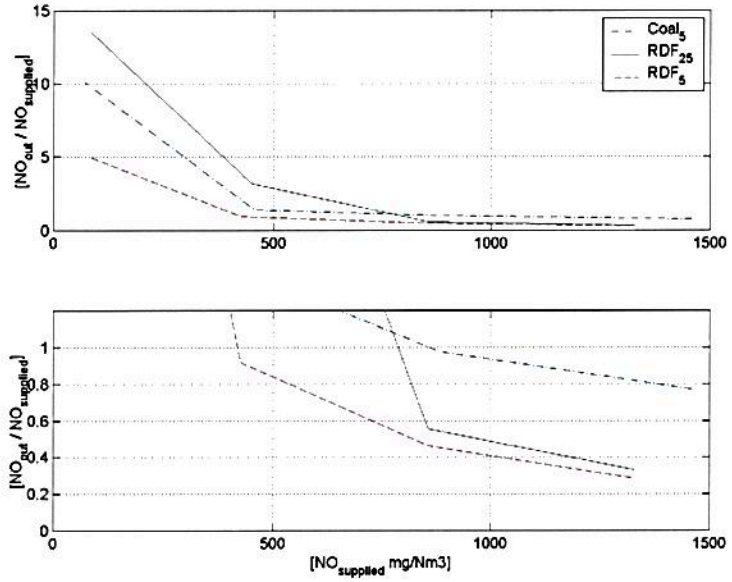

Figure 4.3: Main plot: $NO_{out}/NO_{supplied}$ as a function of NO $_{supplied}$ during advanced reburning experiments with 25 wt % urea and RDF; 5 wt % urea and RDF; 5 wt % urea and coal. Subplot: Close-up of the main plot.

$NO_{supplied}$ versus $Urea_{supplied}$

These experiments show that increasing amounts of $NO_{supplied}$ improve (lower) the ratio $NO_{out}/NO_{supplied}$ (NO reduction), see Figure 4.3.

The molar ratio of urea supplied to the CFBC reactor with respect to $NO_{supplied}$ (urea/$NO_{supplied}$) is shown in Figure 4.4. Figure 2.15 shows that the NO reduction depends on the molar ratio of NH_3 and NO at inlet conditions ($(NH_3/NO)_{in}$). The inlet conditions in this experiment are changed while the urea feed is kept constant, as opposed to previous experiments. Figure 4.4 shows a descending trend for the NO emissions from the CFBC reactor with increasing (urea/$NO_{supplied}$) molar ratio. The optimum is not possible to determine without further experiments, but apparantly (urea/$NO_{supplied}$) molar ratios above 3 - 5 do not contribute to lower NO emissions. A similar trend is found during the full-scale experiments, see Figure 3.13.

4.3.4 Combustion without circulating mass

The experiments without circulating mass were executed with:

- RDF,
- coal,
- AM and
- SHW.

The experiments were carried out with a four-step variation in the NO supplied (74 - 1450 mg /Nm^3). There was no supply of tertiary air during the experiments without circulating mass. The overall excess air ratio was between 1.52 and 1.82.

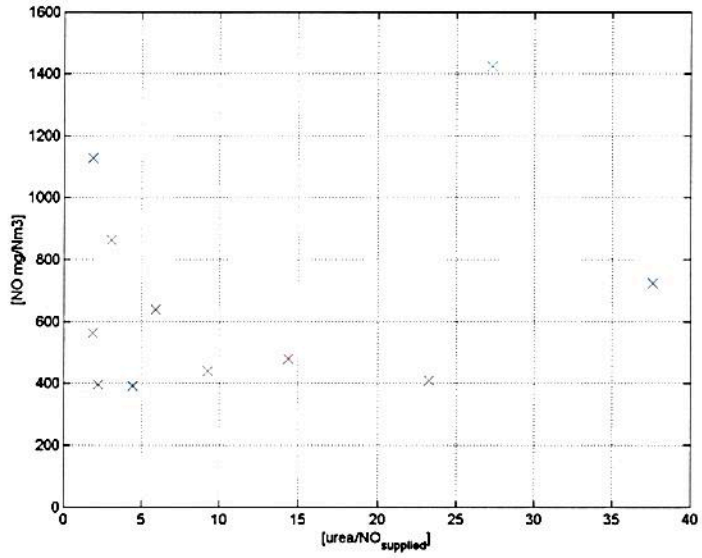

Figure 4.4: NO_{out} as a function of the ratio urea/$NO_{supplied}$, without consideration of alternative fuel type.

Two sets of particle sizes were tested to investigate the impact on combustion behavior. The particles were ground and classified into two groups:

- $d_p \leq 1$ and
- $d_p \leq 2$ mm[2]

Particle size influence on NO reduction

Figure 4.6 shows NO emissions, including a close-up in a subplot. A fuel with a particle size below 2 mm has almost twice the break-even point ($NO_{out}/NO_{supplied}$ = 1), i.e. smaller particles give higher NO reduction, see also Figure 4.7. Figure 4.7 shows a distinctly different behavior for AM, with a relatively horizontal trend with increasing supply of NO.

The experiments show that the NO reduction depends on fuel type, particle size and amount of NO supplied.

Heterogeneous NO reduction

It must be emphasized that the experiments during combustion without circulating mass is conducted without staged combustion (reburning). Hence, the reduction of NO is possibly due to heterogeneous reactions by which NO_x can be both formed and reduced by reactions involving the solid fuel, see Equation 2.15 and 2.16.

Shimizu et al. (1992) state that the net amount of NO_x formed from heterogeneous reactions is strongly dependent on the intrinsic reactivity and internal surface area of the char (Shimizu, Sazawa & Adschiri 1992).

[2]The set of fuels with a diameter below 2 mm was tested out in a period when the analyzer was not fully functional on TOC, NO_2 and N_2O. The temperature nodes during the experiment with $AM_{d<2mm}$ was out of function. However, a comparison with the fuels ground below 1 mm gives important information.

Skaarup Jensen et al. (2000) found that temperature only has a weak effect on the intrinsic NO formation selectivity, and no noticeable effect of O_2 concentration was found on NO selectivity. Furthermore, it was stated that reduction of NO by reaction with char is the main reaction accounting for net NO formation from char combustion being significantly lower than 100 % (Skaarup Jensen et al. 2000). These characteristics will, as shown, possibly vary with fuel-type and particle size.

The amount of nitrogen retained in coal char after devolatilization is reported to be 10 - 30 % at temperatures above 1127 - 1227 $°C$ (Hill & Smoot 2000). Table 4.4 shows that the fraction of nitrogen retained in the char of RDF, coal and AM at 800 $°C$ are 4, 99, and 28 %, respectively. At 950 $°C$ the corresponding values are 2.5, 96 and 14 %, respectively.

Figure 4.8 and 4.9 shows the release of N_2O and NO during combustion experiments with coal and animal meal in a single particle furnace, respectively. The experiments were executed with the same fuels as those used in the CFBC reactor at 21 vol-% oxygen (Voll 2002). In the coal experiment, the fuel nitrogen is released (as NO and N_2O) during a considerable part of the char combustion period, whereas in the AM experiment most of the fuel nitrogen is released during pyrolysis. These experiments verify the analysis on retained nitrogen in the char according to Table 4.4.

It has been suggested that animal meal follows a reduction route similar to advanced reburning or SNCR, which is believed to be due to the release of fuel nitrogen as ammonia in the devolatilization phase. This is probably conditioned by the fuel nitrogen being released during pyrolysis as well as a low O/N ratio. As mentioned previously, both animal meal and coal have a low O/N ratio, but as shown in the experiments, there is a significant difference in the release of fuel nitrogen during pyrolysis. A major part of the nitrogen in animal meal is found in the protein, in which the building blocks are amino acids. The work of Hämäläinen (1995) considered conversion of model-compound N to HCN and NH_3 and to N_2O and NO, including exeperiments on coal and peat. Hence, it must be taken into consideration that the chemistry of animal meal combustion may be different than that of the fuels considered by Hämälainen (1995).

De Soete (1990) and De Soete et al. (1999) report:

- that the amounts of N_2O and NO, measured at the end of the combustion, only account for about 30 to 70 % of total char-nitrogen content, due to heterogeneous reduction of these nitrogen oxides on bound carbon atoms, whereby N_2O is more readily reduced than NO,
- that a suitable heterogeneous adsorption/desorption mechanism of NO and N_2O formation from char-nitrogen can only be proposed in connection with heterogeneous carbon combustion, since, at least at temperatures up to 1300 K oxygen adsorption on (-C) and (-CN) sites controls the overall reactions of both phenomena,
- a triple trade-off between NO, N_2O and N_2, seen from Equation 2.17, 2.18 and 2.19.

Appreciating the investigations from De Soete et al. (1990 and 1999), but also Zevenhoven and Hupa (1998), and considering the amount of nitrogen contained in the coal char it seems likely that NO is reduced by Equation 2.17, 2.18 and 2.19.

In Figure 4.5 shows that N_2O emissions for coal increase with increasing supply of NO. Thus, it is assumed that reduction of NO through Equation 2.18 does not fully complete through Equation 2.19. The N_2O emissions for SHW and RDF show a similar trend but not as evident. In contrast, the N_2O emissions for AM show no correlation with the supply of NO and are about twice as high as for coal and six times higher than for SHW and RDF.

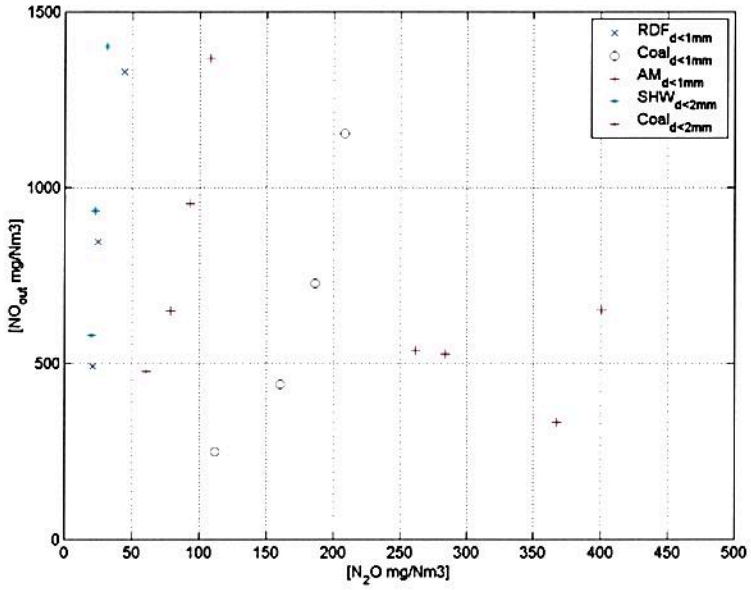

Figure 4.5: Emission of NO versus N_2O during experiments without circulating mass. Exepriments with $RDF_{d<1mm}$, $Coal_{d<1mm}$, $AM_{d<1mm}$, $SHW_{d<2mm}$, $Coal_{d<2mm}$.

Animal meal

The distinctly different behavior (horizontal trend) of AM is possibly due to the assumed release of ammonia during volatilization as previously discussed. Hence, a higher NO reduction potential for AM is shown in Figure 4.7 for both experiments. The relatively high emissions of N_2O in combination with the assumption of a higher NH_3/HCN ratio leads to the assumption of an incomplete termination of Equation 2.38 and/or Equation 2.19.

Precalciner conditions

These investigations show substantial NO reduction at higher levels of NO supply, like in a precalciner, when a favorable fuel and particle size is chosen. At conditions similar to those in a precalciner (1000 mg/Nm^3 $NO_{supplied}$) NO reductions of up to 6, 18 and 45 % for $RDF_{d<1}$, $coal_{d<1}$ and $AM_{d<1}$, respectively, can be expected. Furthermore, it can be seen that $SHW_{d<2}$, $coal_{d<2}$ and $AM_{d<2}$ reach break-even at conditions similar to those in a precalciner (1000 mg/Nm^3 $NO_{supplied}$).

4.4 Conclusion of laboratory experiments

The largest difference between the CFBC reactor and the precalciner is the different turbulence level. However, from the dimensionless numbers and the literature review it has been found that experiments in the laboratory CFBC reactor are as good as experiments in the full-scale precalciner.

The principal laboratory experiments showed:

- almost no correlation between the level of NO supplied and the CO emissions,

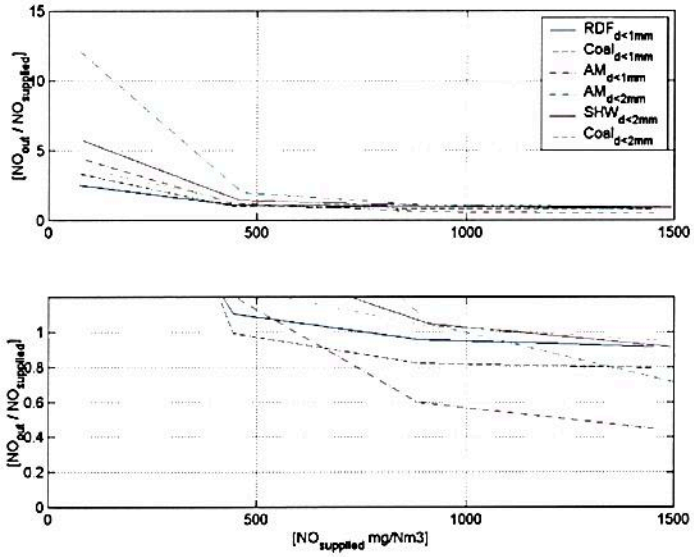

Figure 4.6: Main plot: $NO_{out}/NO_{supplied}$ as a function of $NO_{supplied}$ during experiments without circulating mass. Experiments with $RDF_{d<1mm}$, $Coal_{d<1mm}$, $AM_{d<1mm}$, $SHW_{d<2mm}$, $Coal_{d<2mm}$, $AM_{d<2mm}$. Subplot: Close-up of the main plot.

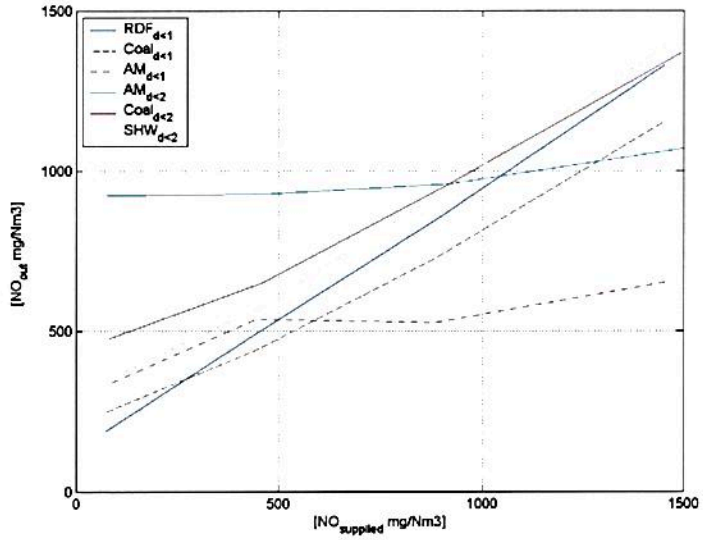

Figure 4.7: NO_{out} as a function of $NO_{supplied}$ during experiments without circulating mass. Experiments with $RDF_{d<1mm}$, $Coal_{d<1mm}$, $AM_{d<1mm}$, $SHW_{d<2mm}$, $Coal_{d<2mm}$, $AM_{d<2mm}$.

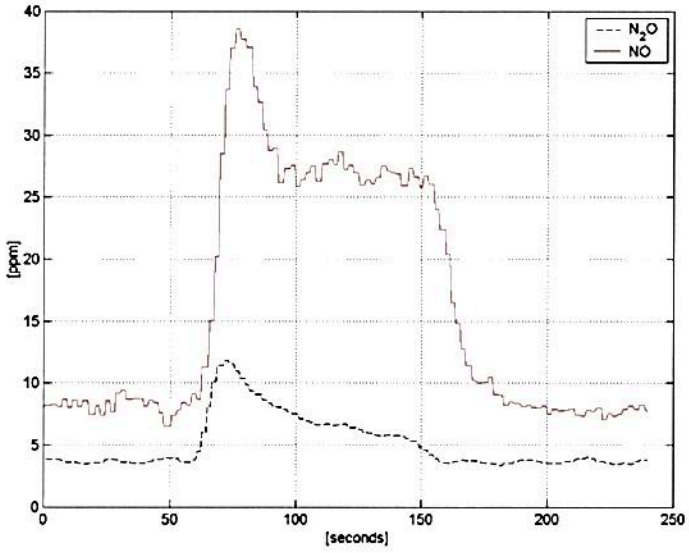

Figure 4.8: The development of N_2O and NO during combustion of coal in a single particle furnace at 900 $°C$ (Voll 2002).

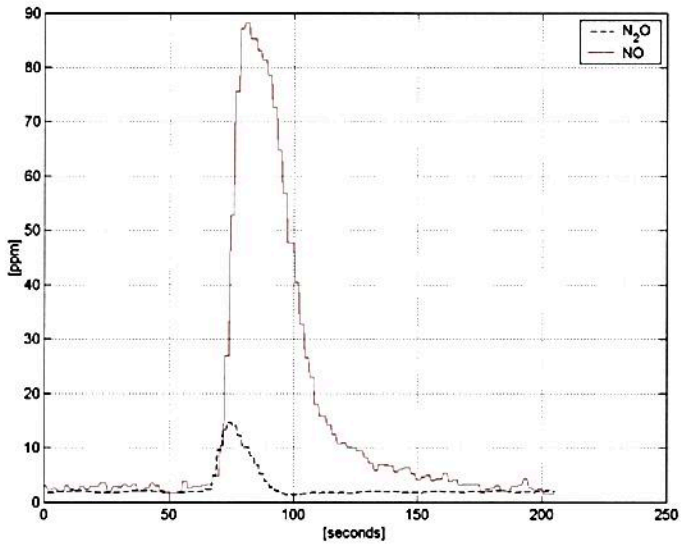

Figure 4.9: The development of N_2O and NO during combustion of animal meal in a single particle furnace at 1000 $°C$ (Voll 2002).

- that larger particle sizes give increased CO emissions and less good fuel particle burnout,
- that increasing the particle size changes the ranking of fuels with highest CO emissions,
- that animal meal gives NO_x reduction by a route similar to that of SNCR or advanced reburning, the preconditions for this, if animal meal corresponds to the work of Hämäläinen (1995), being a low O/N ratio and that the fuel nitrogen is released during pyrolysis, and
- higher CO emissions during reburning with animal meal than during combustion (in a lean environment) without circulating mass.

The increased CO emissions during reburning with animal meal are probably due to competition for the OH radical between the oxidation of CO and the oxidation of NH_3. However, when animal meal is burnt in a lean environment the CO emissions are low and the competition between Equation 2.30 and 2.55 seems to be of minor importance.

A probable cause is that:

- for lean flames, the critical amine free radical NH_2 is reduced directly by Equation 2.33 or Equation 2.34 through 2.36, and/or
- the increased amount of hydrogen radicals increases the production of OH radicals in Equation 2.56.

4.4.1 Reburning

RDF gave better results in laboratory experiments than in full-scale trials. This is possibly due to the difference in particle size.

At conditions similar to those in a precalciner (1930 mg/Nm^3 $NO_{supplied}$) the reburning experiments showed the following order of optimal NO reducing fuels and mixtures:

- RDF/AM (up to 41.4 % improvement relative to coal),
- RDF (up to 39.5 % improvement relative to coal),
- CC/AM (up to 34.5 % improvement relative to coal),
- AM (up to 25 % improvement relative to coal),
- coal/AM (up to 18.3 % improvement related to coal), and
- coal.

4.4.2 Advanced reburning

The advanced reburning experiments showed:

- that the surplus of urea, which did not contribute to a reduction in the NO and was not emitted as ammonia, is found as an increase in the NO_2 and N_2O,
- in advanced reburning, RDF is a better fuel than coal. This is probably due to the higher amount of volatiles in RDF,

- that increased amount of $NO_{supplied}$ improves (lower) the ratio $NO_{out}/NO_{supplied}$ and
- that the NO reduction depends on the ratio of (urea/$NO_{supplied}$), an optimum is not possible to determine without further experiments, but apparantly (urea/$NO_{supplied}$) ratios above 3 - 5 do not contribute to lower NO emissions. A similar trend is found during the full-scale experiments.

At conditions similar to those in a precalciner (1000 mg/Nm^3 $NO_{supplied}$) the advanced reburning experiments showed the following order of optimal NO reducing fuels and urea mixtures:

- RDF_5 (up to 60 %),
- RDF_{25} (up to 50 %) and
- $coal_5$ (up to 8 %)

4.4.3 Combustion without circulating mass

The combustion experiments without circulating mass showed that:

- smaller particles gave larger NO reduction - almost the double at the prevailing conditions,
- heterogeneous reactions are possibly the main reason for the NO reduction with increasing $NO_{supplied}$ during combustion of coal, RDF and SHW. The increased N_2O emissions during coal combustion are probably due to the heterogeneous reactions in Equation 2.18. However, a combination with homogencous reactions is likely,
- homogeneous reactions are possibly the main reason for the NO reduction with increasing $NO_{supplied}$ during combustion of animal meal. Hence the increased N_2O emissions for animal meal are probably due to the homogeneous reaction in Equation 2.37. Animal meal is, as mentioned above, probably governed by the ammonia released during devolatilization, but a combination with heterogeneous reduction reactions are likely
- the distinctly different behavior of animal meal is due to the assumed release of ammonia during the devolatilization phase and
- increased amounts of $NO_{supplied}$ improve (lower) the ratio $NO_{out}/NO_{supplied}$.

At conditions similar to those in a precalciner (1000 mg/Nm^3 $NO_{supplied}$) the combustion experiments without circulating mass showed the following order of optimal NO reducing fuels:

- $AM_{d<1}$ (up to 45 %),
- $coal_{d<1}$ (up to 18 %) and
- $RDF_{d<1}$ (up to 6 %).

Accordingly, $AM_{d<2}$, $SHW_{d<2}$ and $coal_{d<2}$ reach break-even ($NO_{out}/NO_{supplied}$=1) at similar conditions.

Chapter 5

Flow calculations

The objective of this chapter is to describe the flow pattern in the precalciner at kiln 6 in Brevik by using computational fluid dynamics (CFD). Subsections 2.3.2 and 3.1.2 characterize the precalciner with reference to previous work, whereas Subsection 3.1.1 describe the traverse measurements in the precalciner. In order to verify and compare flow regime characterization from previous work and to explain results from full-scale experiments it is useful to do CFD simulations.

Euler-Euler granular multiphase simulations are accomplished with FLUENT 4 (version 4.5.6) in order to substantiate the assumption of dilute flow and the importance of particle-particle collisions in a precalciner. Using Euler-Euler granular multiphase simulations in FLUENT 4 it is not possible to make simulations with combusting particles. Hence, simulations are also performed with an Euler-Lagrangian model in FLUENT 6 (version 6.0.12) to investigate combusting particles and raw meal behavior, e.g. particles-trajectory, retention time and species concentration[1] (FLUENT 1998), (FLUENT 2001).

5.1 CFD grid

A structured grid is generated with GAMBIT, using 240,000 cells. Figure 5.1 shows the outer surface of the precalciner model with its inlets and outlets. The alternative fuel and raw meal inlet on the tertiary air gas side is located opposite to the corresponding inlets on the kiln gas side, and is therefore not shown in Figure 5.1. The full-scale precalciner outlet divides into two cyclones, namely 4.1 and 4.2, see Figure 3.1. In order to simplify the geometric it is chosen to prolong the outlet of the precalciner model as if there were only one cyclone stage. The model height is 42.8 meter with a cross-section of 3.56m×3.27m at the inlets section, and a diameter at the mid- and top region of 3.74 and 2.61 meter, respectively.

5.2 Euler-Euler granular approach

The Euler-Euler granular approach has the advantage, compared to Euler-Langrangian granular approach, that particle-particle collisions are included in the model. Therefore, Euler-Euler simulations is accomplished to study the importance of particle-particle collisions in a precalciner.

The Eulerian multiphase model solves a set of momentum and continuity equations for one gas and one solid phase. Coupling is achieved through the pressure,

[1] This study has been carried out in collaboration with Dr. Vidar Mathiesen at Telemark University College.

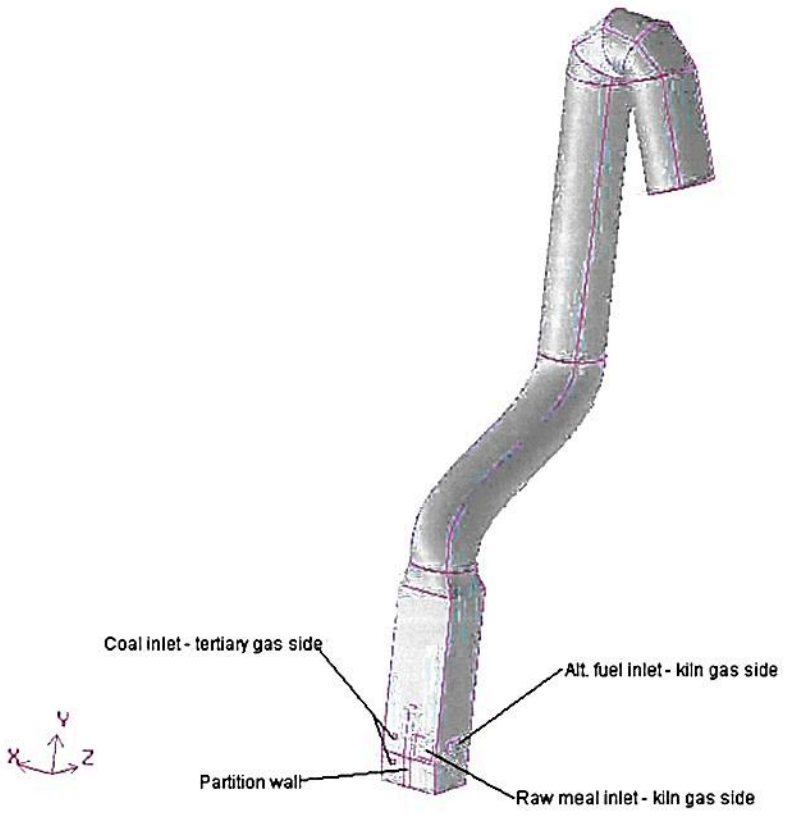

Figure 5.1: The figure shows the precalciner model with its inlets and outlets. The alternative fuel inlet and the raw meal inlet on the teriary gas side are located on the opposite side and are not shown in the figure.

viscosity and the interphase exchange coefficients. Kinetic theory for granular flow described by e.g. Gidaspow (1990) is applied to determine the granular temperature in the particle phases. The granular temperature is defined as one-third times the fluctuating velocity squared. The solid phase pressure, bulk viscosity and shear viscosity are deduced from this theory (Gidaspow 1990).

5.2.1 Governing equations

In the following sections, the general equations for continuity, momentum, turbulent kinetic energy and the dispersed turbulence model are presented. Further details can be found in e.g. FLUENT manuals (FLUENT 1998).

Continuity equations

The general conservation of mass for the gas phase (g) and for the solid phase (s) are shown in Equation 5.1 and 5.2. α, ρ and u_j denote volume fraction of gas or solid, density and the j-th direction velocity component, respectively. No mass transfer is allowed between the phases in this simulations.

When the dispersed turbulence model is applied, as in this simulation, see Equation 5.1 and 5.2. Where $\mu_{j,g}$ and $\mu_{j,s}$ denote the viscosity for solids and gas, respectively.

$$\frac{\partial}{\partial t}(\alpha_g \rho_g) + \frac{\partial}{\partial x_j}(\alpha_g \rho_g u_{j,g}) = 0 \tag{5.1}$$

$$\frac{\partial}{\partial t}(\alpha_s \rho_s) + \frac{\partial}{\partial x_j}(\alpha_s \rho_s u_{j,s}) = 0 \tag{5.2}$$

Momentum equations

Gas phase The conservation of momentum for the gas phase (g) is given by Equation 5.3, where $\tau_{ij,g}$ and K_{gs} denote shear stress for the gas phase, gas-solid particle exchange coefficient and additional forces besides drag and gravity forces, respectively. The shear stress is related to the gradients of velocity components and a turbulent viscosity given by Equation 5.4. k_g and $\mu_{eff,g}$ denote the turbulence kinetic energy and the dynamic effective gas viscosity, respectively.

$$\frac{\partial}{\partial t}(\alpha_g \rho_g u_{i,g}) + \frac{\partial}{\partial x_j}(\alpha_g \rho_g u_{j,g} u_{i,g}) = -\alpha_g \frac{\partial P}{\partial x_i} + \frac{\partial \tau_{ij,g}}{\partial x_j} + \alpha_g \rho_g g_i + \sum_{s=1}^{n} K_{gs}(u_{i,s} - u_{i,g}) \tag{5.3}$$

$$\tau_{ij,g} = -\frac{2}{3}\alpha_g \rho_g k_g \delta_{ij} + \alpha_g \mu_{eff,g}\left[\left(\frac{\partial u_{i,g}}{\partial x_j} + \frac{\partial u_{j,g}}{\partial x_i}\right) - \frac{2}{3}\delta_{ij}\frac{\partial u_{k,g}}{\partial x_k}\right] \tag{5.4}$$

Particle phase The conservation of momentum for the solid phase (s) is given by Equation 5.5, where K_{sg}, K_{ss} and P_s denote the solid-gas exchange coefficient, solid-solid exchange coefficient and the solid phase pressure, respectively. The total stress tensor for the solid phase is shown in Equation 5.6, where λ_s is the bulk viscosity.

$$\frac{\partial}{\partial t}(\alpha_s \rho_s u_{i,s}) + \frac{\partial}{\partial x_j}(\alpha_s \rho_s u_{j,s} u_{i,s}) = -\alpha_s \frac{\partial P}{\partial x_i} - \frac{\partial P_s}{\partial x_i} + \frac{\partial \tau_{ij,s}}{\partial x_j} \tag{5.5}$$

$$+\alpha_s\rho_s g_i + K_{sg}(u_{i,g} - u_{i,s}) + \sum_{l=1}^{m} K_{ss}(u_{i,l} - u_{i,s})$$

$$\tau_{ij,s} = \alpha_s\mu_s(\frac{\partial u_{i,s}}{\partial x_j} + \frac{\partial u_{j,s}}{\partial x_i}) + (\alpha_s\lambda_s - \alpha_s\mu_s\frac{2}{3})\delta_{ij}\frac{\partial u_{k,s}}{\partial x_k} \tag{5.6}$$

Granular temperature equation

The transport equation for granular temperature is derived from kinetic theory for granular flow (Ding & Gidaspow 1990):

$$\frac{2}{3}\left[\frac{\partial}{\partial t}(\rho_s\alpha_s\theta_s) + \frac{\partial}{\partial x_j}(\rho_s\alpha_s u_{j,s}\theta_s)\right] = (-P_s\delta_{ij} + \tau_{ij,s})\frac{\partial u_{i,s}}{\partial x_j} \tag{5.7}$$

$$+\frac{\partial}{\partial x_j}\left(\kappa\frac{\partial\theta_s}{\partial x_j}\right) - \gamma + 3K_{gs}\theta_s$$

κ, γ and ϕ denote diffusion coefficient for granular energy, collisional dissipation of energy due to particle collisions, and dissipation due to gas-particle interactions. The term $(-P_s\delta_{ij} + \tau_{ij,s})\frac{\partial u_{i,s}}{\partial x_j}$ is the energy generation by the solid stress tensor.

Dispersed turbulence model

The dispersed turbulence model applies a modified $k-\epsilon$ turbulence model for the gas phase supplemented with terms including the interphase turbulent momentum transfer. There is no additional turbulence model for the solid phase. Hence, the solids phase turbulence is included in the gas phase.

The modified $k-\epsilon$ turbulence model for the gas phase is shown in Equation 5.8 for kinetic energy (k) and 5.9 for dissipation (ε). $\prod_{k_g}$ and $\prod_{\varepsilon_g}$ denote the influence of the solid particle phase on the gas phase. G_g denotes generation of kinetic energy (k).

$$\frac{\partial}{\partial t}(\alpha_g\rho_g k_g) + \frac{\partial}{\partial x_j}(\alpha_g\rho_g u_{j,g}k_g) = \frac{\partial}{\partial x_j}\left[\alpha_g(\mu_g + \frac{\mu_{t,g}}{\sigma_k})\frac{\partial k_g}{\partial x_i}\right] \tag{5.8}$$

$$+\alpha_g\rho_g(G_g - \varepsilon_g) + \alpha_g\rho_g\prod_{k_g}$$

$$\frac{\partial}{\partial t}(\alpha_g\rho_g\varepsilon_g) + \frac{\partial}{\partial x_j}(\alpha_g\rho_g u_{j,g}\varepsilon_g) = \frac{\partial}{\partial x_j}\left[\alpha_g(\mu_g + \frac{\mu_{t,g}}{\sigma_\varepsilon})\frac{\partial\varepsilon_g}{\partial x_i}\right] \tag{5.9}$$

$$+\alpha_g\rho_g\frac{\varepsilon_g}{k_g}(C_{1\varepsilon}G_g - C_{2\varepsilon}\varepsilon_g) + \alpha_g\rho_g\prod_{\varepsilon_g}$$

5.2.2 Numerical flow conditions

Isothermal conditions are applied and no chemical species are solved in the Euler-Euler simulation. A steady state simulation is performed. The boundary conditions for raw meal (inert), kiln gas and tertiary gas can be found in Table 5.1 and 5.2. The gas and particle density are set to 0.27 and 2745 kg/m^3, respectively. The pressure is set to $1 \cdot 10^5$ Pa.

All the wall boundaries are modeled in a standard way with standard wall functions, and no-slip conditions for the gas as well as the particle phase.

A zero flux of granular temperature at the wall is assumed. The density is set constant and the walls are set adiabatic. The simulation is done without fuel particles since their contribution are insignificant compared to the amount of raw meal.

Table 5.1: Boundary conditions for the precalciner model during Euler-Euler simulations.

Inlets	Flow rates
Air, raw meal inlet 1 (k.g.)	0.83 kg/s
Air, raw meal inlet 2 (t.a.)	0.83 kg/s
Kiln gas	25 m/s
Tertiary gas	16.4 m/s

Table 5.2: Boundary injections for the precalciner model during Euler-Euler simulations.

Injections	Flow rates [kg/s]	Velocity [m/s]	Particle size [μm]
Raw meal 1 (k.g.)	30	10	52
Raw meal 2 (t.a.)	30	10	52

5.2.3 Computational results and discussions

Figure 5.2 shows the volume fraction of the solid phase in the precalciner. The raw meal volume fraction is below $1 \cdot 10^{-3}$ in the precalciner during Euler-Euler simulations, which is in accordance with the characteristics in Subsection 3.1.2.

It was found that gas-particle interactions are more important than particle-particle interactions.

Appendix N shows raw meal volume fraction, gas velocity and kinetic energy of turbulence in three cross-sections, in accordance with Figure 3.2. (All CFD figures in Appendix N follow the view of Figure 3.3.) The raw meal seems to rise in two plumes from the inlets until it disperses between the first and second bend, and increases the volume fraction at the wall, see Figure N.1, N.4 and N.7. Figure 5.2 shows indications of core-annulus flow from the first bend and up to the swan's neck.

Figure 5.3 show the gas velocity in the axial direction where the velocity is at about 40 m/s at its largest. The lowest cross-section plot, Figure N.2, shows increased velocities from 32 to 40 m/s on the side opposite to the raw meal inlets. Thereafter, the velocity in the mid cross-section reaches 53 m/s, see Figure N.5. The increased velocity on the side opposite to the raw meal inlet (lowest cross section) is probably due to displacement of the gas through-put, i.e. the raw meal blocks part of the tertiary- and kiln gas inlet before it disperses further up.

The kinetic energy of turbulence in Figure 5.4, N.3, N.6 and N.9 can be seen to follow the raw meal volume fraction in Figure N.1, N.4 and N.7. Hence, the particles seem to enhance turbulence. According to the proposed map of Elgobashi (1991), and taking into account that the raw meal volume fraction is less than $1 \cdot 10^{-3}$, it can be stated that the raw meal particles are in the region of two-way coupling and possibly enhancing turbulence, see Figure 2.26. It must be emphasized that the velocity gradient could have an impact on the magnitude of turbulence.

5.3 Euler-Lagrangian approach

Euler-Lagrangian simulations do not include particle-particle interactions in the model, only gas-particle interactions. The gas phase will impact the particle phase whereupon the particle phase trajectories affect the continuum.

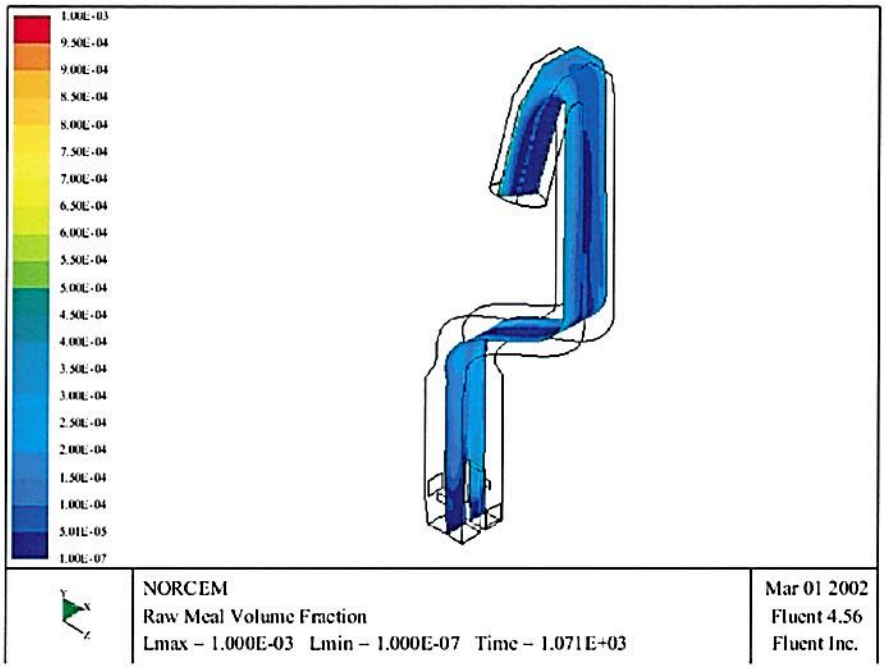

Figure 5.2: Raw meal volume fraction in the precalciner during Euler-Euler simulations. The tertiary gas inlet can be seen on the right hand side of the partition wall.

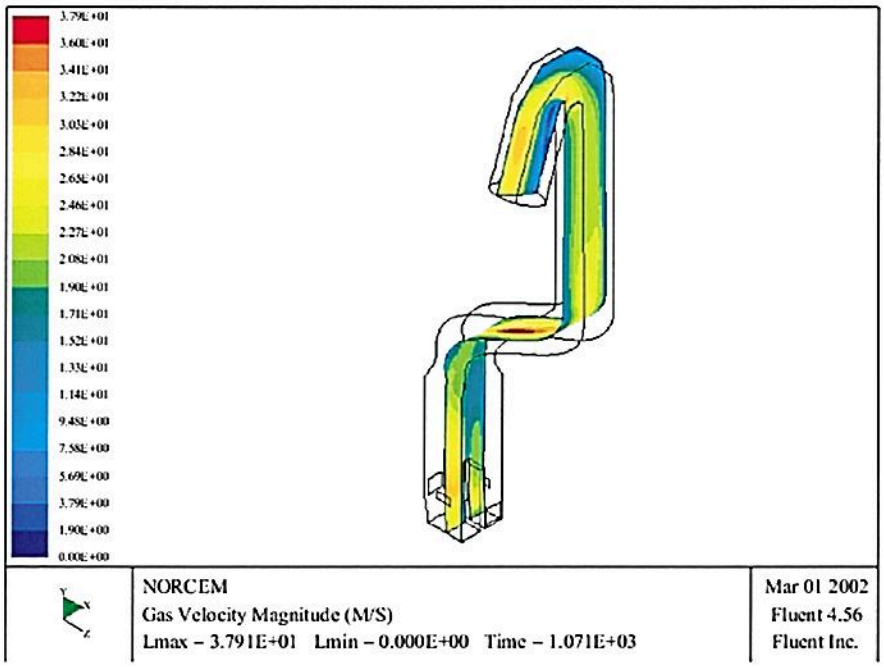

Figure 5.3: Gas velocity in the precalciner during Euler-Euler simulations. The tertiary gas inlet can be seen on the right hand side of the partition wall.

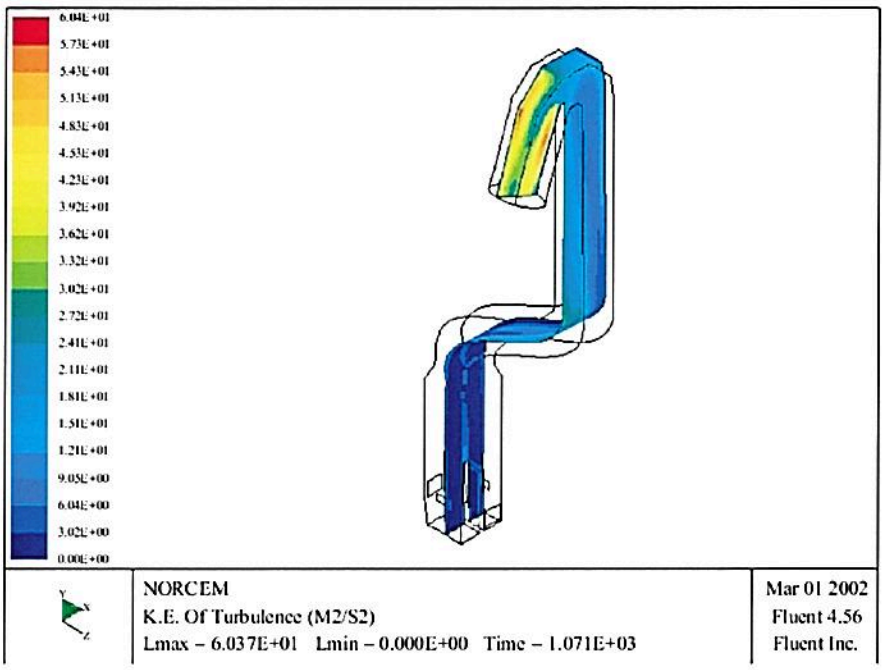

Figure 5.4: Kinetic energy of turbuelence in the precalciner during Euler-Euler simulations. The tertiary gas inlet can be seen on the right hand side of the partition wall.

5.3.1 Discrete and continuous phase coupling

The two-way coupling is accomplished by alternately solving the continuous and discrete phase equations until a converged solution in both phases is achieved.

5.3.2 The fluid phase

The fluid phase is treated as a continuum with a numerical solution of the steady state differential equations for energy, mass, chemical species, momentum, turbulent kinetic energy and dissipation rate.

Equation 5.10 shows the differential expression, where ϕ is the general variable; x_j is the position; u_j is the velocity; Γ is the diffusion coefficient and S is the source term (Patankar 1980). The particle influence on the gas phase is included in the source terms.

$$\frac{\partial}{\partial x_j}(\rho u_j \phi) = \frac{\partial}{\partial x_j}\left(\Gamma \frac{\partial \phi}{\partial x_j}\right) + S \tag{5.10}$$

5.3.3 The discrete second phase

The discrete second phase follows the Euler-Lagrangian approach, which is solved by tracking a certain number of particles through the flow field.

The particle force balance

The particle force balance equates the particle inertia with the forces acting on the particle:

$$\frac{d\vec{u}_p}{dt} = F_D(\vec{u}_g - \vec{u}_p) + \vec{g}\frac{(\rho_p - \rho_g)}{\rho_p} + \vec{F} \tag{5.11}$$

$F_D(\vec{u}_g - \vec{u}_p)$ is the drag force per unit particle mass and F_D is given by Equation 5.12.

$$F_D = \frac{18\mu}{\rho_p d_p^2}\frac{C_D \,\mathrm{Re}}{24} \tag{5.12}$$

Here, u_g is the gas phase velocity, u_p is the particle velocity, μ is the dynamic viscosity of the fluid, ρ_g is the fluid density, ρ_p is the density of the particle, and d_p is the particle diameter. Re is the relative particle Reynolds number, which is defined as

$$\mathrm{Re} = \frac{\rho d_p \,|\vec{u}_g - \vec{u}_p|}{\mu} \tag{5.13}$$

The drag coefficient, C_D, is a function of the relative Reynolds number, from the the model of Haider and Levenspiel (1989):

$$C_D = \frac{24}{\mathrm{Re}_p}(1 + b_1 \,\mathrm{Re}_p^{b_2}) + \frac{b_3 \,\mathrm{Re}_p}{b_4 + \mathrm{Re}_p} \tag{5.14}$$

Equation 5.14 is a function of the shape factor (ϕ) through the empirical Equation 5.15 and 5.16, where s is the surface area of a sphere having the same volume as the particle, and S is the actual surface area of the particle (Haider & Levenspiel 1989).

$$\begin{aligned} b_1 &= 2.3288 - 6.4581\phi + 2.4486\phi^2 \\ b_2 &= 0.0964 + 0.5565\phi \\ b_3 &= 4.905 - 13.8944\phi + 18.4222\phi^2 - 10.2599\phi_3 \\ b_4 &= 1.4681 + 12.2584\phi - 20.7322\phi^2 - 15.8855\phi_3 \end{aligned} \tag{5.15}$$

$$\phi = \frac{s}{S} \tag{5.16}$$

The shape factor is set to 0.03 in the simulation performed in this study.

Integration of the trajectory equations

Trajectory and auxiliary equations for heat and mass transfer to or from the particle, are solved by stepwise integration over discrete time steps. Integration in time of Equation 5.11 yields the velocity of the particle at each point along the trajectory, with the trajectory itself predicted by Equation 5.17.

$$\frac{dx}{dt} = \vec{u}_p \tag{5.17}$$

Turbulent dispersion of particles

FLUENT models turbulent dispersion either by a stochastic discrete-particle approach or a cloud representation of a group of particles about a mean trajectory. In this study the stochastic tracking approach is applied. This is known as the Discrete Random Walk (DRW) model, also called the eddy lifetime model.

The stochastic tracking approach predicts the turbulent dispersion of particles by integrating the trajectory equations for individual particles, using the instantaneous

fluid velocity, $\bar{u}+\acute{u}(t)$, along the particle path during the integration. By computing the trajectory in this manner for a sufficient number of representative particles, the random effects of turbulence on the particle dispersion may be accounted for.

The integral time

The fluctuating velocity components are discrete piecewise constant functions of time, and kept constant over an interval of time given by the characteristic lifetime of the eddies. The raw meal in a cement kiln has a particle size of about 52 μm and from this accepting that the particles move with the fluid (zero drift velocity), the integral time becomes the fluid Lagrangian integral time (T_L). An approximation is found as:

$$T_L = C_L \frac{k}{\epsilon} \tag{5.18}$$

C_L is set to 0.15 in this study.

The eddy lifetime model

In the eddy lifetime model, the interaction of a particle with a succession of discrete conventionalized fluid phase turbulent eddies is simulated. Each eddy is characterized by a:

- Gaussian distributed random velocity fluctuation, u', v' and w'
- time scale, τ_e.

The values of u',v', and w' that prevail during the lifetime of the turbulent eddy are sampled by assuming that they obey a Gaussian probability distribution, see Equation 5.19.

$$u' = \zeta\sqrt{\overline{u'^2}} \tag{5.19}$$

ζ is a normally distributed random number, and the remainder of the right-hand side is the local rms value of the velocity fluctuations. Since the kinetic energy of turbulence is known at each point in the flow, these values of the rms fluctuating components can be obtained by assuming isotropy for the k-ϵ model and its variants, see Equation 5.20.

$$\sqrt{\overline{u'^2}} = \sqrt{\overline{v'^2}} = \sqrt{\overline{w'^2}} = \sqrt{2k/3} \tag{5.20}$$

The characteristic lifetime of the eddy (τ_e) is defined as:

$$\tau_e = 2T_L \tag{5.21}$$

Inert heating and cooling

Inert heating and cooling is applied while the particle temperature is less than the vaporization temperature:

$$T_p < T_{vap}$$

and after the volatile fraction, f_{v0}, of a particle has been consumed:

$$m_p \leq (1 - f_{v0}) m_{p0}$$

where T_p , T_{vap}, m_{p0} and m_p denote the particle temperature, the vaporization temperature, the initial mass of the particle and its current mass, respectively.

$T_p < T_{vap}$ is applied until the temperature of the particle/droplet reaches the vaporization temperature. Then a non-inert particle/droplet proceeds by obeying one of the mass-transfer laws e.g. devolatilization and/or surface combustion. Following, application of $m_p \leq (1 - f_{v0})m_{p0}$ when the volatile portion of the particle/droplet has been consumed, i.e. for a combusting particle containing residual ash, reverts to the inert heating law.

A simple heat balance is applied to relate the particle temperature ($T_p(t)$) to the convective heat transfer at the particle surface, see Equation 5.22. Where, m_p, c_p, A_p, T_∞ and h denote particle mass, particle heat capacity, particle surface area, local temperature of the continuous phase and convective heat transfer coefficient, respectively. Negligible internal resistance to heat transfer is assumed, i.e., the particle is at a uniform temperature. Radiative heat transfer is not included in this model.

$$c_p \frac{d(T_p m_p)}{dt} = hA_p(T_\infty - T_p) \tag{5.22}$$

Devolatilization

The devolatilization law is applied to a combusting particle when the temperature of the particle reaches the vaporization temperature (T_{vap}):

$$T_p \geq T_{vap} \; and \; T_p \geq T_{bp}$$

and remains in effect while the mass of the particle (m_p) exceeds the mass of the non-volatiles in the particle:

$$m_p > (1 - f_{v0} - f_{w0})m_{p0}$$

where T_{bp} and f_{w0} denote boiling point temperature of the particle and volume fraction of the evaporating/boiling material if wet combustion is selected.

The volume fraction (f_{w0}) is set to zero in this simulation.

There are three devolatilization models in FLUENT:

- the constant rate model (the default model)
- the single kinetic rate model
- the two competing rates model

The model with two competing rates is used in this study, and a discussion of this model follows.

The kinetic devolatilization rate expressions, where R_1 and R_2 are competing rates that may control the devolatilization over different temperature ranges, are shown in Equation 5.23 and 5.24 (Kobayashi, Howard & Sarofim 1976).

$$R_1 = A_1 \exp(-E_1/RT_p) \tag{5.23}$$

$$R_2 = A_2 \exp(-E_2/RT_p) \tag{5.24}$$

The two kinetic rates are weighted to yield an expression for the devolatilization, see Equation 5.25, where $m_v(t)$, m_{p0}, $\alpha_{1 \; and \; 2}$ and m_a denote the volatile yield up to time t, initial particle mass at injection, yield factors and ash content in the particle, respectively. The yield α_1, which represents the devolatilization at low temperatures, is recommended to be set similar to the fraction of volatiles from proximate analysis.

$$\frac{m_v(t)}{m_{p0} - m_a} = \int_0^t (\alpha_1 R_1 + \alpha_2 R_2) \exp(-\int_0^t (R_1 + R_2) dt) dt \tag{5.25}$$

Particle Swelling During Devolatilization

The particle diameter changes during the devolatilization according to the swelling coefficient (C_{sw}), see Equation 5.26, where d_{p0} and d_p denote the initial particle diameter and current particle diameter, respectively.

$$\frac{d_p}{d_{p0}} = 1 + (C_{sw} - 1)\frac{(1 - f_{w0})m_{p0} - m_p}{f_{v0} m_{p0}} \tag{5.26}$$

The term $[((1 - f_{w0})m_{p0} - m_p)/f_{v0}m_{p0}]$ in Equation 5.26 is the ratio of the mass that has been devolatilized to the total volatile mass of the particle.

Heat Transfer to the Particle During Devolatilization

Heat transfer to the particle during the devolatilization process includes contributions from convection and the heat consumed during devolatilization, see Equation 5.27.

$$c_p \frac{d(T_p m_p)}{dt} = hA_p(T_\infty - T_p) + \frac{dm_p}{dt} h_{fg} \tag{5.27}$$

Radiation heat transfer to the particle is not included in this model.

Surface combustion

After the volatile component of the particle is completely evolved, a surface reaction begins, which consumes the combustible fraction (f_{comb}) of the particle. Thus, char combustion starts when all volatiles are evolved and continues until the combustible fraction is consumed:

$$m_p > (1 - f_{v0} - f_{w0} - f_{comb})m_{p0}$$

When the combustible fraction (f_{comb}) has been consumed, the combusting particle may contain residual ash that reverts to the inert heating law, described by Equation 5.22.

The surface combustion law consumes the reactive content of the particle as governed by the stoichiometric requirement (S_b) of the surface burnout reaction, see Equation 5.28. S_b is defined as mass of oxidant per mass of char.

$$char(s) + S_b O(g) \rightarrow Products(g) \tag{5.28}$$

There are three heterogeneous surface reaction rate models for combusting particles in FLUENT:

- the diffusion-limited rate model (the default model)
- the kinetics/diffusion-limited rate model
- the intrinsic model

The kinetics/diffusion-limited rate model is applied in this simulation, and a discussion of this model follows.

The kinetic/diffusion-limited rate model assumes that the surface reaction rate is determined either by kinetics or by a diffusion rate. The standard FLUENT

model is applied. Equation 5.29 and 5.30 show the diffusion rate and kinetic rate, respectively. In Equation 5.31 they are weighted to yield a char combustion rate.

$$R_1 = C_1 \frac{[(T_p + T_\infty)/2]^{0.75}}{d_p} \tag{5.29}$$

$$R_2 = C_2 \exp(-E/RT_p \tag{5.30}$$

$$\frac{dm_p}{dt} = -\pi d_p^2 Po \frac{R_1 R_2}{R_1 + R_2} \tag{5.31}$$

P_O is denoted the partial pressure of oxidant species in the gas surrounding the combusting particle. The kinetic rate R_2 incorporates the effects of chemical reaction on the internal surface of the char particle (intrinsic reaction) and pore diffusion. The particle size is assumed to remain constant in this model, whereas the density is allowed to decrease.

Heat and Mass Transfer During Char Combustion

The surface reaction consumes the oxidant species in the gas phase, i.e. it supplies a (negative) source term during the computation of the transport equation for this species. The product of the heterogeneous surface reaction appears in the gas phase as a user-selected chemical species.

The particle heat balance during surface reaction is shown in Equation 5.32. H_{reac} denotes the heat released by the surface reaction.

$$c_p \frac{d(T_p m_p)}{dt} = hA_p(T_\infty - T_p) + f_h \frac{dm_p}{dt} H_{reac} \tag{5.32}$$

The particle absorbs a fraction (f_h) of the heat released by the surface reaction, i.e. a portion $(1 - f_h)$ of the energy produced by the surface reaction appears as a heat source in the gas phase.

5.3.4 Numerical flow conditions

General conditions

The particle drag parameter is set to 0.63 for fuel (coal-hv) and circulating mass ($CaCO_3$) (Kunii & Levenspiel 1991).

The viscous model applied in FLUENT 6 includes the standard two equation k-ϵ turbulence model and the standard wall functions.

The precalciner is highly turbulent (Re $\approx$ 700.000). Therefore, the eddy-dissipation-model reaction rates (the Magnussen-Hjertager model) and/or the Arrhenius reaction rate model are used. The reactions are volumetric and diffusion energy source and full multicomponent diffusion are included. The segregated solver is applied including its default (first-order upwind) discretization scheme.

The species included in the model are CO, CO_2, O_2, H_2O, N_2 and volatiles from the coal (coal-hv). CO_2 is selected as the product of the heterogeneous surface reaction. Chosing CO_2 as the product of the heterogeneous surface reaction do not fulfil Equation 2.81, but it simplify identification of products from pyrolysis (CO). Energy is included with its standard solution. Radiation is not included in order to simplify the calculations at this stage. This is a reasonable assumption since the gas and particle mixture is fairly homogeneous.

The boundary inlet conditions and injections

The boundary inlet injections and conditions are given in Table 5.3 and Table 5.4, respectively. All injections have a turbulence intensity of 3 %. Simulations including both the upper and the lower coal inlet led to a large pressure build-up between the two inlets. Therefore, the simulations are simplified by applying only the upper coal inlet. The abbreviation *k.g.* and *t.a.* in Table 5.3 and Table 5.4 denote kiln gas and tertiary air (flowing on separate sides of the precalciner bottom section).

Table 5.3: Boundary conditions for the precalciner model during Euler-Lagrangian simulations.

Inlets	Flow rates	T [K]	O_2 [wt%]	N_2 [wt%]	CO_2 [wt%]	H_2O [wt%]
Air, coal	0.1 kg/s	298	23.3	76.7	-	-
Air, alt.fuel (k.g.)	0.1 kg/s	298	23.3	76.7	-	-
Air, alt.fuel (t.a.)	0.1 kg/s	298	23.3	76.7	-	-
Air, raw meal 1 (k.g.)	0 kg/s	973	23.3	76.7	-	-
Air, raw meal 2 (t.a.)	0 kg/s	973	23.3	76.7	-	-
Kiln gas	25 m/s	1173	3.2	76.5	17.8	2.4
Tertiary gas	16.4 m/s	923	23.3	76.7	-	-

Table 5.4: Boundary injections for the precalciner model during Euler-Lagrangian simulations.

Injections	Flow rates [kg/s]	T [K]	Velocity [m/s]	Particle size [μm]
Coal	1.5	298	25	40
Alt.fuel (k.g.)	0.5	298	0.5	200
Alt.fuel (t.a.)	1.5	298	0.5	200
Raw meal 1 (k.g.)	30	973	10	52
Raw meal 2 (t.a.)	30	973	10	52

The precalciner outlet

Pressure outlet boundary conditions are applied on the precalciner outlet, which is used to define the static pressure at flow outlets.

The exterior walls

The exterior walls are set to be conducting with a heat flux of 1293 W/m^2, while the interior partition wall is set to a constant temperature of 1048 K. In scarcity of better heat flux, taking into consideration that the temperature and construction (thermal resistance) of different precalciners are comparable, results found by Giddings et al. (2000) are applied. For simplicity, the simulations were carried out with no wall roughness and no slip.

Particulate phase modelling

The mass ratio of particles to gas is 0.88. Hence, it is expected that the discrete phase (particles) has a significant effect on the enthalpy and momentum of the continuous phase (gas). Therefore, interaction with the continuous phase is included.

The particles (mean path) trajectory is simulated. Hence, the dispersion of particles due to turbulence in the fluid phase is not predicted. Coal and raw meal injections have a uniform diameter distribution with the stochastic model of random eddy lifetime. Table 5.4 shows the particle size and flow rates.

Calcination modelling of raw meal was not possible to implement in FLUENT 6 with application of the devolatilization model for combusting particles. This is due to the fact that FLUENT 6 does not accept more than one type of combusting particles, e.g. coal. Thus, the energy requirement in the precalciner model is highly affected. A realistic precalciner temperature is the major quality assurance for well accomplished simulations. The precalciner temperature is found, in full-scale experiments, to be from 820 to 960 $°C$, see Table 3.7.

The energy balance can be fulfilled to obtain an expected precalciner temperature in three ways:

- The fuel heat of reaction for burnout can be reduced, or
- an energy sink within the computational domain can be defined, or
- an endothermic reactant (e.g. $CaCO_3$) can be fed into the precalciner along with the raw meal.

To obtain the energy balance (achieve precalciner temperature) it is chosen to reduce the reaction for burnout.

The injection rates for inert $CaCO_3$ particles are similar to those found in the full-scale precalciner in Brevik. The fuel flow rates are based on previous experiments with precalciner alternative fuels (SHW, RDF, AM).

The devolatilization model applies the two competing rates model, and the kinetic/diffusive limited combustion model is used. Furthermore, CO is selected as the devolatilization species, whereas CO_2 is selected as the product from char combustion. All reaction constants, physical constants and chemical constants are set equal to FLUENT standard values, except α_1, which represents the devolatilization at low temperatures in Equation 5.25. It is recommended to set the devolatilization at low temperatures (α_1) similar to the fraction of volatiles from proximate analysis. Hence, a trade-off between coal and the alternative fuels is necessary. The volatiles fractions are 31.6, 53, 59.7 and 46.3 % for coal, RDF, AM and SHW, respectively. As an approximation $\alpha_1$is set to 0.5.

The particle size of the alternative fuels in the precalciner kiln is fuel specific and varies between 0.5 and 30 mm. It is chosen to simulate with a particle size of 200 μm for the injections of alternative fuels in order to investigate the particle trajectories and burnout, see Table 5.4. The alternative fuel injections are executed with coal-hv since FLUENT 6 only allows for simulations with one fuel-type. The swelling index is set to 2, which is appropriate for coal (FLUENT standard). However, the swelling index is not representative for the alternative fuels. Since it is of interest to simulate the alternative fuels inlets with a larger particle size, and execution of simulations with particles larger than 200 μm gave numerical instability, a swelling index of 2 is an acceptable assumption. This means that, after devolatilization, the alternative fuel particles obtain a particle diameter of 400 μm.

5.3.5 Computational results and discussions

Figure 5.5 and 5.6 show that the product species from devolatilization (CO) is lower (is generated slower) for the alternative fuel inlet on the kiln gas side than the one on the tertiary air gas side. Hence, a delayed devolatilization will delay the initialization of char combustion with subsequent lower char conversion, see Table 5.5.

It is believed that the slower devolatilization of the fuel on the kiln gas side can be caused by:

- the lower mass flow rate of fuel, compared to the tertiary kiln gas side and/or
- the suppressing effect of raw meal in the upstream, which can be due to the location of the raw meal inlet. The raw meal inlet on the kiln gas side is at the same level as the alternative fuel inlet, in contrast to the tertiary air gas side, where the alternative fuel inlet is placed lower.

A suppressing effect of raw meal will probably lower the heat transfer to the fuel particles, which results in a slower devolatilization rate on the kiln gas side, even though the temperature is 200 K higher than on the tertiary air gas side. Previous work has shown that the devolatilization rate is governed by heat transfer (Zevenhoven, Karlsson, Hupa & Frankenhaeuser 1997), (Bjerkebo 2000).

It can be seen from Figure 5.5 and 5.6 that the coal fuel, on the tertiary air gas side, follows and incorporates into the alternative fuel feed stream.

Figure 5.7 shows the contours of O_2 in the precalciner. In the lower section of the precalciner there is a low degree of mixing between the tertiary air gas side (23.3 wt-% O_2) and the kiln gas side. This phenomenon explains the successful utilization of reburning (for NO reduction) on the kiln gas side of the precalciner. However, delayed mixing represents less oxidizing conditions for the alternative fuels on the kiln gas side, followed by a delayed burnout. The reburning zone could probably, with success, be shortened by means of change in the flow pattern to improve the oxidizing conditions on the kiln gas side.

The CO is concentrated in a smaller region in Figure 5.8 compared to Figure 5.9. Traverse CO measurements in full-scale experiments showed a similar result, but the locations were not the same as those found in the CFD simulations, see Figure 3.3. This is possibly due to the differences in the particle size distribution of the alternative fuels, which will affect the flow pattern.

Figure 5.10 shows a high degree of turbulence intensity in the three cross-sections.

It can be shown, from application of Equation 2.99 and 2.100 together with the precalciner characteristics in Table 3.8, that previous work on the particle retention time in a CFB reactor should be used with caution on a precalciner, see Section 2.3.2. Also, different calciners most likely have different particle retention times. Table 5.5 shows calculated particle retention times for the fuel and raw meal from the different inlets. The gas retention time ($\tau_g = 1.9$ sec.) is analogous to the lowest retention time for the alternative fuel and raw meal. A comparison to the retention time for the raw meal ($\tau_s = 3.6$ sec.) gives an average ratio τ_s/τ_g of about 2. Previous experiments from Hundebøl et al. (1987) in a FLS-ILC industrial calciner give an approximate ratio τ_s/τ_g of 4. Hundebøl et al. (1987) explained this with backmixing ("showers") or so called core-annulus flow, which is also confirmed from previous work on CFBC reactors by several authors, see Section 2.3.2. From this, it can be assumed that the precalciner at kiln 6 in Brevik has a lower degree of backmixing / core-annulus flow compared to previous work, which is probably due to the large gas velocity. Furthermore, it can be seen from Table 5.5 that the fuel particles retention time is lower than for raw meal, which is probably due to the different flow pattern.

It can be seen from Figure 5.11 that the temperature is simulated to be in the upper range (820 - 960 $°C$) of previous measurements in the precalciner.

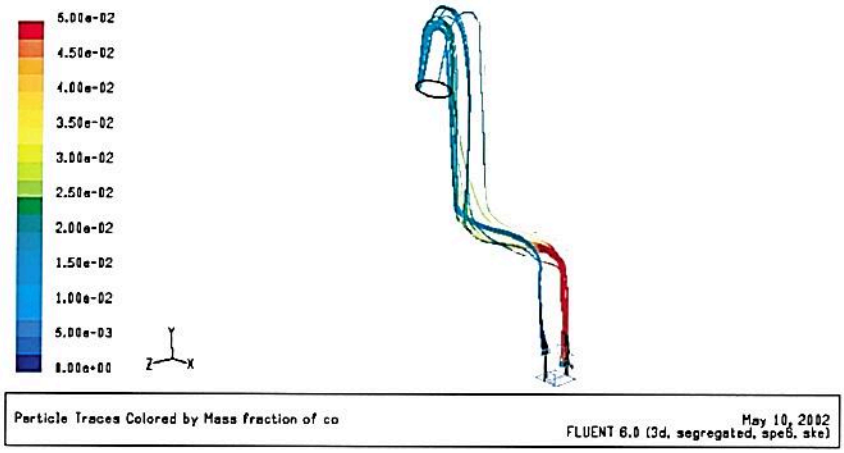

Figure 5.5: Fuel particle traces coloured by mass fraction of CO during Euler-Lagrangian simulations. The tertiary air gas side is nearest in the figure.

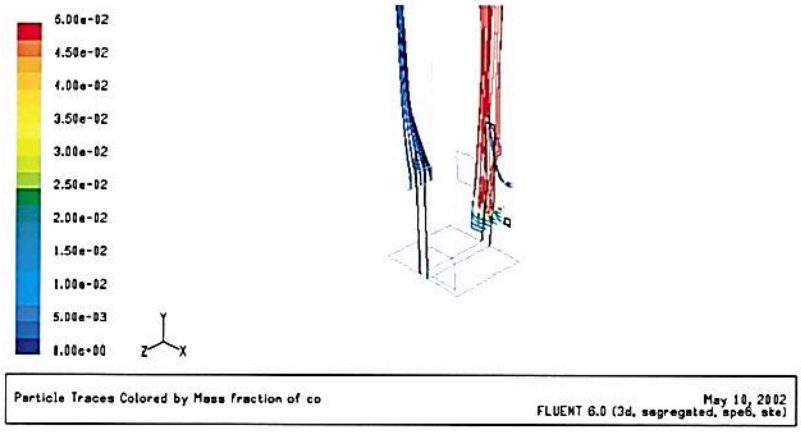

Figure 5.6: Close-up: Inlet section of Figure 5.5. Particle (fuels) traces coloured by mass fraction of CO during Euler-Lagrangian simulations. The tertiary air gas side is nearest in the figure.

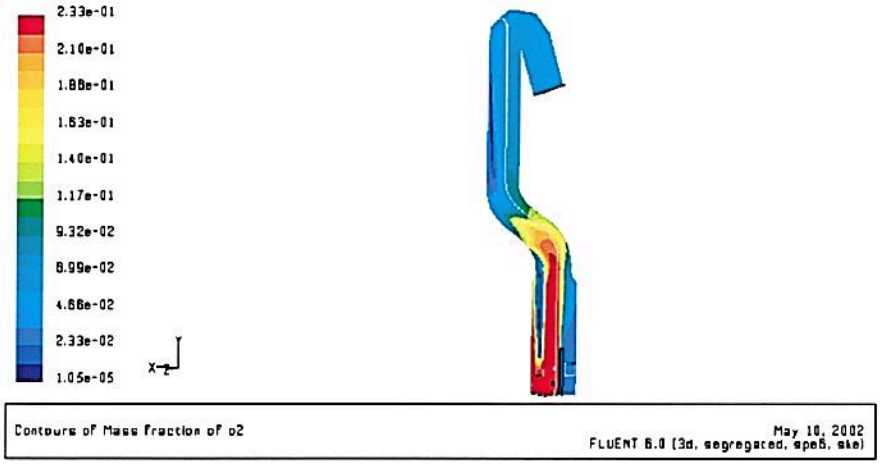

Figure 5.7: Contours of O_2 mass fraction during Euler-Langrangian simulations.

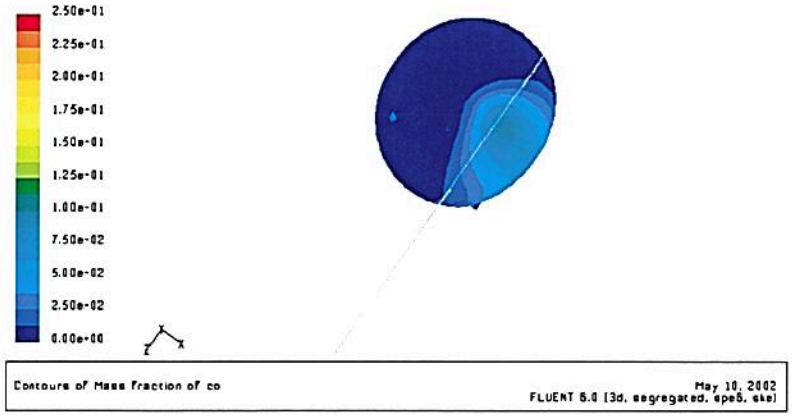

Figure 5.8: Contours of CO mass fraction during Euler-Lagrangian simulations. The cross-section refers to sampling points 3 to 6 in Figure 3.2

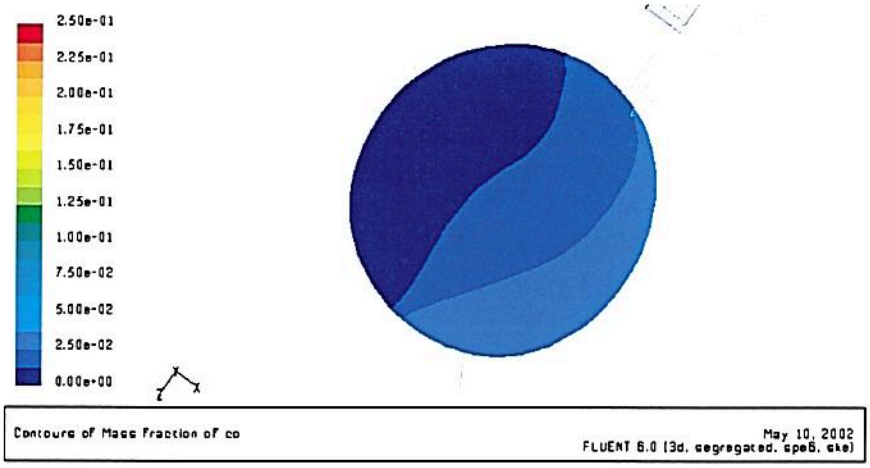

Figure 5.9: Contours of CO mass fraction during Euler-Lagrangian simulations. The cross-section refers to sampling points 8 to 11 in Figure 3.2

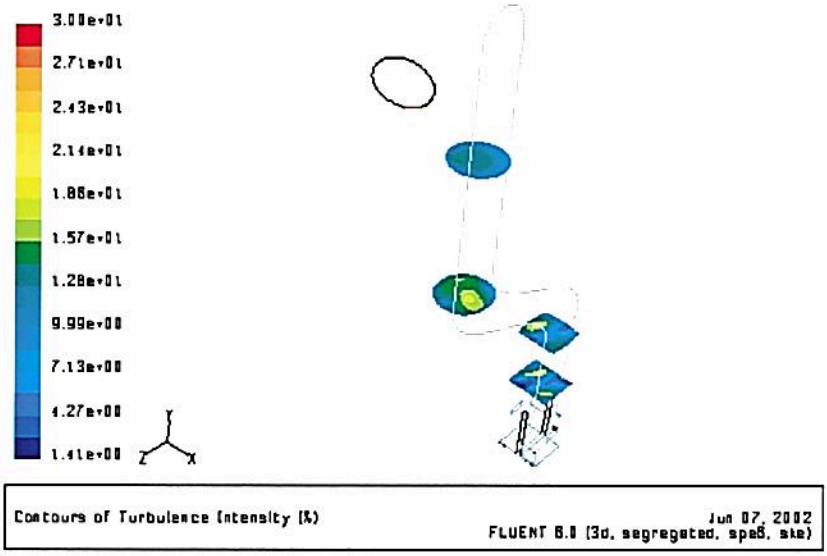

Figure 5.10: Turbulence intensity (%) during Euler-Langrangian simulations. The three lowest cross-sections correspond to the positions of the sampling points in Figure 3.3 and 3.2.

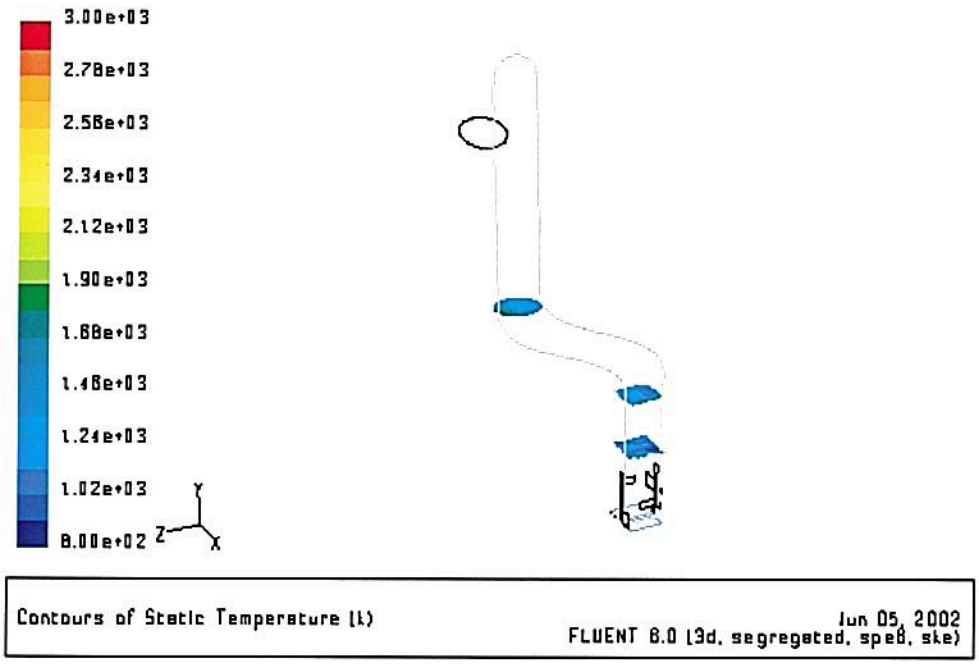

Figure 5.11: Temperature (K) during Euler-Langrangian simulations, The cross-sections correspond to the positions of the sampling points in Figure 3.2.

5.4 Conclusion of CFD simulations

Euler-Euler simulations of the precalciner were performed. The obtained flow pattern verified the assumption of dilute flow and the importance of gas-particle interaction in a precalciner. It has been found that the raw meal:

- volume fraction is below $1 \cdot 10^{-3}$, which is in accordance with previous characteristics,
- rises in two plumes from the injection points until it disperses between the first and second bend and increases the particle volume fraction close to the wall,
- obstructs part of the tertiary- and kiln gas inlet, which increases the local gas velocity, before it disperses and becomes uniformly distributed in the upper parts, and
- particles seem to enhance turbulence.

Euler-Langrangian simulations of the precalciner were performed as well. The particle-trajectory, retention time and species concentration were successfully calculated. The simulations revealed important information for further utilization of alternative fuel in the precalciner. The Euler-Langrangian simulations showed:

- delayed devolatilization on the kiln gas side, which is most likely due to the suppressing effect of raw meal in the upstream, giving a lower heat transfer. Replacement of the raw meal inlet could improve the devolatilization, since the raw meal inlet is at the similar level as the alternative fuel inlet, in contrast to the tertiary gas side.

Table 5.5: Particle retention time, volatile and char conversion during Euler-Lagrangian simulations.

Injections	Part. size [μm]	Part. retention time [s] Mean (Range)	Volatile Conversion [%]	Char Conversion [%]
Coal	40	2.1 (2.0 - 2.2)	100	100
Alt.fuel (k.g.)	200	2.0 (1.9 - 2.7)	100	84.4
Alt.fuel (t.a.)	200	3.0 (2.6 - 5.1)	100	100
Raw meal 1 (k.g.)	52	3.4 (2.0 - 6.9)	-	-
Raw meal 2 (t.a.)	52	3.6 (1.9 - 6.7)	-	-

- low degree of mixing between the kiln- and the tertiary air gas side, which means poor oxidizing conditions for the alternative fuel on the kiln gas, and a delayed burnout. (However, to obtain a successful utilization of reburning and advanced reburning for NO reduction in the precalciner, delayed mixing is required.) A reduction (optimization) of the reburning zone will improve the delayed burnout.

- that CO is concentrated in certain regions, as also shown in full-scale measurements, however not at the same locations. This is probably due to differences in particle size and particle size distribution of the alternative fuels, which may change the flow pattern.

- that the ratio of solids- to gas retention time τ_s/τ_g in the precalciner is about 2, i.e. only half of the value found by Hundebøl et al. (1987) in experiments on an FLS-ILC calciner. Comparing previous work on CFBC reactors and precalciners with the CFD simulations, shows that particle retention time has to be considered for the specific CFBC reactor or precalciner. Furthermore, previous work explains the ratio of τ_s/τ_g with back mixing / core-annulus flow, which is low in this precalciner due to the high gas velocity.

- that the difference between fuels- and raw meal particle retention times are probably due to their difference in flow paths or inlet locations.

Chapter 6

Conclusions

In this work several techniques have been employed to increase the knowledge about combustion and flow regimes in the precalciner of kiln 6 at Norcem Brevik. Focus has been on NO_x reduction by reburning and advanced reburning.

A comprehensive study on theory and previous work on fluidization regimes showed that the extensive work on CFBC reactors can be applied to the investigation of precalciners.

A CFBC reactor has been designed and constructed, and experiments with several fuels, i.e. refuse derived fuel, animal meal, solid hazardous waste, char coal and coal, have been performed with this reactor.

Full-scale experiments in the precalciner have also been carried out, using same type of fuels. In addition, advanced reburning rich using urea has been tested.

Moreover, full-scale and laboratory experiments have been combined with CFD simulations to investigate the impact of flow pattern on burnout, to characterize alternative fuels and to improve the understanding of utilizing such fuels in cement kilns.

Detailed discussions of full-scale experiments, laboratory experiments and CFD simulations can be found in Sections 3.4, 4.4 and 5.4, respectively. In the following, main conclusions and suggestions for further work are given.

6.1 Main conclusions

This work showed that:

- the CFBC reactor is well suited for characterization of alternative fuels burnt in a precalciner regime.
- experiments with and without circulating mass in the laboratory CFBC reactor demonstrate the importance of executing combustion experiments under conditions similar to those prevailing where the results are to be applied - in the precalciner. However, the complex operation of such a large CFBC reactor will give certain variations in stability.
- advanced reburning and reburning during utilization of SHW and animal meal appear to be well suited for NO_x reduction in the precalciner at kiln 6 in Brevik . However, a optimum with regard to emissions, influence on clinker quality and operation was not found. RDF showed the highest capacity to reduce NO_x during reburning and advanced reburning in laboratory experiments. However, previous experiments in full-scale experiments show a higher NO_x reduction for animal meal than for RDF.

- animal meal is believed to follow the reduction route of SNCR and/or advanced reburning. This is likely due to the release of fuel nitrogen as a NH_3 to a higher extent than HCN. This may be explained by the phenomenon that fuel nitrogen is released during pyrolysis and the fact that the fuel has a low O/N ratio.

- increasing amount of NO supplied at the reactor inlet improves the ratio of $NO_{out}/NO_{supplied}$ for all fuels during laboratory experiments with advanced reburning and combustion without circulating mass.

- laboratory experiments confirm the special ability of animal meal to reduce NO_x during increased supplies of NO at the reactor inlet. Previous work confirms that fuels with a high nitrogen content, such as animal meal, do not necessarily lead to fuel-NO. Previous work by others also shows that the HCN/NH_3 ratio in pyrolysis gases decreases with fuel O/N ratio. This result gives possibilities in the utilization of alternative fuels with a high nitrogen content and for which a higher proportion of the nitrogen is released during pyrolysis, as shown in the full-scale and laboratory experiments.

- an increasing ratio of $urea/NO_{supplied}$ lowers the NO_x emissions. The optimum is not possible to determine without further experiments, but apparantly $(urea/NO_{supplied})$ ratios above 3 - 5 do not contribute to lower NO emissions. A similar trend is found during the full-scale experiments. It must be emphasized that these findings apply to a precalciner regime.

- increased CO emissions during advanced reburning and reburning (with animal meal) is most likely to be due to the competition for the OH radical during oxidation of CO and reduction of NH_3. However, combustion of animal meal in a lean environment without circulating mass showed low CO emissions. This is probably because the critical amine free radical NH_2 finds another path and/or because an increased amount of hydrogen radicals increases the production of OH radicals.

- heterogeneous reactions is likely to reduce NO with an increasing amount of NO supplied. This was shown during combustion without circulating mass in a lean environment in the laboratory experiments. This finding can possibly demonstrate that NO reduction is governed not only by one phenomenon, but several phenomena.

- smaller particles reduce CO and NO emissions in the laboratory experiments.

- CFD simulations reveal important information about the flow regime and its importance for improved burnout.

6.2 Further work

Increasing utilization of alternative fuels in cement kiln 6 in Brevik will demand better understanding and further work on several issues.

Further work will be to:

- increase the understanding of the pyrolysis and char products (e.g. NH_3, HCN), under conditions chemically comparable to those in a cement kiln, in order to follow the specific reduction/oxidation routes. These investigations should be executed in single particle drop tube or equivalent equipment.

- increase the understanding of blending of alternative fuels. It is found that animal meal or similar fuels increase the emissions of N_2O. Furthermore, it is known that free carbon sites contribute to the reduction of N_2O. Hence, it is of interest to execute further studies on blends of e.g. char coal and animal meal to test the reducing effect on N_2O emissions. Moreover, it is probable that the future will bring new alternative fuels into the cement production as e.g. sewage sludge, car scrap, photochemical waste etc. Hence, it will be of interest to understand the effects of blending various fuels and their effects on combustion and not at least the effect on the product quality and production stability.

- increase the understanding of increased level of HCl in the precalciner. An increased utilization of RDF in the precalciner will increase the levels of HCl. Previous work shows that both NO and HCl inhibit the oxidation of CO. Hence, an increased amount of HCl will affect the CO reduction since scrubbing of HCl is prevailing in the preheater at temperatures below 650 and 700 $°C$. Furthermore, it is known that adding O_2 to the reaction system has been found to strongly reduce the CO oxidation rate in the presence of HCl.

- improve/extend the CFD simulations to include the calcination reaction and include reactions like e.g. NO. Furthermore, it will be of interest to change the configuration on the inlets and imposing increased mixing to investigate improved burnout.

- execute CFD simulations of the CFBC reactor in order to study the flow regime and combustion of fuel particles.

There is a need to make a joint assessment of all possible effects that contribute to improved utilization of alternative fuels in the precalciner kiln 6 in Brevik regarding the product quality, production stability and emissions.

In order to utilize more alternative fuels and to keep the emissions low, a first assessment would be to consider the impact of:

- HCl, N_2O, CO, NH_3, NO, calciner temperature, particle size, fuel inlet configurations and mixing in the precalciner for improved oxidation of CO and TOC,

- controlling the flame temperature in the main burner by keeping a stable composition of the feed of raw materials, fuels, primary and secondary air, which will possibly lower the NO at the kiln inlet (or keeping it stable),

- controlling the excess air ratio in the reburning zone at the kiln gas side of the precalciner for improved NO_x reduction during reburning or advanced reburning and

- controlling the ratio of $NH_3/NO_{supplied}$ or urea/$NO_{supplied}$ in the precalciner for improved NO_x reduction during reburning with animal meal or advanced reburning.

6.3 End statement

This work shows the complexity of the chemical reactions, heat transfer and fluid dynamics in a cement kiln precalciner. The work is quite unique in the sense that a large laboratory reactor has been used for execution of experiments under conditions similiar to those in a cement kiln precalciner, and laboratory experiments as well as full-scale experiments have also been combined with CFD simulations. Further

success on the utilization of alternative fuels will depend on continued research employing full-scale tests, laboratory experiments and simulations.

Part I

Appendixes - Representative sampling

Appendix A

Representative sampling

A.1 Basic theory

This section will present basic theory important for the comprehension of the assumptions and tools behind the investigation. For a deeper understanding it is recommended to study Dr. Pierre Gy's sampling theory (Gy 1998), (Pitard 1989*a*), (Pitard 1989*b*).

A.1.1 Definition of representativeness

The sampling selection is representative when the mean square of the sampling error $r^2(SE)$, i.e. the sum of the bias $m^2(SE)$ and the variance $s^2(SE)$, is smaller than a certain standard of representativeness $r_0^2(SE)$ considered as acceptable (Gy 1998), (Pitard 1989*a*):

$$r^2(SE) = m^2(SE) + s^2(SE) \leq r_0^2(SE) \tag{A.1}$$

The value of $r_0^2(SE)$ can be fixed by legislation, technical standards or individually by the quality management of the company.

Representativety requires the attainment of two objectives that are independent of each other: *accuracy* (i.e., $|m(SE)| \leq m_0$ where m_0 is the maximum bias allowed) and *reproducibility* (i.e., $s^2(SE) \leq s_0^2$ where s_0^2 is the maximum allowed variance).

The technical way to increase the representativety is to increase the *accuracy* of the sample (i.e. reduction of the sample bias). It is impossible to control *accuracy* directly, but *accuracy* can be controlled indirectly (Pitard 1989*a*). A correct sampling method is always structurally accurate and can easily be reached with correct sampling equipment (Gy 1998). The optimal result of *accuracy* ($m(SE) = 0$) is theoretically possible to reach, but impossible in practice. A small remnant of bias can be disregarded in practical use if the sampling method is completely correct. In this case the representativety will only be influenced by the *reproducibility* ($s^2(SE)$ of the sampling error ($r^2(SE)$). The main factors influencing the sampling error $r^2(SE)$ is:

- the heterogeneity of the material that is sampled,
- the sampling interval,
- the sample mass and the sampling equipment.

It is assumed in the following that the *accuracy* ($m(SE) = 0$) can be disregarded and the representativety only will be influenced be the *reproducibility* ($s^2(SE)$ of the sampling error).

A.1.2 The sampling error (SE)

When we apply the model to real functions represented by the real unknown critical content of the selected, extracted, and prepared increments, the calculated total sampling error (TE) involves the following sequence (Pitard 1989*a*): the sampling error (SE) and the preparation error (PE). This error is the total sampling error (TE):

$$TE = SE + PE \tag{A.2}$$

Sampling is a combination of only two categories of operations (Pitard 1989*a*): an immaterial selection process which leads to the continuous selection error (CE) and a materialization process which leads to the delimitation error (DE), and the extraction error (EE) of the actual increment.

The sampling error (SE) is, see Equation A.3:

$$SE = CE + DE + EE \tag{A.3}$$

The total sampling is given by Equation A.4:

$$TE = CE + DE + EE + PE \tag{A.4}$$

When all the conditions for correctness are satisfied, in other words when the sampling is correct, and only then, Equation A.5 and A.6 (Gy 1998) apply:

$$DE = EE = PE = 0 \tag{A.5}$$

and

$$TE = SE = CE \tag{A.6}$$

It clearly follows that the total sampling error (TE) of a correctly taken and prepared sample reduces to the continuous selection error CE, the only error that can be modelled mathematically. It will be shown later that the error-generating functions of the variogram can be a useful tool to estimate the continuous selection error (CE), and at the same time to estimate the representativeness of a correctly taken sample (Gy 1998).

Estimation of the delimitation error (DE) and the extraction error (EE) is pointless. The only appropriate way is to eliminate these errors by using correct sampling equipment (Gy 1998).

A.1.3 The overall estimation error (OE)

The analytical error (AE) comes in addition to all other errors and it is not known how to eliminate this error completely. The analytical error is beyond the scope of this work. It is much easier in practice to detect, correct, and minimize analytical errors than sampling errors (Pitard 1989*a*).

The overall estimation error (OE) is equal to the sum of the total sampling error (TE) and the analytical error (AE), see Equation A.7.

$$OE = TE + AE \tag{A.7}$$

Equation A.8 is valid if the conditions of sampling correctness are rigorously respected (Gy 1998), (Pitard 1989*a*).

$$OE = CE + AE \tag{A.8}$$

A.1.4 Annotation

The first-stage sampling must be seen as the crucial source of error within this special sampling problem. Therefore, it is possible to state that the representativeness of the taken sample is only influenced by the sampling error (SE) of the first sampling step, see Figure 3.4. A second presumption, for the moment, is that the sampling system is correct (i.e., correct sampling and preparation equipment is used). It follows that the representativeness of the taken sample mainly will be influenced by the heterogeneity of the lot and the sampling plan.

A.1.5 How to study the heterogeneity of a lot

It is important to catergorize the lot. The lot is classified in the following dimensions (Gy 1998), (Pitard 1989*a*):

- zero-dimensional (e.g., truck, railroad car, jar, and etc.),
- one-dimensional (conveyor belt),
- two-dimensional and
- three-dimensional (e.g., a compact solid such as a block inside a mineral deposit).

The present sampling problem will be considered as a one-dimensional lot, describing the alternative fuel feed stream on the conveyor belt. One-dimensional lots are continuous and elongated piles, material on conveyor belts, streams, or series of trucks, railroad cars, bags, jars, etc., as long as these objects are considered as sets of non-random, discontinuous units making up the lot with a high relevance of the sequence.

When the one-dimensional lot is sampled by increments, it must be treated as a chronological or geometric series of units. The order of the units is of paramount importance and must be taken into consideration because of the possibility that some degree of auto-correlation may exist between them (Gy 1998).

A finite number of quasi-punctual increments must be sampled in order to study the heterogeneity of a one-dimensional lot.

The description and characterization of the heterogeneity of this chronological lot necessitates the use of continuous functions whose continuity fills the existing gaps between the punctual increments.

The study of a chronological set of increments, and the quantification of all the forms of heterogeneity fluctuations carried out by this set, random or non-random, is called variography. The most important and powerful tool used in variography is called the variogram.

A.1.6 The total heterogeneity of an one-dimensional lot

The one-dimensional lot L can be considered made of N_u discrete units (e.g. increments) arranged in chronological order, and U_m one of these units with $m = 1, 2, \ldots, N_u$. The total heterogeneity carried by the unit U_m of a one-dimensional lot can be expressed as in Equation A.9 (Pitard 1989*a*).

$$h_m = N_u \frac{(a_m - a_L)}{a_L} \cdot \frac{M_m}{M_L} \tag{A.9}$$

M_m : The weight of the component U_m
a_m : The component of interest content, or critical content of U_m
a_L : The content of interest content of lot L

N_u : Number of units U_m in lot L
M_L : Mass of the lot L. It is the sum of the masses M_m of the N_u units U_m
The total heterogeneity of a one-dimensional lot is found in Equation A.10.

$$h_m = h_{1m} + h_{2m} + h_{3m} \tag{A.10}$$

The three independent kinds of fluctuations can be defined as follows:

- A short-range term, mainly random, discontinuous at every instant, reflecting the random nature of constitution heterogeneity within one unit or one increment. For liquids, these fluctuations are usually negligible but not nil. This term is defined as the heterogeneity h_{1m} carried by one unit.
- A long-range term, non-random, mainly continuous, representing trends between units. This term is a non-random form of the heterogeneity defined as h_{2m}.
- A cyclic term, continuous, such as cycles introduced by reclaiming operations or corrective actions to maintain a parameter between two known limits. Such a cycle is nearly always detrimental to quality, therefore to sampling, and is defined as the non-random form of heterogeneity h_{3m}.

A.1.7 The variogram

The variogram is a plot of the average differences in a characteristic such as the value of the various h_m, between pairs of units selected as a function of time or distance, where the pairs are chosen in whole-number multiples (e.g., every minute, 2 minutes, 3 minutes, etc.). When a variogram is calculated, units regularly spaced along a one-dimensional lot is considered, and the measurement of a continuity index of their heterogeneity h_m as a function of time is determined (Pitard 1989*a*).

For each value of $m + j < N_u$ the increase $\Delta h(m + j, m)$ in the heterogeneity h_m between the final observation at time $t_{(m+j)}$ and the instant t_m at which the observations started, is calculated. By definition $\Delta h(m + j, m) = h(m + j) - h_m$.

These two points are separated on the time axis by an interval of $[t_{(m+j)} - t_m] = j\Theta_{min}$, which is called 'lag'$(j = \Theta/\Theta_{min})$. What is important is not the value or sign of each individual $\Delta h(m+j, m)$; it is instead their quadratic mean at each lag. This is why the function called the variogram $V(j\Theta_{min})$, or more simply $V(j)$, is defined as the semi-mean square of the increment, see Equation A.11 (Gy 1998).

$$V(j) = 1/2(N_u - j) \sum_m [\Delta h(m + j, m)]^2 \tag{A.11}$$

A more detailed description of the theory can be found in the references (Gy 1998) and (Pitard 1989*a*).

A.2 Execution of experiments

A.2.1 Sampling and preparation

It must be emphasized that the first-stage sampling method is not suitable to provide a correct sample, as described in the sampling theory. However, the intention was to get practical experience in the utilization of variography without large investments in new sampling equipment. Therefore, a simple sampling system was designed. It will be shown that this target was reached with a sufficient precision for the moment.

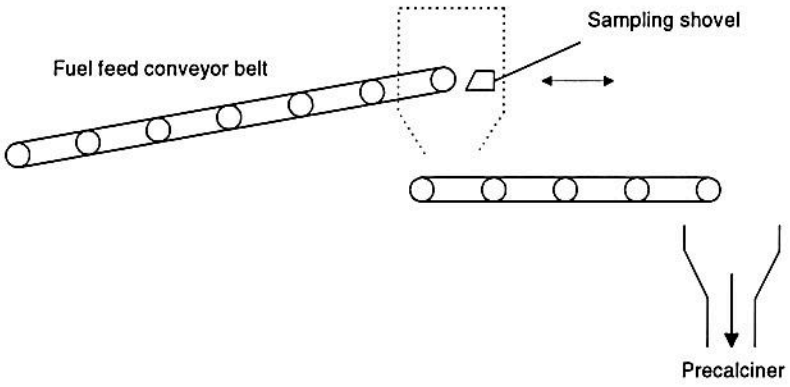

Figure A.1: The sample point (Piechatzek et al. 2000).

Figure A.2: Structure of a general RDF.

First-stage sampling: Gross sample

The first-stage sampling was an incremental sampling, see Figure A.1. With the aid of a specially designed shovel, increments were extracted from the end of the fuel feed conveyor belt. RDF was collected in four series of 32 increments, at intervals of 30 seconds, 1 minute (two series) and 10 minutes. The shovel and the conveyor belt had the same width.

Secondary sampling: From gross sample to laboratory sample

The gross samples (I_q) were at first air-dried according to ASTM standard E 329 and secondly ground and then split down to approximately 0.05 kg. The necessary number of splits (N) was according to Equation A.12, see Figure A.5. The laboratory samples were filled into labelled sample containers after splitting. The structure of a general RDF sample and a RDF sample from the variographic experiment at Brevik Norcem are shown in Figure A.2 and A.3, respectively.

$$N = \frac{I_{q\ Mass\ of\ increment}}{I^*_{q\ Mass\ of\ increment}} \tag{A.12}$$

Figure A.3: Structure of a RDF sample from the variographic experiments at Brevik Norcem.

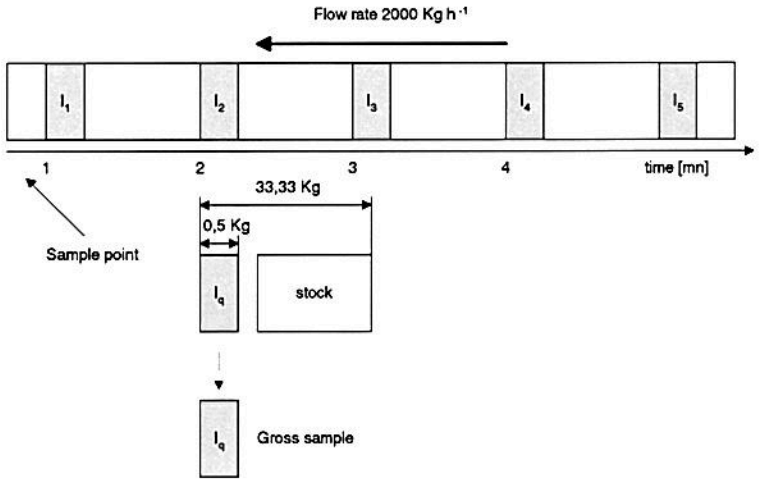

Figure A.4: Incremental sampling at the conveyor belt (Piechatzek et al. 2000).

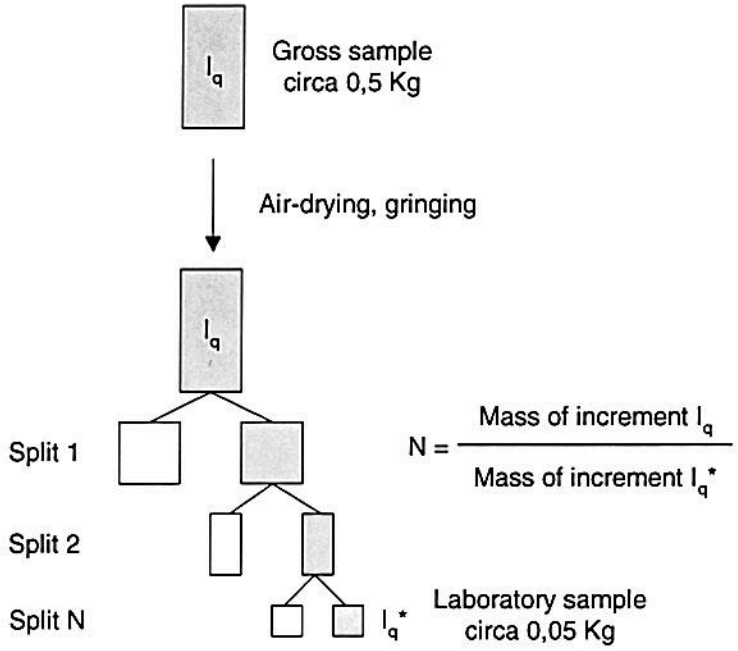

Figure A.5: Splitting of the gross sample (Piechatzek et al. 2000).

Third-stage sampling: From laboratory sample to analysis sample

The analytical sample, with an average weight of 0.001 kg, was composed of four to five increments from the laboratory sample. The first step in the is to shake the container in order to ease the material. Then the first increment is withdrawn using a spatula. Before withdrawal of each of the following increments, the container is turned four times around its own axes.

A.2.2 Analytical techniques

It is of interest to investigate all chemical and physical parameters of the RDF e.g. the gross calorific value as well as the content of Hg, Cl, S, metals and alkali metals. The number of samples and the demand for parallels add up to a large number of analyses, which affect the cost and manpower. Therefore, only the most fluctuating parameters were selected for analysis: In consultation with Norcem R&D, gross calorific value and chlorine content were selected. The samples were analyzed at Norcem R&D and at the combustion laboratory at Telemark University College, see (Piechatzek et al. 2000) for results.

Gross calorific value

The gross calorific value was analyzed with an automatic Leco AC-350 and a Leco AC-300 at Telemark University College and Norcem R&D, respectively. The analytical equipment was in close agreement with ASTM standard E 711. All air-dried samples were analyzed in two parallels whereupon the arithmetic average was applied in the variographic calculations (Piechatzek et al. 2000).

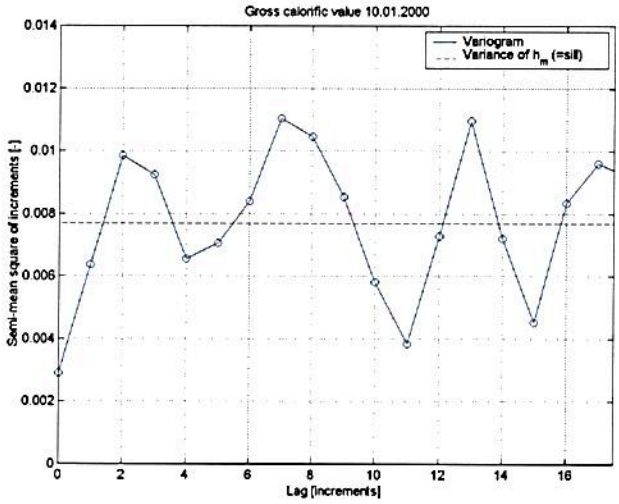

Figure A.6: Variogram of the gross calorific value from the the 10th of January 2000. Sample increments of 1 minute (Piechatzek et al. 2000).

Chlorine content

The principle determination of the total chlorine content is combustion of the sample in an oxygen atmosphere (bomb calorimeter) followed by conversion to chlorides and absorption of the chlorides in an alkaline solution. The content of the water-soluble chloride form was quantitated by a potentiometric titration system.

The chlorine content determined at Norcem R&D was performed in conformity with a Norcem standard for analysis of chlorine and fluorine content in coal. A corresponding standard was applied at Telemark University College, but the titration was performed manually (Piechatzek et al. 2000).

A.2.3 Calculation of the variogram and the error-generating functions

The theory of the one-dimensional model of a lot and point-by-point interpretation of the variogram was programmed in MATLAB® by Dr. Ing. L.-A. Tokheim; the program was named VARIO (Piechatzek et al. 2000).

VARIO calculates the variogram, the auxiliary functions and the error-generating functions with the aid of the point-by-point calculation of an integral. The estimation of the ordinate $V(0)$ of the variogram is performed by a simple extrapolation of the points $V(2)$ and $V(1)$ to zero. Figure A.6 shows an example of the calculation results from VARIO of the gross calorific value (Piechatzek et al. 2000).

A.3 Results and discussion

The continuous component of the (long-range) heterogeneity is nil for the gross calorific value and chlorine content in all series. In practice this implies that the mean value of the gross calorific value and chlorine content is constant in the long-range.

Generally, the periodic heterogeneity shows cyclic fluctuations of about 5 minutes around a constant mean value for all series, see Figure A.6 as an example.

This indicates that the gross calorific value and the chlorine content oscillate with a period of about 5 minutes around a constant mean value. Calculations show values in between of 17.8 to 20.9 MJ/kg and 0.3 to 0.5 % for the gross calorific value and the chlorine content, respectively. The physical cause of these fluctuations remain unexplained, but can be caused by an upstream delivery- or preparation plant.

It has been shown that the produced selection error is nearly independent of the sampling interval and the number of taken increments (Piechatzek et al. 2000). Since the preparation cost for analysis is proportional to the weight of the gross sample, the sample interval is chosen with regard to an economical optimum in sample weight. An economical optimum between the preparation cost and the variance of the sampling-error ought to be found. The sampling interval is rarely greater than 20 minutes (Gy 1998). Hence, the sampling interval should be between 5 and 20 minutes, and not a multiple of a 5-minutes periods. The periodic fluctuation of the heterogeneity shows a sinusoidal behavior (i.e. a very simple behavior). Therefore, it is not necessary to install a stratified random sampling system. The gross calorific value can with a 95 % confidence interval have a relative standard deviation lower than 0.14 % (Piechatzek et al. 2000). An even larger heterogeneity of the chlorine (up to hundred times larger compared to the gross calorific value) gives a relative standard deviation of about 20 % (Piechatzek et al. 2000). This leads to an important question: *How representative are the results from the chlorine content determinations?*

The sampling system gives valuable results, even though it is simple and far from correct in the first-stage sampling. The results show an increase in the representativeness of sampling in comparison to grab sampling from containers, which is the general sampling practice in most process operations. A systematic incremental sampling system reached a relative standard deviation of about 0.06% compared to grab sampling from a container of 6.3 % for the gross calorific value (Piechatzek et al. 2000). This means that grab sampling from e.g. containers will not give representative samples. Furthermore, a precise continuous sampling system will provide precise and representative information which will improve quality and process control, not only for the RDF fuel feed stream but also for all other feed materials.

Part II

Appendixes - Full-scale experiments

Appendix B

Experimental results and discussion

In this appendix more details of the full-scale experiments are presented.

Table B.1 gives an overview of sampling points, frequency, method and parameters.

Table B.1: Sampling points during the experiments in the precacalciner kiln 6

Sample points	**Sampling period**	**Method**	**Parameter**
Cyclone 4.1 and 4.2	Two per shift		Calcination degree
Cooler	Daily		Minerals
Chimney, string 1	Continously	FTIR	O_2, CO, CO_2, SO_2, NO, NO_2, N_2O, HCl, H_2O, HF, TOC
Chimney, string 2	Continously	FTIR	O_2, CO, CO_2, SO_2, NO, NO_2, N_2O, HCl, H_2O, HF, TOC
Rotary kiln inlet	Continously	NDIR	O_2, CO, CO_2
Rotary kiln inlet	Exper.period	Orsat	O_2, CO, CO_2
Cyclone 4.2	Continously	NDIR	O_2, CO, CO_2, SO_2, NO_x, N_2O
Precalciner	Exper.period	NDIR	O_2, CO, CO_2 (Traverse measurements)
Precalciner	Exper.period	Th.el.(K)	Temperature (Longitudinal direction)

Figure B.1 shows that the fuel-nitrogen supply is substantially higher in experiment 7, 8, 13, 14 and 15 because of the utilization of animal meal in the precalciner and in the main burner.

Figure B.2 shows the ratio ($\kappa_{N-ratio}$) of emitted NO_x (as nitrogen) to fuel-nitrogen supplied, see Equation B.1.

$$\kappa_{N-ratio} = \frac{mass\ nitrogen\ emitted}{mass\ fuel\ nitrogen\ supplied} \tag{B.1}$$

The bars in Figure B.2 show $\kappa_{N-ratio}$ based on:

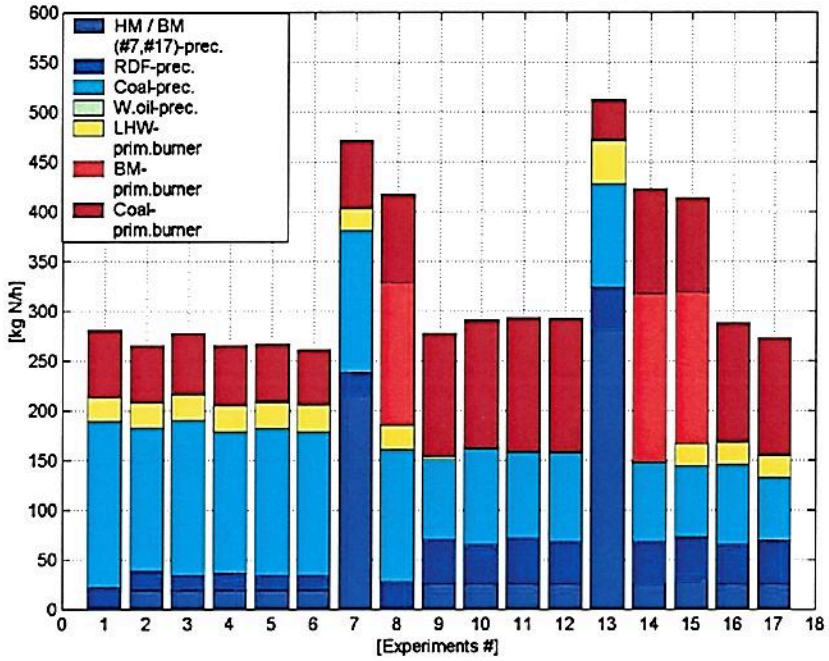

Figure B.1: Fuel-N supplied into kiln 6 during experiment 1 to 17.

- NO_x emissions from string 1 and 2, and total supply of fuel nitrogen into the process,
- NO_x emissions from the rotary kiln, and supply of fuel nitrogen into the main burner.

Figure B.2, B.3, B.4 and B.5 show a trend of decreasing NO_x, HCl and HF emissions throughout the February campaign (experiment 1 to 7) and the April campaign (experiment 8 to 17). However, no specific trend of decreasing NO_2 with decreasing NO_x can be seen, see Figure B.6.

The NO_x reduction system Thermalonox® applies direct injection of elemental phosphorus into the flue gas stream, which reacts with the NO and converts it to NO_2. Subsequently the NO_2 is removed using a conventional flue gas scrubber (Digest 2000). Table 3.4 shows that animal meal in experiment 7 and 13 contain up to 8.3 wt % phosphorus. However, no increase is found in the NO_2 emissions during combustion of animal meal in experiment 7 and 13. (But a higher concentration of phosphorus in the clinker is found.) The NO_2 emissions, based on all experiments, is on average about 1.6 % of the total NO_x emissions. Low and stable NO_2 emissions can be due to scrubbing effects in the cooling tower.

The decreasing NO_x emissions can be explained with reburning in experiment 2 and 9, increasing supply of urea (AR) in experiment 3 to 6 and 10 to 12, and utilization of animal meal in experiment 7 and 13.

Table B.2 shows average NO_x and CO emissions for experiment 1 to 17. The alterations refer to experiment 1 for series 2 to 7 (February campaign) and experiment 8 for series 9 to 17 (April campaign). It can be seen from Table B.2 that AR and animal meal give NO_x reduction up to 73 % and 63 %, respectively.

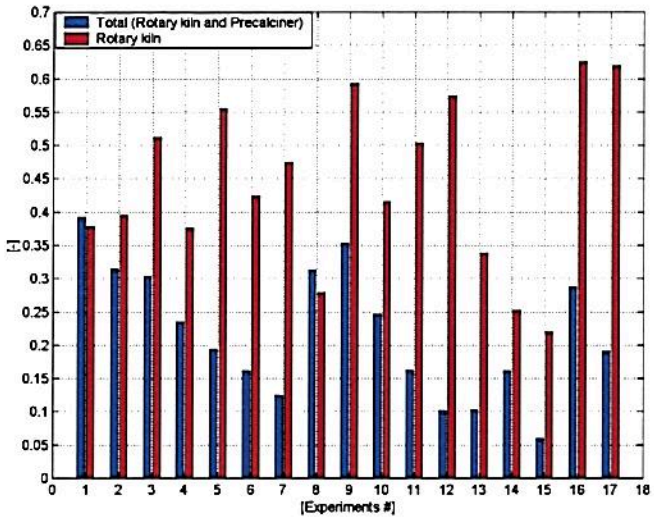

Figure B.2: Ratio of N emitted and fuel-N supplied ($\kappa_{N-ratio}$) during experiment 1 to 17.

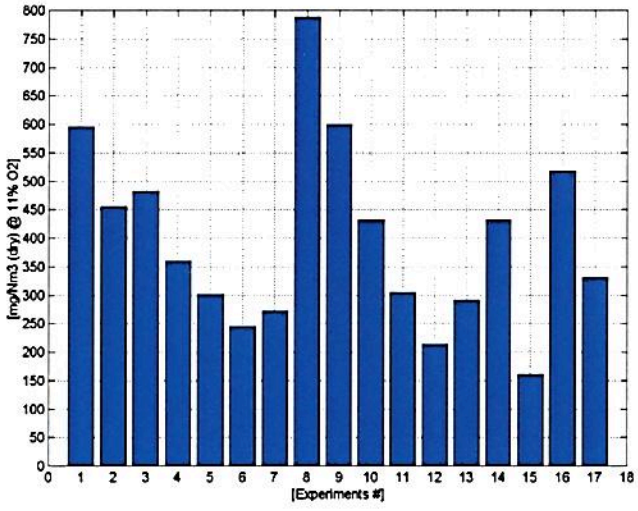

Figure B.3: NO_x emitted from kiln 6 during experiment 1 to 17.

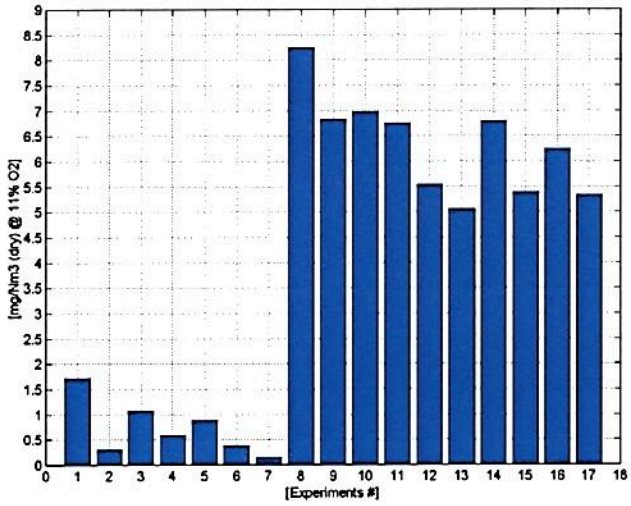

Figure B.4: HCl emitted from kiln 6 during experiment 1 to 17.

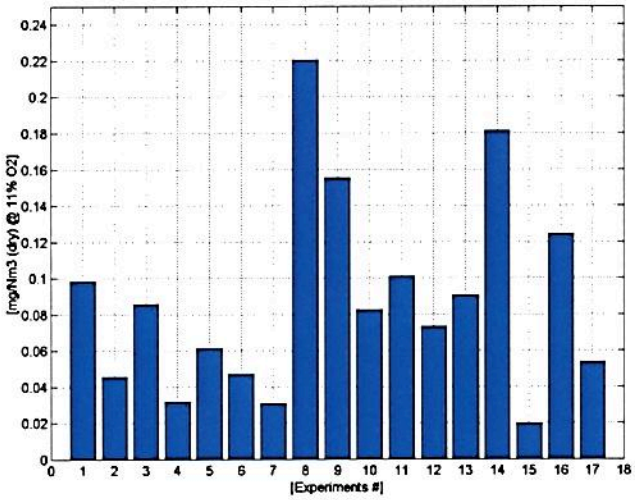

Figure B.5: HF emitted from kiln 6 during experiment 1 to 17.

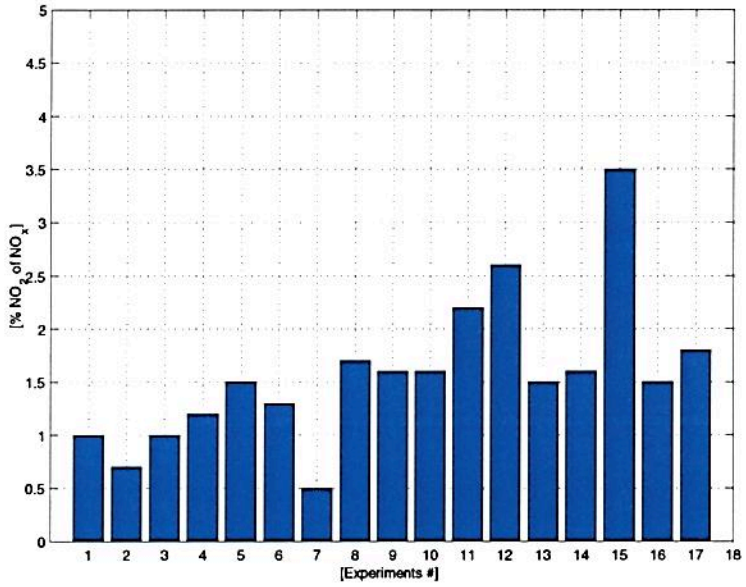

Figure B.6: NO_2 emissions in % of NO_x ($NO + NO_2$) duringe full scale experiments.

Additional supply of animal meal into the main burner in experiment 14 compared to experiment 9 gives an increase in NO_x reduction of about 21 %, see Figure B.2, B.3 and Table B.2. A similar trend can be seen in experiment 15, 11 and 17, which increase the NO_x reduction with about 19 %. The NO_x level at the kiln inlet is lower in experiment 14 and 15 than in experiment 9, 11 and 17, even though the supply of fuel-nitrogen, mainly from animal meal, into the main burner increases, see Figure B.1 and B.7.

It is obvious that a supply of animal meal in the main burner, even though it has a higher fuel-nitrogen content, gives lower NO_x emissions at the kiln inlet. The overall NO_x reduction with additional animal meal in the main burner can not be explained with lower NO_x levels at the kiln inlet, since the relative reduction in the kiln inlet is 4 % and 2 % compared to the overall reduction of 21 % and 19 %. The NH_3 released by the animal meal in the main burner probably follows a reduction route similar to SNCR.

The emissions are kept below the limits given by the Norwegian State Pollution Control Agency (SFT), with the exception of TOC, for which the emission level is above the limit in most of the experiments, see Figure B.8 . (The SFT limit value for TOC is 10 mg/Nm^3.)

The HCl and HF emissions decrease throughout experiment 1 to 7 and experiment 8 to 13, see Figure B.4 and B.5. It is likely that the increased release of NH_3 in the process also affects the HCl and HF emissions. The probable cause is that the chlorine in lack of hydrogen radicals does not form HCl, but finds other forms. The primary reduction reaction for NH_3 can be seen from Equation 2.30. It follows that during rich conditions, reactions with hydrogen make a significant contribution, see Equation 2.32. Hence, the ammonia reaction will dissipate hydrogen radicals, thus the chlorine finds another elemental form. The same argument can be applied to fluorine.

The increased HCl emissions in experiment 8 to 17 compared to experiment 1 to 7 is probably due to different raw material compositions.

Figure 2.13 show that for more fuel rich conditions, a stoichiometric ratio lower than 0.9, the additional fuel-N and possible prompt NO will decrease the overall

Table B.2: Average NOx and CO emissions and alterations during experiments in February and April 2001.

Experiment		NO_x		CO	
		Average mg/Nm^3	Alteration %	Average mg/Nm^3	Alteration %
1	No feed	584 (ref.)	0 (ref.)	2755 (ref.)	0 (ref.)
2	SHW	456	-22	5102	85
3	SHW + 38 kg/h urea	483	-17	3346	21
4	SHW + 153 kg/h urea	360	-38	4518	64
5	SHW + 269 kg/h urea	302	-48	3488	27
6	SHW + 386 kg/h urea	245	-58	4567	66
7	Bone Meal	272	-53	6331	130
8	No feed	788 (ref.)	0 (ref.)	441 (ref.)	0 (ref.)
9	SHW	600	-24	1495	644
10	SHW + 153 kg/h urea	432	-45	2456	458
11	SHW + 386 kg/h urea	305	-61	3757	753
12	SHW + 770 kg/h urea	214	-73	4836	998
13	Bone Meal	292	-63	4251	865
14	SHW	431	-45	2345	432
15	SHW + 386 kg/h urea	161	-80	6617	1402
16	SHW + 153 kg/h urea	518	-34	2428	451
17	SHW + 386 kg/h urea	331	-58	4082	826

NO_x reduction. (Chen et al. (1998) indicated optimum conditions for NO reduction (AR) with reaction temperatures at 800 $°C$, stoichiometric ratio at about 0.99 and minimal air addition to give slightly fuel lean conditions (SR =1.02).) It can be seen from Table B.3 that the excess air ratio in the reburning zone, on the kiln gas side of the precalciner, is mainly varying between 0.65 and 0.87 during the reburning and AR experiments. (The excess air ratio is calculated by means of the oxygen concentration measurement at the kiln inlet. Values measured at the kiln inlet must be used with caution because of the difficult measurement environment in this part of the kiln system.) This is below what is recommended value for optimum NO_x reduction. Nevertheless, a substantial NO_x reduction has been achieved.

A common statement is that particularly oxidation of CO could generate significant amount of radicals via chain branching, which play an important role in the conversion of the NO, HCN and NH_3 species to N_2 or NO during burnout. It is also stated that an excess of radicals can reduce the NO reduction efficiency by promoting the oxidation of the key intermediate, NH_2. The important role of CO oxidation is supported by previous AR experiments that report an increase of about 30 % in CO emissions.

The CO and TOC emissions follow the same pattern, indicating that these

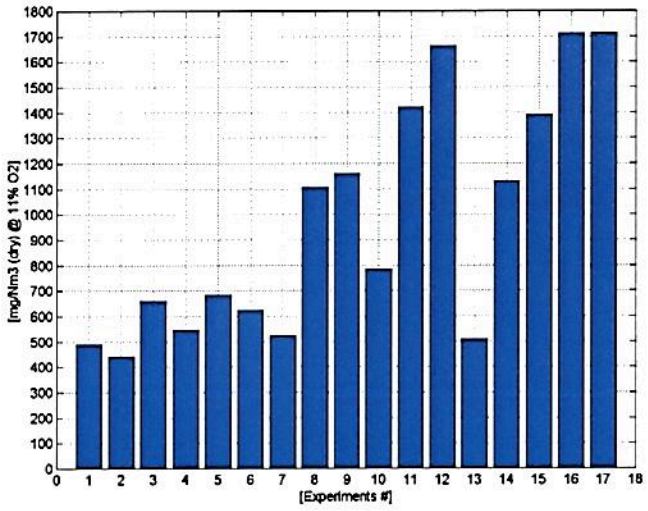

Figure B.7: NO_x emitted from the inlet (rotary kiln) of kiln 6 during experiment 1 to 17.

emissions result from incomplete combustion, see Figure B.8 and B.9. However, the increased CO emissions are probably due to the increased amount of NH_3 in the process during supply of urea and animal meal for experiment 1 to 17. Equation 2.30 and 2.55 are the primary reduction reactions for NH_3 and CO, respectively.

It is reasonable to believe that a higher excess air ratio during experiment 1 to 17 would decrease the CO emissions and probably result in a higher NO_x reduction.

The ammonia (NH_3) emissions were measured during experiments with reburning (#9), AR (#10, #12) and supply of animal meal in the precalciner (#13) and main burner (#14) during the April campaign, see Table B. (The full report of the mean values presented in Table B is found in (Axelsen 2001*b*).) The results are interesting and point out a trend for the ammonia emissions. It can be seen from Table B that the lowest amount of ammonia results when animal meal is supplied into the main burner in experiment 14. Furthermore, it can be seen an increasing trend when urea is supplied into the precalciner during experiment 10 and 12. The highest ammonia emissions originate from combustion of animal meal in experiment 13, namely with animal meal in the precalciner. The slip of ammonia during combustion of animal meal and SHW should support that a low O/N ratio signify a smaller HCN/NH_3 ratio as discussed previously. There is no emission limit value on NH_3 in the Directive 2000/76/EC on the incineration of waste.

The SO_2 emissions are shown in Figure B.10.

The thermal energy input to the kiln system is shown in Figure B.11.

B.0.1 Advanced reburning rich in the precalciner

The trends for experiments 3 to 6 (February campaign) and experiments 10, 11, 12, 16 and 17 (April campaign) are shown in Appendix C.

The CO and TOC emissions are observed to follow the inverse trend of the NO_x emissions during the experiments in February and April, see Figure C.1 - C.5. The influence of the alteration in the urea feed on the CO, TOC and NO_x emissions is distinct and rapid. Table B.0.1 lists the molar ratio of urea and NO in the different urea experiments.

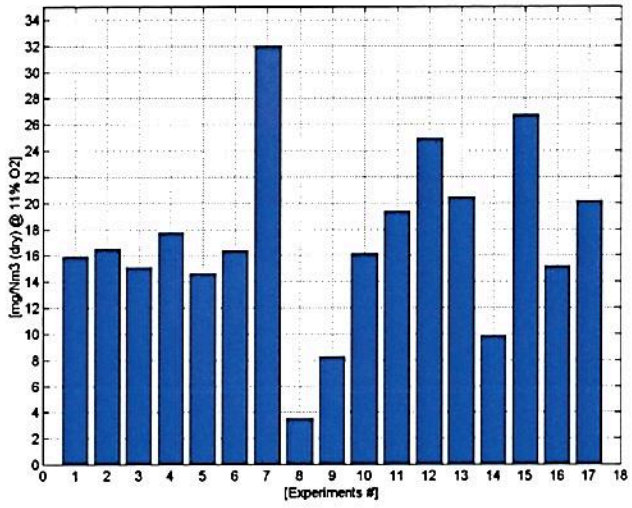

Figure B.8: TOC emitted from kiln 6 during experiment 1 to 17.

A change in the SO_2 emissions during alteration of the urea feed is also observed, although less distinct, see Figure C.6 and C.7. This indicates that the urea supply impacts the internal cycle of sulphur in the kiln system.

In Figure C.8 and C.9 overall descending trends of HCl emissions are seen, both in the February and the April campaign. These trends have been discussed previously, see also Figure B.4.

The N_2O emissions are fairly stable during alteration of the urea feed with a mean value of about 46 mg/Nm^3, see Figure C.10. It is previously reported that thermal DeNO$_x$ control, with urea or cyanuric acid injection, gives N_2O emissions of about 10 - 15 % of the NO$_x$ reduction. If this statement is transferable to AR, at a supply rate of 153 kg/h urea (average of the February and April campaign), it would give N_2O emissions between 29 - 44 mg/Nm^3. Previous experiments have shown a correlation between CO and N_2O. Hence, it is important to limit the CO emissions.

Experiment 15 was carried out with feed of animal meal (bone meal) into the main burner in combination with AR in the precalciner, see Figure C.11 - C.14. The combination of AR in the precalciner and animal meal in the main burner gives a higher NO$_x$ reduction. Furthermore, a substantial NO$_x$ reduction is observed with animal meal in the main burner and SHW being fed to the precalciner (reburning).

In general, the trends indicate that all experiments preferably could have been carried out for a longer period of time in order to stabilize the process conditions between each new setpoint.

B.0.2 Combustion of animal meal in the precalciner

The trends during experiment 7 and 13 are shown in Appendix D.

The emission trends are to those in the previous subsection; Advanced reburning rich in the precalciner. (In Figure D.5, the error in the first part of the emission measurement period should be ignored.)

The N_2O emissions during experiment 13 show a continuously increasing trend (except for the last 35 minutes), with a mean value of 74 mg/Nm^3, see Figure

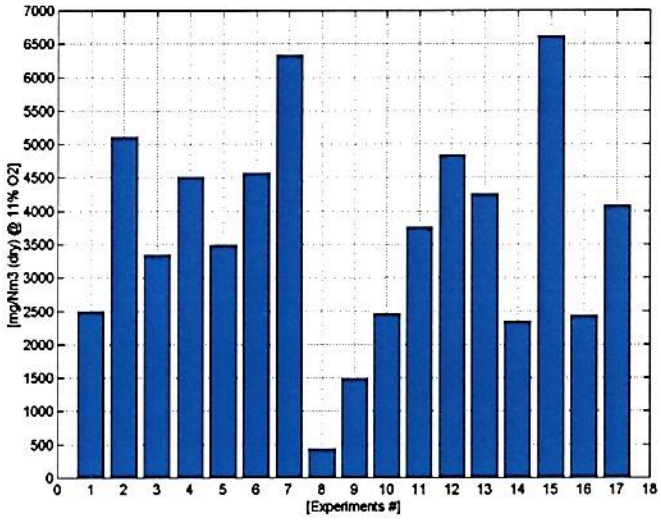

Figure B.9: CO emitted from kiln 6 during experiment 1 to 17.

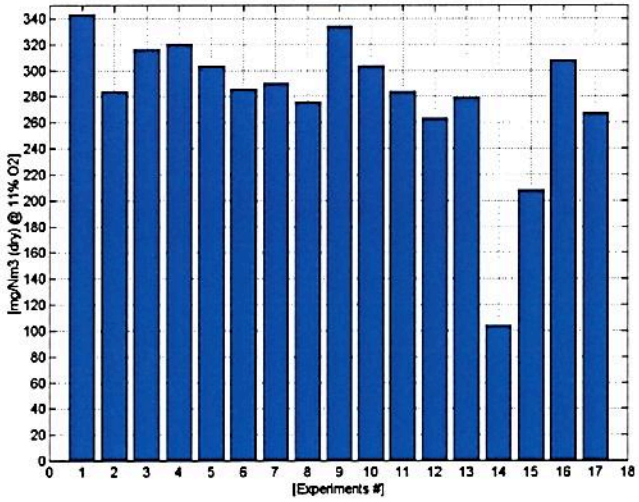

Figure B.10: SO_2 emitted from kiln 6 during experiment 1 to 17.

Table B.3: Excess air ratio in the reburning zone, on the kiln gas side during experiments in February and April 2001.

Experiment		Excess air ratio
# 1	No feed	1.16
# 2	SHW	0.87
# 3	SHW + 38 kg/h urea	0.87
# 4	SHW + 153 kg/h urea	0.87
# 5	SHW + 269 kg/h urea	0.87
# 6	SHW + 386 kg/h urea	0.87
# 7	Bone Meal	0.65
# 8	No feed	1.16
# 9	SHW	0.65
# 10	SHW + 153 kg/h urea	0.65
# 11	SHW + 386 kg/h urea	0.65
# 12	SHW + 770 kg/h urea	0.65
# 13	Bone Meal	0.56
# 14	SHW	0.65
# 15	SHW + 386 kg/h urea	0.65
# 16	SHW + 153 kg/h urea	0.65
# 17	SHW + 386 kg/h urea	0.65

Table B.4: Ammonia (NH3) emissions from kiln 6 during experiments in April 2001.

Experiment		NH_3 mg/Nm^3 @ 11% O_2	$NH_3 \rightarrow NO_2$ mg/Nm^3 @ 11% O_2	NO_x reduction %
# 9	SHW	2.6	7	3.7
# 10	SHW + 153 kg/h urea	25.7	69,5	19.5
# 12	SHW + 770 kg/h urea	37.9	102.6	17.9
# 13	AM	62.9	170.2	34.3
# 14	SHW	1.1	3	0.8

D.11. The previously discussed statement, that 10 - 15 % of the NO_x reduction is converted to N_2O, would give emissions of 50 - 74 mg/Nm^3.

No correlation between CO and N_2O is observed in experiment 13.

B.0.3 Combustion of animal meal in the main burner

The trends during experiment 14 are shown in Appendix E.

Combustion of animal meal in the main burner gives a distinct increase in CO and TOC, with a trend inverse to that of NO_x, HCl and SO_2, see Figure E.1, E.2, E.3, E.10 and E.12. Furthermore, it can be observed an increased level of CO and NO_x in the kiln inlet according to previous discussions, see Figure E.4 and E.5.

The N_2O emissions shown in Figure E.6 have a much longer sampling period than the rest of the emissions of experiment 14. The period from 480 to 730 minutes correspond to the period of the other measurement trends. In this period, the mean value of N_2O is 49 mg/Nm^3.

Another N_2O emission measurement was carried out at conditions similar to those in experiment 14, only 12 hours later. For this new measurement time, the

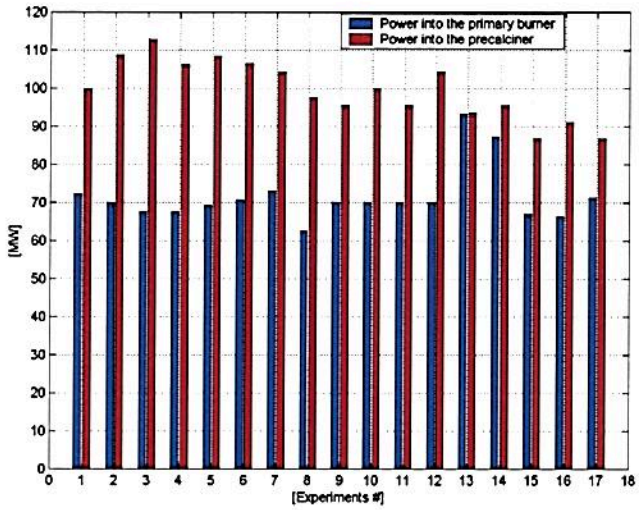

Figure B.11: Average thermal energy input to the primary burner and precalciner during experiment 1 to 17.

Table B.5: The molar ratio of (urea/NO) into the precalciner.

Experiment		$\mathbf{(Urea/NO)_{in}}$
# 3	**SHW + 38 kg/h urea**	0.36
# 4	**SHW + 153 kg/h urea**	1.75
# 5	**SHW + 269 kg/h urea**	2.46
# 6	**SHW + 386 kg/h urea**	3.62
# 10	**SHW + 153 kg/h urea**	1.30
# 11	**SHW + 386 kg/h urea**	1.51
# 12	**SHW + 770 kg/h urea**	2.72
# 15	**SHW + 386 kg/h urea**	1.54
# 16	**SHW + 153 kg/h urea**	0.52
# 17	**SHW + 386 kg/h urea**	1.32

mean value is 24 mg/Nm^3, see Figure E.8. The two nitrous oxide emission measurement experiments, carried out under approximately similar conditions, indicate that there is a considerable element of uncertainty connected to N_2O emission measurements. Nitrous oxide is reported to be catalytically destroyed over calcium compounds. The high catalytic activity of CaO surfaces towards N_2O is well documented. Furthermore, nitrous oxide measurements are reported to be disturbed by interference from CH_4, H_2O and SO_2 and to a minor extent from NH_3. Hence, it is difficult to state if the uncertainty is caused by the measurement technology or by process operations.

Appendix C

Figures - AR-rich in the precalciner

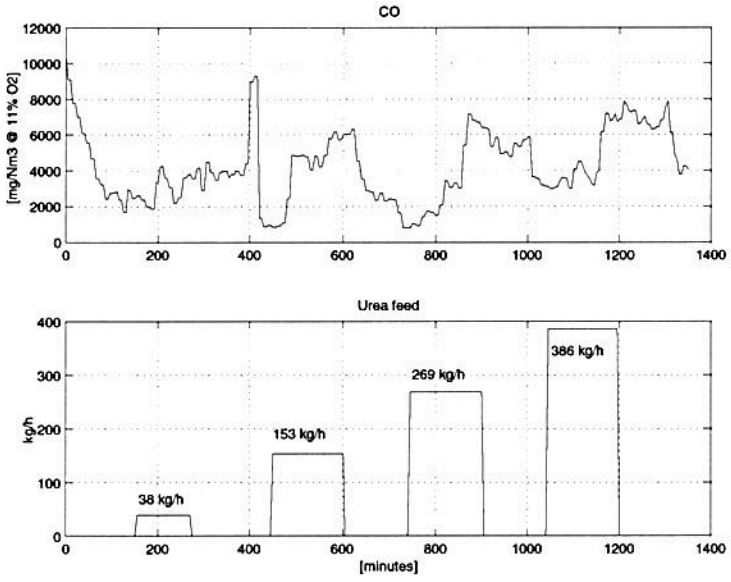

Figure C.1: CO emissions during alteration in urea feed into kiln 6. Experiment 3 to 6 (February campaign).

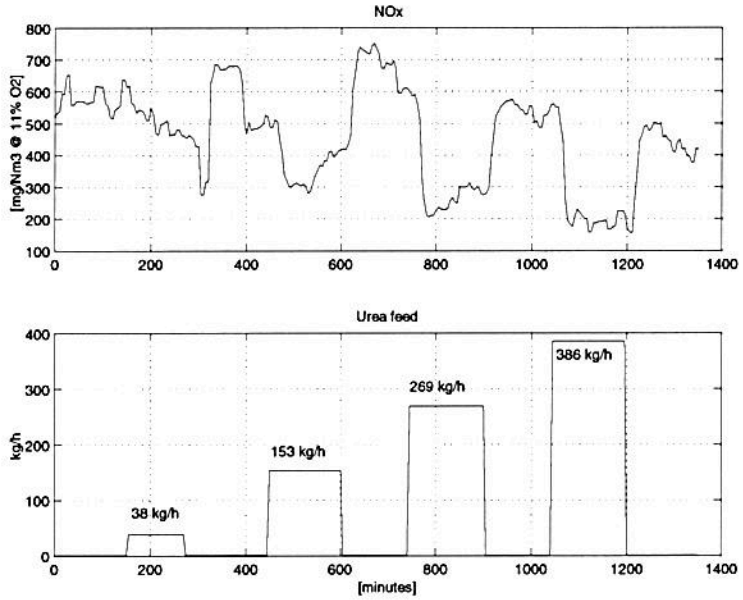

Figure C.2: NO_x emissions during alteration in urea feed into kiln 6. Experiment 3 to 6 (February campaign).

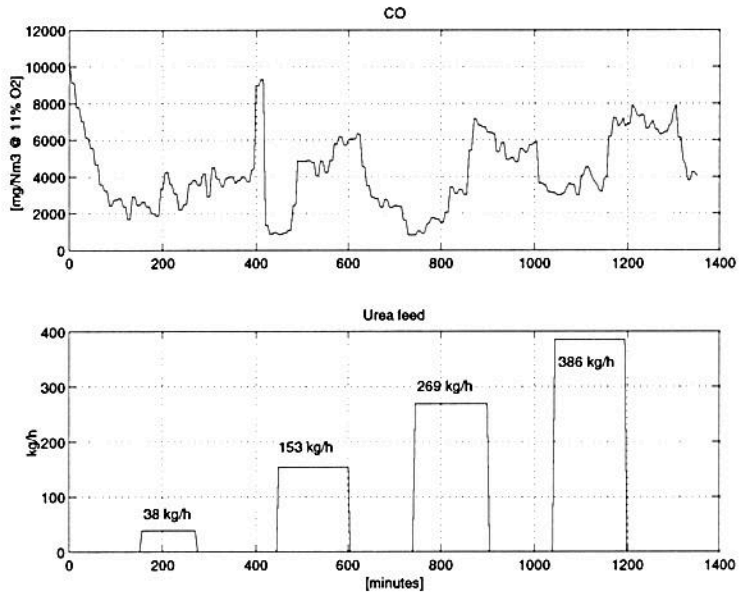

Figure C.3: CO emissions during alteration in urea feed into kiln 6. Experiments 10, 11, 12, 16 and 17 (April campaign).

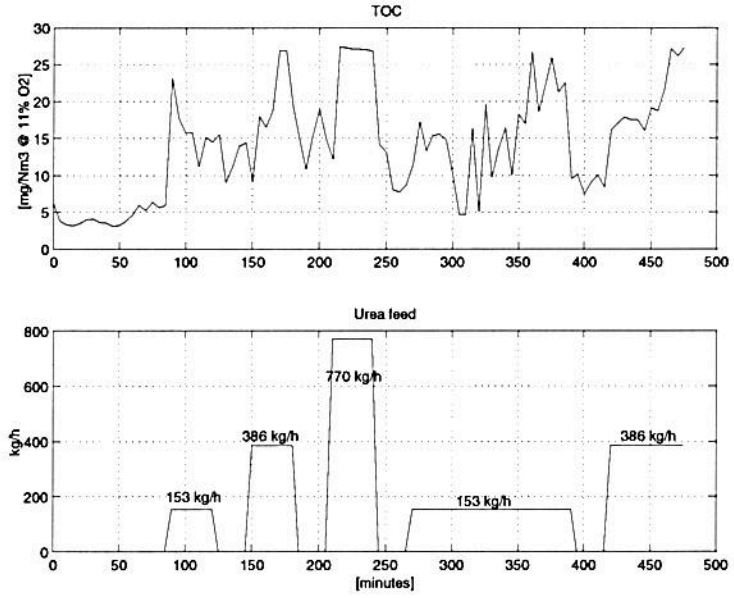

Figure C.4: TOC emissions during alteration in urea feed into kiln 6. Experiments 10, 11, 12, 16 and 17 (April campaign).

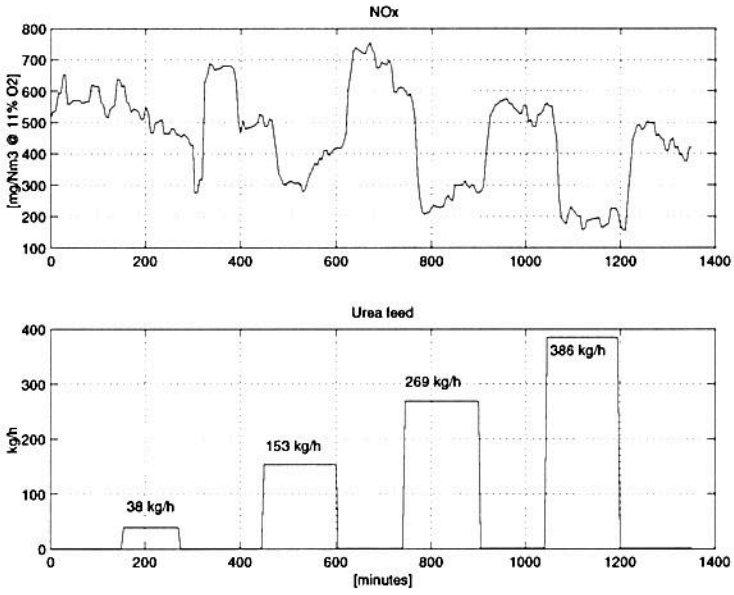

Figure C.5: NO_x emissions during alteration in urea feed into kiln 6. Experiments 10, 11, 12, 16 and 17 (April campaign).

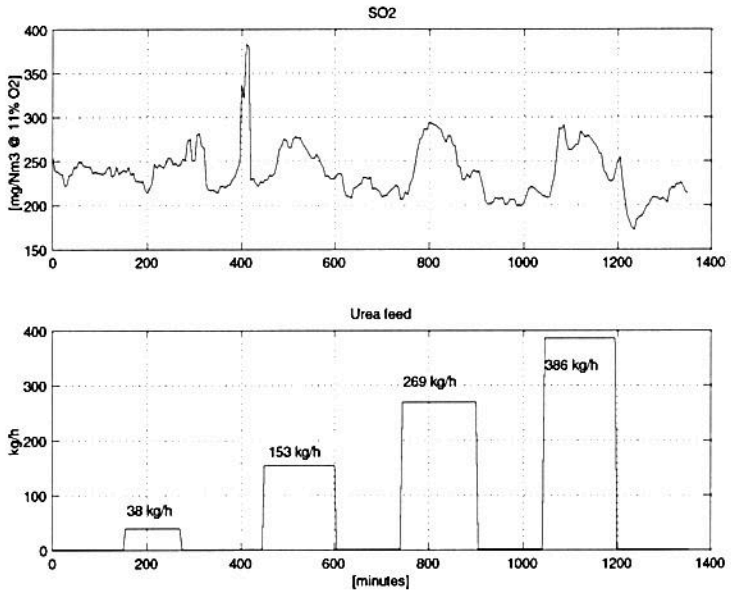

Figure C.6: SO_2 emissions during alteration in urea feed into kiln 6. Experiments 3 to 6 (February campaign).

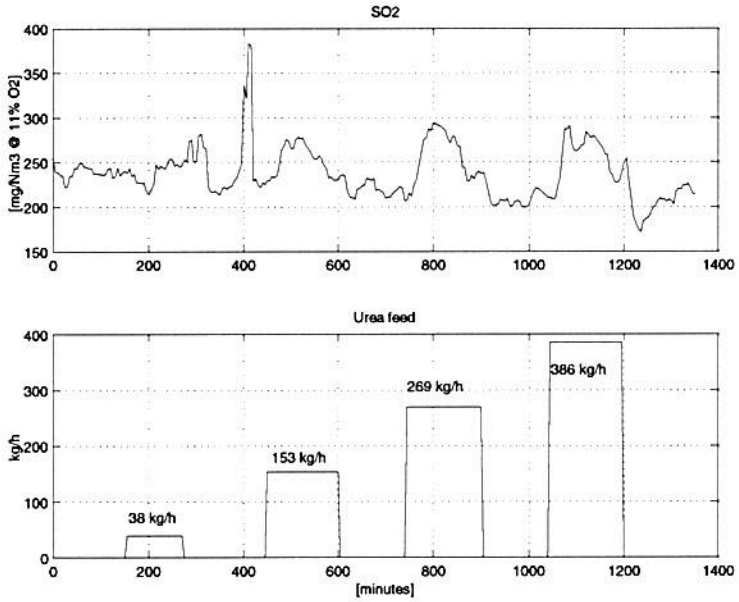

Figure C.7: SO_2 emissions during alteration in urea feed into kiln 6. Experiments 10, 11, 12, 16 and 17 (April campaign).

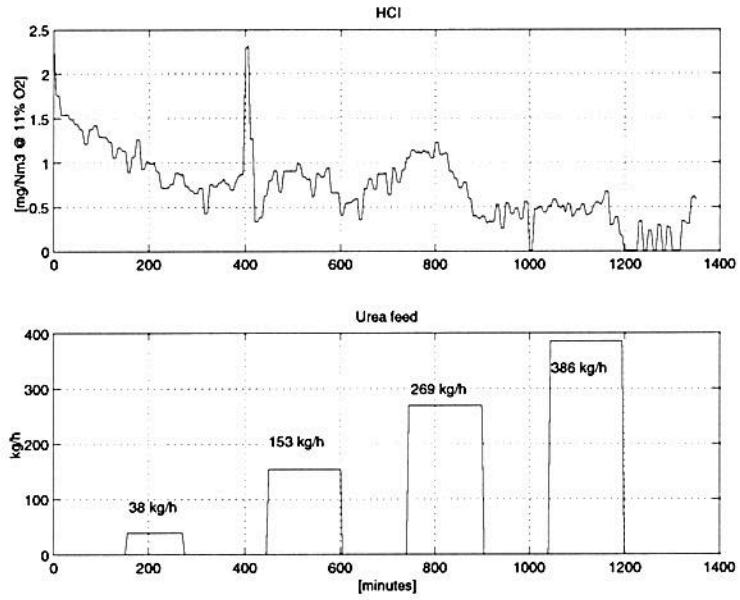

Figure C.8: HCl emissions during alteration in urea feed into kiln 6. Experiments 3 to 6 (February campaign).

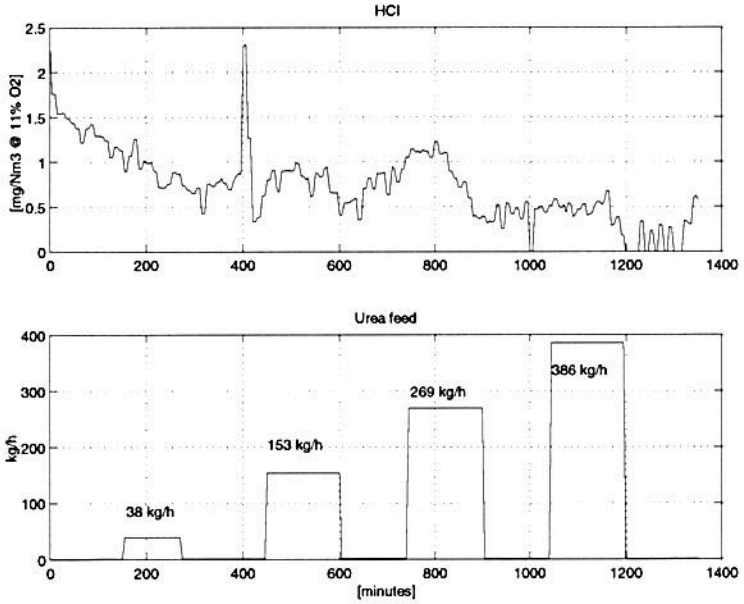

Figure C.9: HCl emissions during alteration in urea feed into kiln 6. Experiments 10, 11, 12, 16 and 17 (April campaign).

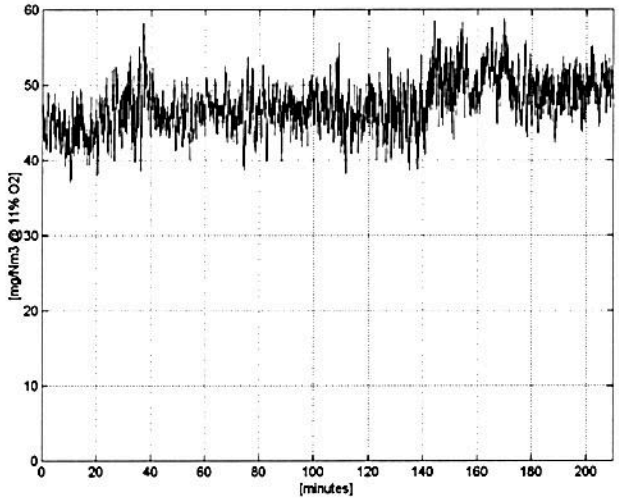

Figure C.10: N_2O emissions during alteration in urea feed into kiln 6. Experiments 10, 11 and 12 (April campaign).

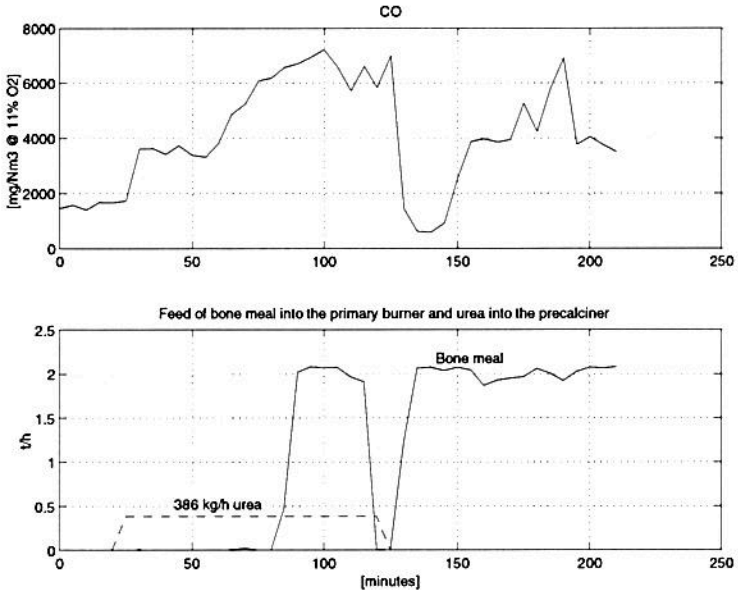

Figure C.11: CO emissions during feed of bone meal into the main burner and urea into the precalciner. Experiment 15 (April campaign).

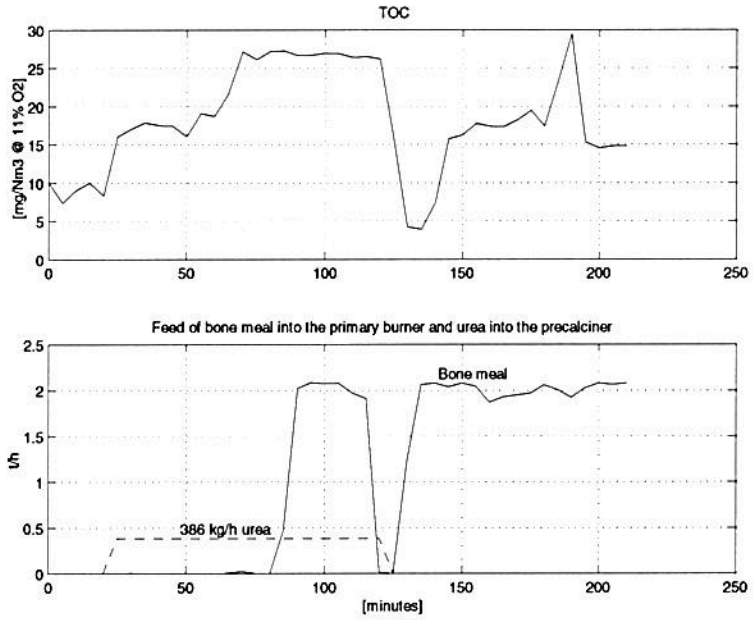

Figure C.12: TOC emissions during feed of bone meal into the main burner and urea into the precalciner. Experiment 15 (April campaign).

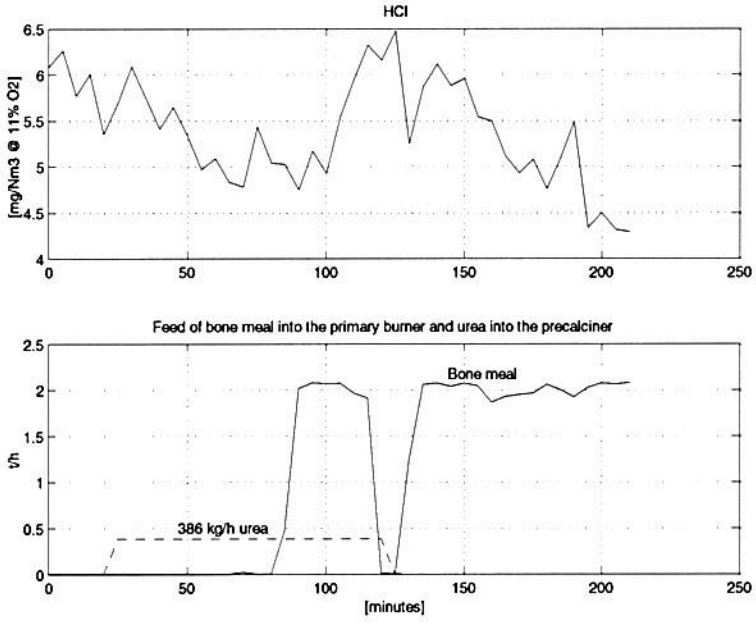

Figure C.13: HCl emissions during feed of bone meal into the main burner and urea into the precalciner. Experiment 15 (April campaign).

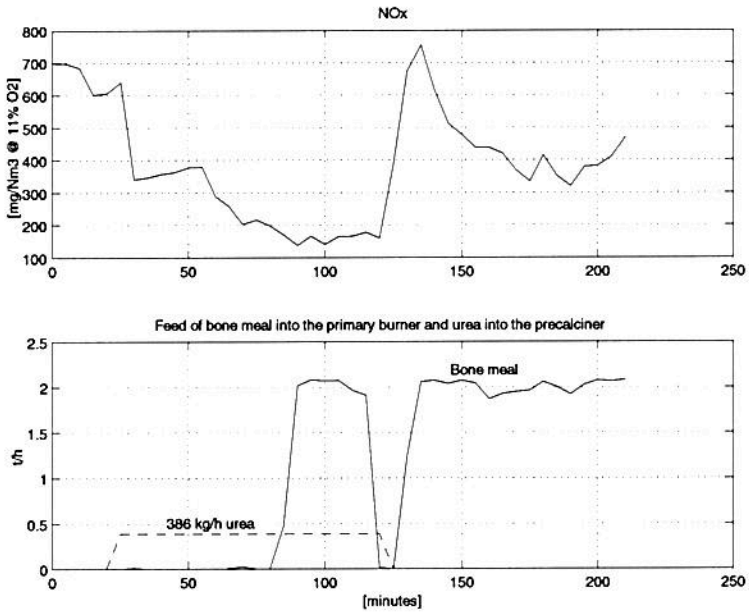

Figure C.14: NO_x emissions during feed of bone meal into the main burner and urea into the precalciner. Experiment 15 (April campaign).

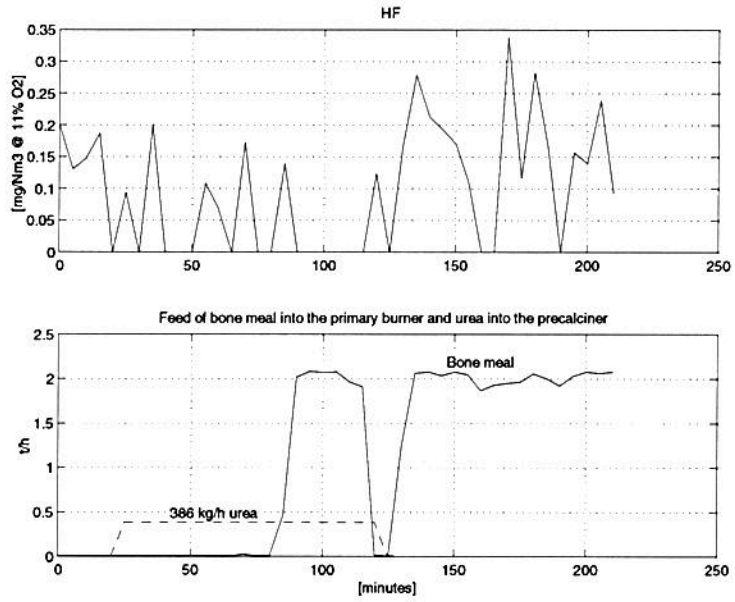

Figure C.15: HF emissions during feed of bone meal into the main burner and urea into the precalciner. Experiment 15 (April campaign).

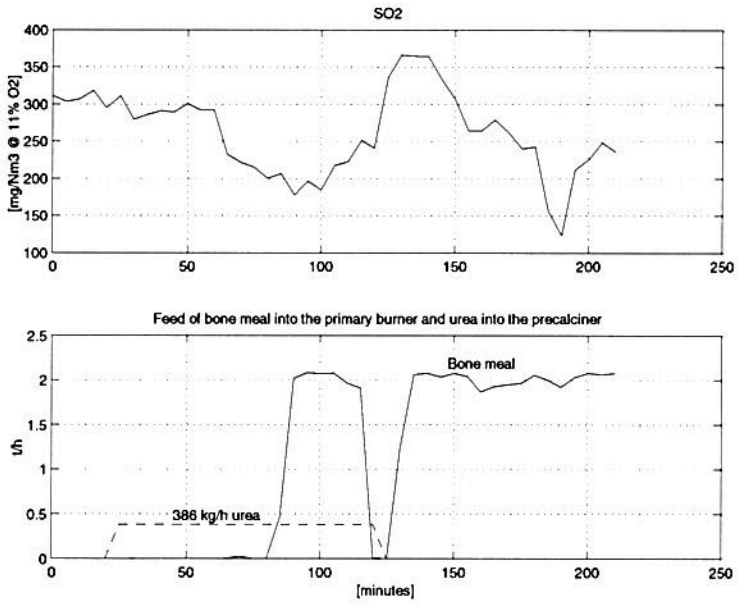

Figure C.16: SO_2 emissions during feed of bone meal into the main burner and urea into the precalciner. Experiment 15 (April campaign).

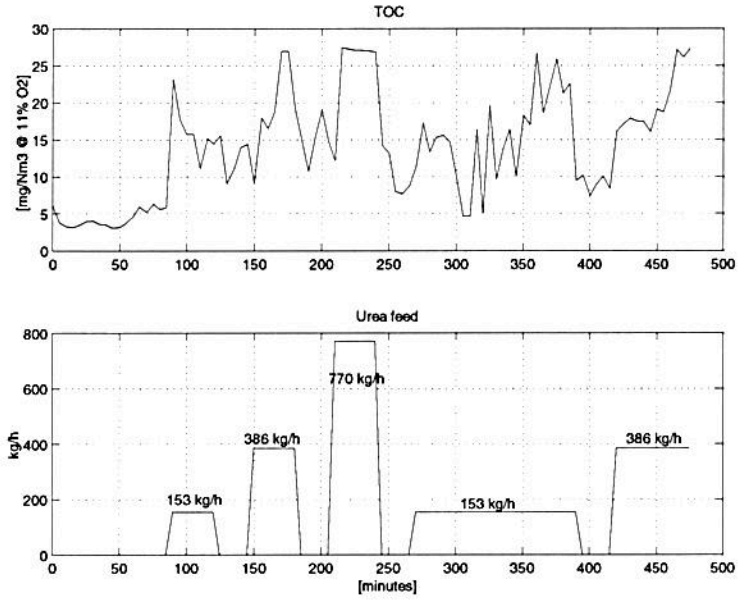

Figure C.17: TOC emissions during alteration in urea feed into kiln 6. Experiments 3 to 6 (February campaign).

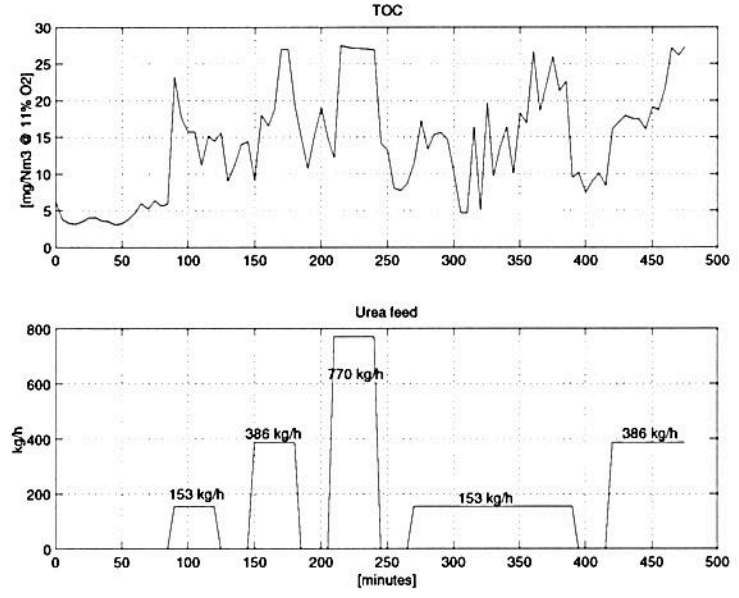

Figure C.18: TOC emissions during alteration in urea feed into kiln 6. Experiments 10, 11, 12, 16 and 17 (April campaign).

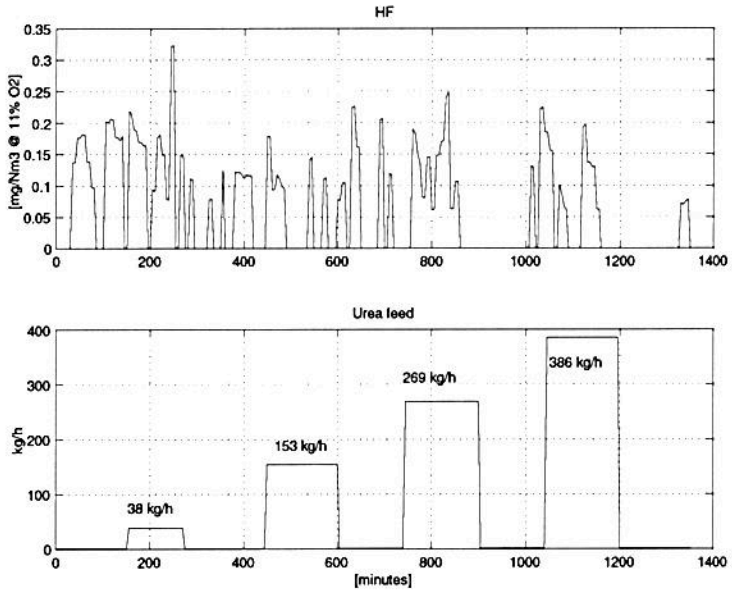

Figure C.19: HF emissions during alteration in urea feed into kiln 6. Experiments 3 to 6 (February campaign).

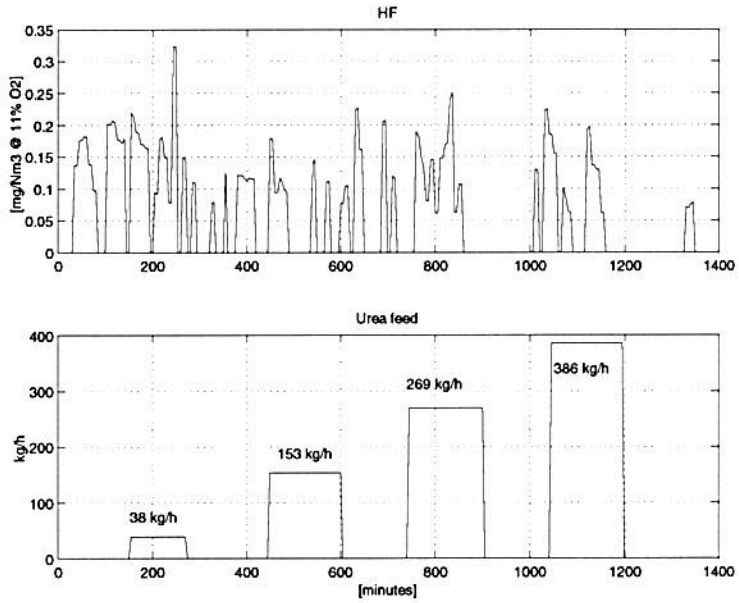

Figure C.20: HF emissions during alteration in urea feed into kiln 6. Experiments 10, 11, 12, 16 and 17 (April campaign).

Appendix D

Figures - AM combustion in the precalciner

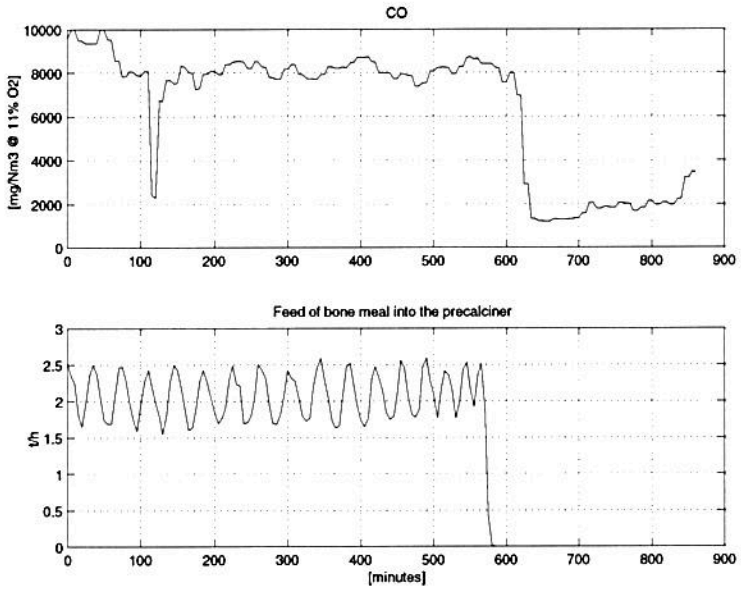

Figure D.1: CO emissions during combustion of bone meal in the precalciner. Experiment 7 (February campaign).

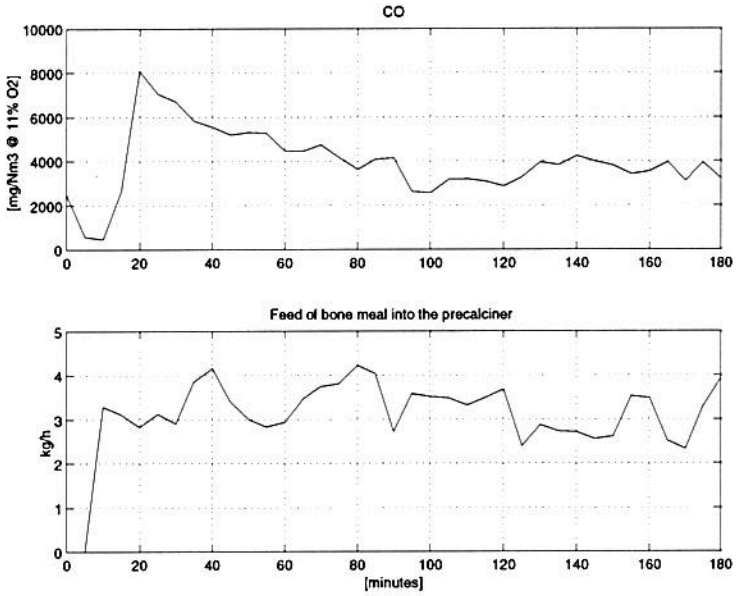

Figure D.2: CO emissions during combustion of bone meal in the precalciner. Experiment 13 (April campaign).

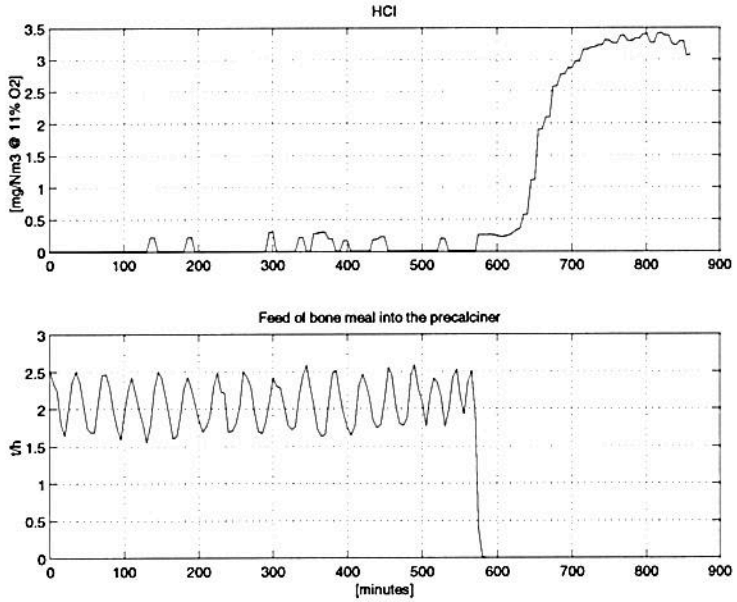

Figure D.3: HCl emissions during combustion of bone meal in the precalciner. Experiment 7 (February campaign).

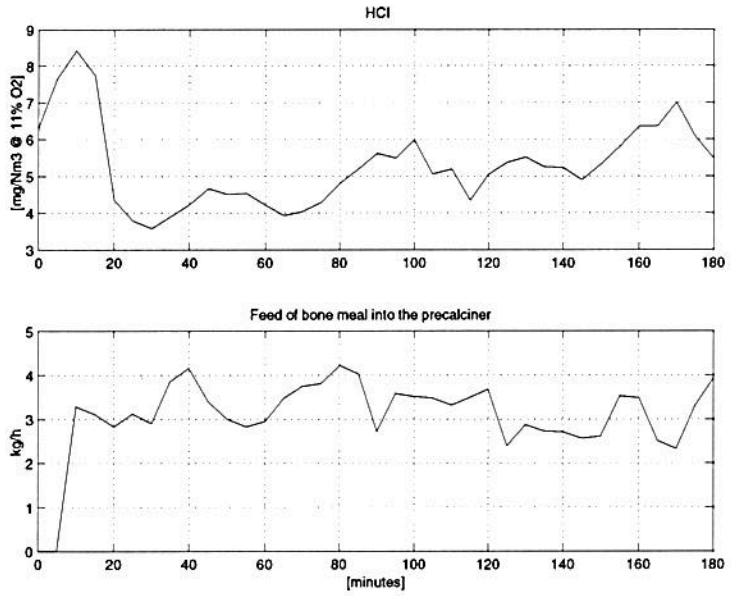

Figure D.4: HCl emissions during combustion of bone meal in the precalciner. Experiment 13 (April campaign).

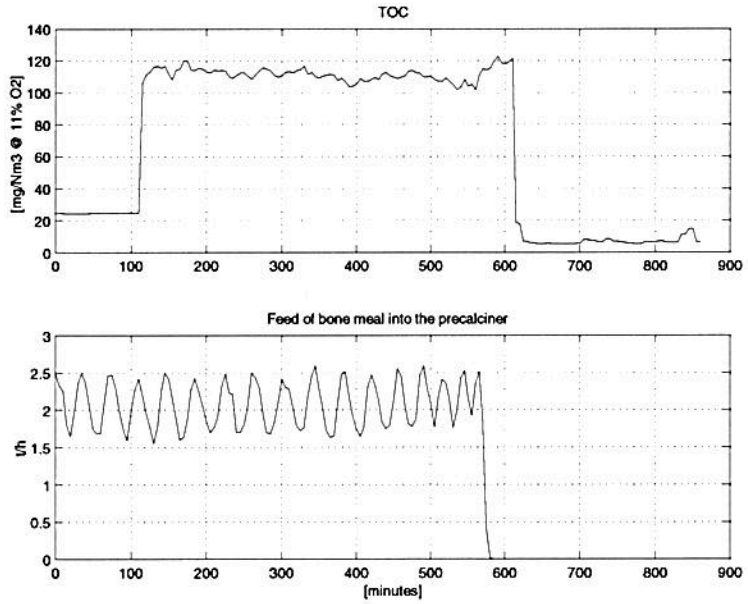

Figure D.5: TOC emissions during combustion of bone meal in the precalciner. Experiment 7 (February campaign).

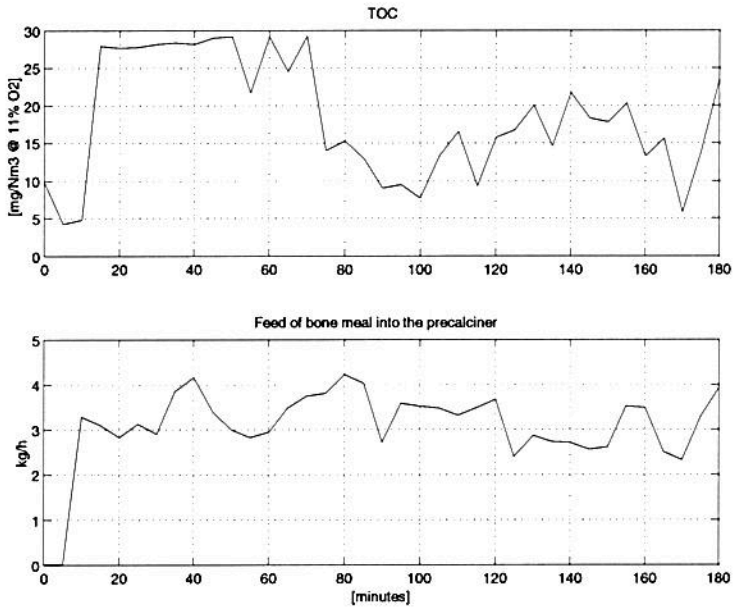

Figure D.6: TOC emissions during combustion of bone meal in the precalciner. Experiment 13 (April campaign).

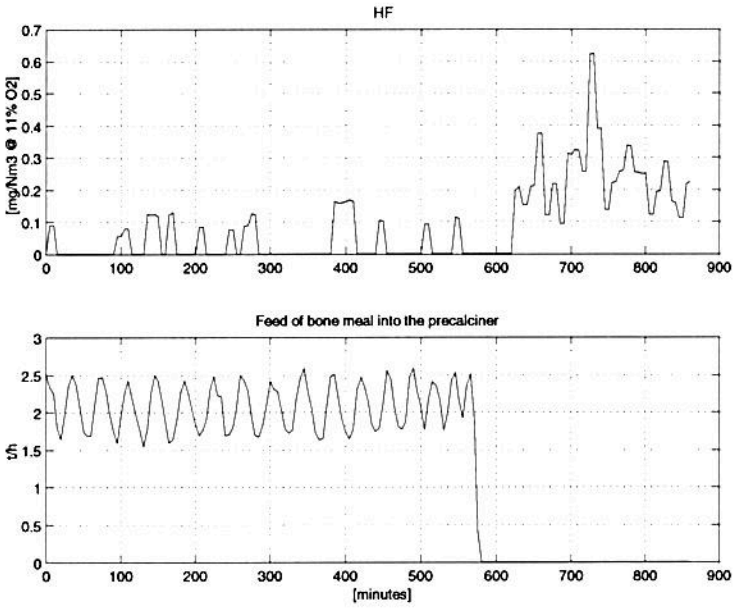

Figure D.7: HF emissions during combustion of bone meal in the precalciner. Experiment 7 (February campaign).

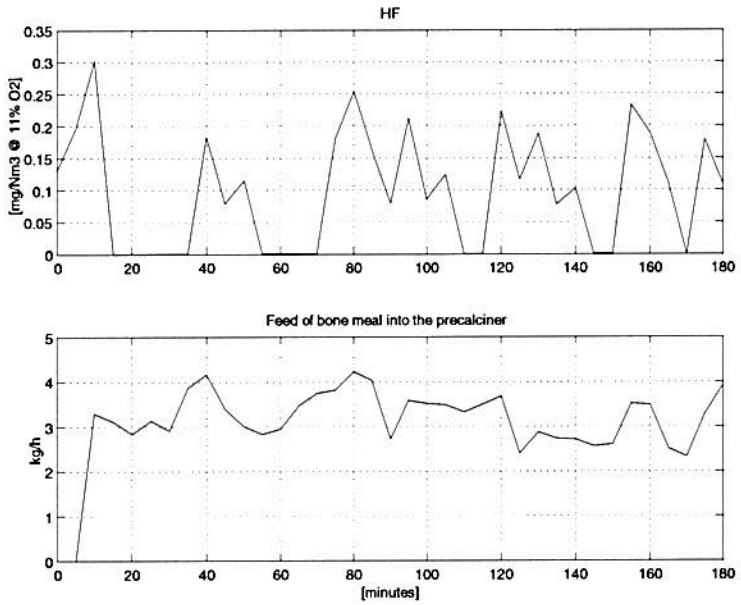

Figure D.8: HF emissions during combustion of bone meal in the precalciner. Experiment 13 (April campaign).

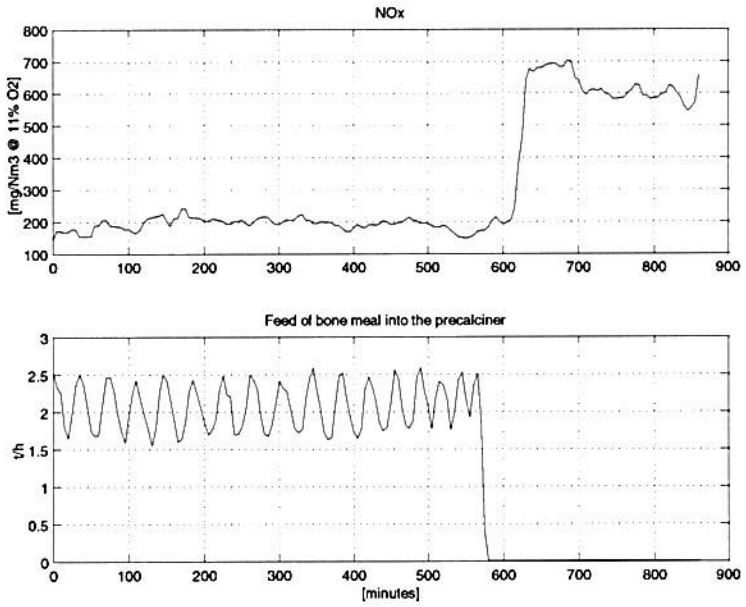

Figure D.9: NO_x emissions during combustion of bone meal in the precalciner. Experiment 7 (February campaign).

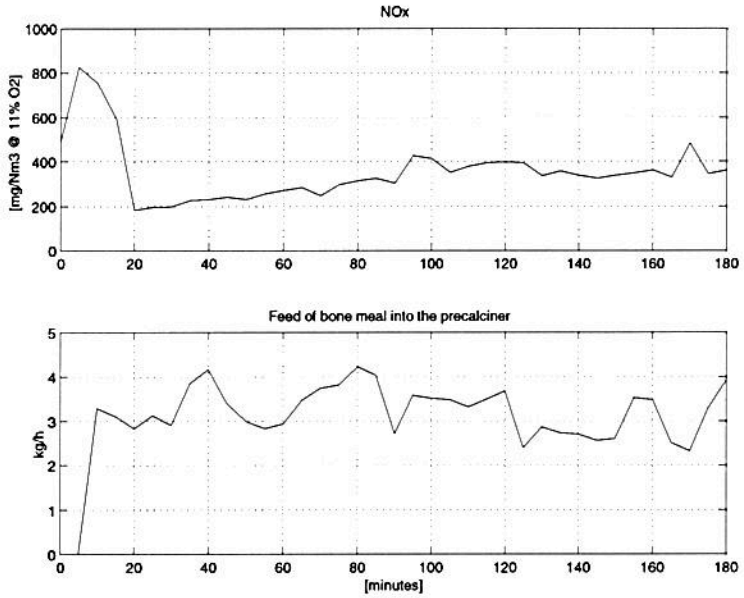

Figure D.10: NO_x emissions during combustion of bone meal in the precalciner. Experiment 13 (April campaign).

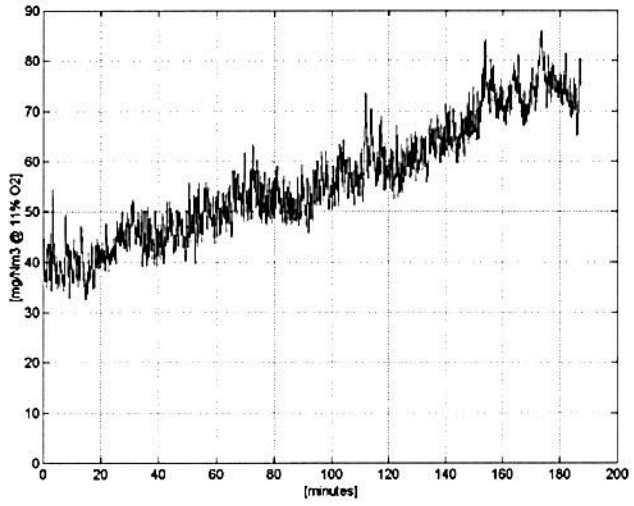

Figure D.11: N_2O emissions during combustion of bone meal in the precalciner. Experiment 13 (April campaign).

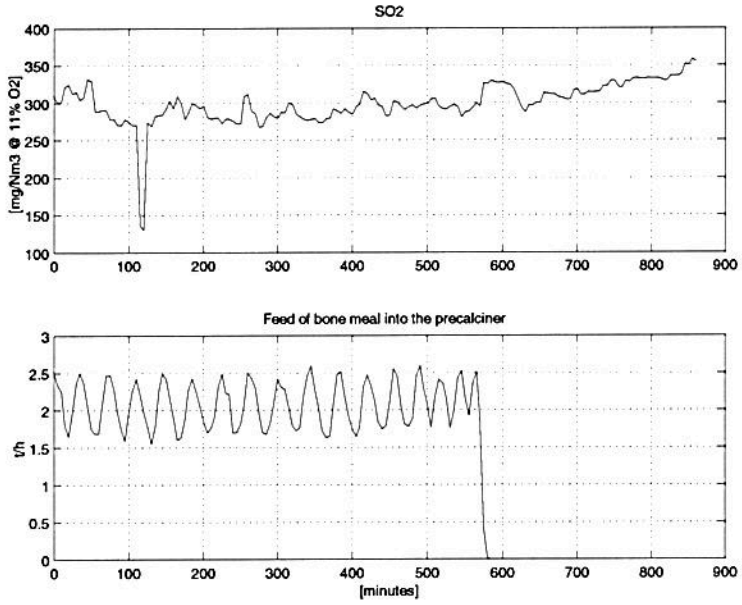

Figure D.12: SO_2 emissions during combustion of bone meal in the precalciner. Experiment 7 (February campaign).

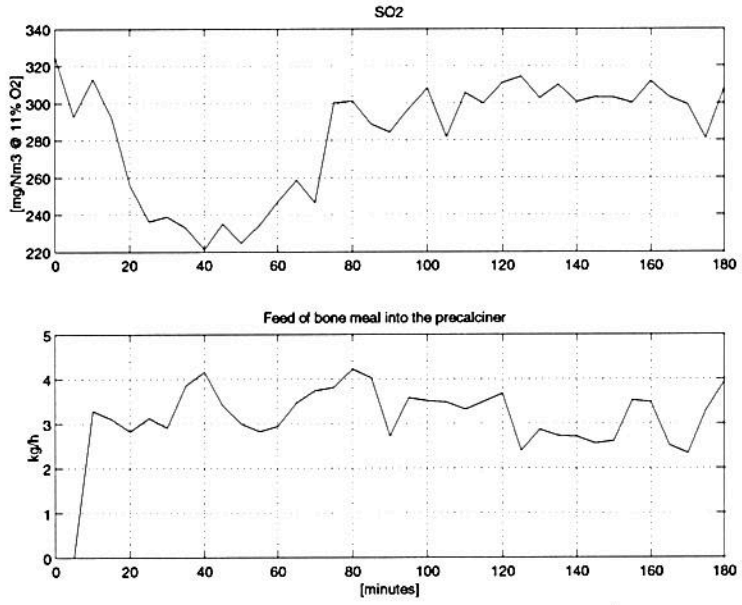

Figure D.13: SO_2 emissions during combustion of bone meal in the precalciner. Experiment 13 (April campaign).

Appendix E

Figures - AM combustion in the main burner

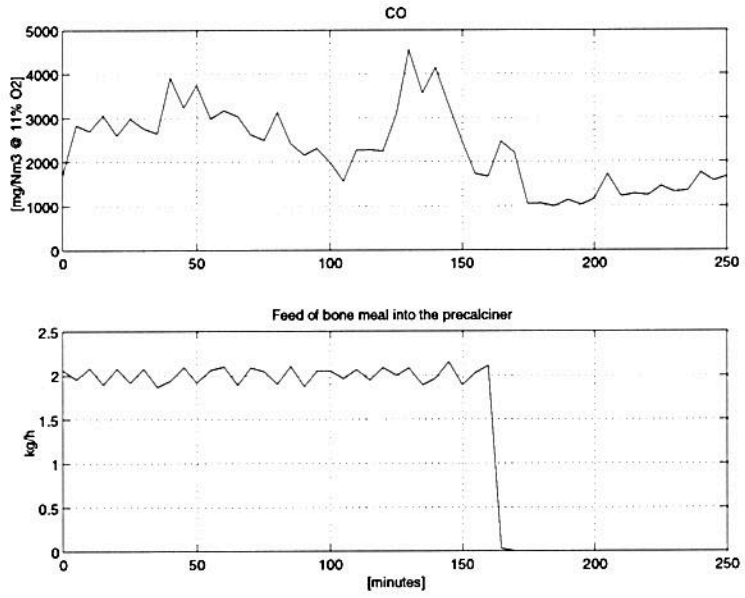

Figure E.1: CO emissions during combustion of bone meal in the primary burner. Experiment 14 (April campaign).

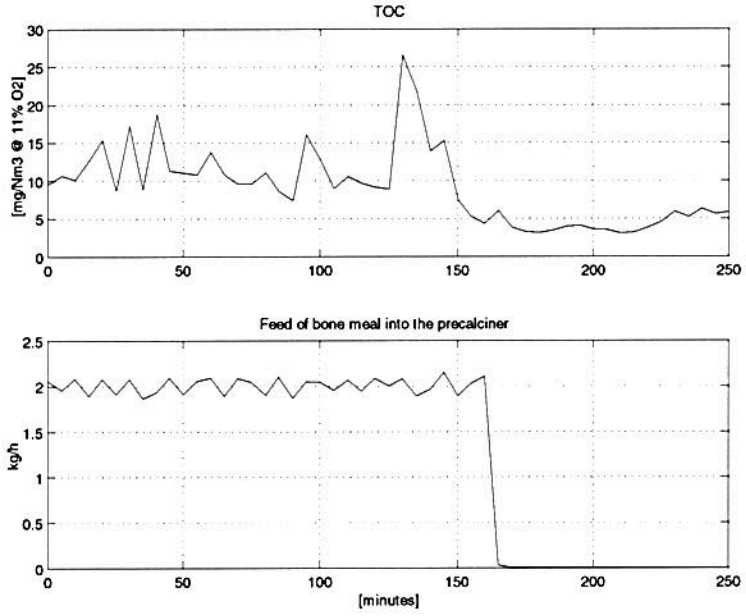

Figure E.2: TOC emissions during combustion of bone meal in the primary burner. Experiment 14 (April campaign).

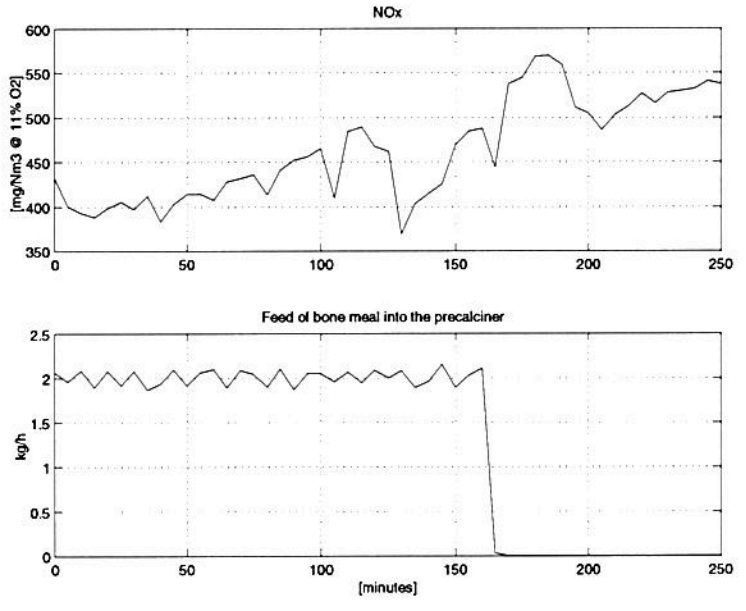

Figure E.3: NO_x emissions during combustion of bone meal in the primary burner. Experiment 14 (April campaign).

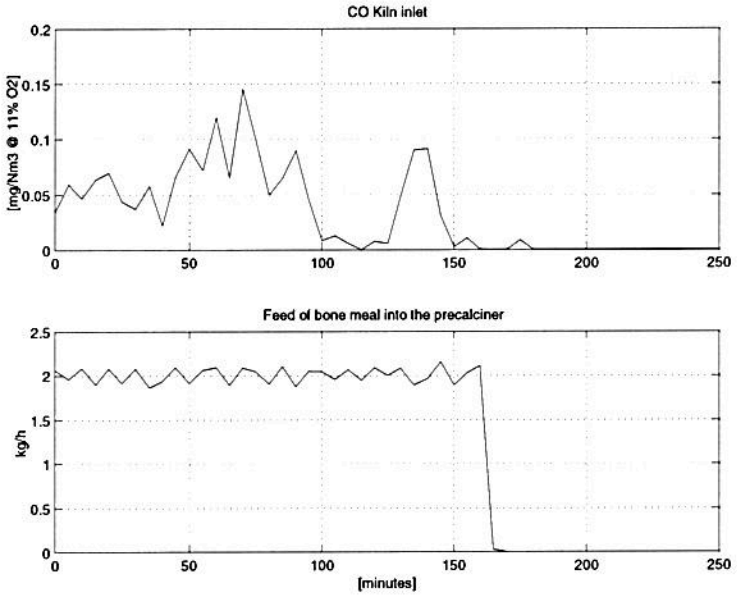

Figure E.4: CO level at the kiln inlet during combustion of bone meal in the primary burner. Experiment 14 (April campaign).

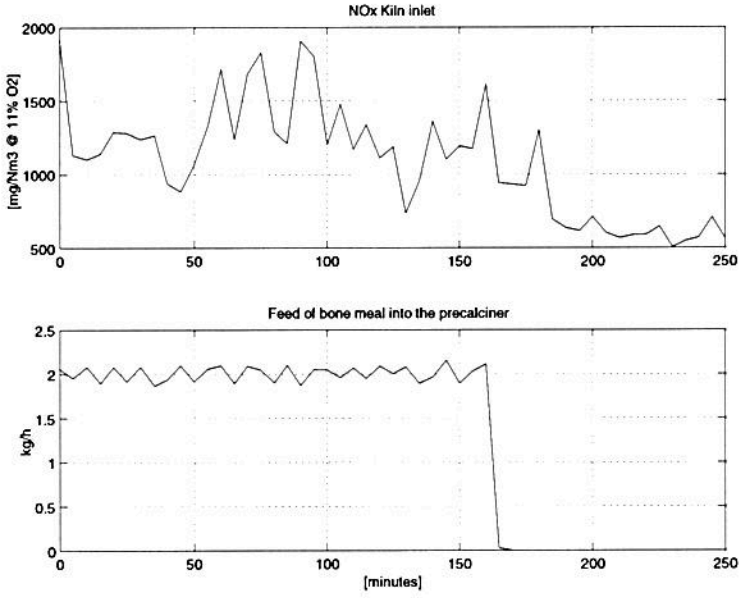

Figure E.5: NO_x level at the kiln inlet during combustion of bone meal in the primary burner. Experiment 14 (April campaign).

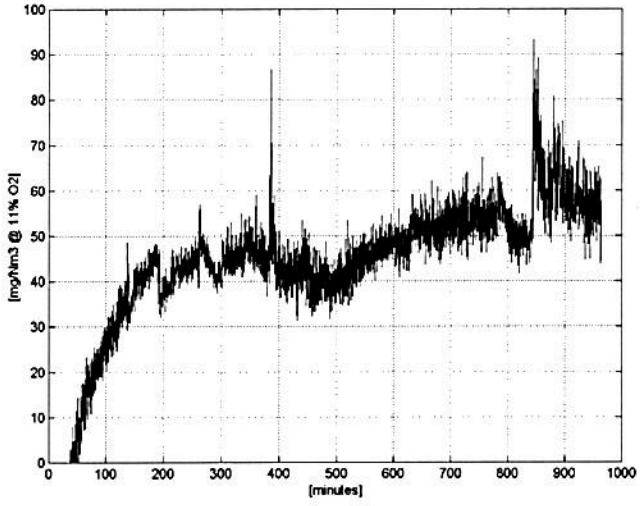

Figure E.6: N_2O emissions during combustion of bone meal in the primary burner, measured at the outlet of cyclone 4.2. Experiment 14 (April campaign).

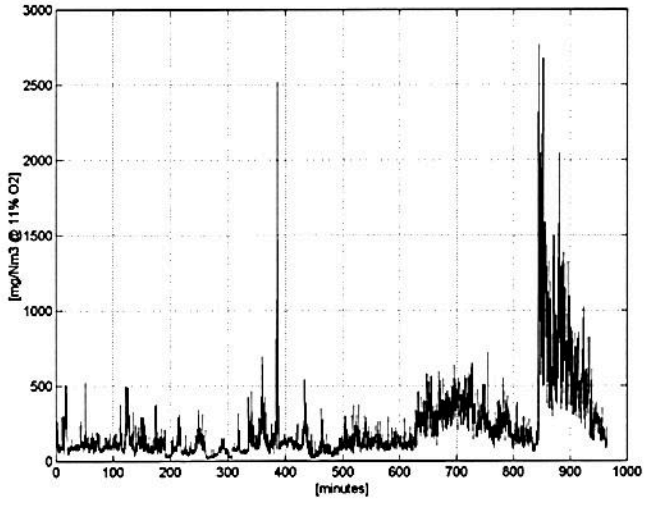

Figure E.7: CO emissions during combustion of bone meal in the primary burner, measured at the outlet of cyclone 4.2. Experiment 14 (April campaign).

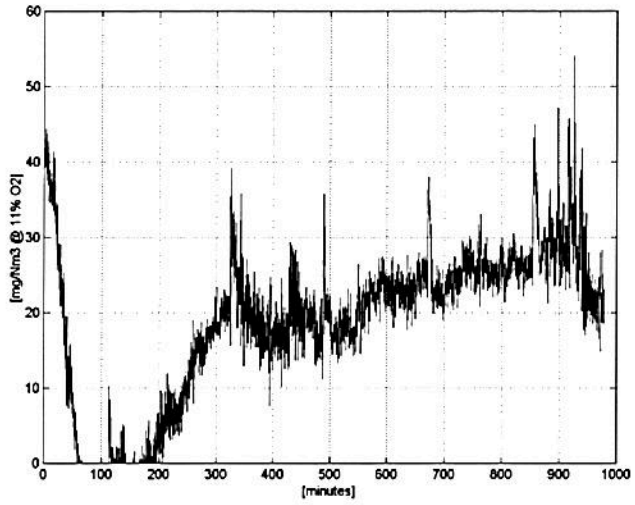

Figure E.8: N_2O emissions during combustion of bone meal in the primary burner, measured at the outlet of cyclone 4.2; similar conditions as in experiment 14 (April campaign).

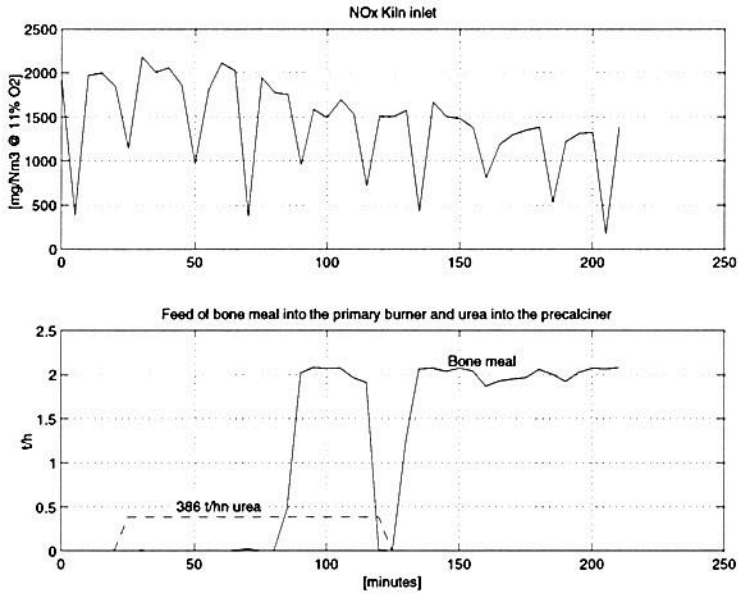

Figure E.9: NO_x level at the kiln inlet during feed of bone meal into the main burner and urea into the precalciner. Experiment 15 (April campaign).

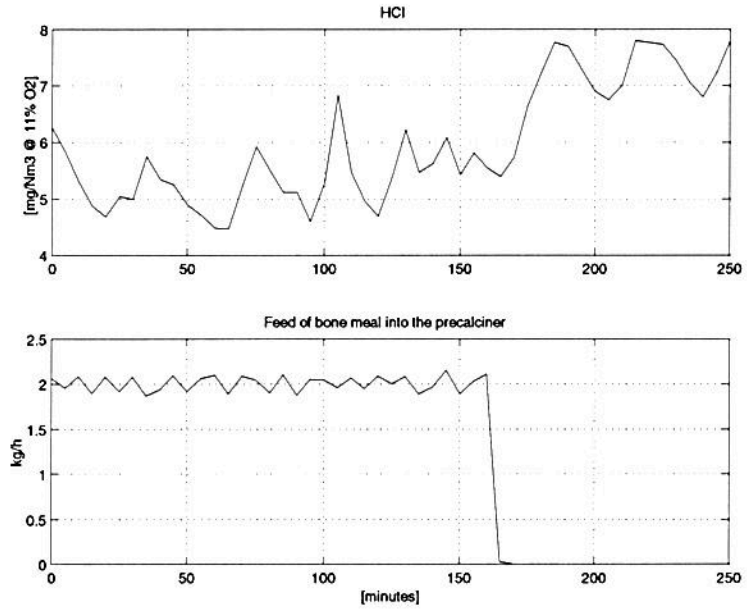

Figure E.10: HCl emissions during combustion of bone meal in the primary burner. Experiment 14 (April campaign).

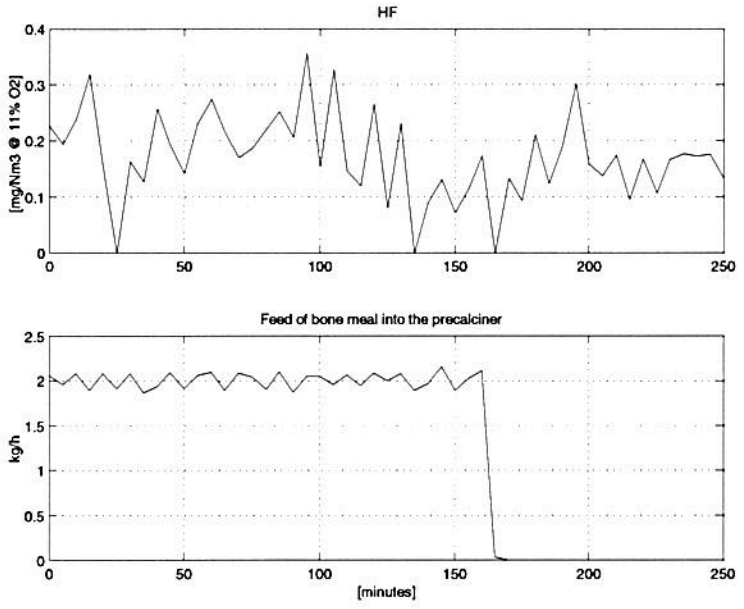

Figure E.11: HF emissions during combustion of bone meal in the primary burner. Experiment 14 (April campaign).

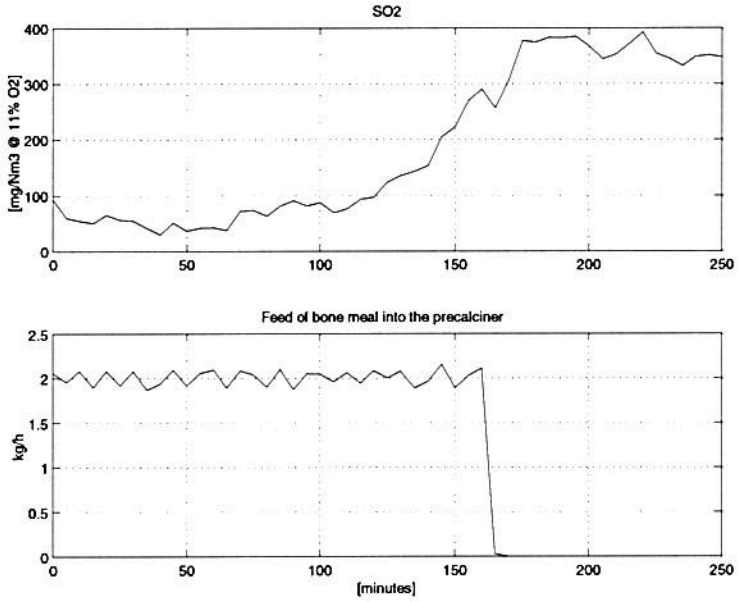

Figure E.12: SO_2 emissions during combustion of bone meal in the primary burner. Experiment 14 (April campaign).

Appendix F

NH_3 versus CO competition

It can be seen from Figure F.1 that the primary abstraction reaction constant for NH_3 is about ten times faster than the CO oxidation.

However, it would not be correct to evaluate the NH_3 versus CO competition only through the reaction constants. Therefore, it is useful to make an evaluation of the reaction rates for the two components to obtain a more correct picture (even though it is an approximation).

$$r_{NH_3} = k_{NH_3}[OH][NH_3] \tag{F.1}$$

$$r_{CO} = k_{CO}[OH][CO] \tag{F.2}$$

$$N + \frac{3}{2}H_2 \rightarrow NH_3 \tag{F.3}$$

$$C_s + \frac{1}{2}O_2 \rightarrow CO \tag{F.4}$$

F.1 Approach

To simplify the problem it is necessary to consider only one fuel particle and (partly) leaving out interactions with other fuel particles, circulating mass, wall effects etc.

A fuel particle that releases most of the fuel nitrogen during pyrolysis, and that has a low O/N ratio, is considered. Such a particle releases most of its nitrogen as NH_3, according to previous discussions, see Section 2.1.3. (An uncertainty is the ratio of HCN/NH_3 in the gases released from the fuel particle.)

Char combustion does not begin until the release of pyrolysis products is finished (Tillmann 1991), and at temperatures similar to those in a precalciner most of the carbon is released as CO, according to Equation F.4, see Section 2.2.

F.2 Assumptions

- The OH radicals are assumed to be equally accessible for both reaction rates. Hence, the proportionality of NH_3 and CO is evaluated, see Equation F.1 and F.2.
- Combustion of animal meal occurs according to Table 4.4, where the molar fraction of C and N are 0.312 and 0.057, respectively.

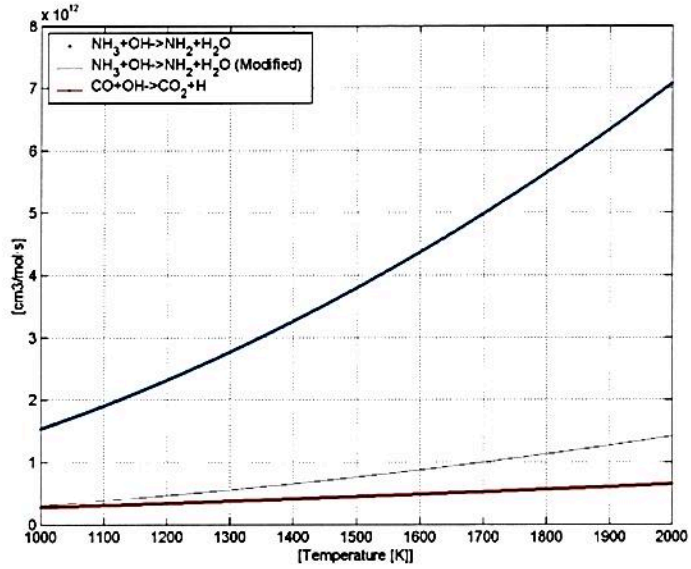

Figure F.1: Comparision between the reaction rate constants for reaction: $CO + OH \rightarrow CO_2 + H$ and $NH_3 + OH \rightarrow NH_2 + H_2O$ (Warnatz et al. 1999).

- Formation of CO and NH_3 occur according to the global reactions in Equations F.3 and F.4.
- The fuel nitrogen is released in equal amounts of HCN and NH_3.
- Up to 95 % of the C is released as CO, according to Equation 2.81 at 1300 K.
- It is assumed that nitrogen released (as NH_3) during pyrolysis and carbon released (as CO) during char combustion competes simultaneously for the OH radical.

Based on these assumptions, calculations give molar fractions of CO and NH_3 of 0.1136 and 0.02345, respectively. This shows that the concentration of CO released from a burning particle of animal meal is about five times higher than that of NH_3.

Modifying the reaction constant for NH_3 to a fifth part of the original, the three reaction constants are plotted together in Figure F.1.

The lower limit is set to 1000 K, since the rate coefficient of CO is nearly independent of temperature. Hence, quenching of CO at lower temperatures principally occurs by depletion of radical species, such as OH, by recombination reactions (Bartok & Sarofim 1991).

F.3 Conclusion

It can be seen from Figure F.1 that the modified reaction constant for NH_3, expressing the development of a simplified reaction rate, is about twice as fast as the CO oxidation. Furthermore, it must be taken into account that NH_3 is released prior to CO and therefore probably will have an advantage in the competition for the OH radical.

Taking into account the simplicity of this evaluation, a conclusion is that an increased amount of NH_3 present in the combustion chamber (precalciner), by advanced reburning with urea pellets or reburning with animal meal, leads to competition for the OH followed by an increase in the CO emissions.

Part III

Appendixes - Laboratory experiments

Appendix G

Introductory experiments - CFBC

G.1 Experiments with circulating mass

The experiments were carried out using a circulating mass with a particle distribution different from that of Millisil®M6 and raw meal, as discussed earlier. The reason for carrying out experiments with a different circulating mass is to achieve experience about operation of the CFBC reactor. The circulating mass had a median particle size of about 300 μm (Axelsen 2001*a*).

Five experiments were executed, with alteration of the superficial gas velocity in each experiment, see Table G.1. Solids circulation rate and excess air ratio were held constant. No secondary air was supplied during the experiments. The primary fuel throughout all experiments was propane.

Table G.1: Alteration between experiment A to E.

		A	B	C	D	E
Parameters	**Unit**	**Avg.**	**Avg.**	**Avg.**	**Avg.**	**Avg.**
q	kW	21.7	20.3	19.2	17.8	16.4
τ_g	$sec.$	1.30	1.40	1.52	1.68	1.84
v_{riser}	m/s	3.3	3.1	2.8	2.6	2.3
G_s	kg/h	19	19	19	19	19

The experiments reflect the overall stable conditions in the CFBC reactor for the prevailing state-parameters. A test plan with different plots of the experiments is found in (Axelsen 2001*a*).

The experiments will be addressed as A, B, C, D and E according to the chronological order of the experiments, see (Axelsen 2001*a*). Averages and standard deviations of the parameters in experiments A and E, which have highest and lowest superficial gas velocity, respectively, are shown in Table G.2. The CO emissions, BFB pressure and average CFB temperature in the riser as a function of retention time are shown in Figures G.1, G.2 and G.3.

It can be seen from Table G.2 and Figure G.2 that increased gas retention time (decreased superficial gas velocity) increases bed voidage (lower pressure drop over the riser) and the pressure in the BFB. This indicates increased hold up of solids in the bottom region in accordance with previous experiments (Bai, Jin, Yu & Zhu 1992). An increasing solids hold up in the bottom region indicates a higher splashing zone with a lower dense region and an upper dilute region according to

Table G.2: Comparison of averages and standard deviations of the parameters in experiment A and E.

		A		E	
Parameters	**Unit**	**Avg.**	**Sdev.**	**Avg.**	**Sdev.**
CO @ 11% O_2	ppm	39.6	9.72	188.0	20.67
CO_2 @ 11% O_2	%	4.4	0.0106	4.0	0.0046
SO_2 @ 11% O_2	ppm	-2.92	0.0552	-3.2	0.0398
NO @ 11% O_2	ppm	35.2	0.39	34.3	0.41
N_2O @ 11% O_2	ppm	15.9	0.15	21.8	0.19
O_2	%	7.3	0.0411	7.6	0.0342
$\lambda(O_2)$	[−]	1.35	0.0046	1.35	0.0040
		(1.53)		(1.56)	
P_{BFB}	$mbar$	21.4	7.97	37.1	1.61
ΔP_{riser}	$mbar$	0.37	2.22	0.14	2.68
T_{BFB}	$°C$	904.8	1.62	800.6	2.39
$T_{average:1-10}$	$°C$	785.4	0.37	706.4	0.83
q	kW	21.7		16.4	
τ_g	$sec.$	1.34		1.86	
v_{riser}	m/s	3.3		2.3	
ε_{riser}	[−]	0.99999442		0.9999782	
G_s	kg/h	19			

Figure 2.28. The increasing solids hold up in the bottom region, giving a better heat transfer from the BFB, can also be seen from Figure G.5 where temperature nodes 1 and 3 are closer than in Figure G.4.

The increasing CO emissions are probably due to lower temperature and/or poorer gas- and solids mixing in the riser. At temperatures lower than 800 K the hydroxide radical (OH) freezes out, impeding the completion of the oxidation of CO into CO_2 (Turns 1996). Bartok and Sarofim (1989) state that at temperatures below 1000 K, the rate coefficient is nearly independent of temperature. Hence quenching of CO at lower temperatures principally occurs by depletion of radical species, such as OH, by recombination reactions. The CO emissions show a sharp increase when the retention time is at a maximum, whereas the temperature decreases smoothly throughout the experiments, see Figures G.1 and G.3.

The solids loading in the CFBC reactor is increasing with falling superficial gas velocity giving a higher splashing zone (increased dense region). At the point of maximum retention time the CFBC reactor starts the phenomenon of choking (slugging) that gives poorer gas- and solids mixing. This phenomenon in combination with temperature is the probable reason for higher CO emissions at the point of maximum retention time. It should also be taken into account that cold spots in the CFBC reactor might freeze out the hydroxyl radical. The low temperature is most likely the reason for the increased CO emissions.

The emissions of sulphur dioxide are just below zero, since no sulphur is supplied from the fuel or circulating mass. A zero point error in the SO_2 emissions can be seen from Table G.2.

The NO concentration is 34.5 ppm and is not varying much between experiment A and E. The concentration of nitrous oxide is varying from 15 to 22 ppm, which is high compared to previous work (Hulgaard & Dam-Johansen 1992). Hulgaard et al. (1992) state that nitrous oxide emissions usually are low (0-5 ppm), and that such measurements are disturbed by interferences from CH_4, H_2O, SO_2 and to a minor extent from NH_3. After calibration of the the H&B analyzer, an experiment with 250 ppm SO_2 in N_2 was made in order to check any interference could be detected.

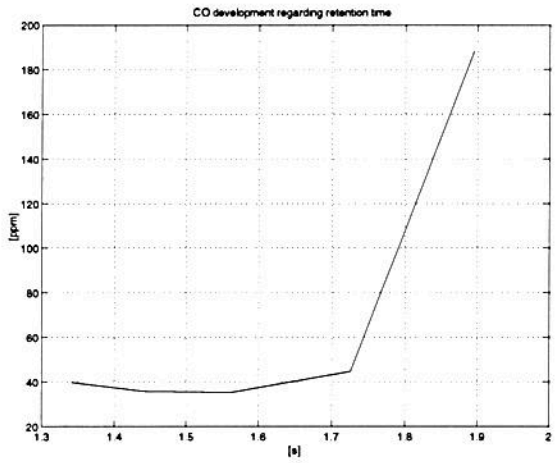

Figure G.1: CO in the CFBC reactor as a function of retention time for experiments: A, B, C, D and E.

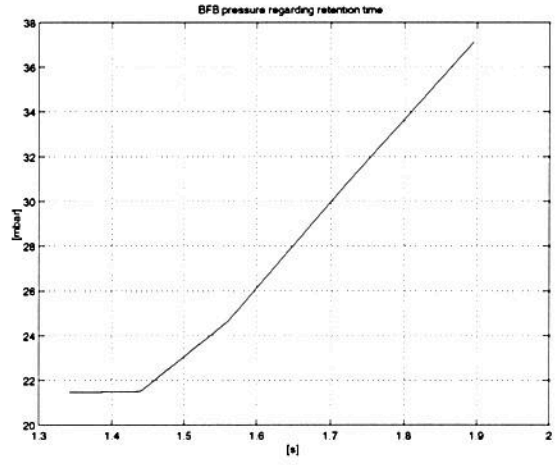

Figure G.2: Pressure in the BFB as a function of retention time for experiments: A, B, C, D and E.

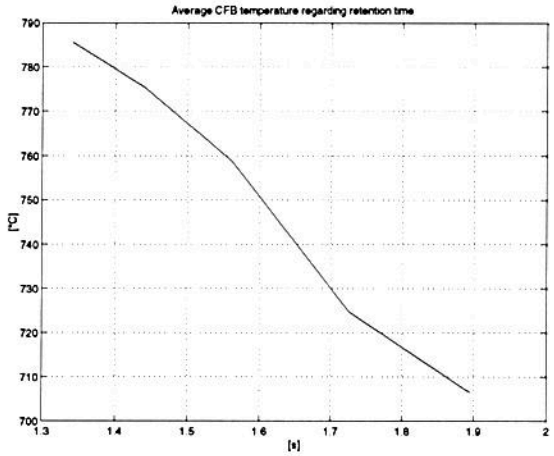

Figure G.3: Average temperature in the CFB as a function of retention time for experiments: A, B, C, D and E.

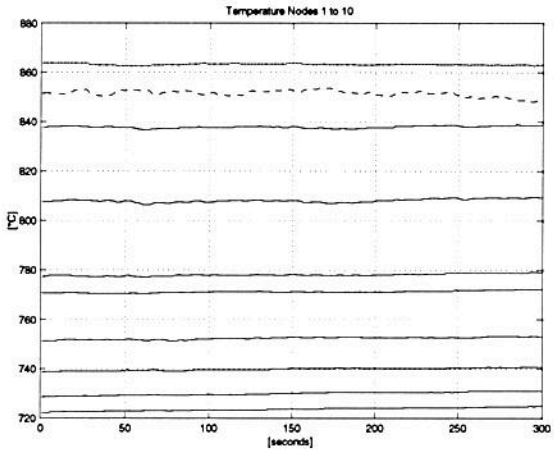

Figure G.4: Temperature distribution for experiment A. Nodes in descending order: 2, 1, 3...10.

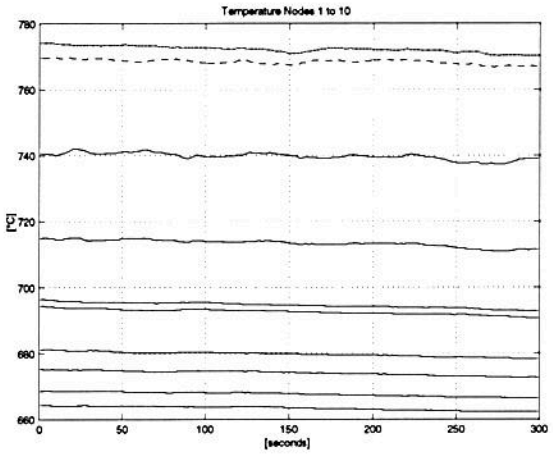

Figure G.5: Temperature distribution for experiment E. Nodes in descending order: 2, 1, 3...10.

However, no influence of SO_2 on the H&B analyzer was observed.

The emissions of CO and the differential pressure in the riser are the parameters with the highest standard deviation. It can be seen from Table G.2 that the standard deviation of CO decreases significantly with higher solids hold up in the bottom region. The standard deviation for the differential pressure is large in all experiments, but is significantly higher in experiment E. This can be explained by the increased solids hold up in the bottom region giving a more unstable splashing zone. In contrast, a higher solids hold up in the bottom region gives a more stable pressure measurement (less standard deviation) in the BFB.

G.2 Experiments with wood chippings

An experiment with fine wood chippings without circulating mass in the CFBC reactor was performed. Table 4.5 shows the composition of the wood chippings, which had a particle size of about 4×1×1 mm, corresponding to a spherical diameter of about 2 mm. The experiment was carried out in four steps with increasing input of alternative fuel, see Table G.3.

Table G.3: Paremeters for the experiment with fine wood chippings carried out in four steps.

Parameters	**Unit**	**1**	**2**	**3**	**4**
Running − time	*sec*	0 - 300	300 - 1200	1200 - 2460	2460 - 3250
Alternative fuel	*% (of energy)*	0	6.5	11.7	0
λ	[−]	1.51	1.41	1.33	1.51
q	kW	15.4	16.4	17.4	15.4
τ_g	*sec*	1.76	1.74	1.73	1.76
v_{riser}	m/s	2.7	2.7	2.7	2.7
ε_{riser}	[−]	1	1	1	1
G_s	kg/h	0	0	0	0

Figures G.6 - G.11 show the development of O_2, CO, N_2O, NO, temperature nodes 1 to 10 and average temperature in the riser. All figures and a test plan can

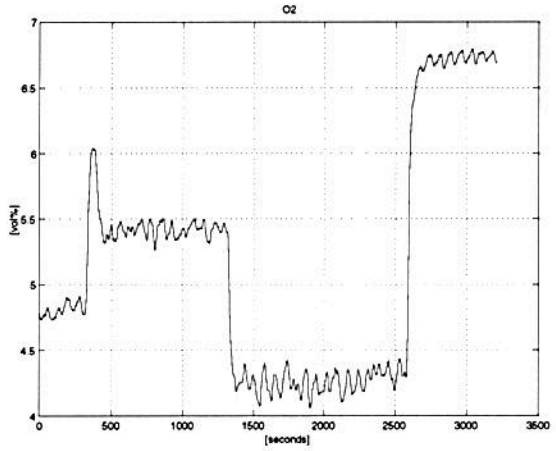

Figure G.6: Development of O_2 during the experiment with fine wood chippings.

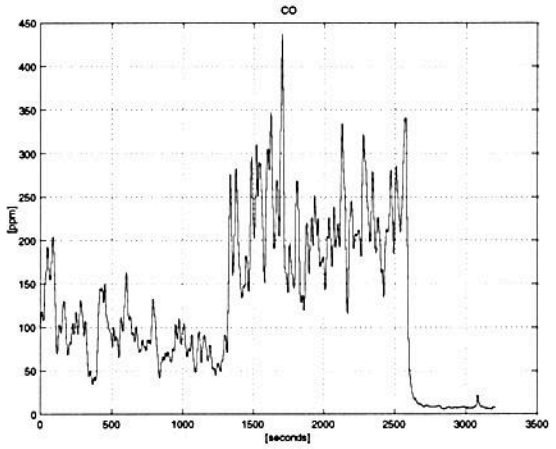

Figure G.7: Development of CO during the experiment with fine wood chippings.

be found in (Axelsen 2001*a*). Average and standard deviation for each step of the experiment are not presented since the intention was to investigate the development of temperature and emissions during increasing input of alternative fuel.

The magnitude of nitrous oxide is very high, as it was in the experiment with circulating mass. Most interesting is the similar development of both NO, N_2O and CO with increasing feed of alternative fuel. However, the NO emissions can be seen to follow every change in the fuel feed steps, in contrast to the CO and N_2O emissions. This is due to the increased supply of fuel nitrogen from the wood chippings.

The figures for emission measurements show a somewhat fluctuating trend during the experiment. In the literature review was found a statement from Mathiesen et al. (2000) that a gas/solid flow system, such as circulating fluidized bed, never will reach a normal steady state condition. The system will exhibit a fluctuating behavior, see Figure 2.32 (Mathiesen et al. 2000). The largest fluctuations are found in the emission measurements of CO. The reason for this is probably a combination of chamber instability and system instabilities (Williams 1985). Investigations of Figure G.7 shows that the CO emissions are lower in step four than in step one.

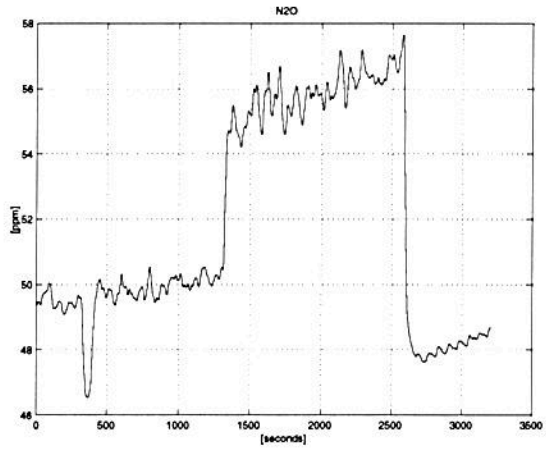

Figure G.8: Development of N_2O during the experiment with fine wood chippings.

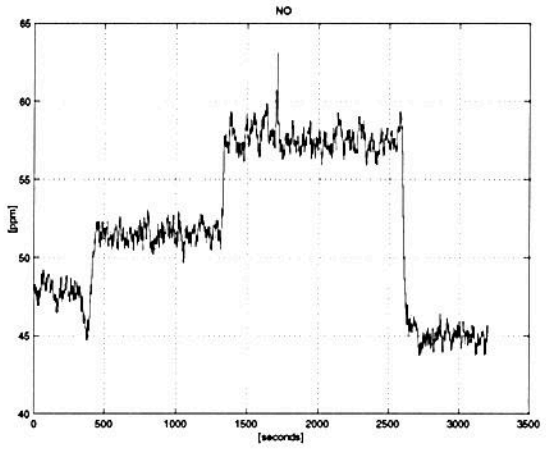

Figure G.9: Development of NO during the experiment with fine wood chippings.

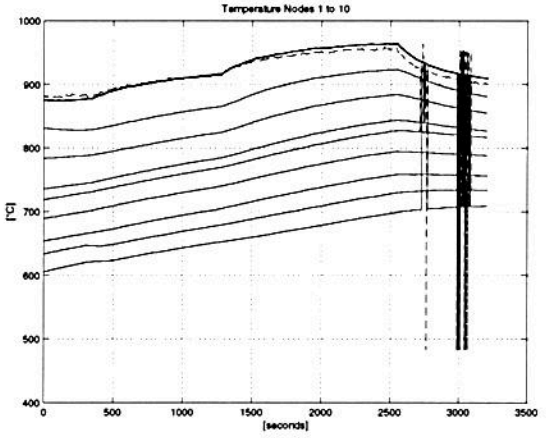

Figure G.10: Development of temperature in node 1 to 10 during the experiment with fine wood chippings. Nodes in descending order from the start: 2, 1, 3...10.

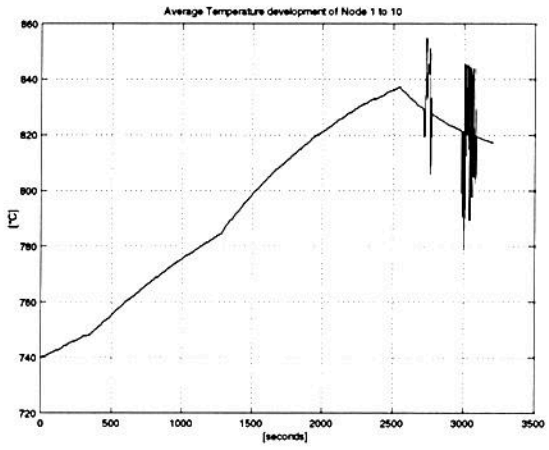

Figure G.11: Development of the average temperature in node 1 to 10 during the experiment with fine wood chippings.

This is probably because of different temperature profiles as a result of steady state conditions not being achieved.

It can be seen from Figure G.10 that increasing supply of alternative fuel increases the temperature in the riser. The temperature in the BFB increases with increasing supply of alternative fuel. The reason for this is probably deposition of fuel particles into the BFB. Furthermore G.10 shows that temperature node 2 increases and moves above node 1 when the CFBC reactor is fed with alternative fuel. Different fuels with varying volatility will probably show different temperature profiles in the CFBC reactor. (The disturbances in Figure G.10 and G.11 is due to failure in the signals from the thermoelements.)

The average temperature development in the riser shows a continuous increase, see Figure G.11. This means that it is of importance to be aware of the average temperature development in the riser in order to achieve stable conditions during experiments. CFB stability is indicated by the average temperature profile in the riser flattening out.

G.3 Conclusion of the introductory experiments

Introductory experiments with circulating mass showed the phenomena of:

- increasing holdup,
- higher splashing zone with a lower dense region and
- an upper dilute region.

The experiment showed an increase in CO emissionss that was probably due to the combination of lower temperature with reduced gas- and solids mixing in the riser. Therefore backmixing is an interesting phenomenon in further investigations of the use of alternative fuels (Axelsen 2001*a*).

By performing experiments in a laboratory reactor it is possible to control the conditions more thoroughly than in a full-scale reactor, such as a calciner. For instance, using a well-defined particle size for different fuels, makes it easier to determine whether an increase in CO emissions is due to different fuel characteristics or subject to a change in flow pattern (backmixing). In this way, the CFBC reactor

may be a useful tool for investigations of fuel specific emissions from combustion in a regime equivalent to that in a precalciner (Axelsen 2001*a*).

Appendix H

Reactor stability

H.0.1 Reactor stability

Reactor instability is a major challenge during execution of experiments due to operational complexity, such as variable influx and composition. Reactor instability and reactor stability during start-up are shown for O_2 in Figure H.1 and Figure H.2, respectively. The instability in Figure H.1 ended in a stoppage with subsequent preparation of the reactor.

Figure H.3 and H.4 show O_2 and temperature stability during an advanced reburning experiment after the start-up in Figure H.2.

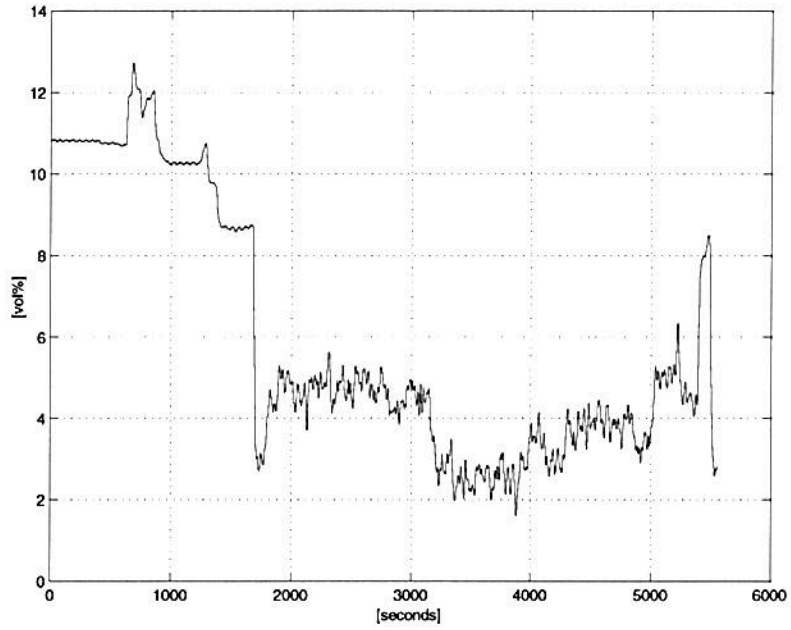

Figure H.1: Emissions of O_2 during start-up of an advanced reburning experiment with RDF (5 wt % urea), showing reactor instability.

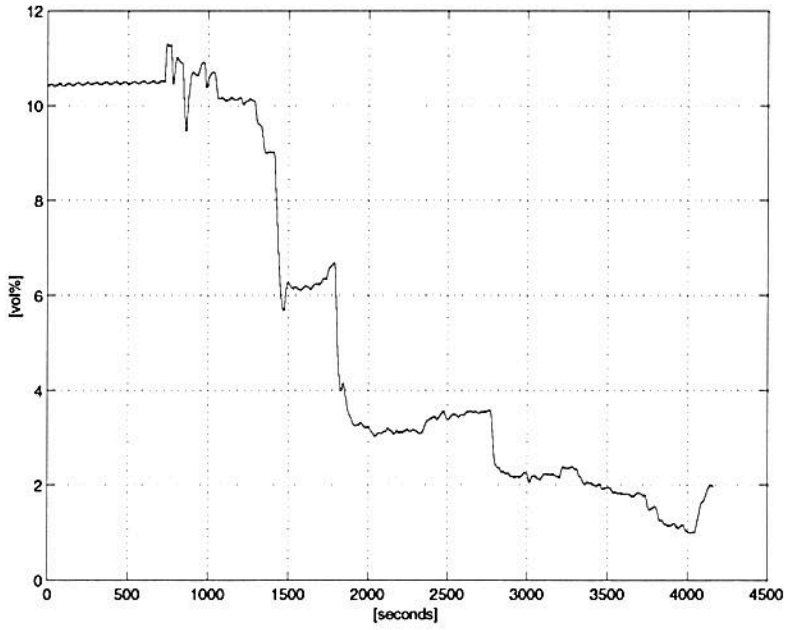

Figure H.2: Emissions of O_2 during start-up of an advanced reburning experiment with coal (5 wt % urea), showing reactor stability.

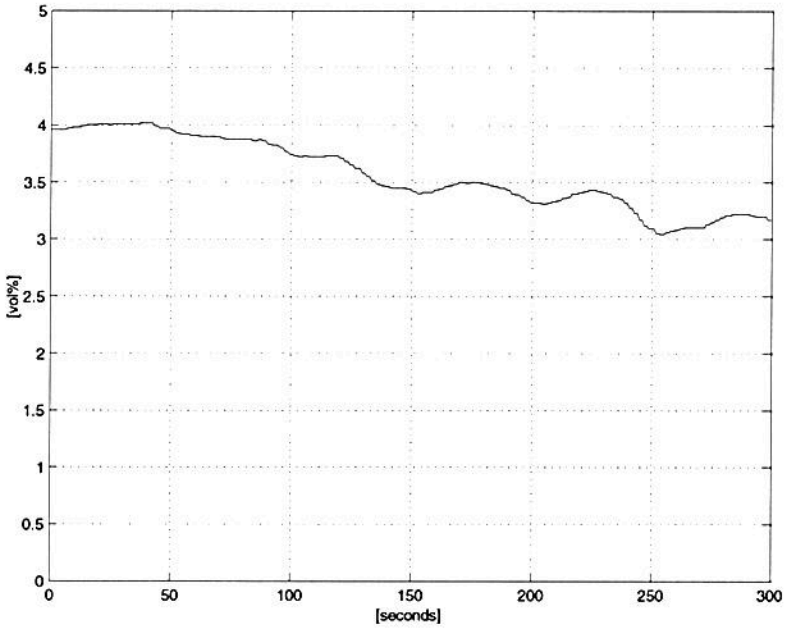

Figure H.3: Emissions of O_2 during an advanced reburning experiment with coal (5 wt % urea), showing reactor stability after start-up.

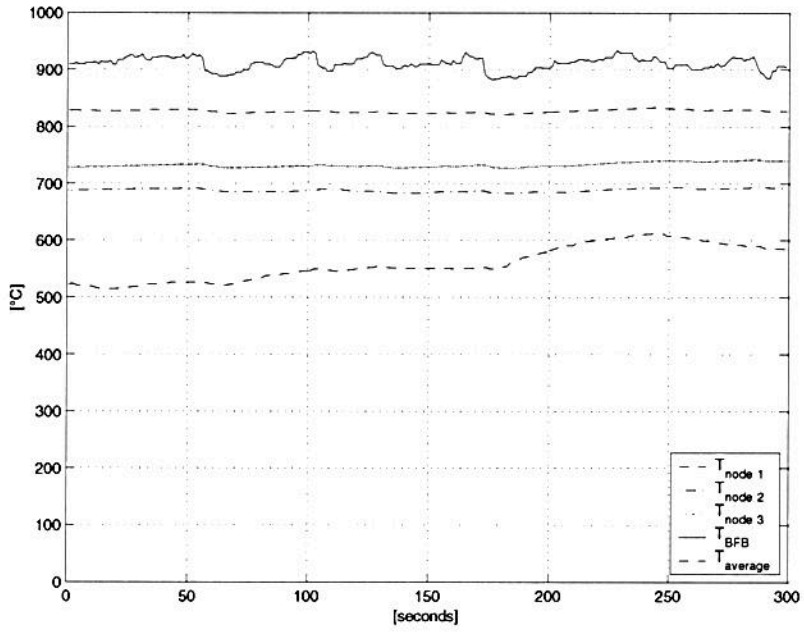

Figure H.4: Temperature development during an advanced reburning experiment with coal (5 wt % urea), showing reactor stability after start-up.

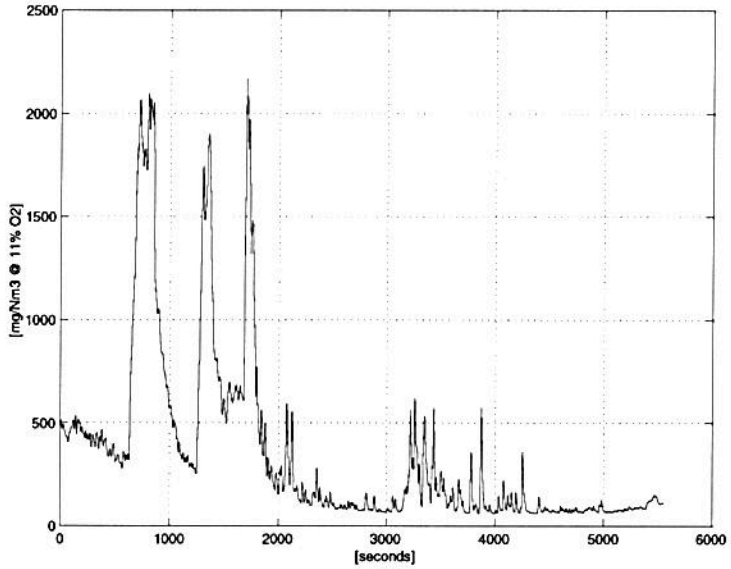

Figure H.5: Emissions of CO during start-up of an advanced reburning experiment with RDF (5 wt % urea), showing reactor instability.

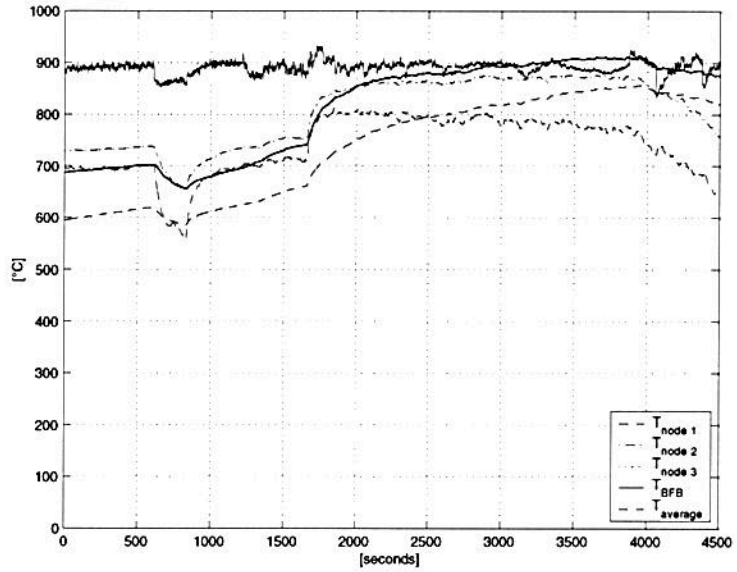

Figure H.6: Temperature development during start-up of an advanced reburning experiment with RDF (5 wt % urea), showing reactor instability.

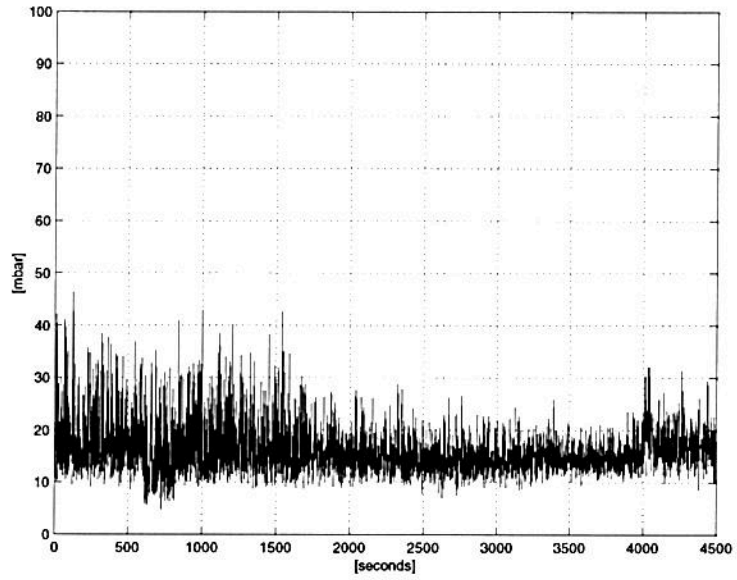

Figure H.7: Pressure development in BFB during start-up of an advanced reburning experiment with RDF (5 wt % urea), showing reactor instability following.

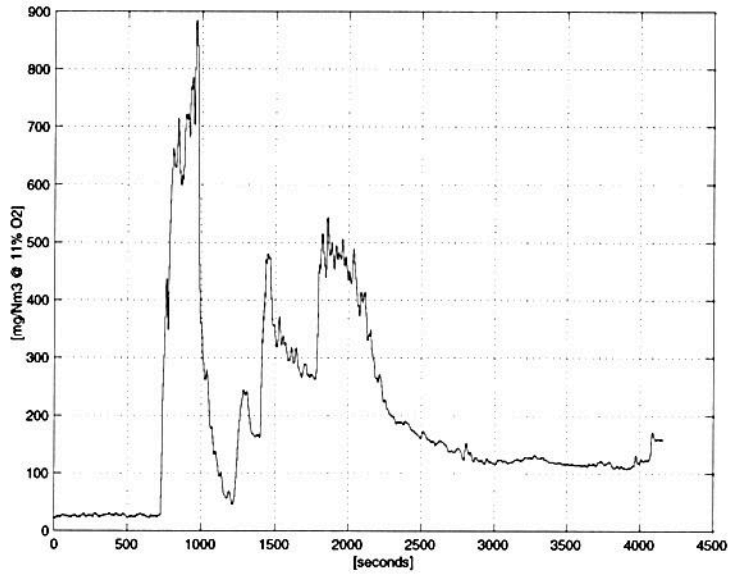

Figure H.8: Emissions of CO during start-up of an advanced reburning experiment with coal (5 wt % urea), showing reactor instability.

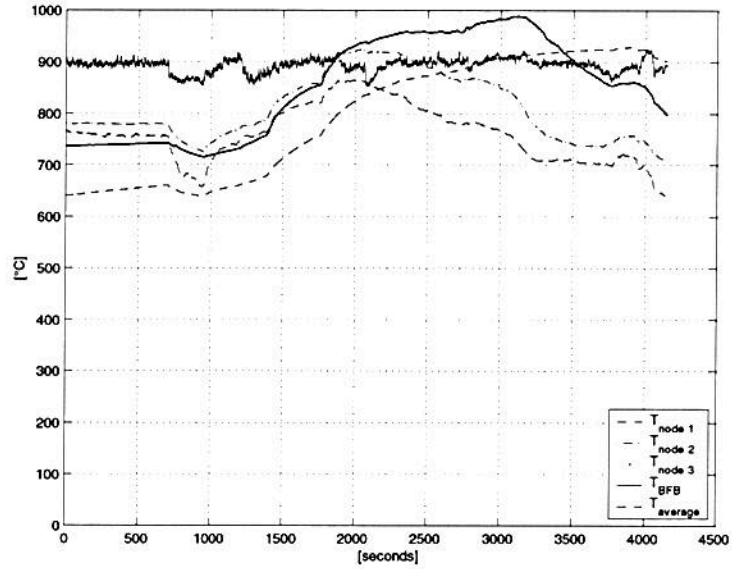

Figure H.9: Temperature development during start-up of anadvanced reburning experiment with coal (5 wt % urea), showing reactor stability.

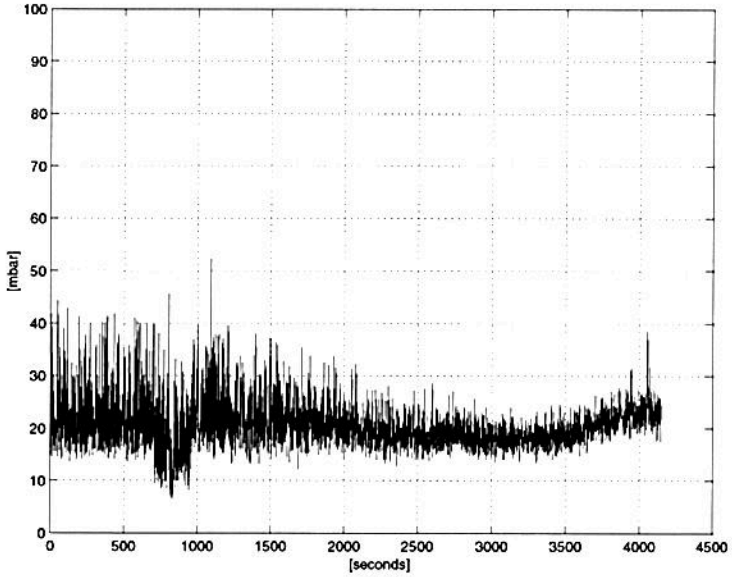

Figure H.10: Pressure development in BFB during start-up of an advanced reburning experiment with coal (5 wt % urea), showing reactor stability.

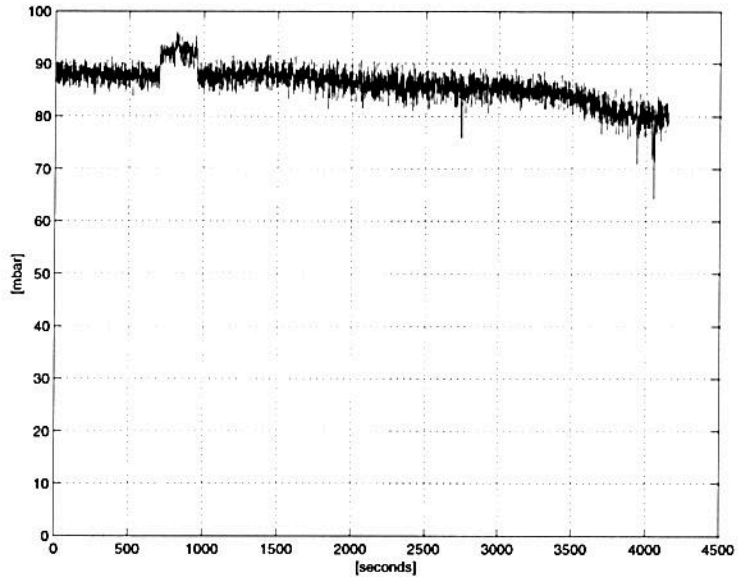

Figure H.11: Differential pressure development in the riser during start-up of an advanced reburning experiment with coal (5 wt % urea), showing reactor stability.

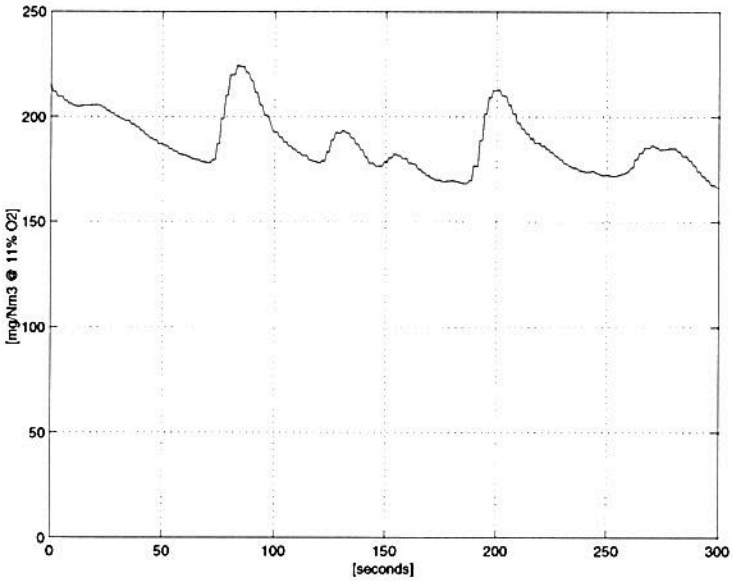

Figure H.12: Emissions of CO during an advanced reburning experiment with coal (5 wt % urea), showing reactor stability after start-up.

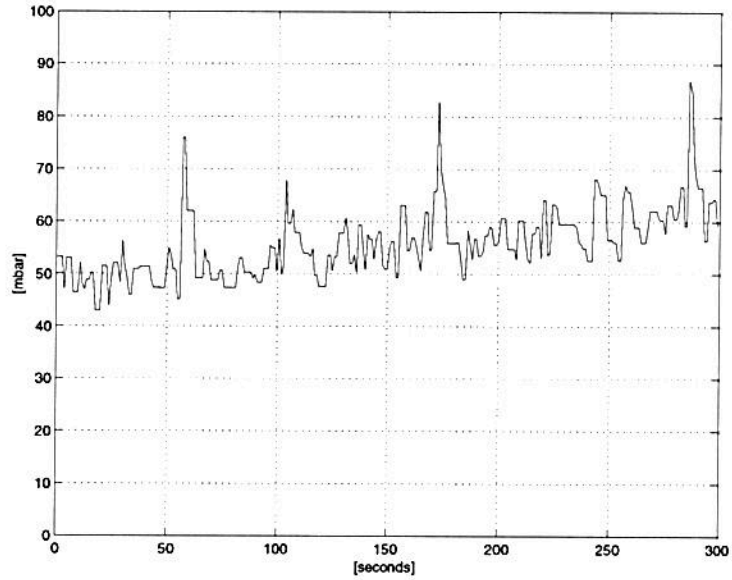

Figure H.13: Pressure development in BFB during an advanced reburning experiment with coal (5 wt % urea), showing reactor stability after start-up.

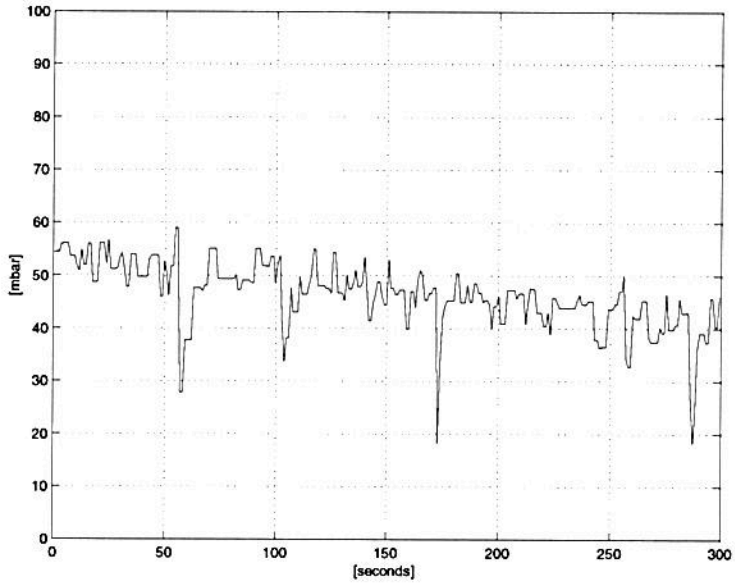

Figure H.14: Differential pressure development in the riser during accomplishment of an advanced reburning experiment with coal (5 wt % urea), showing reactor stability after start-up.

Appendix I

N_2O emissions

Table I.1: Parallel batch analysis of N2O with a gas chromatograph compared to continous measurements with the Uras 14 NDIR analyser.

Experiment	**NDIR**	**GC**
	$mg/Nm^3@11\%O_2$	$mg/Nm^3@11\%O_2$
Animal meal	59.5	28.3
Animal meal/Char coal	58	20.2

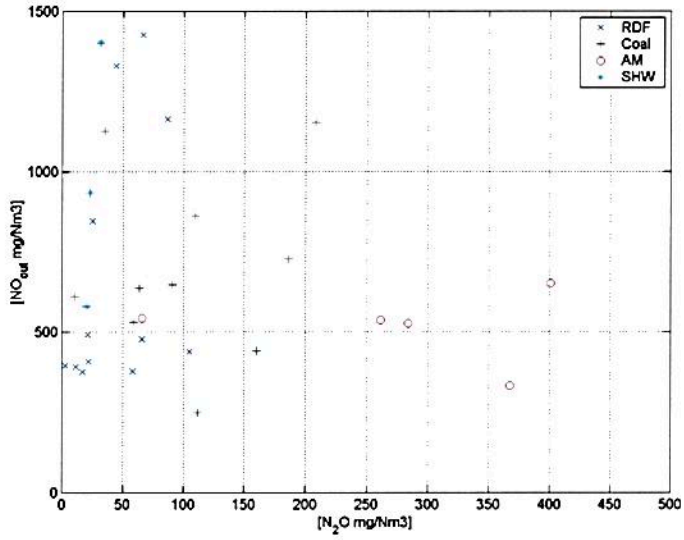

Figure I.1: Emissions of NO versus N_2O during reburning, advanced reburning and experiments without circulating mass.

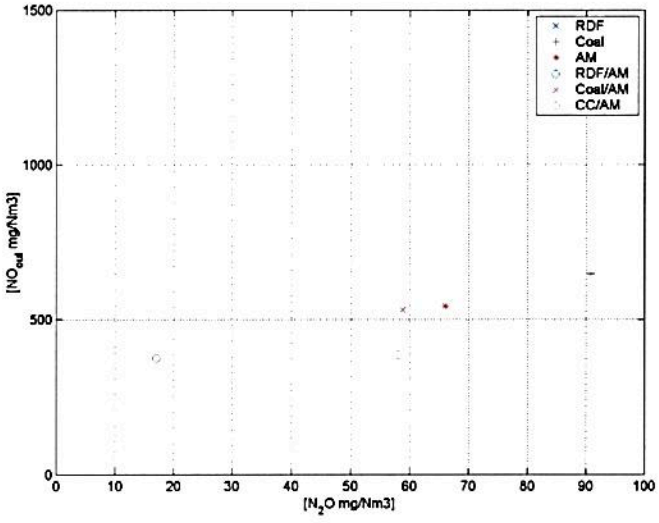

Figure I.2: Emission of NO versus N_2O during reburning experiments with RDF, coal, AM, RDF/AM, coal/AM and CC/AM.

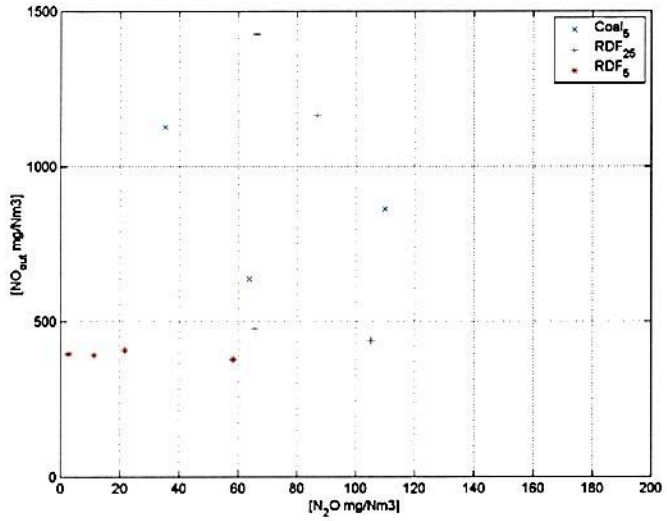

Figure I.3: Emission of NO versus N_2O during advanced reburning experiments with 25 wt % urea and RDF; 5 wt % urea and RDF; 5 wt % urea and coal.

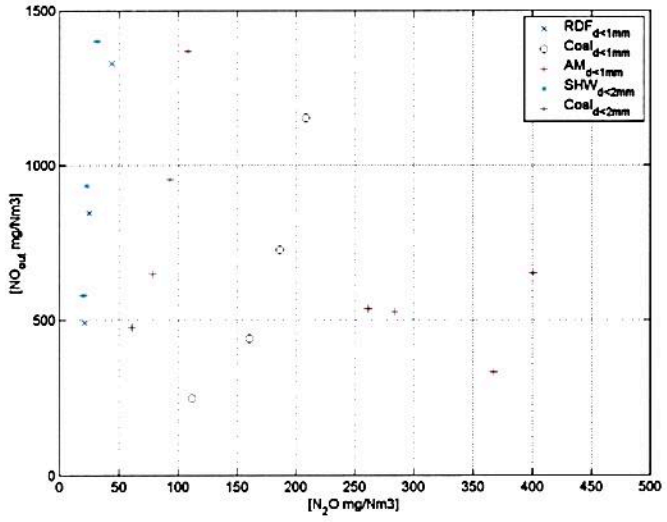

Figure I.4: Emission of NO versus N_2O during experiments without circulating mass. Exepriments with $RDF_{d<1mm}$, $Coal_{d<1mm}$, $AM_{d<1mm}$, $SHW_{d<2mm}$, $Coal_{d<2mm}$.

Appendix J

SO_2 emissions

J.1 Sulphur mass balance

A mass balance on sulphur is carried out based on the results from the advanced reburning experiments with coal. Table J.1 shows the calculated sulphur into and out of the CFBC reactor. Note that only 50 % of the circulating mass is raw meal. About 65 % of the sulphur balance is fulfilled.

An accumulation of sulphur in the CFBC reactor during the experiments was observed. The color of the accumulated circulating mass was brown/yellow and the amount was varying between 1 to 5 kg. The missing sulphur may be due to inaccuracies in the:

- SO_3 analysis of the raw meal,
- SO_3 analysis of the calcined meal,
- S analysis of the coal,
- mass flow of coal,
- mass flow of circulating mass,
- SO_2 analysis of the gas and
- accumulation of sulphur in the CFBC reactor.

However, sulphur in the gas amounts to less than 1 % of the sulphur balance. Taking into consideration the uncertainty in the mass balance (accumulation), it is chosen not to emphasize the SO_2 emissions in this thesis.

Table J.1: Presents a sulphur mass balance of the CFBC reactor during advanced reburing experiments with coal.

Sulphur in (g/h)		**Sulphur out (g/h)**	
Coal	46.60	Gas	0.44
Circulating mass	34.80	Circulating mass	52.20
Sum	*81.40*	*Sum*	*52.64*

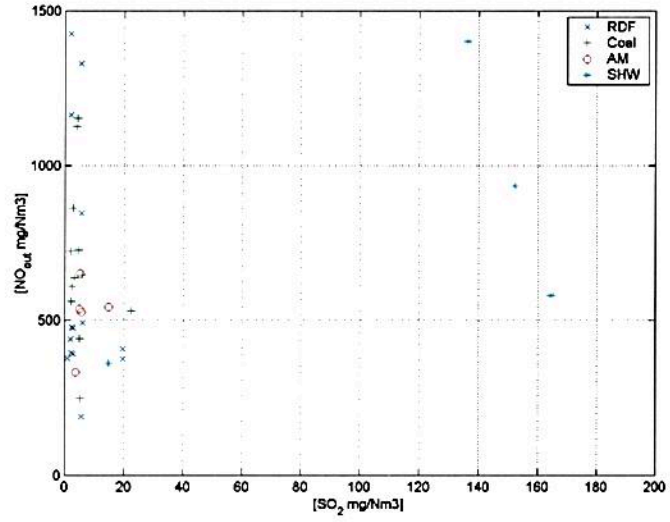

Figure J.1: Emission of SO_2 with respect to NO during reburning, advanced reburning and experiments without circulating mass.

Appendix K

NO_2 emissions

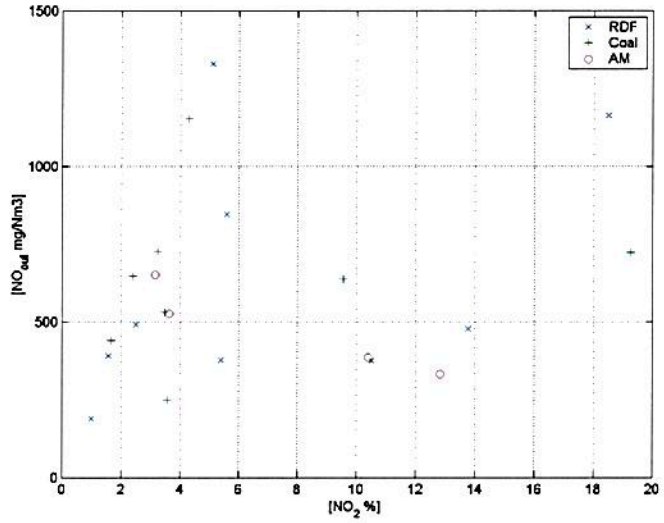

Figure K.1: Emissions of NO versus NO_2 during reburning, advanced reburning and experiments without circulating mass.

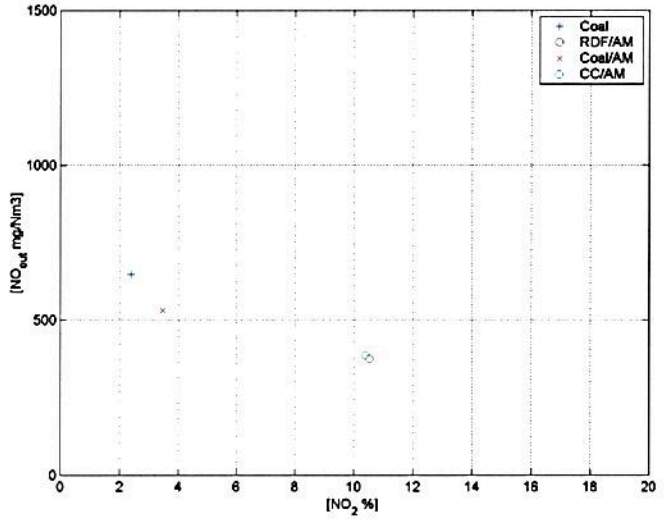

Figure K.2: Emissions of NO versus NO_2 during reburning experiments with RDF, coal, AM, RDF/AM, coal/AM and CC/AM.

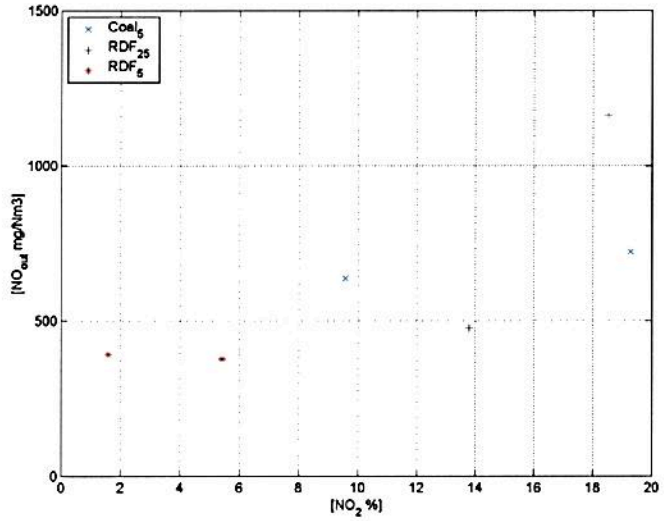

Figure K.3: Emissions of NO versus NO_2 during advanced reburning with 5 wt % urea and coal; 25 wt % urea and RDF; 5 wt % urea and RDF.

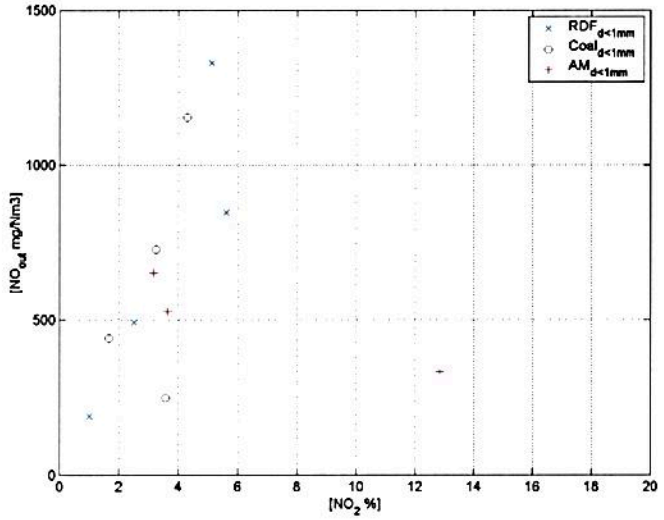

Figure K.4: Emissions of NO versus NO_2 during experiments without circulating mass with RDF, coal and animal meal (AM).

Appendix L

CO and TOC emissions

L.1 Reburning

The competition for the OH radical between Equation 2.30 and 2.55 is probably the reason for the increased CO and TOC emissions of up to 5 and 15 times, respectively, during combustion of AM.

L.2 Advanced reburning

The CO and TOC emissions show two almost vertical groupings with RDF and coal. The vertical groupings indicate that coal emits a higher amount of CO than RDF does, and the other way around for the TOC emissions, see Figure L.5 and L.6. There seems to be no correlation between the level of NO and the CO or TOC emissions. The deviation in the CO and TOC emissions in one of the RDF experiments is most likely due to a lower average temperature (about 850 $°C$) in the riser compared to the rest of the experiments (about 900$°C$).

L.3 Combustion without circulating mass

The CO and TOC emissions show three distinct vertical groupings with RDF, SHW and coal. The vertical groupings show almost no influence of the level of NO on the CO emissions, see Figure L.7. In contrast, AM has, for both particle sizes, CO emissions with a random development regarding the level of NO. From Figure L.8 it can be seen that $AM_{d<1}$ has an almost horizontal development of the TOC emissions and no distinct trend with increasing NO.

It is important to emphasize that $coal_{d<1}$ emits more than twice the amount of CO compared to $RDF_{d<1}$ and $AM_{d<1}$ at similar conditions. In contrast, $AM_{d<2}$ emit a larger amount of CO compared to $SHW_{d<2}$ and $coal_{d<2}$. A comparison of $coal_{d<2mm}$ and $coal_{d<1mm}$ shows higher CO emissions with increased particle size.

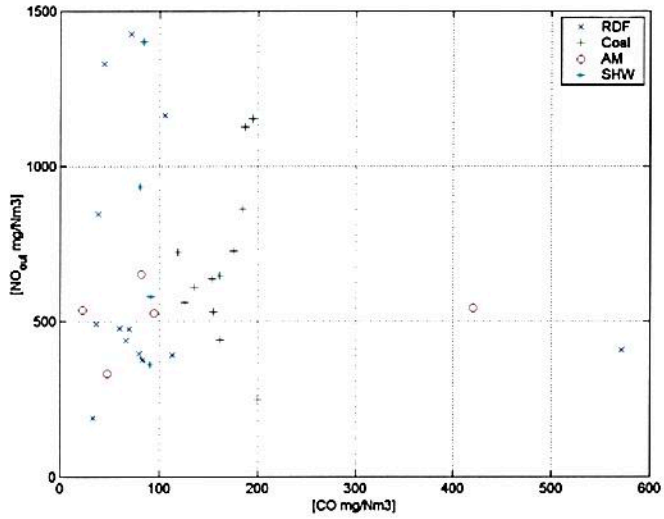

Figure L.1: Emissions of NO versus CO during reburning, advanced reburning and experiments without circulating mass.

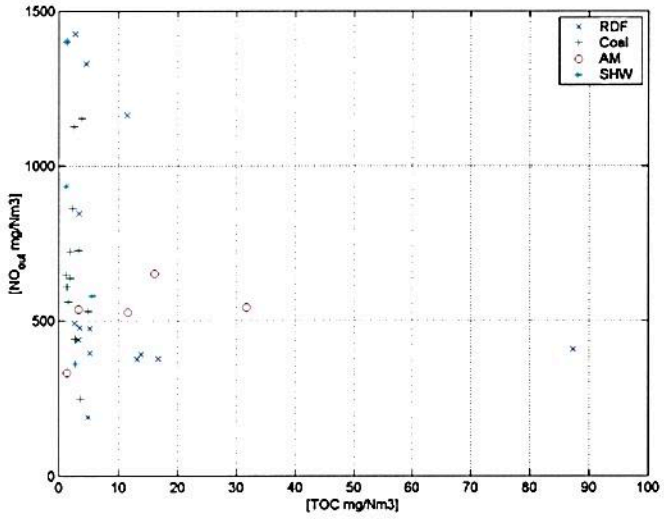

Figure L.2: Emissions of NO versus TOC during reburning, advanced reburning and experiments without circulating mass.

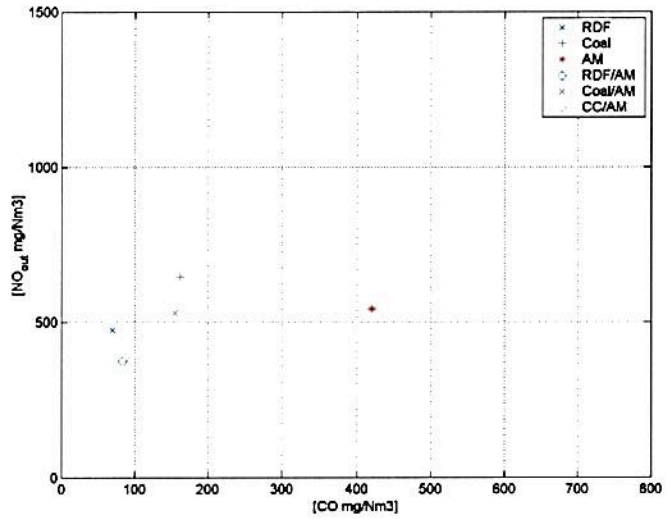

Figure L.3: Emission of CO with respect to NO during reburning experiments with RDF, coal, AM, RDF/AM, coal/AM and CC/AM.

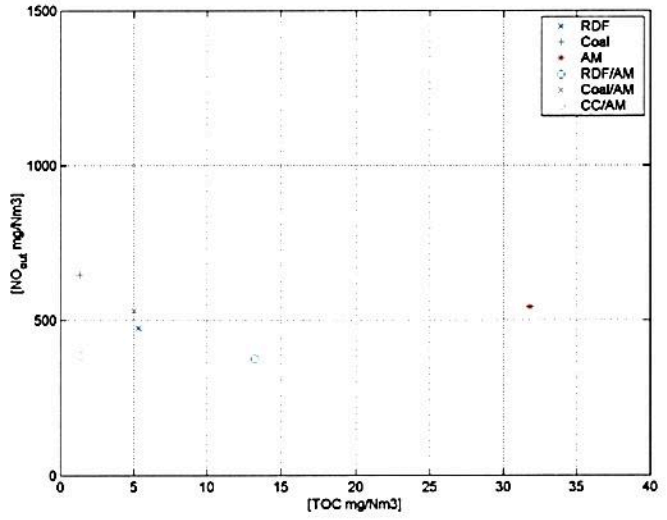

Figure L.4: Emission of TOC with respect to NO during reburning experiments with RDF, coal, AM, RDF/AM, coal/AM and CC/AM.

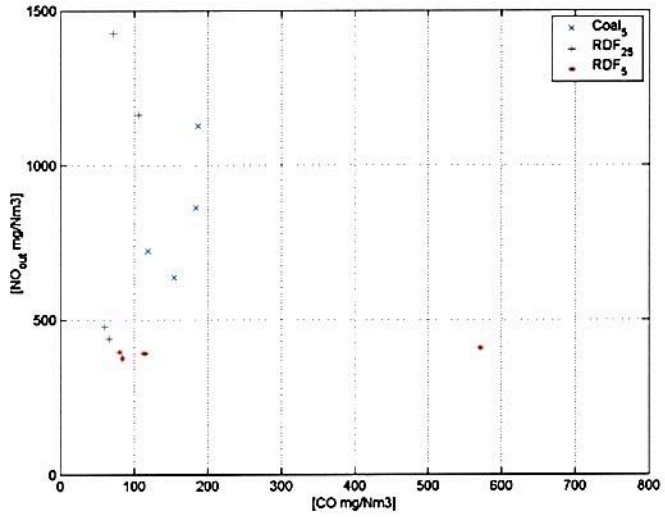

Figure L.5: Emissions of NO versus CO during advanced reburning experiments with 25 wt % urea and RDF; 5 wt % urea and RDF; 5 wt % urea and coal.

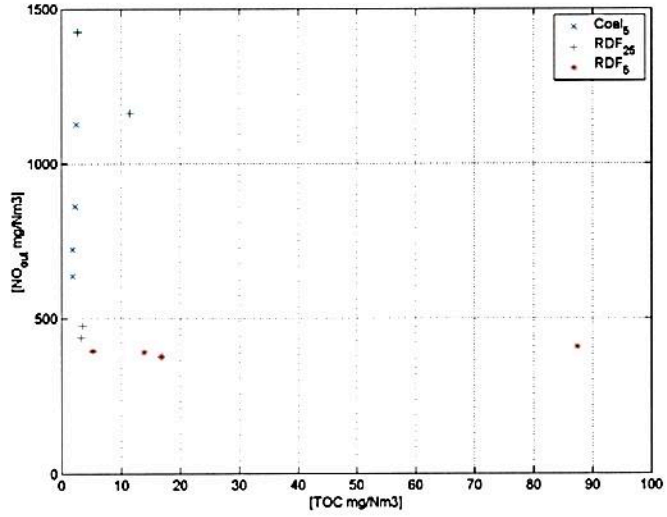

Figure L.6: Emission of NO versus TOC during advanced reburning experiments with 25 wt % urea and RDF; 5 wt % urea and RDF; 5 wt % urea and coal.

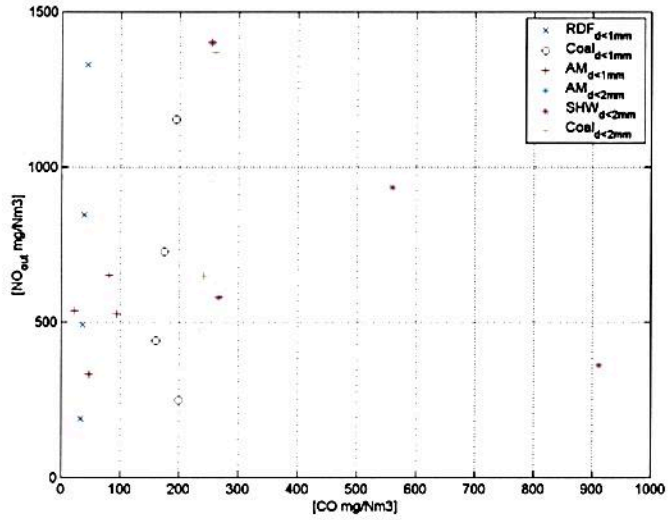

Figure L.7: Emissions of NO versus CO during experiments without circulating mass. Experiments with $\mathrm{RDF}_{d<1mm}$, $\mathrm{Coal}_{d<1mm}$, $\mathrm{AM}_{d<1mm}$, $\mathrm{SHW}_{d<2mm}$.

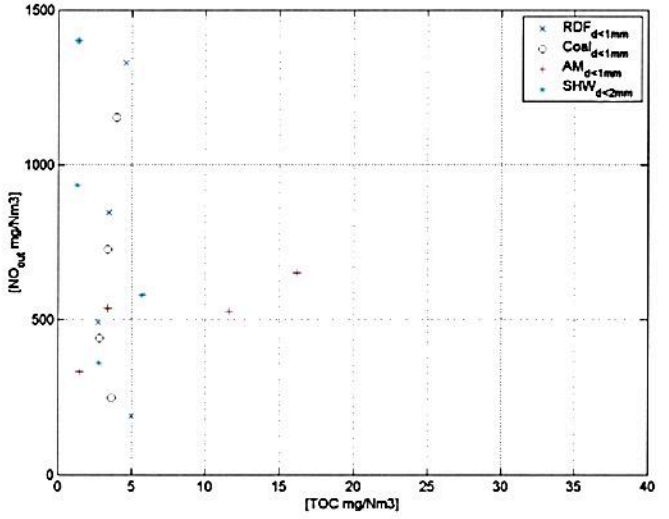

Figure L.8: Emission of NO versus TOC during experiments without circulating mass. Experiments with $\mathrm{RDF}_{d<1mm}$, $\mathrm{Coal}_{d<1mm}$, $\mathrm{AM}_{d<1mm}$, $\mathrm{SHW}_{d<2mm}$.

Appendix M

Temperature profiles

M.1 Reburning

Figure M.1 shows the temperature profile during the reburning experiments. The temperature nodes are evenly distributed with 0.4 m from the diaphragm (node 1) to the reactor outlet (node 10), see Figure 4.1 and (Axelsen 2001*a*). The temperature drop at node 4 is due to the secondary air inlet, which has a temperature of about 20 $°C$. Figure M.1 show a gentler development from node 6 to 10 for coal and coal/AM than for the remaining fuels. This can be explained with a higher ratio of fixed carbon to volatiles for coal and coal/AM, see Table 4.4 and 4.5.

M.2 Advanced reburning

Figure M.2 shows the temperature profile during the advanced reburning experiments. There is a distinct difference between combustion of coal and RDF. RDF shows a gentle downward slope from node 6, in contrast to coal combustion. This can be explained with a higher ratio of fixed carbon to volatiles for coal, see Table 4.4. The profiles of the two RDF experiments demonstrate reproducibility.

M.3 Combustion without circulating mass

Figure M.3 shows the temperature profile during the experiments without circulating mass. The fixed carbon to volatiles ratios are almost similar for RDF, SHW and AM in contrast to coal, see Table 4.4. Therefore, it is as expected that $AM_{d<1}$, $SHW_{d<2}$ and $RDF_{d<1}$ have corresponding maximas, see Figure M.3. Combustion of $coal_{d<2mm}$, compared to $coal_{d<1mm}$, shows a slower burnout, with a higher temperature in the upper part of the reactor, as expected.

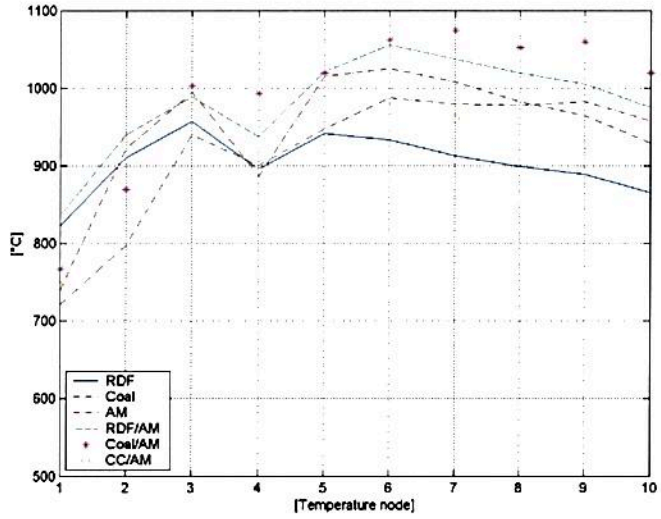

Figure M.1: Temperature profile during reburning experiments with RDF, coal, AM, RDF/AM, coal/AM and CC/AM. Temperature nodes 1 (diaphragm) to 10 (outlet) have an equal spacing of 0.4 m.

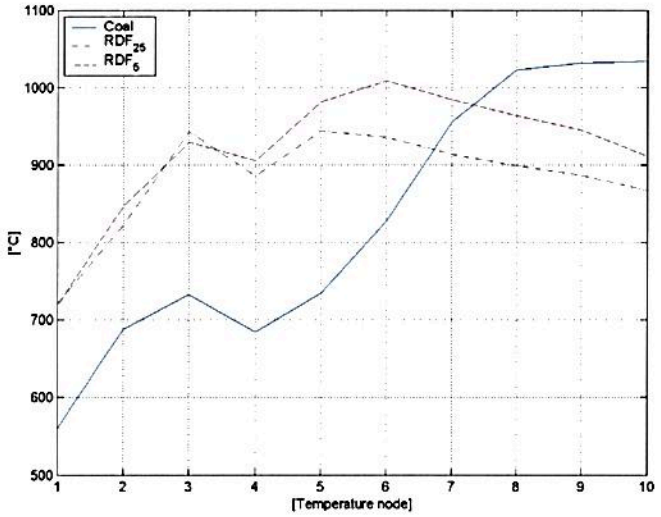

Figure M.2: Temperature profile during advanced reburning experiments with 25 wt % urea and RDF; 5 wt % urea and RDF; 5 wt % urea and coal. Temperature nodes 1 (diaphragm) to 10 (outlet) have an equal spacing of 0.4 m.

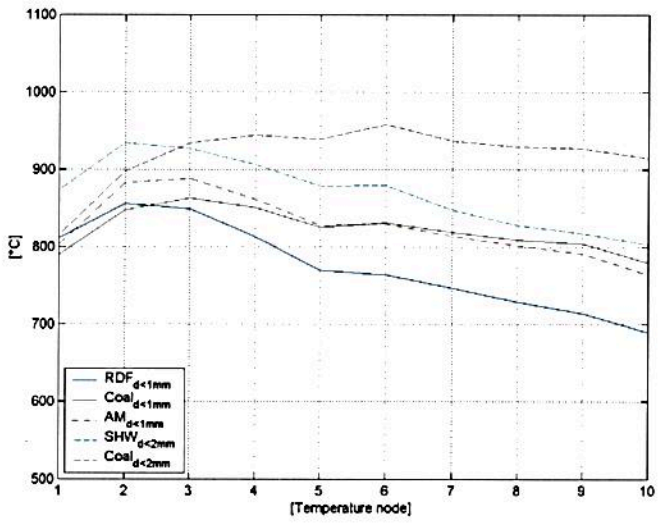

Figure M.3: Temperature profile during experiments without circulating mass with RDF, coal, AM and SHW. Temperature nodes 1 (diaphragm) to 10 (outlet) have an equal spacing of 0.4 m.

Part IV

Appendixes - Flow calculations

Appendix N

Euler-Euler approach

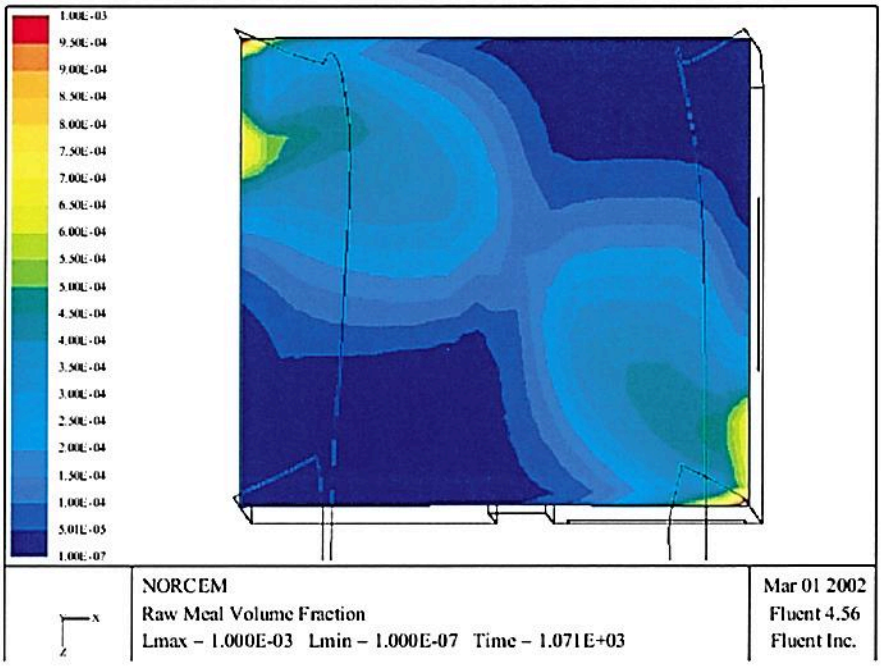

Figure N.1: Raw meal volume fraction during Euler-Euler simulations. The cross-section refers to sampling point 1 and 2 in Figure 3.2.

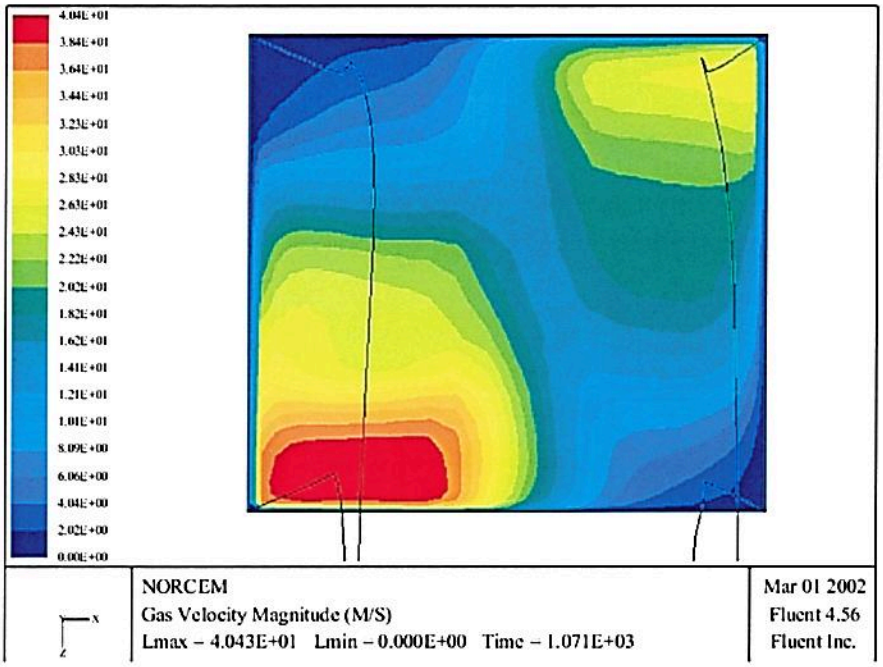

Figure N.2: Gas velocity during Euler-Euler simulations. The cross-section refers to sampling point 1 and 2 in Figure 3.2.

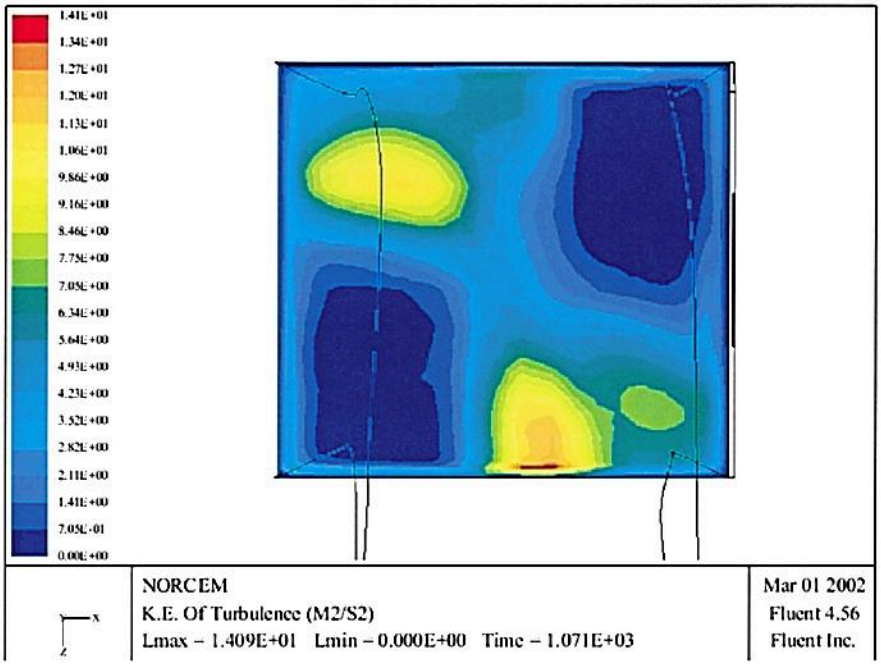

Figure N.3: Kinetic energy of turbulence during Euler-Euler simulations. The cross-section refers to sampling point 1 and 2 in Figure 3.2.

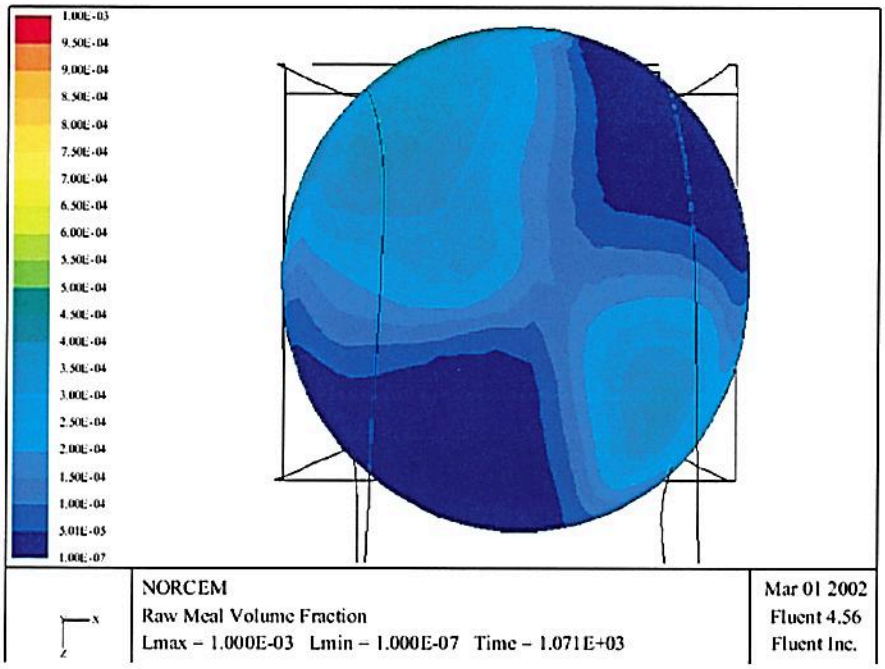

Figure N.4: Raw meal volume fraction during Euler-Euler simulations. The cross-section refers to sampling point 3 and 6 in Figure 3.2.

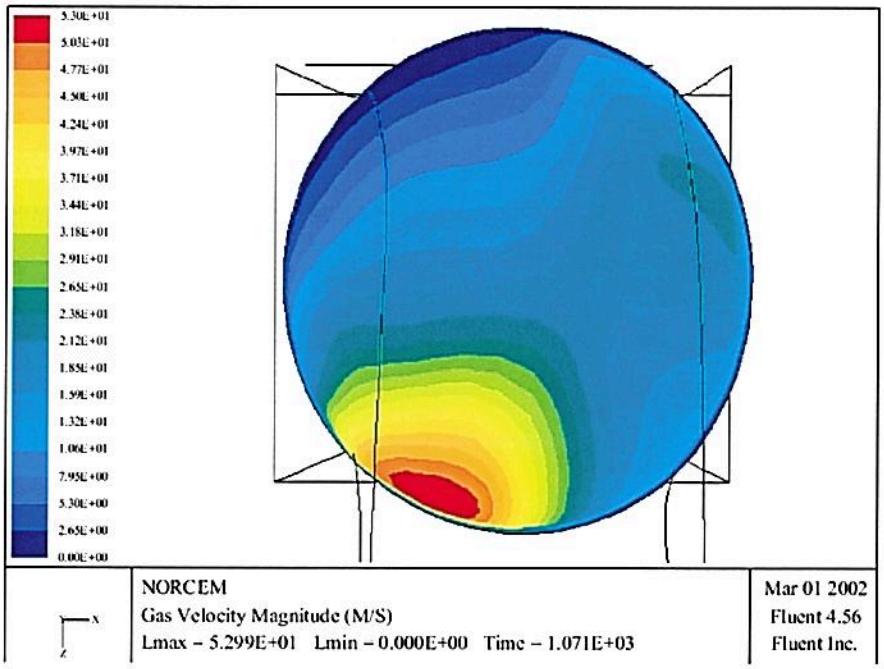

Figure N.5: Gas velocity during Euler-Euler simulations. The cross-section refers to sampling point 3 to 6 in Figure 3.2.

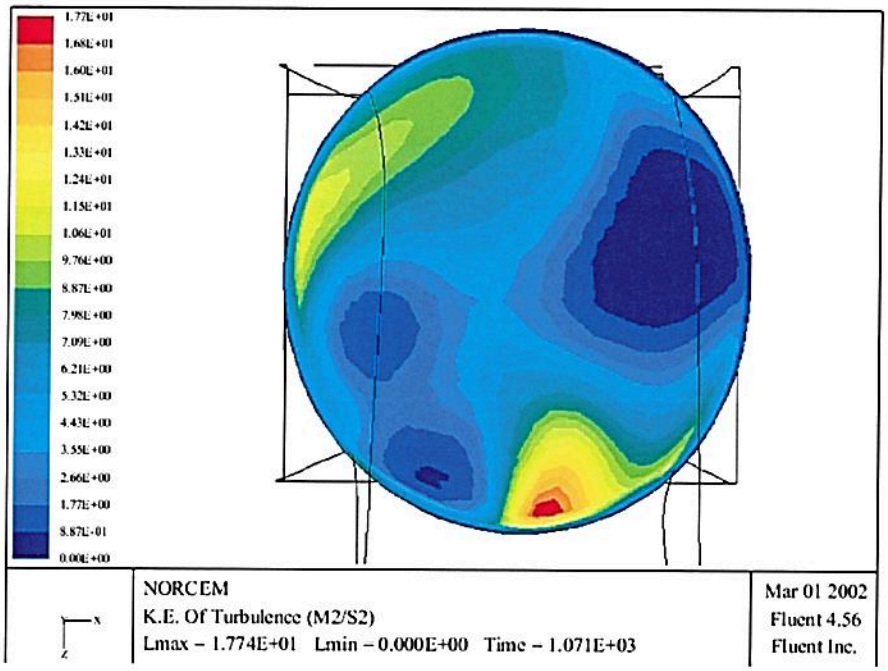

Figure N.6: Kinetic energy of turbulence during Euler-Euler simulations. The cross-section refers to sampling point 3 to 6 in Figure 3.2.

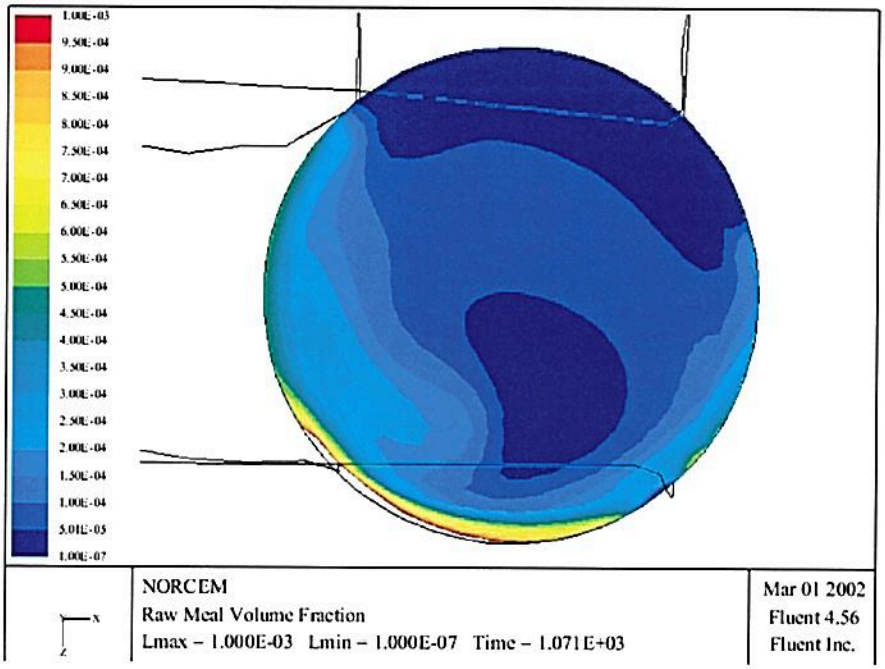

Figure N.7: Raw meal volume fraction during Euler-Euler simulations. The cross-section refers to sampling point 8 and 11 in Figure 3.2.

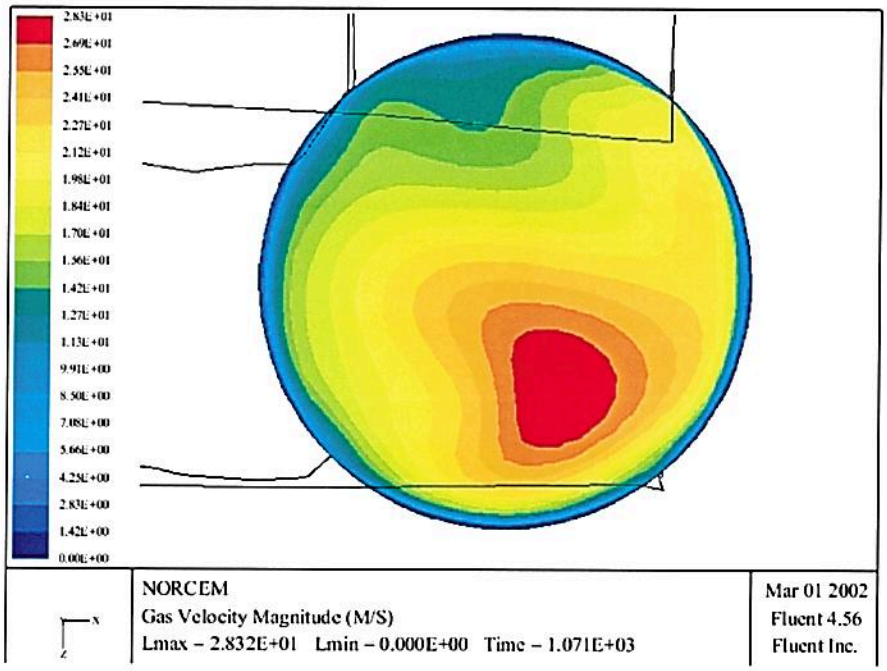

Figure N.8: Gas velocity during Euler-Euler simulations. The cross-section refers to sampling point 8 to 11 in Figure 3.2.

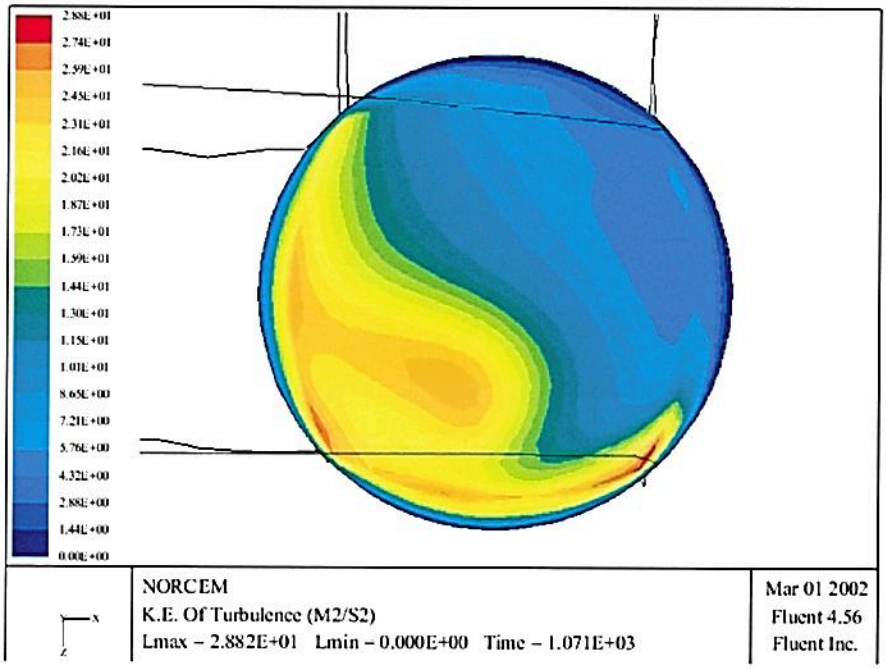

Figure N.9: Kinetic energy of turbulence during Euler-Euler simulations. The cross-section refers to sampling point 8 to 11 in Figure 3.2.

Bibliography

Axelsen, E. P. (1998), Forbrenningsforsøk - NOx reduksjon i sementovn, Master's thesis, Høgskolen i Telemark.

Axelsen, E. P. (2001*a*), Laboratory circulating fluidizing bed combustor - design and preliminary experiments - comparative study to the precalciner at Norcem Brevik, Technical report, Scancem Int. ANS.

Axelsen, E. P. (2001*b*), Utilisation of alternative fuels in the precalciner at Norcem Brevik - NOx reduction with additional effort to reduce the CO emissions, Technical report, Scancem Int. ANS.

Bai, D.-R., Jin, Y., Yu, Z.-Q. & Zhu, J.-X. (1992), 'The axial distribution of the cross-sectionally averaged voidage in fast fluidized beds', *Powder Technology* .

Bai, D., Yi, J., Jin, Y. & Yu, Z. (1992), 'Residence time distributions of gas and solids in a circulating fluidized bed', *Fluidization - Engeineering Foundation Conference - 7th* pp. 195–202.

Bartok, W. & Sarofim, A. F. (1991), *Fossil Fuel Combustion A Source Book*, John Wiley Sons, Inc.

Belot, C., Goffe, D., Grouset, D., Bertrand, C., Homassel, B. & Philippe, J. L. (1993), 'Optimization of a cement plant preheating tower, equipped with a precalciner, burning pulverized coal', *Combustion Science and Technology* **93**, 9–25.

Berruti, F., Chaouki, J., Godfroy, L., Pugsley, T. S. & Patience, G. S. (1995), 'Hydrodynamics of circulating fluidized bed risers: A review', *The Canadian Journal of Chemical Engineering* **73**, 579–602.

Bews, I. M., Hayhurst, A. N., Richardson, S. M. & Taylor, S. G. (2001), 'The order, Arrhenius parameters, and mechanism of the reaction between gaseous oxygen and solid carbon', *Combustion and Flame* **124**, 231–245.

Bi, H. T., Grace, J. R. & Zhu, J.-X. (1993), 'Types of choking in vertical pneumatic systems', *Int. J. Multiphase Flow* **19**, 1077–1073.

Bierl, T. W. & Gajdos, L. T. (1982), Phenomenological modelling of reaction experiments in risers, Technical Report Final Report, DOE/MC-14249-1149, Environmental Research and Technology, Inc.

Bjerkebo, N. (2000), Karakterisering av foredlet biobrensel (in Norwegian), Master's thesis, Telemark University College, Norway.

Bjerketvedt, D. & Høidalen, Ø. (1994), NOx reduction by staged combustion in precalsiner kilns. A preliminary study, Technical report, Norcem FoU.

Bowman, C. T. (1992), 'Control of combustion-generated nitrogen oxide emissions: Technology driven by regulation', *Twenty-Fourth Symposium (International) on Combustion/The Combustion Institute* pp. 859–879.

Broll, A. C. (2000), Utslippsmålinger fra punktvarmekilder, Master's thesis, Høgskolen i Telemark.

Brooks, C. L., Blankenship, J. E. & Daugherty, K. E. (1992), 'Co-firing of RDF in cement kilns', *International Cement Review* pp. 54–57.

Brouwer, J., Heap, M. P., Pershing, D. W. & Smith, P. J. (1996), 'A model for prediction of selective noncatalytic reduction of nitrogen oxides by ammonia, urea and cyanuric acid with mixing limitations in the presence of CO', *Twenty-Sixth Symposium (International) on Combustion / The Combustion Institute* pp. 2117–2124.

Carrasco, F., Bredin, N., Gningue, Y. & Heitz, M. (1998), 'Environmental impact of the energy recovery of scrap tires in a cement kiln', *Environmental Technology* **19**, 461–474.

CBR (2001), Influence of the P2O5 content in clinker on the performances of cement, Technical Report February - June, CBR Cement, Belgium.

Chen, S. L., Cole, J. A., Heap, M. P. & Kramlich, J. C. (1988), 'Advanced NOx reduction processed using -NH and -CN compounds in conjunction with staged air addition', *Twenty-Second Symposium (International) on Combustion / The Combustion Institute* pp. 1135–1145.

Chen, S. L., Heap, M. P., Pershing, D. W. & Martin, G. B. (1982), 'Influence of coal composition on the fate of volatile and char nitrogen during combustion', *19th. Symposium (International) on Combustion. The Combustion Institute.* p. 1271.

Chen, S. L., Kramlich, J. C., Seeker, W. R. & Pershing, D. W. (1989), 'Optimization of reburning for advanced NOx control on coal-fired boilers', *Air & Waste Management Association* **39**, 1375–1379.

Chen, W., Smoot, L. D., Fletcher, T. H. & Boardman, R. D. (1996), 'A computational method for determining global fuel-NO rate expressions', *Energy & Fuels* **10**, 1036–1045.

Chen, W., Smoot, L. D., Hill, S. C. & Fletcher, T. H. (1996), 'Global rate expression for nitric oxide reburning', *Energy & Fuels* **10**, 1046–1052.

Chomiak, J. (2000), *Turbulent Reacting Flows*, Department of Thermo and Fluid Dynamics, Chalmers University of Technology, Gotenborg, Sweden.

de Silva, S. R. (2001), *Introduction to Powder Technology (in Norwegian)*, Tel Tek, Kjølnes Ring, 3918 Porsgrunn, Norway.

De Soete, G. G. (1990), 'Heterogeneous N2O and NO formation from bound nitrogen atoms during coal char combustion', *Twenty-Third Symposium (International) on Combustion / The Combustion Institute* pp. 1257–1264.

De Soete, G. G., Croiset, E. & Richard, J.-R. (1999), 'Heterogeneous formation of nitrous oxide from char-bound nitrogen', *Combustion and Flame* **117**, 140–154.

Desroches-Ducarne, E., Dolignier, J. C., Marty, E., Martin, G. & Delfosse, L. (1998), 'Modelling of gaseous pollutants emissions in circulating fluidized bed combustion of municipal refuse', *Fuel* **77**, 1399–1410.

Digest, W. (2000), 'AEP to test phosphor based NOx reduction system', *World Digest, Modern Power Systems* p. 11.

Diguet, S. (1996), Contribution á l'etude de la déshydratation du carbonate de sodium monohydrate en lit fluidisé dense et mise en oeuvre en lit fluidisé circulant: étude experimentale et modélisation, PhD thesis, L'Institut National Polytechnique de Toulouse, France.

Ding, J. & Gidaspow, D. (1990), 'A bubbling fluidization model using kinetic theory of granular flow', *AIChE Journal* pp. 523–538.

Dusome, D. (1995), 'Staged combustion for NOx control at the calaveras tehachapi plant', *World Cement* pp. 2–8.

Elgobashi, S. E. (1991), 'Particle-laden turbulent flows: Direct simulation and closure models', *Applied Scientific Research* **48**, 301–314.

European Commision, D.-G. J. (1999), Integrated pollution prevention and control (IPPC), Technical report, European Commision, Directorate-General, Joint Research Center.

Feria, J., Loland, R., Pleym, T., Thoresen, G. I. & Ulltang, T. (1999), Forbrenning av alternative brensler i fluidisert gassfase reaktor, Technical Report 1, Høgskolen i Telemark.

FLUENT, I. (1998), *FLUENT 4.5 Update Manual*, Inc. FLUENT.

FLUENT, I. (2001), *FLUENT 6 Users Guide Release 6.*, december edn, Fluent Inc.

Fogler, S. H. (1992), *Elements of Chemical Reaction Engineering*, Prentice-Hall International, Inc., ISBN 0-13-253220-4.

Gajewski, S. & Hoenig, V. (1999), 'Influence of pulverized coal fineness on the formation of NOx in rotary kilns in the cement industry', *ZKG International* **1**, 44–53.

Geankoplis, C. J. (1993), *Transport Process and Unit Opreations. Third Edition*, Prentice-Hall International, Inc.

Gidaspow, D. (1990), *Multiphase Flow and Fluidization*, Academic Press, ISBN 0-12-282470-9.

Giddings, D., Eastwick, C. N., Pickering, S. J. & Simmons, K. (2000), 'Computational fluid dynamics applied to a cement precalciner', *Proc. Instn. Mech. Engrs* **214 Part A**, 269–280.

Giddings, D., Pickering, S. J., Simmons, K. & Eastwick, C. N. (2000), 'Using CFD to investigate combustion in a cement manufacturing process', *IMechE Journal of Power and Energy* .

Giugliano, M., Cernuschi, S., Ghezzi, U. & Grosso, M. (1999), 'Experimental evaluation of waste tires utilization in cement kilns', *Journal of Air & Waste Management Association* **49**, 1405–1414.

Glassman, I. (1996), *Combustion, Third Edition*, Academic Press.

Goel, S., Zhang, B. & Sarofim, A. F. (1996), 'NO and N2O formation during char combustion: Is it HCN or surface attached nitrogen?', *Combustion and Flame* **104**, 213–217.

Gokulakrishnan, P. & Lawrence, A. D. (1999), 'An experimental study of the inhibiting effect of chlorine in a fluidized bed combustor', *Combustion and Flame* **116**, 640–652.

Gore, R. A. & Crowe, C. T. (1989), 'Effect of particle size on modulating turbulent intensity', *Int. J. Multiphase Flow* **15**, 279–285.

Grace, J. R., Avidan, A. A. & Knowlton, T. M. (1997), *Circulating Fluidized Beds*, Chapman & Hall.

Greco, C. (2000), 'A burning advantage', *World Cement* pp. 67–72.

Gy, P. (1998), *Sampling for Analytical Purposes*, John Wiley & Sons Ltd, Baffins Lane, Chichester, West Sussex PO19 1UD, England.

Haider, A. & Levenspiel, O. (1989), 'Drag coefficient and terminal velocity of spherical and nonspherical particles', *Powder Technology* **58 (1)**, 63–70.

Hämäläinen, J. (1995), Effect of Fuel Composition on the Conversion of Fuel-N to Nitrogen Oxides in the Combustion of Small Single Particles, PhD thesis, Department of Chemistry, University of Jyväskylä.

Hansen, P. F. B., Dam-Johansen, K., Johnsson, J. E. & Hulgaard, T. (1992), 'Catalytic reduction of NO and N2O on limestone during sulfur capture under fluidized bed combustion conditions', *Chem. Eng. Sci.* **47**, 2419.

Harpe, V. T. (1998), 'Modified NOxOUT and NOx control', *World Cement* pp. 28–33.

Harting, A. (2000), 'Alternative fuels at phoenix', *European Cement Magazine* pp. 12–14.

Hayhurst, A. N. & Parmar, M. S. (1998), 'Does solid carbon burn in oxygen to give the gaseous intermediate CO or produce CO2 directly? Some experiments in a hot bed of sand fluidized by air', *Chemical Engineering Science* **53**, 427–438.

He, Y. & Rudolph, V. (1995), 'Gas-solids flow in the riser of a circulating fluidized bed', *Chemical Engineering Science* **50**, 3443–3453.

Helmreich, C. (2000), 'Innovative burning', *International Cement Review* pp. 53–55.

Helmreich, C. (2002), 'In the firing line', *World Cement* **April**, 66–69.

Herat, S. (1997), 'Protecting the environment from waste disposal: The cement kiln option', *Environment Protection Engineering* **23**, 25–35.

Hill, S. & Smoot, L. D. (2000), 'Modelling of nitrogen oxides formation and destruction in combustion systems', *Progress in Energy and Combustion Science* **26**, 417–458.

Ho, W.-P., Barat, R. B. & Bozzelli, J. W. (1992), 'Thermal reactions of CH2Cl2 in H2/O2 mixtures. implications for chlorine inhibition of CO conversion to CO2', *The Combustion Institute* .

Hock, U. (2001), 'The burning alternative', *International Cement Review* **January**, 37 – 38.

Hoenig, V., Høidalen, Ø. & Bergamaschi, C. (1997), NOx emissions from cement manufacture and evaluation of various possibilities for NOx reduction in the cement industry, Technical Report EV5V-CT94-551, Forschungsinstitut der Zementindustrie, Düsseldorf Deutschland.

Hoenig, V., Hoppe, H. & Bodendiek, N. (2001*a*), 'Options and limitations in NOx abatement in the cement industry, part 1', *ZKG International* **54**, 165–171.

Hoenig, V., Hoppe, H. & Bodendiek, N. (2001*b*), 'Options and limitations in NOx abatement in the cement industry, part 2', *ZKG International* **54**, 356–361.

Høidalen, Ø. (1990), 'Modernisation and increase of capacity of rotary kiln 6 in the dalen plant of norcem A/S', *ZKG International* (3).

Hulgaard, T. & Dam-Johansen, K. (1992), 'Nitrous oxide sampling, analysis, and emission measurement form various combustion systems', *Environmental Progress* **11**, 302–309.

Hundebøl, S. & Kumar, S. (1987), 'Retention time of particles in calciners of the cement industry', *Zement - Kalk - Gips* pp. 422–425.

Inverardi, M. (1993), Refuse derived fuel: A clever auxiliary fuel for cement kilns, *in* EniChem, ed., 'APC-PWMI Joint Meeting', ECP EniChem Polimeri.

Jeschar, R., Jennes, R., Kremer, H. & Kellerhof, T. (1999), 'Reducing NOx and CO emissions by burning plastics in the calciner of rotary cement kiln plant', *ZKG International* **52**(10), 534–549.

Jin, Y., Yu, Z.-Q., Qi, C.-M. & Bai, D.-R. (1988), 'The influence of exit structure on the axial distribution of voidage in fast fluidized bed', *Science and Technology* **Fluidization '88, (eds. M. Kwauk and D. Kunii)**, 165–173.

Johnsson, J. E. (1994), 'Formation and reduction of nitrogen oxides in fluidized-bed combustion.', *Fuel* **73**, 1398–1415.

Kaldeway, F. (1985), 'Successful handling of alternative fuels', *World Cement* pp. 344–346.

Kicherer, A., Spliethof, H., Maier, H. & Hein, K. R. G. (1994), 'The effect of different reburning fuels on NOx-reduction', *Fuel* **73**, 1443–1446.

Kilpinen, P. T. & Norstrom, T. N. (2000), 'New simplified rate equation for gas-phase CO oxidation at combustion', *Energy & Fuels* **14**, 1156–1160.

Kobayashi, H., Howard, J. B. & Sarofim, A. F. (1976), 'Coal devolatilization at high temperatures', *16th Symp. (Int'l.) on Combustion, The Combustion Inst., Cambridge, MA* pp. 15–20.

Kramlich, J. C. & Linak, W. P. (1994), 'Nitrous oxide behaviour in the atmosphere, and in combustion and industrial systems', *Progress in energy and combustion science* **20**, 149–202.

Kristensen, P. G., Glarborg, P. & Dam-Johansen, K. (1996), 'Nitrogen chemistry during burnout in fuel-staged combustion', *Combust. Flame* **107**, 211–222.

Kruse, M., Schoenfelder, H. & Werther, J. (1995), 'A two-dimensional model for gas mixing in the upper dilute zone of a circulating fluidized bed', *The Canadian Journal of Chemical Engineering* **73**, 620–634.

Kunii, D. & Levenspiel, O. (1991), *Fluidization Engineering*, Butterworth-Heinemann.

Lidal, R., Kleppe, A., Bjørnson, O. & Andreassen, T. F. (2000), Strømnings- og energibetrakninger i CFB-reaktor, Technical Report 1, Høgskolen i Telemark.

Liebl, P. & Gerger, W. (1993), 'Benefits and limitations when using secondary materials', *Zement-Kalk-Gips* **10**, 632–638.

Lim, K. S., Zhu, J. X. & Grace, J. R. (1995), 'Hydrodynamics of gas-solid fluidization', *Int. J. Multiphase Flow* **21**, 141–193.

Lockwood, F. C. & Ou, J. J. (1993), 'Review: Burning refuse-derived fuel in a rotary cement kiln', *Proc Instn Mech Engrs* **207**, 65–70.

Lyngfelt, A., Åmand, L.-E. & Leckner, B. (1998), 'Reversed air staging - a method for reduction of N2O emissions from fluidized bed combustion of coal', *Fuel* **77**, 953–959.

Malcus, S., Chaplin, G. & Pugsley, T. (2000), 'The hydrodynamics of the high-density bottom zone in a CFB riser analyzed by means of electrical capacitance tomography (ECT)', *Chemical Engineering Science* **55**, 4129–4138.

Maly, P. M., Zamansky, V. M., Ho, L. & Payne, R. (1999), 'Alternative fuel reburning', *Fuel* **78**, 327–334.

Mantus, E. K. (1992), All fired up, burning hazardous waste in cement kilns, Technical Report ISBN 0-9631944-1-0, Environment Toxicology International.

Mathiesen, V., Solberg, T., Arastoopour, H. & Hjertager, B. H. (1999), 'Experimental and computational study of multiphase gas / particle flow in a CFB riser', *AIChe Journal* **45**, 2503–2516.

Mathiesen, V., Solberg, T. & Hjertager, B. H. (2000), 'An experimental and computational study of multiphase flow behaviour in a circulating fluidized bed', *International Journal of Multiphase Flow* **26**, 387–419.

McCarthy, J. M., Moller, E. C., Ho, L., Cole, J. A., Kramlich, J. C. & Chen, S. L. (1988), An investigation to define the physical/chemical constraints which limit NOx emission reduction achieved by reburning, Technical report, Energy and Environmental Research Corporation.

Miller, A. J. & Bowman, C. (1989), 'Mechanism and modeling of nitrogen chemistry in combustion', *Prog. Energy Combust. Sci.* **15**, 287–338.

Neuffer, W. J. (1994), Alternative control techniques document - NOx emissions from cement manufacturing, Technical Report (919) 541-5435, U. S. Environmental Protection Agency, Emission Standards Divison.

Neumann, E. (1992), 'The energy alternatives - the substitution of fossil fuels in cement kilns', *Fuels & Environment* pp. 61–67.

Neumann, E., Duerr, M. & Kreft, W. (1990), 'The substitution of fossil fuels in cement kilns', *World Cement* pp. 80–88.

Norcem (1999), Miljørapport 1999, Technical report, Norcem AS.

Patankar, S. V. (1980), *Numerical Heat Transfer and Fluid Flow*, Taylor & Francis, ISBN 0-89116-522-3.

Peirano, E. & Leckner, B. (1998), 'Fundamentals of turbulent gas-solid flows applied to circulating fluidized bed combustion', *Prog. Energy Comb. Sci.* **24**, 259–296.

Piechatzek, T., Axelsen, E. P., Tokheim, L. A. & Bjerketvedt, D. (2000), Practical sampling of a continuous RDF fuel feed stream for quality assurance and process control, Technical report, Telemark Technological R&D Center.

Pitard, F., F. (1989*a*), *Pierre Gy's Sampling Theory and Sampling Practice. Volume I Heterogeneity and Sampling*, CRC Press, Inc., Boca Raton, Florida, USA.

Pitard, F. F. (1989*b*), *Pierre Gy's Sampling Theory and Sampling Practice. Volume II Sampling Correctness and Sampling Practice.*, CRC Press, Inc., Boca Raton, Florida, USA.

Rhodes, M. J., Zhou, S., Hirama, T. & Cheng, H. (1991), 'Effects on operating conditions on longitudinal solids mixing in a circulating fluidized bed reactor.', *AIChE Journal* **37**, 1450–1458.

Roesler, J. F., Yetter, R. A. & Dryer, F. L. (1992), 'Detailed kinetic modeling of moist CO oxidation inhibited by trace quantities of HCl', *Combust. Sci. and Tech.* **85**, 1–22.

Roesler, J. F., Yetter, R. A. & Dryer, F. L. (1995), 'Kinetic interactions of CO, NOx and HCl emissions in postcombustion gases', *Combustion and Flame* **100**, 495–504.

Rose, D., Adler, K. & Erpelding, R. (2001), 'NOx abatement with the SNCR process in kiln plants with staged combustion', *ZKG International* **54**, 362–371.

Rutar, T., Kramlich, J. C., Malte, P. C. & Glarborg, P. (1996), 'Nitrous oxide emissions control by reburning', *Combustion and Flame* **107**, 453–463.

Schäfer, S. & Hoenig, V. (2001), 'Operational factors affecting the mercury emissions from rotary kilns in the cement industry', *ZKG International* **54**, 591–599.

Scheuer, A. (1987), Theoretische und Betriebliche Untersuchungen Zur Bildung und Zum Abbau Von Stickstoffmonoxid in Cementdrehofenanlagen., PhD thesis, Verein Deuscher Zementwerke e. V. , Düsseldorf.

Schmidthals, H. & Rose, D. (2001), 'Untersuchungen zur thermishen nutzung stückiger sekundärbrennstoffe im zementbrennprozess', *ZKG-International* **54**, 180–188.

Schwab, J., Wilber, K., Riley, J. & Hawks, R. (1999), 'And SO2 can you', *International Cement Review* pp. 54–55.

Sharp, D. W. A. (1990), *Dictionary of Chemistry*, Penguin Books.

Shimizu, T., Sazawa, Y. & Adschiri, T. (1992), 'Conversion of char-bound nitrogen to nitric oxide during combustion', *Fuel* **71**, 361–365.

Skaarup Jensen, L., Jannerup, H. E., Glarborg, P., Jensen, A. & Dam-Johansen, K. (2000), 'Experimental investigation of NO from pulverized char combustion', *Proceedings of the Combustion Institute* **28**, 2271–2278.

Smart, J. P. & Jenkins, B. G. (1999), 'Studies on NOx emissions from an experimental rotary cement kiln fired with mono and multi-channel burners', *ZKG International* **52**, 420–432.

Smolders, K. & Baeyens, J. (2000), 'Overall solids movement and solids residence time distributrion in a CFB-riser', *Chemical Engineering Science* **55**, 4101–4116.

Smoot, L. D., Hill, S. C. & Xu, H. (1998), 'NOx control through reburning', *Prog. Energy Combust. Sci.* **24**, 385–402.

Stephan, D., Knöfel, D. & Härdtl, R. (2001), 'Examination of the influence of Cr, Ni and Zn on the manufacture and use of cement', *ZKG International* **54**, 335–346.

Steuch, V. H. E., Hille, J., Sun, W. H., Bisnett, M. J. & Kirk, D. W. (1996), 'Reduction of NOx emissions from a dry process preheater kiln through the use of the NOxOUT process', *ZKG International* **49**(1), 1–11.

Syverud, T., Thomassen, A. & Gautestad, T. (1994), 'Utilization of chipped car tyres for reducing NOx emissions in a precalciner kiln', *World Cement* .

Syverud, T., Thomassen, A. & Høidalen, Ø. (1994), 'Reducing NOx at the brevik cement works in norway - trails with stepped fuel supply to the calciner', *ZKG International* (3).

Taylor, N. & Isaksson, R. (2001), *Introduction to Kiln Technology - Improved Process Performance*, Scancem Research and Intec Services P/L.

Thorne, L. R., Branch, M. C., Chandler, D. W., Kee, R. J. & Miller, J. A. (1986), 21st symposium (international) combustion, The Combustion Institute, Pittsburgh, pp. 965–977.

Thyholdt, P. (2002), Limit of P2O5 in cement production at Norcem Brevik, Norway, Technical report, Norcem Brevik, Norway - Personal dialogue.

Tillmann, D. A. (1991), *The Combustion of Solid Fuels and Wastes*, Academic Press, Inc.

Tokheim, L.-A. (1999), The Impact of Staged Combustion on the Operation of a Precalciner Cement Kiln, PhD thesis, Norwegian University of Science and Technology.

Tokheim, L.-A. (2000*a*), Alternative fuels in Scancem's precalciner cement kilns, Technical Report 1, Norcem AS.

Tokheim, L.-A. (2000*b*), Calciner performance test at Norcem Brevik May/June 2000, Technical report, Norcem AS.

Tokheim, L.-A. & Bjerketvedt, D. (1998*a*), Full scale trial on kiln no. 6, Norcem Brevik, Technical Report 220288-4, Tel-Tek, Dep. Combustion and Environment.

Tokheim, L.-A. & Bjerketvedt, D. (1998*b*), 'NOx reduction by staged combustion in a precalciner cement kiln using alternative fuels', *Work-in-progress poster no. 1G18, Symposium (International) on Combustion, 27, The Combustion Institute, USA* .

Tokheim, L., Bjerketvedt, D., Husum, I. & Hoidalen, O. (1998), 'NOx-minderung in einem zementofen mit vorcalcinierung durch reduzierende verbrennung von kunststoff', *ZKG International* **1**, 12–23.

Turnell, V. J. (2001), 'Impact of fuel change', *International Cement Review* pp. 65–67.

Turns, S. R. (1996), *An Introduction to Combustion, Concepts and Applications*, McGraw-Hill Book Co.

Van der Meer, E. H., Thorpe, R. B. & Davidson, J. F. (1999), 'Dimensionless groups for practicable similarity of circulating fluidised beds', *Chemical Engineering Science* **54**, 5369–5376.

Van der Meer, E. H., Thorpe, R. B. & Davidson, J. F. (2000), 'Flow patterns in the square cross-section riser of a circulating fluidised bed and the effect of riser exit design', *Chemical Engineering Science* **55**, 4079–4099.

Voll, S. (2002), Karakterisering av alternative brensler (in Norwegian), Master's thesis, Telemark University College.

Warnatz, J., Maas, U. & Dibble, R. W. (1999), *Combustion*, Springer-Verlag Heidelberg Berlin 2nd edn. ISBN 3-540-65228-0.

Werther, J., Hartge, E. U. & Krause, M. (1992), 'Radial gas mixing in the upper dilute core of a circulating fluidized bed', *Powder Technology* **70**, 293–301.

Werther, J. & Ogada, T. (1999), 'Sewage sludge combustion', *Progress in Energy and Combustion Sciences* **25**, 55 – 116.

Williams, F. A. (1985), *Combustion Theory*, Addison-Wesley Publishing Company.

Wojtowicz, M. A., Pels, J. R. & Moulijn, J. A. (1993), 'Combustion of coal as a source of N2O emission', *Fuel Processing Technology* **34**, 1–71.

Xeller, H. (1999), 'New developments in NOx abatement in the cement industry', *ZKG International* **51**, 208–210.

Xu, H., Smoot, L. D. & Hill, S. C. (1998), 'A reduction kinetic model for NOx reduction by advanced reburning', *Energy & Fuels* **12**, 1278–1289.

Xu, H., Smoot, L. D. & Hill, S. C. (1999), 'Computational model for NOx reduction by advanced reburning', *Energy & Fuels* **13**, 411–420.

Zamansky, V. M., Maly, P. M. & Ho, L. (1997), 'Family of advanced reburning technologies: Pilot scale development', *Joint Power Generation Conference* **EC-Vol. 5**, 107–113.

Zevenhoven, R. (2001), Personal dialogue, e-mail, *in* 'HCl Capture in FBC', Helsinki University of Technology, ron.zevenhoven@hut.fi.

Zevenhoven, R., Axelsen, E. P., Kilpinen, P., Hupa, M., Elomaa, M. & Liukkonen, V.-P. (2000), The behaviour of nitrogen from polymers and plastics in waste-derived fuels during combustion, Technical Report Final report, Åbo Akademi University, Process Chemistry Group.

Zevenhoven, R. & Hupa, M. (1998), 'The reactivity of chars from coal, peat and wood towards NO, with and without CO', *Fuel* **11**, 1169–1176.

Zevenhoven, R., Karlsson, M., Hupa, M. & Frankenhaeuser, M. (1997), 'Combustion and gasification properties of plastics particles', *Air & Waste Management Association* **47**, 861–870.

Zheng, Q. Y., Wei, X. & Lou, F. (1992), 'Experimental study on radial gas dispersion and its enhancement in circulating fluidized beds', *Fluidization VII* **Engineering Foundation, New York**, 258–293.

Zorzi, E. D. (1988), 'Burning of municipal solid waste in cement kilns', *IEEE Cement Industry Conference, Quebec, Canada* pp. 461–477.

Errata

Pg. 64	Table 3.8	Reference (?)
Should be:		Kunii & Levenspiel (1991)
Pg. 72	Line 4	…%(#14) in NOx reduction in comparison to 73 % (#11)…
Should be:		…%(#15) in NOx reduction in comparison to 73 % (#12)…
Pg. 73	Line 22	…see Table 3.13 and B…
Should be:		…see Table 3.13 and Appendix B…
Pg. 80	Table 4.1	Reference (?)
Should be:		Kunii & Levenspiel (1991)
Pg. 93	2. line bottom	…no supply of tertiary air…
Should be:		…no supply of secondary air…